Durham E-Theses

Geothermics of the Malay basin, offshore Malaysm

Wan Ismail Wan Yusoff

How to cite:

Yusoff, Wan Ismail Wan (1993) *Geothermics of the Malay basin, offshore Malaysm.* Masters thesis, Durham University.

Use policy

The full-text may be used and/or reproduced, and given to third parties in any format or medium, without prior permission or charge, for personal research or study, educational, or not-for-profit purposes provided that:

- a full bibliographic reference is made to the original source
- a https://etheses.durham.ac.uk/id/eprint/5537/ is made to the metadata record in Durham E-Theses
- the full-text is not changed in any way

The full-text must not be sold in any format or medium without the formal permission of the copyright holders.

Please consult the [full Durham E-Theses policy](https://etheses.durham.ac.uk) for further details.

GEOTHERMICS
OF THE MALAY BASIN,
OFFSHORE MALAYSIA

Wan Ismail Wan Yusoff

UNIVERSITY OF DURHAM

1993

GEOTHERMICS
OF THE MALAY BASIN,
OFFSHORE MALAYSIA

by

Wan Ismail Wan Yusoff

(Bachelor of Science, University of Malaya)

A thesis submitted for the

Master of Science degree

at the University of Durham

Graduate Society   November 1993

Declaration

The content of this thesis is the original work of the author and has not been previously published for a degree at this university or any other institution. The work of others is acknowledged throughout this thesis by reference.

Wan Ismail W. Yusoff, BSc. University of Malaya
Department of Geological Sciences
University of Durham
England

ABSTRACT

A review of the temperature, thermal conductivity and heat flow data of the Malay Basin has been carried out by analysing data from fifty nine exploration wells. The thermal conductivity of each well have been determined from logs which has been calibrated to measured thermal conductivity of cores. The formation temperature of the well at logging depth has been estimated by Horner plot by using a new model for derivation of effective circulation time. The effective circulation time has been approximated empirically from the well log data.

Revised heat flow, geothermal gradient and thermal conductivity maps of the Malay Basin have been constructed from the new data. A vertical thermal profile of the basin has been analysed. The heat flow anomalies have been observed from the areal as well as vertical profiles of heat flow.

The Malay Basin is found to have an average heat flow of 86 mWm^{-2}. The average geothermal gradient is 47 °C/km. Both the heat flow and geothermal gradient are high. The heat flow varies over the basin, with regional highs in the Northwest, South and Central portions and a lower heat flow in the Southeastern part and Northeast peripherals.

The anomalous heat flow is found to be related to the subsurface fluid movement and the overpressures. The temperature is not related to the top of onset of overpressures directly, however the various mechanisms of overpressuring can be speculated from the regional distribution of the temperatures at tops of the overpressures. Thermal maturity modelling has been carried out for selected wells. It was found that the basin thermal history can be matched to a rifted basin thermal model.

CONTENT

LIST OF FIGURES

LIST OF TABLES

CHAPTER 1

Introduction

1.1   Scope of work

Thermal parameters of a sedimentary basin are crucial in the assessment of tectonophysical and chemical properties of a basin. Heat is one of the agents that controls many of the processes in the basin which include basin development, mineralization and generation of hydrocarbons. Consequently, the main aim of this study is to re-evaluate and analyse the thermal constituents of the Malay Basin based on thermal data acquired from exploration wells. Previous researchers have observed that subsurface petroleum accumulations can induce heat flow anomalies and that variations of heat flow values with depth are a manifestation of subsurface fluid flow.

Another aspect of this study is to gain insight into thermal maturity and the temperature history of the basin by combining burial history analysis with organic maturity data. The analysis in pressure is included to complement the thermal data. The study intended to provide important background analysis for use in exploring for petroleum.

The heat flow components in sedimentary basins consist mainly of conduction and advection. Heat flow by radiation is not relevant in sedimentary basins because of low temperatures. The conduction heat flow is often related to the heat energy transferred from the deeper crust plus in situ radioactive heat generation and igneous intrusion. The advection heat transfer is associated with the subsurface fluid flow. It has been shown that, generally

conductive heat is more prominent over the advective heat components in studies over Northwestern Kansas (Forster and Merriam, 1993) and Michigan Basin (Speece et al. 1985).

With regards to the above, any improvement in the estimation of thermal conductivity and formation temperatures is vital for this study. The determination of the thermal conductivity of sediments and the formation temperatures are made primarily by measuring thermal conductivity of core samples and taking temperature readings of production tests. The vertical thermal profiles are generated from empirical evaluation of the measured thermal conductivity and formation temperature by calibration to log responses.

The resulting thermal values shall be used to evaluate the vertical and aerial thermal distributions over the basin. A two dimensional fluid flow model can be deduced from the relationship between heat flow temperature gradient and horizontal heat flow variation. Vitrinite reflectance is used to calibrate the thermal maturity estimates derived from modelling of thermal and subsidence histories of selected wells.

1.2   Location and general statement of study area

The study area is located in Malay Basin, offshore Peninsular Malaysia parallel to the Northeast coast from Kota Bharu in the Northwest to Kuala Terengganu in the South. The Malay Basin is under water of 40 m to 80 m and is approximately 450 km long and 160 km wide (Figure 1.1). It is one of the venues for active petroleum exploitation in SE Asia. Since 1968 Esso is the major oil company operating in the area. Recently several other companies joined in the search for petroleum which include PETRONAS Carigali, Japex-Taiyo, Texaco and Hamilton oil. The Malay Basin has been producing oil and gas from fields mainly discovered by Esso since 1978 (Figure 1.2). New discoveries have been made lately by Esso and other oil companies.
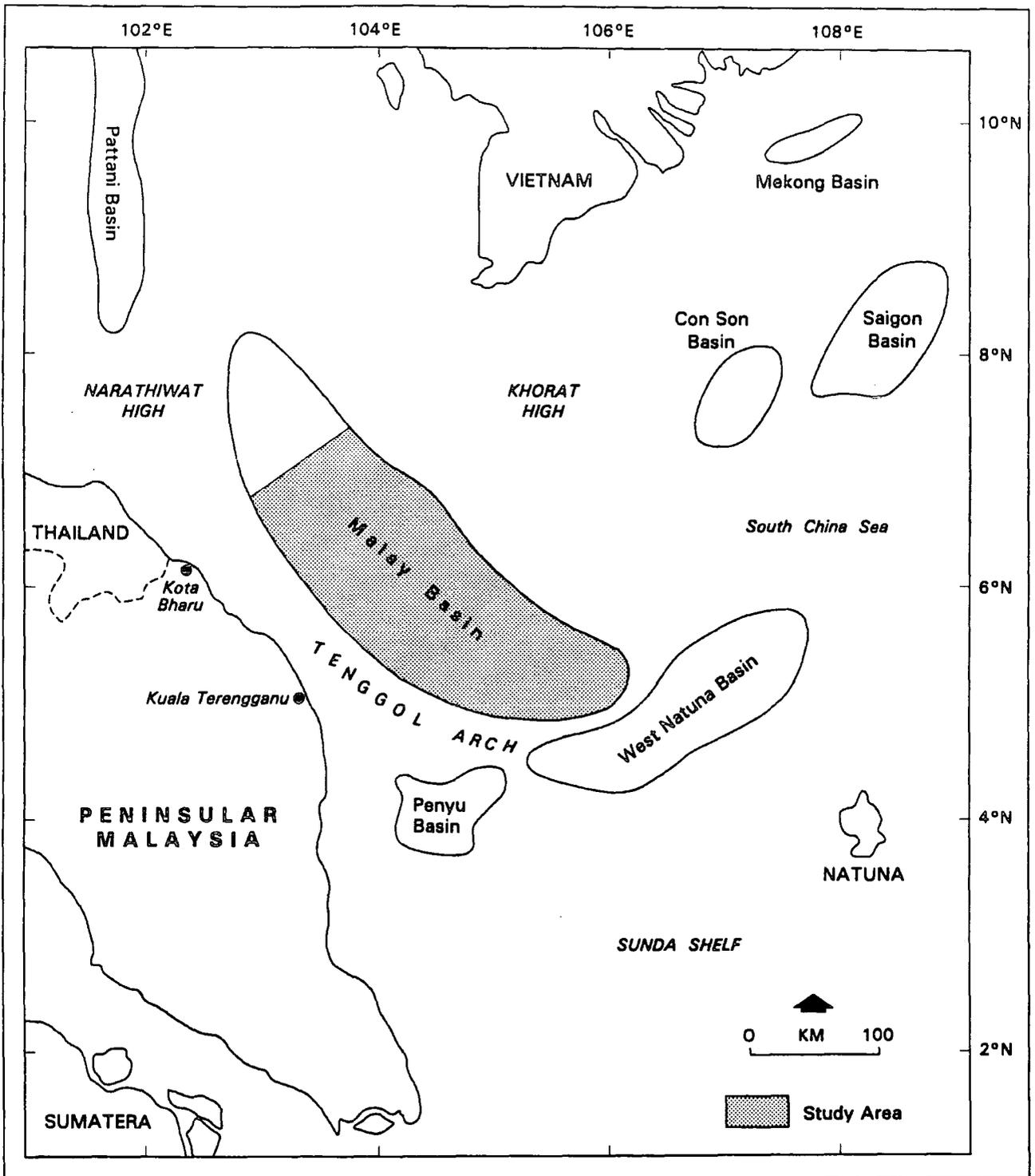
Figure 1.1 :   Location of study area and Malay Basin with adjacent
sedimentary basins of South East Asia
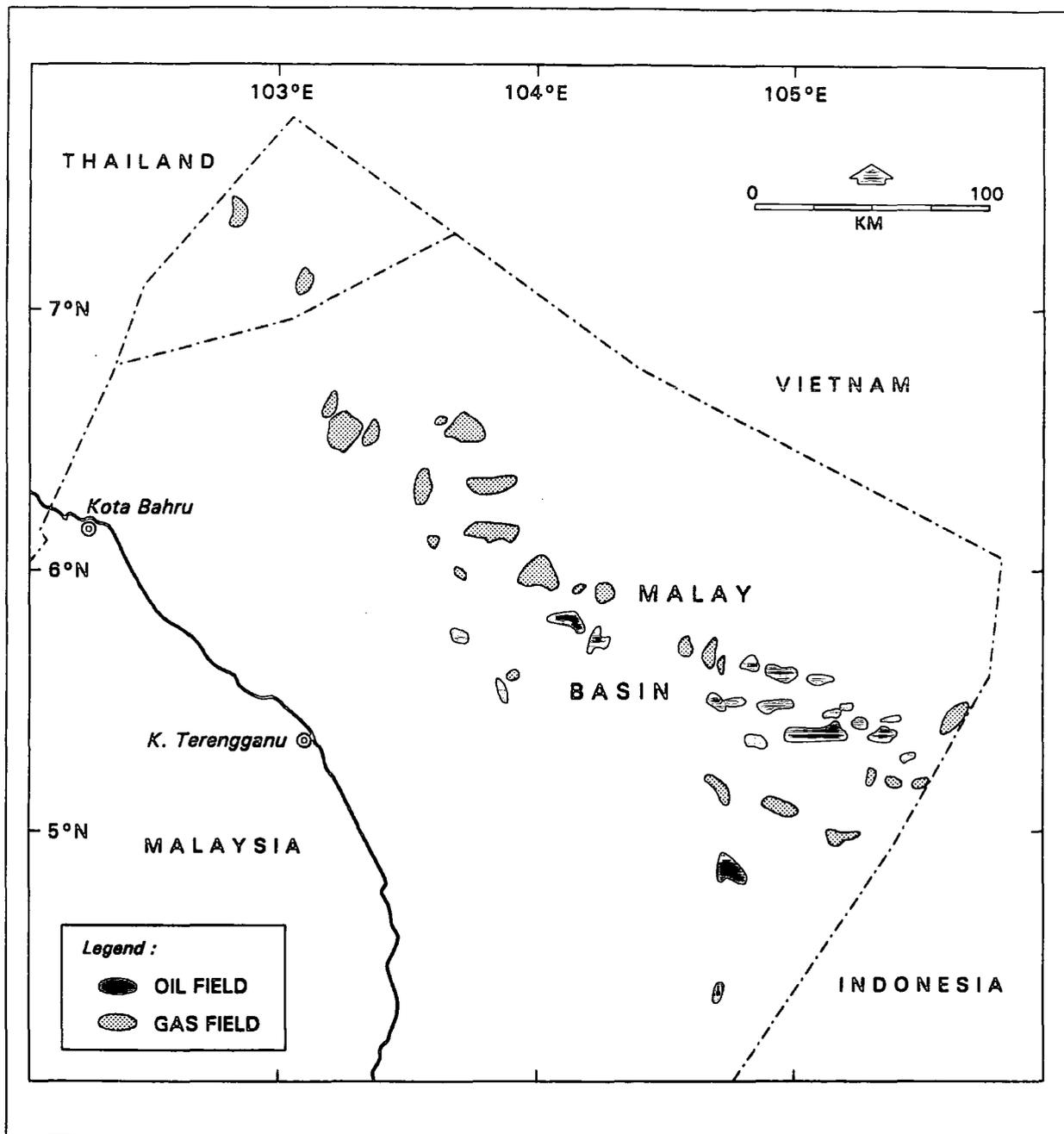
Figure 1.2 : Distribution of oil and gas fields in Malay Basin

4

1.3   Geological setting

The Malay Basin is an intracratonic basin which lies within the Sunda platform close to the boundaries between several major tectonic plates. i.e. the Pacific, Indian, and Eurasian (Figure 1.3) and Australian to the south. Although the mechanism and timing of basin development is still speculative, it has been suggested by several workers that basin initiation began with rifting which is in Early Oligocene times. The basin has East-West grabens which are mostly seen in the South Eastern part of the basin. The SW edges are bounded by basin inception growth faults which runs parallel to the present coast. The late compressive features overlie the extensional features in the SE but over the NW the extension persists to the present. The SE portion was uplifted in Late Miocene and Pliocene which caused erosion and produced unconformity.

Tapponier et al. (1982) considered the basin to be a wrench or shear basin formed due to the continental collision between India and Tibet and associated wrench faulting to the South and East. The collision has resulted in a southeastward extrusion of part of the mainland Asia (Figure 1.3) which has activated a sinistral strike-slip fault system and initiated the formation of the sedimentary basins of SE Asia. Hutchison (1986) suggested that the basin emplacement mechanism is rifting with the extensional tectonics processes combined with wrench faults. He believed that the basins have formed as a consequence of the Indian and Eurasian continent's collision in the Eocene which resulted in the propagation of a major wrench fault and the reactivation of the older suture zone in this region.

A more comprehensive model for the mechanism of the formation of the Malay Basin was described in Daly et al. (1991). The observation was based from their reconstructed plate tectonic history of the region. They described that the Malay Basin was formed by the similar
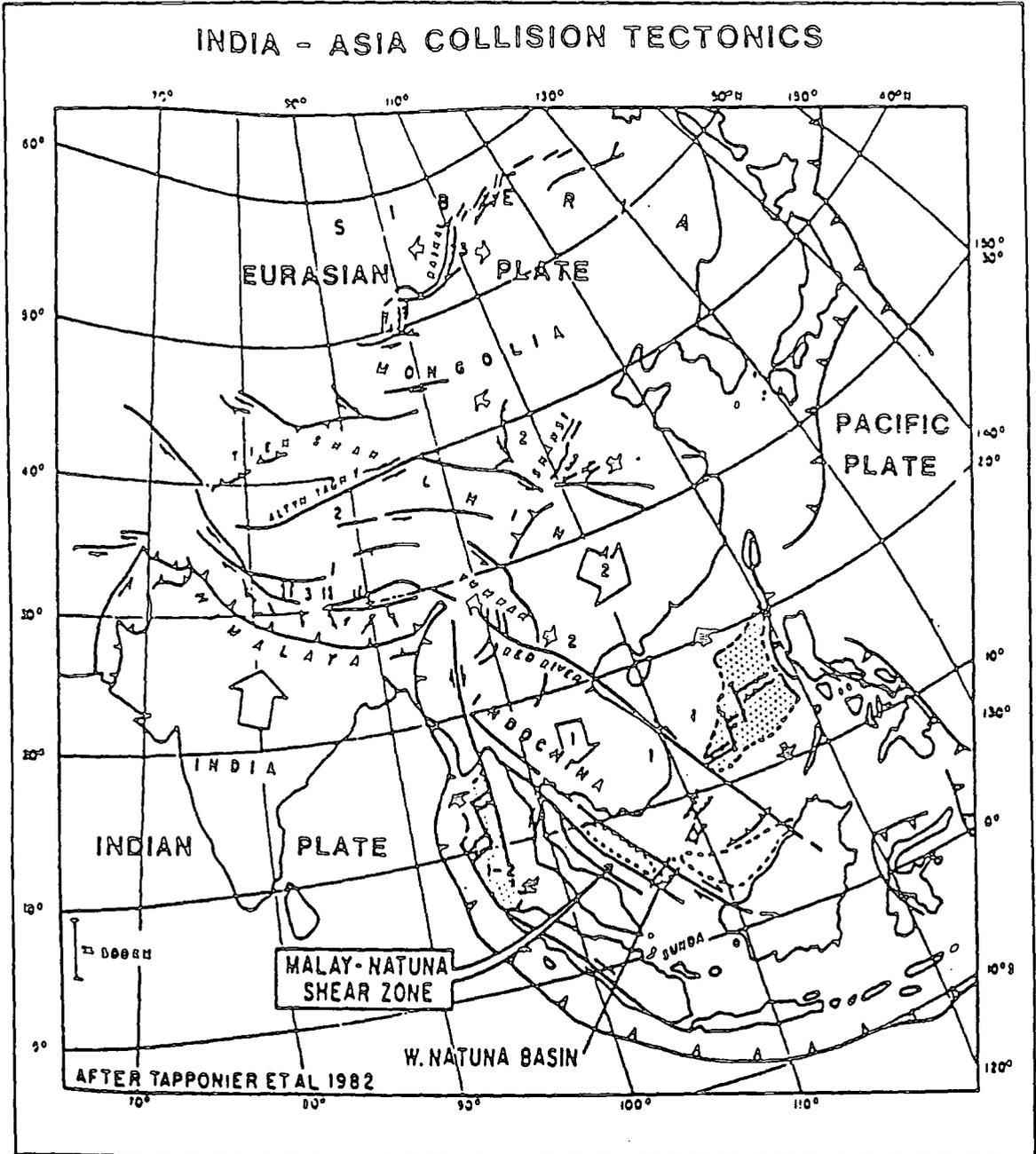
Figure 1.3 :   Location of Malay Basin within tectonic plates framework
in East Asia. The white arrows indicate the block motions
with respect to Siberia while the black arrows show the
direction of extrusion-related extension.
(after Tapponier et al., 1982)

6

mechanism as explained by Hutchison (1986). Further, they said that the Thai-Malay Basin were formed due to a strike slip movement as a result of increasing convergence between the Indian plates and Eurasia and the consequent clockwise rotation of the SE Asian mainland. They showed that the deformation in the region was due to the contraction of mainland Asia rather than large scale Eastward extrusion.

The Malay basin is believed to have been affected by a thermal perturbation which occurred as a result of the opening of the S China sea. In Late Eocene to Late Oligocene, drift or thermal subsidence was postulated to have affected the S China sea basins covering areas of up to the West Natuna basins which was believed to have been connected to the Malay basin (Ru and Pigott, 1986; Nik Ramli, 1988 and Daly et al., 1991)

Seismic quality generally deteriorates below 2.5 s two-way time (TWT), as such the basement has hardly been recognised. At the deepest part of the basin, sediment thickness is estimated from geophysics to be about 13,000 m . Five peripheral wells have encountered basement consisting of granite and metamorphosed sedimentary rocks, including quartzite, phylite, argilite and arenite with Cretaceous age (Esso, 1976).

1.3.1 Structures

The structural patterns of the basin has been mapped by Esso (1976). The structural anomalies identified are mainly anticlinal. These anomalies vary in complexity from simple domes to faulted structures, of which some are basement related. In the SE part of the basin, major faults and fold lineaments are mainly trending E-W and NW-SE, while in the Northwestern one third of the basin, the lineaments is in N-S direction. (Figure 1.4). The basin is asymmetrical in cross section. Esso, (1976) suggested that structural evolution of the basin can be divided into three tectonic deformation stages.

Legend :

	BASEMENT HIGH
	BASIN MARGIN FAULT
	COMPRESSIONAL ANTICLINE
	FAULT CLOSURE

Kota Bahru

PENINSULAR
MALAYSIA

K. Terengganu
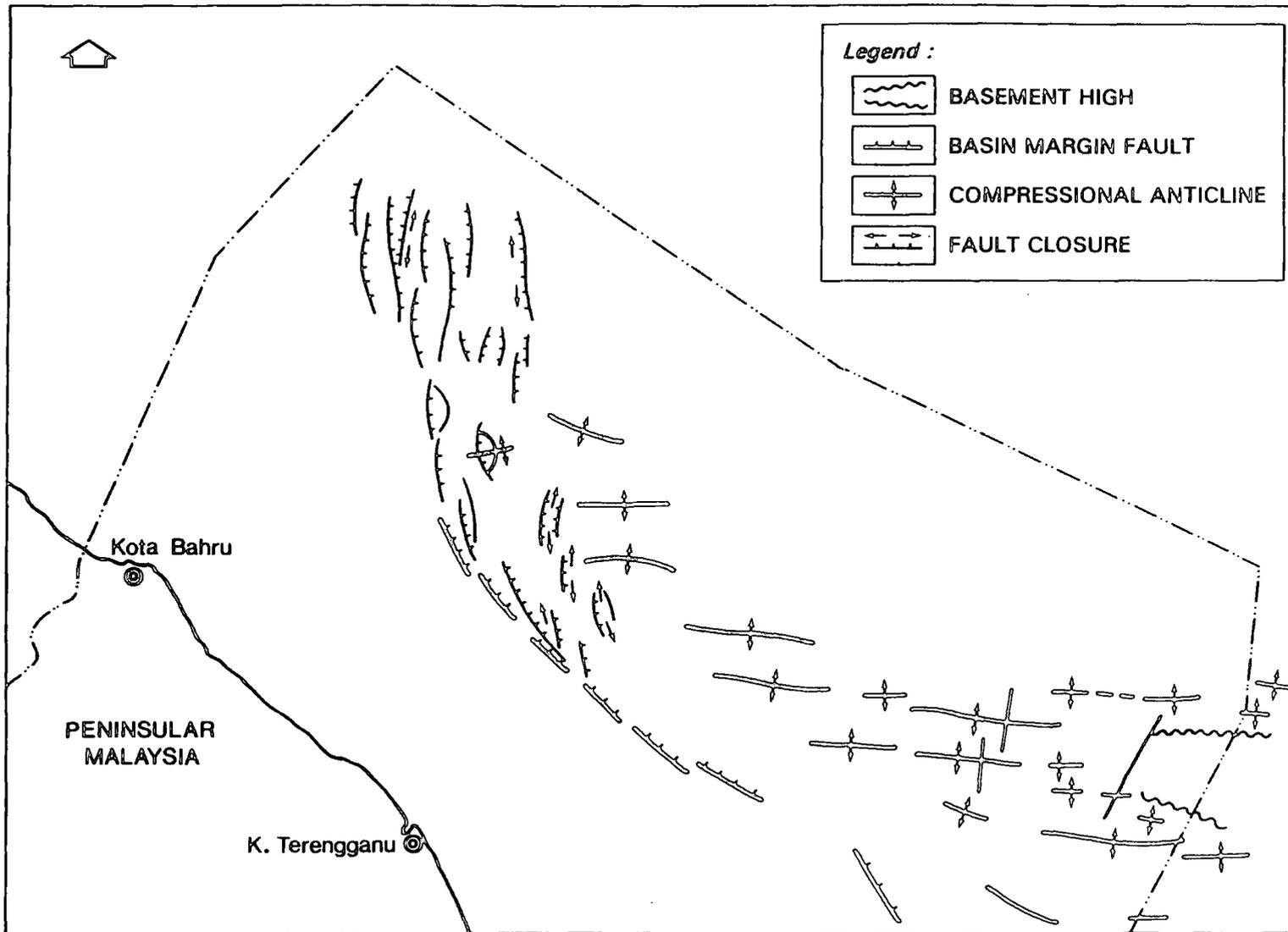
Figure 1.4 :   Structural pattern of Malay Basin showing basin margin faults,
the N-S extensional faults, compressional anticline alignments
and basement highs   (Esso, 1976)

In the earliest stage, a mainly N-S tensional stress produced a series of E-W half grabens. This extensional event started in Early Oligocene. The half grabens are generally faulted along their southern flanks as can be seen in the Southeastern part of the basin (Figure 1.4). In the Northwestern section of the basin, its earlier structural style can not be seen due to poor seismic data quality. By Early Miocene, a stage of compressive stress acted on the area which resulted in the formation of the folds. This compressional stage ended in Pliocene. The latest episode of structural developments is a result of an E-W extension. This event is shown by the N-S fault alignments occurring over the basin. In Late Miocene to Pliocene, a regional unconformity was developed due to the relative fall in sea-level. The Southeastern part of the basin was eroded because of the uplift while the Northwestern part was not affected by erosion and the unconformity is marked by disconformity surfaces.

1.3.2 Stratigraphy

The stratigraphy of the Malay Basin is based exclusively on sources from oil companies working in the area. There are three known stratigraphic nomenclature which were originated by workers in Esso, Conoco (which operated in late seventies in Penyu and South Malay Basins area), and Carigali. In this study, Esso's scheme for stratigraphic subdivision is used because it is widely documented over the basin.

Esso's stratigraphy is based on seismic sequence analysis which subdivided the sedimentary column into eleven seismic groups. These groups are named according to alphabetical order, starting with group A, the youngest and ending with group M, the oldest (Figure 1.5).
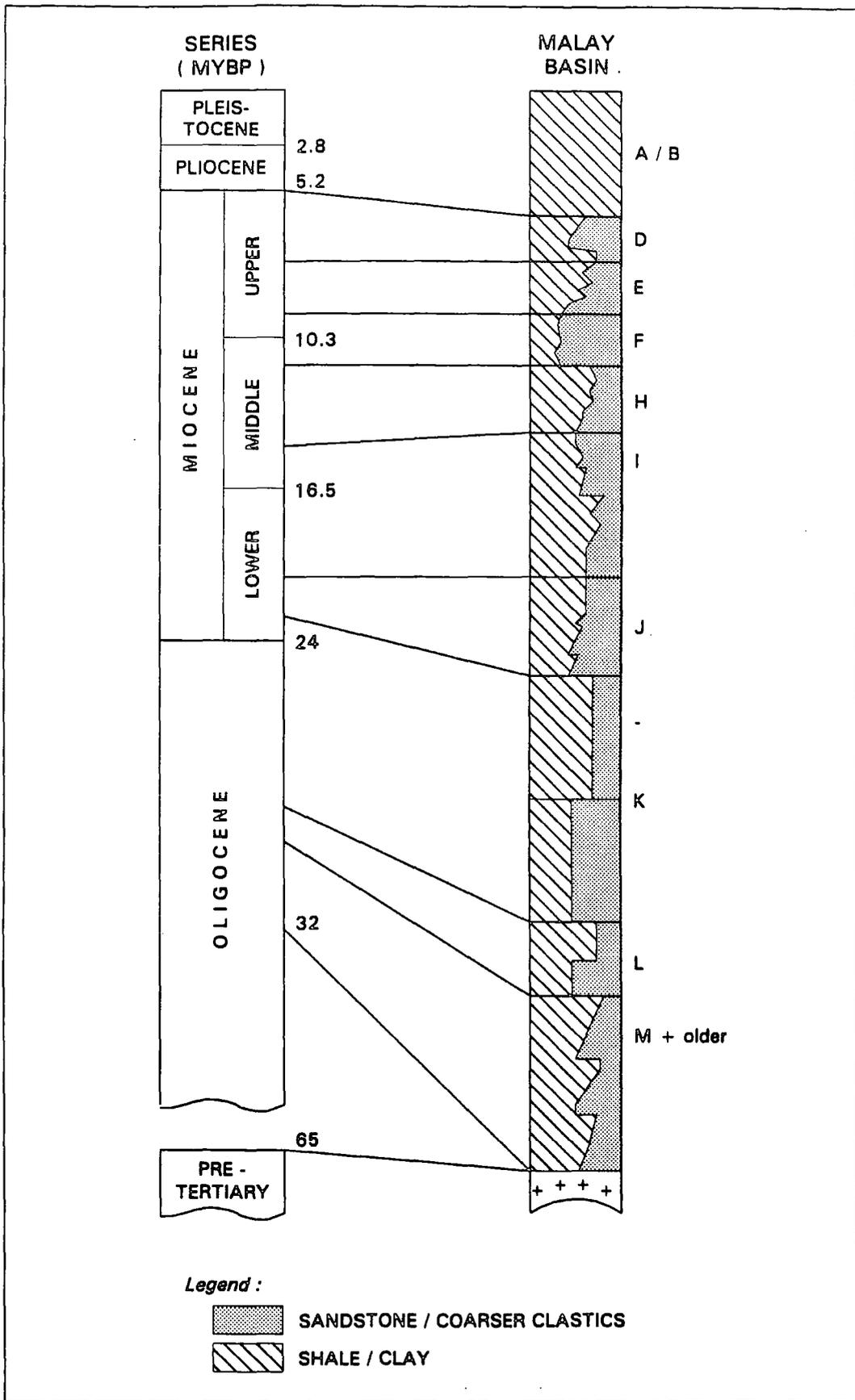
Figure 1.5 :   Sketch of stratigraphic column estimated lithologic
                composition in Malay Basin

The sedimentary rocks in the basin almost entirely consist of clastics, however intermittent calcareous sandstone prevails in some sections. Coal is found predominantly in groups D to H. In the Southeastern sector, red sandstones were penetrated and are believed to be related to a volcanic source. These clastics identified from rocks and logs have been correlated to corresponding seismic groups. Hence the seismic groups would represent sequences of clastic which has been identified and correlated .The base of each lithologic sequence has been identified to correspond with a seismic marker.

The age of these sequences are known mainly from the works of Armitage and Vioti (1977), and proprietary studies of Esso, PETRONAS and Carigali. These studies have been summarised by Ngah (1990) whereby a model chronostratigraphic columns has been introduced. Figure 1.6 is the preferred stratigraphic scheme used here. In this study the numerical age scale has been correlated with the seismic-lithostratigraphic scheme above and the seismic chronostratigraphy after Vail and Mitchum (1979). Hutchison (1989) observed that there is an excellent correlation between eustatic seal level changes and transgression and regression events in all SE Asian basins. The basement age of the granite and metamorphosed rocks has been dated by K/Ar dating to be 80 m.a. and 55.5 m.a. respectively (Esso, 1976).

1.3.3. Sedimentation and tectonic history

The tectonic history of the basin began from the deposition of the oldest stratigraphic groups M, L and K which infilled the half grabens (Figure 1.7). This event corresponds to subsidence of half grabens beginning in the Early Oligocene (Esso, 1976). The top of K sandstones has been interpreted to have been deposited in Late Oligocene (Ngah, 1990). In this report these synrift deposition is considered to have taken place until the Early Miocene at about 22.5 m.a.. The rocks are dominantly of continental and coastal plain origin with some lacustrine sediments. The sediments of these synrift deposit exceeds 8 km at the centre of the

11
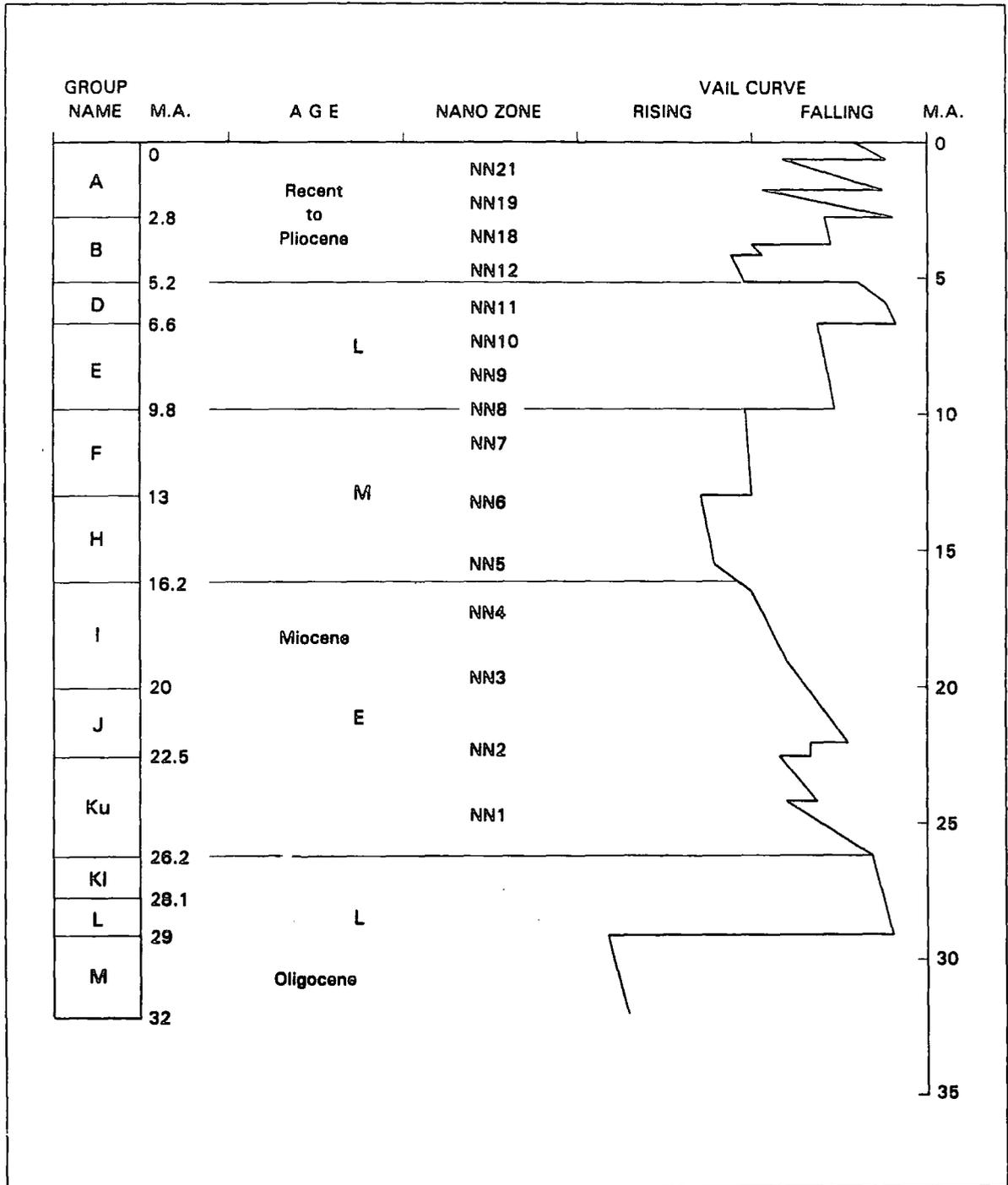
Figure 1.6 :   Adopted stratigraphic scheme of Malay Basin

WEST   EAST

EXTENSION

TENGGOL ARCH   TENGGOL FAULT   SOUTHERN PART OF MALAY BASIN

STABLE BLOCK

HALF
GRABEN   HORST

GRABEN

BASIN FILL

0   10 km
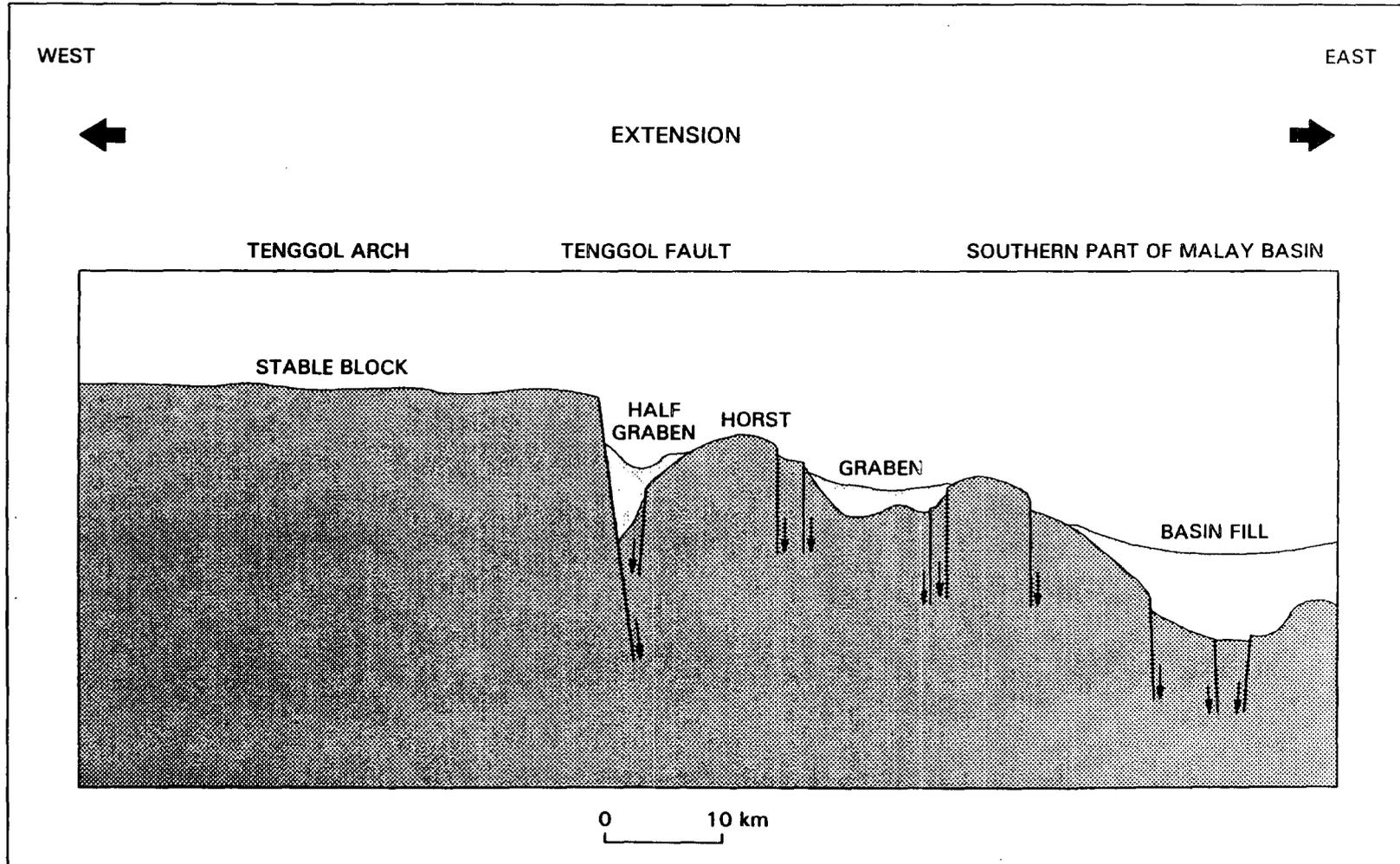
Figure 1.7 :   Structural cross-section of Southern Malay Basin showing half grabens filled
                with synrift sediments of group K, L and M during Early Oligocene to
                Early Miocene   *(modified after Ng T.S., 1985)*

basin. This episode of extensional phase was followed by an episode of inversion which contributed to the growth of the structures in the SE portion of the basin. Some of these structures are believed (Esso, 1976) to be probably associated with re-adjustment of fault blocks especially in the NW part of the basin and or shale diapirism which may be due to deep-seated wrench movements. The structural growth and coeval sediment deposition continued until H time. The sediments of seismic groups J, I, H, F, E and D are composed of dominantly sands and shales of increasing marine influence. These groups have a maximum thickness of about 5 km. The upper groups A and B have thicknesses up to 1.75 km and comprise mostly claystones with interbeds of lignite, sandstone and dolomite.

During H time, some structures in the SE have been uplifted with associated erosion which began to contribute reworked sediment to group F, E and D (Figure 1.8). This has been indicated by the formation of the regional Plio-Miocene unconformity. Along the basin margins, the sediments were eroded at several discrete time intervals resulting in three erosional unconformities, namely L sandstone , K sandstone and J sandstone unconformities. In most of the Northwestern portion, sedimentation continues and the Plio-Miocene unconformity is only marked by an insignificant disconformity (Figure 1.8). However in the northwest, unconformities have been shown to occur during the E and D times where sediments of group D, E, F, H, and I at the basin margin have been eroded. These unconformities have been interpreted to be the result of lowering of eustatic sea levels (Esso, 1976, Hutchison, 1978). The amount of erosion has been estimated to be at least some 800 m (Ngah, 1990) in the SE portion of the basin.

The latest episode is marked by a period of basin rejuvenation with extensive marine incursion and sedimentation during Pliocene-Recent times. The sediments comprise shales with interbeds of lignite, sandstones and dolomite deposited as group A and B. The dolomites record an increasing spread of marine influence. Some structures appear to grow for some
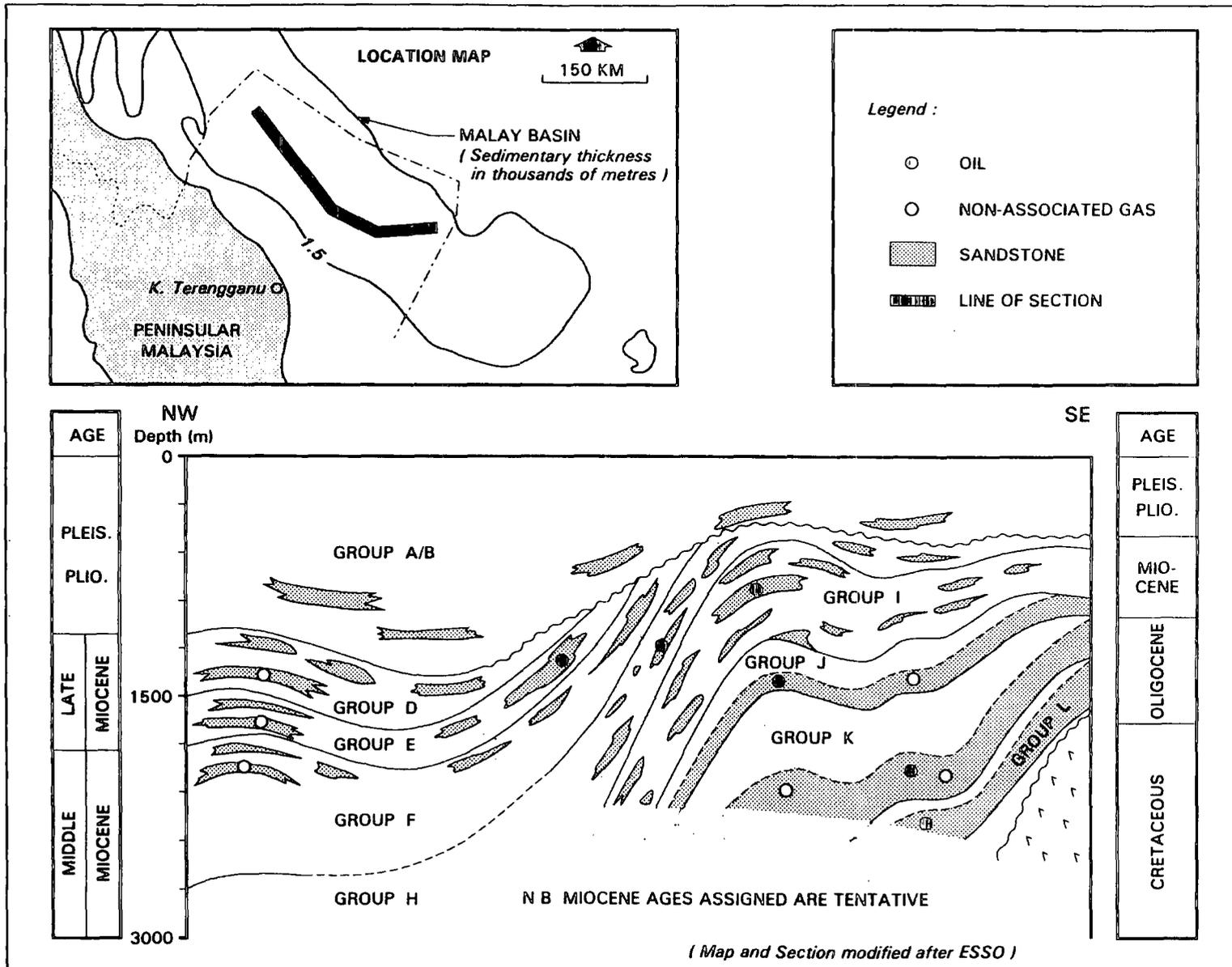
Figure 1.8 : Diagrammatic cross-section of Malay Basin showing regional unconformity and main oil and gas sands distribution   (modified after Wan Ismail, 1984)

times during this period, and are believed to have been caused by basement readjustment which in turn resulted in the probably more ductile sediments, shale, to flow.

1.4   Previous work.

After over a decade since the search for hydrocarbon in Malay Basin began, little is yet known to communities other than the operators about the thermal properties of the basin. The earliest record of a study in geothermics of the basin was carried out by Matsubayashi and Uyeda in 1979. Data used in the study were provided by Esso with the consent of PETRONAS. The conventional cores and logs were used for measuring thermal conductivity as well as lithologic description and for determination of composite percentage of lithologic type of each well studied. Although earlier work in the determination of the regional temperature gradient had been carried out by S. E. Asia Petroleum Exploration Society and Indonesian Petroleum Association (1977), no measurements of thermal conductivity were then available.

Matsubayashi and Uyeda (1979) revealed that the heat flow values were anomalously high (89.2 mWm^{-2}) in Malay Basin that time (9 wells). They suggested that if the simple subsidence-cooling model of sedimentary basins of Turcotte and Ahern (1977) is valid then the heat flow in the basin would be about 50mW/sq. m assuming the basement is Cretaceous. They suggested that the " excess " heat flow observed could indicate some igneous events in the Late Cenozoic which could be correlated with igneous rocks in mainland. But the high heat flow could also be as a result of effect of tectonic events which caused the major unconformity in the Gulf of Thailand in the Late Miocene and the subsequent block movements until Late Pliocene.

16

Many difficulties have been accounted by the above workers in their research due to insufficient data for correction of the formation temperatures and thermal conductivity values. The most severe problem is limitations from the thermal conductivity measurements which are mainly of sandstone. These values are a poor representation of the stratigraphic column, as most of the sediments are made up of mudstone rather than the sandstone. A better approximation would be achieved by correlation between log and thermal conductivity for a range of appropriate lithologies which have actual thermal conductivity measurements.

In 1984, Association of South East Asian Nation (ASEAN) Council on Petroleum (Ascope) and the Committee for co-ordination of joint Prospecting for Mineral Resources for Asian Offshore Areas (CCOP) jointly carried out studies on the terrestrial heat flow over the ASEAN region. This area includes countries such as Indonesia, Malaysia, Thailand, Brunei, Philippines and Singapore. A pilot Malay Basin terrestrial heat flow map was integrated in a regional heat flow map based on the collation of data provided by member countries. The average thermal conductivity of representative samples from selected boreholes were determined by lithostratigraphic average method. In this method, the average thermal conductivity of a well column is determined by using the mathematical average values of each rock type and then applying a harmonic average equation to calculate the stratigraphic average thermal conductivity value. The harmonic average equation is then used on the lithostratigraphic average values to derive thermal conductivity of the well. The report confirmed the earlier findings of Matsubayashi and Uyeda (1979) that the Malay Basin has an anomalously high heat flow.

The use of lithostratigraphic average thermal conductivity in determining the average thermal conductivity of the well, also adopted by Wan Ismail (1984) and reviewed in the Ascope heat flow workshop, seemed to be accepted by some workers. However it can be regarded as inadequate because a single average thermal conductivity of a stratigraphic unit

was used to approximate every well over the basin. A better method to estimate thermal conductivity can be made by using an empirical relation between thermal conductivity and electric log records introduced by Vacquier, et al. (1988), the principle of which forms part of this study.

A pilot study on the thermal history of the Malay basin has been carried out by a British Geological Survey (BGS) team in conjunction with studies on thermal histories of all petroliferous basins in the CCOP region in 1990. The study provided a first estimate of the temperature history of the basin using a software package, HOTPOT (Chadwick, et al. , 1991). The basic thermal data used were acquired from Ascope (Wan Ismail, 1984). The basin's thermal history has been modelled by assuming (i) a constant heat flow through time and (ii) a time variant heat flow method based on instantaneous lithospheric extension (Mackenzie, 1978) using a β factor of 1.6. Although the basin's heat flow ranges from 77 to 95 mW/m^{-2} (Wan Ismail, 1984), a uniform present day conductive heat flow of 83 mW/m^{-2} was adopted to model the temperature evaluation of the basin. They suggested that the large variation in heat flow may be due to data errors or it may suggest large movement of basinal fluids which redistribute the basement heat.

1.5   Objective of the study

The previous studies have been carried out without good supportive data for comparison and calibration of temperature and thermal conductivity values. It is envisaged that the temperature and thermal conductivity data should be re-examined with the hope that improvements can be achieved in estimation of the thermal parameters of the basin. For example, the estimated formation temperatures used in the pervious work were not adequately compared to the production test temperature, which is regarded as the best representation of true formation temperature. Traditionally, Horner plots are used to correct for the cooling effect of mud circulation to the temperature measured on logs. This is a popular method but

18

the accuracy is uncertain unless the resulting temperature is calibrated to the known formation temperatures.

One of the main objectives of this study is to produce an updated thermal map of the Malay Basin by reviewing analytical procedures for the estimation of true formation temperatures and in situ thermal conductivity. Another major objective is to produce a paleotemperature model of the basin based on the observed thermal patterns, geohistory and paleogeothermal indicators (e. g. vitrinite reflectance). The final objective is to address the significance of the present and paleothermal regimes on the understanding of the hydrocarbon occurrences in the Malay Basin.

1.6   Data base, data compilation and analysis

This work is based mainly on well data provided by PETRONAS. The basic data includes the electric logs and well reports. Measured thermal conductivity and gross core description data used are based on the previous work of the author, Wan Ismail, (1984). The core samples, seismic sections and shot point maps made available by PETRONAS are analysed for petrography and stratigraphy, and fluid inclusion analysis carried out in the University of Durham, using in-house laboratory facilities.

The bottom-hole temperature values and neutron, sonic and density log readings are taken directly from the electric log records. The pressure and stratigraphic information are available from the well completion reports and logs. The log data of 59 wells were read manually and later keyed in a spreadsheet software (EXCEL). This is carried out for the calibration and interpretation of thermal conductivity and formation temperature data and constructing vertical thermal profiles. The thermal parameters obtained are analysed by basin

modelling software, BASIMOD for the determination of thermal history of the basin. The contouring of thermal parameters are carried out by a mapping software, UNIMAP.

1.7 Pattern of thesis.

The methodology in calibration of temperature and thermal conductivity data are described in the earlier sections of Chapter 2. The test and limitation of the empirical relationship between the measured and modelled data are discussed. This is followed by discussions on surface heat flow density, thermal conductivity and temperature distributions in Chapter 3. The significance of the anomalous heat flow patterns and the relationship with fluid movement within the basin will be discussed.

The vertical thermal and pressure distributions and fluid flow path within the sedimentary sequences shall be described in the earlier part of chapter 4. The thermal modelling of the selected wells are then described. A discussion on the use of the present day temperature and subsidence curves , heat flow and thermal conductivity data in thermal modelling using BASINMOD programme follows. A description on the heat flow constraints in basin modelling by comparing single time invariant surface heat flow and time variant heat flow is then given. This chapter ends with results of thermal history based on a rifted basin model.

Chapter 5 will give the conclusions from the work done and discussions on the possible future extensions.

CHAPTER 2

Thermal data and the calibration of log records to the measured thermal data

2.1   Introduction

Thermal conductivity is the measurement of the rate of energy transfer across a unit area under the potential of a unit temperature gradient which has been expressed in units of $W(m^{\circ}K)-1$. It is a property of matter and in rock specimens, its value is dependent on direction of measurement since the rocks are anisotropic (Jessop, 1990).

2.1.1   Measurement of thermal conductivity

The direct measurement of thermal conductivity can not be obtained (Jessop, 1990) hence the measurements are often based on the knowledge of the amount of heat input into a system and the consequent temperature changes after a specific time. In this study the thermal conductivity has been measured by a `Quick thermal conductivity meter' (QTM). The meter consists of a probe made up of a known conductive matter (pad) and a thermocouple. In measuring the heat flowing through a rock, the probe is applied on the flat surface of the rock to be measured. The increment in temperature after the electrical energy is passed through the probe into the pad and the rock to be measured is computed by a processor which automatically registers the thermal conductivity of the rocks.

The heat flow through rocks can be expressed as the product of temperature gradient and thermal conductivity and is given by Fourier's law. It states that the heat flow Q is directly proportional to the temperature gradient in the form of

$$Q = -KdT/dy \qquad (2.1)$$

where K is the thermal conductivity, T is the temperature at a given point in the rocks and y is the co-ordinate in the direction of the temperature variation. dT/dy is the temperature gradient. T is in units of °C while Q is in mW/m2. In studies of terrestrial heat flow over the surface heat flow values, Q is also known as heat flow density, HFD (Thamrin, 1985; Correia et al., 1990).

In a sequence of sedimentary rocks where only conductive heat is transferred, with a constant basement heat flux, anomalous temperature fields will be observed over the surface of rocks due to different effective vertical thermal conductivities. The low conductive rocks will transmit heat slower (Figure 2.1-B) and the geothermal gradient is higher producing an iso-temperature surface deeper than normal (such as over a shale diapir). Whereas in a high conductive rocks (Figure 2.1-A) the heat energy is transmitted faster and the geothermal gradient is lower which will raise iso-temperature surface above the normal conductive zones (such as over a salt dome). The changes in the conductivity of the subsurface medium can thus be recognised by the heat flow anomalies for any region of normal conductive heat transfer. But in sedimentary basins where the heat-flow values are normally controlled by basement conductive heat, the heat flow is modified by internal radioactive heat sources as well as fluid movements within the subsurface.
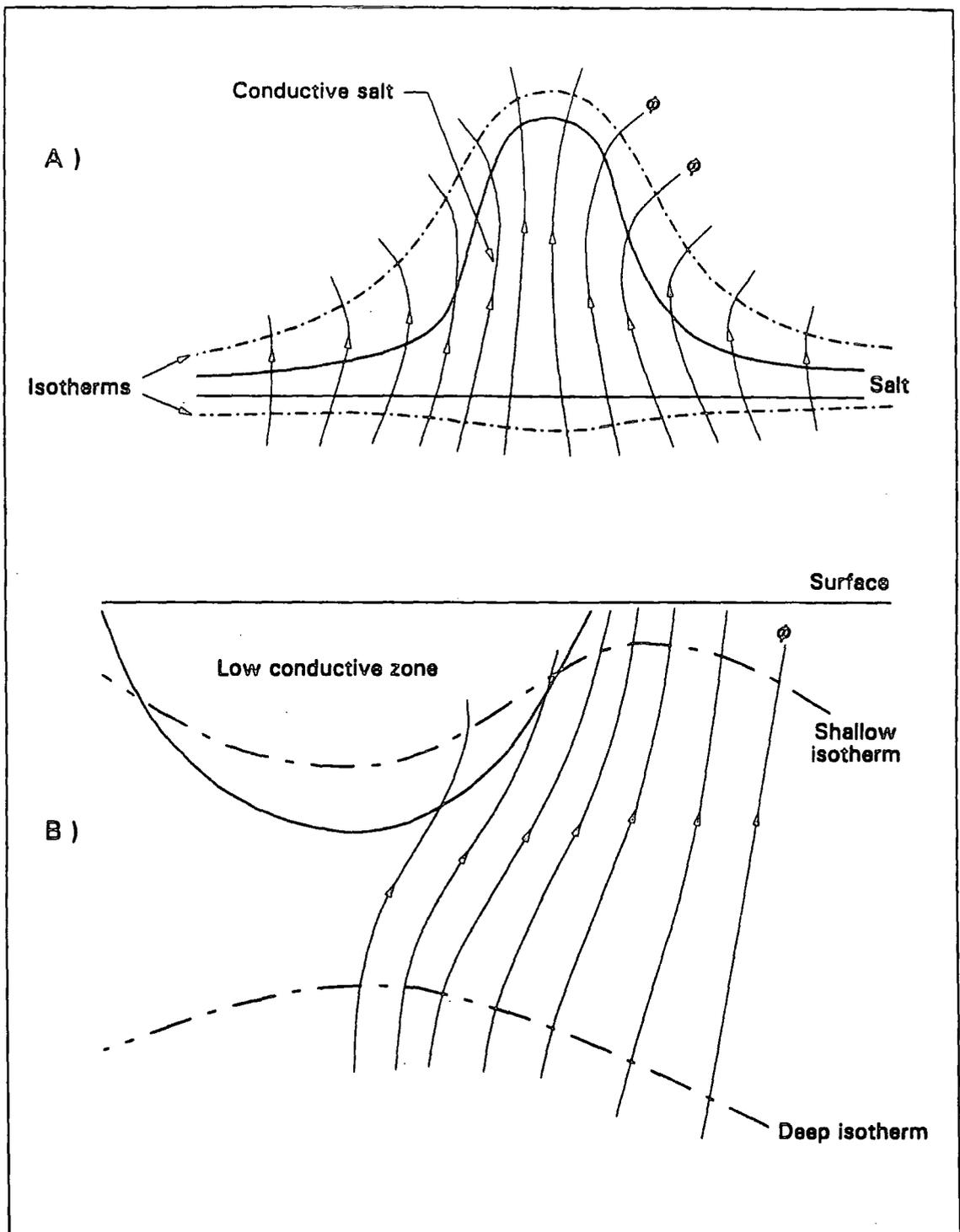
Figure 2.1 : Sketch of rocks in subsurface of different thermal conductivities, resulting in variations of isotherms over (A) higher thermal (B) lower thermal conductive zone (After Robert, 1988).

2.1.2   Factors affecting thermal conductivity of rocks

The thermal conductivity of a rock depends on the lithology and porosity. The rock's porosity is related to the initial porosity at the site of deposition and the degree of compaction and diagenesis (Sclater and Christie, 1980). The amount and type of fluid in pores and water bounded in clays contribute partly to the gross thermal conductivity of the rocks. The changes in lithology of each rock type considerably affect the thermal conductivity due to their compositional variations. Thermal conductivity of quartzitic sandstone is high, about 7.1 to 2.8 W/m/°K whereas those of clay rich sandstone are low with values between 2.1 and 1.9 W/m°K (Brigaud, et. al., 1990). The sandstones in the Malay basin have thermal conductivity of averaged between 2.58 ± 0.74 to 5.14 ± 0.63 W/m°K (in group M) while the claystones give lower thermal conductivity measurements of 1.39 ± 0.14 (in group A & B in Table 2.1).

In clastics, thermal conductivity is normally likely to increase with depth of burial, if only the compaction is the main factor which determines the variation in porosity with depth (Palciauskas, 1986). It has been observed that the averaged thermal conductivity values of clastics differ within different parts of the Malay Basin (Wan Ismail, 1984). Table 2-1 demonstrates a difference between the measured thermal conductivity-burial depth trend for the two sectors as shown by the relation between the thermal conductivity values of different lithology with sequence age. In the Northwest sector the measured thermal conductivity of the sandstone increases proportionately with stratigraphy (and hence depth) which may be explained by dominance of the effects of porosity loss due to compaction on the thermal conductivity values within the cored depth interval (Figure 2.2). This part of the basin has experienced a normal sedimentation history and relatively normal compaction trend which is disrupted often by overpressured zones only at depth near the bottom of the well.Figure 2.3 shows a relation between excess pore pressure and insitu thermal conductivity of a typical well in the North Western part of the basin.

Table 2-1 : Thermal conductivity of different rock types averaged over stratigraphic group in Malay Basin, bracketed are the number of samples measured (after Wan Ismail, 1984).

North Western and Central Malay Basin

Stratigraphic group	Rock type			
	Sandstone	siltstone	Shale	Claystone
A&B	-	-	-	1.39 ± 0.14
	(0)	(0)	(0)	(8)
D	2.58 ± 0.74	3.11 ± 0.00	-	2.01 ± 0.00
	(21)	(4)	(0)	(2)
E	2.90 ± 0.50	2.92 ± 0.63	2.89 ± 0.34	2.36 ± 0.00
	(118)	(70)	(28)	(2)
F	3.02 ± 0.64	3.11 ± 0.59	2.65 ± 0.29	2.50 ± 0.00
	(11)	(15)	(10)	(3)
H	3.63 ± 0.26	3.90 ± 0.55	-	
	(9)	(7)	(0)	(0)

Table 2.1 (continued)

Southern Malay Basin	Rock type			
Stratigraphic group	Sandstone	Siltstone	Shale	Claystone
F	- (0)	- (0)	- (0)	1.87±0.1 (4)
H	1.90± 0.49 (14)	2.97 ± 0.96 (14)	- (0)	2.09±0.36 (8)
I	3.14±1.26 (24)	3.24±0.94 (17)	- (0)	- (0)
J	3.05±0.96 (226)	4.28±0.42 (6)	2.32±0.46 (9)	- (0)
K	2.65±1.28 (84)	3.36±0.56 (23)	2.69±0.45 (3)	- (0)
L	3.35±1.08 (23)	3.98±0.91 (4)	2.55±0.45 (5)	- (0)
M	5.14±0.63 (16)	3.50±0.42 (3)	- (0)	- (0)
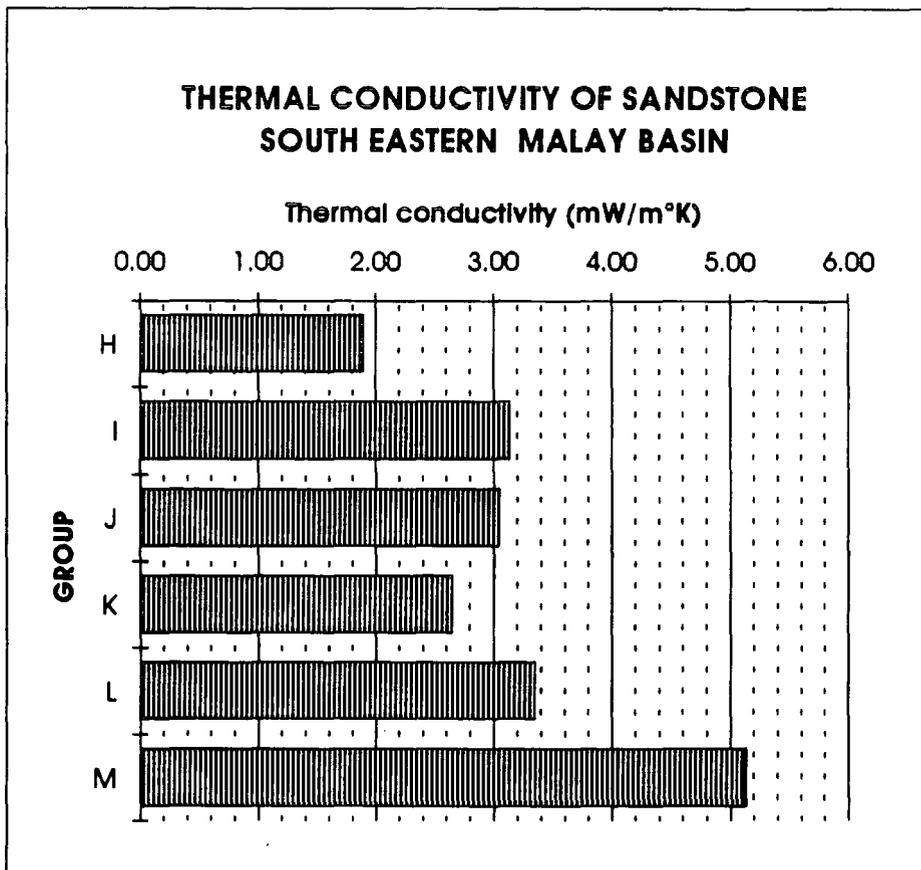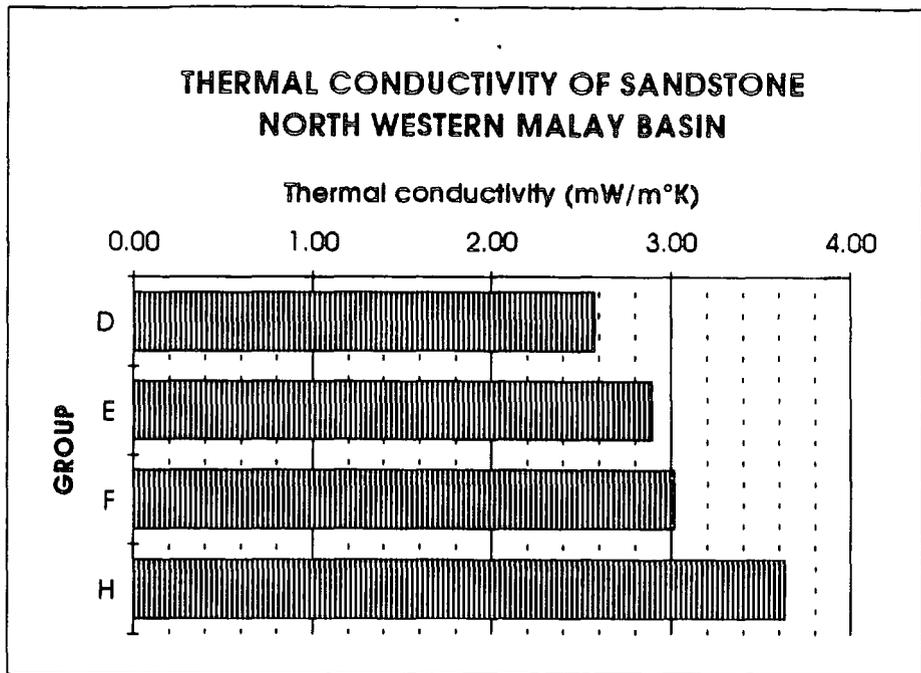
Figure 2.2 Comparison of average measured thermal conductivity
of sandstone in the NW and SE sector of the Malay Basin
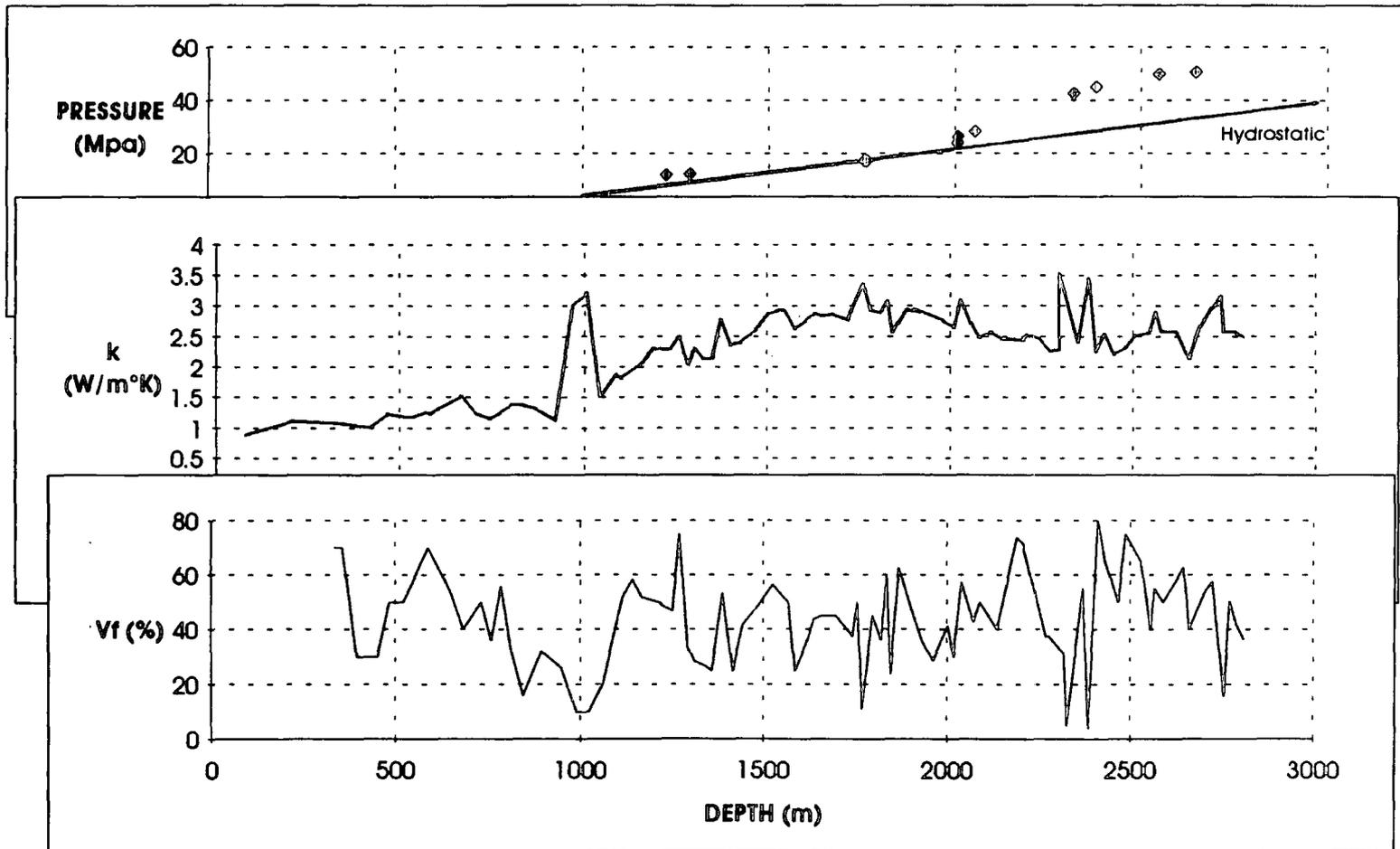
Figure 2.3   Relationship of pressure and thermal conductivity (k) of a well in the north western part of Malay Basin with an overpressured section below 2000m depth. Vf is the volume of fines.

The average measured thermal conductivity of sandstones in group I, J and K is 3.14, 3.05 and 2.65 W(m°K)$^{-1}$ respectively (Table 2.1). The case of lower thermal conductivity values in the J and K sandstone compared to those of overlying I sandstone in SE sector (Figure 2.2) shows there is a complexity which does not permit a general equation relating thermal conductivity to depth. The irregular trend of measured thermal conductivity of sandstones with depth is probably due to effect of diagenesis which overshadows the effect of compaction. For shales there are no good trends of the thermal conductivity versus stratigraphic position or depth which may be due to shale anisotropy (Brigaud, et. al. , 1992) in addition to reason of diagenesis. A regular increase in thermal conductivity with depth is only observed in claystones at shallow depths. Note that some of siltstones have unusually high thermal conductivity relative to sandstone in a similar group but that may be due to the effect of comparatively low porosity.

Therefore, from the observations of the measured thermal conductivity versus stratigraphic age for different lithologies, it seems quite difficult to relate thermal conductivity to either depth or depositional age for all the sequences. Any relationship between thermal conductivity and depth might be made for rocks within only a small interval of the stratigraphic sequence and confined to a uniform localised geological setting. When measured thermal conductivity is not available, the in situ thermal conductivity is therefore best described by considering the relationship of the porosity, matrix and fluid content with known thermal conductivity measured.

2.1.3   Empirical relationship of thermal conductivity with the rocks type and porosity

It has been accepted that thermal conductivity of rocks can be a function of lithology and porosity (Andrew-Speed et al., 1984; Brigaud et al., 1990). An empirical relationship between thermal conductivity and porosity is given by

$$K = k_m^{(1-\emptyset)}k_f^{(\emptyset)}$$

or it can be written as

$$K = k_m(k_f/k_m)^\emptyset \qquad\qquad (2.2)$$

where K is the thermal conductivity of rocks and k_m is the thermal conductivity of matrix, k_f is the thermal conductivity of fluid and $\emptyset$ is the porosity. The above equation which is normally called as geometric means equation is useful for most rocks, but it is not adequate for cases where the matrix conductivity ratio, k_f/k_m is too large or too small. With a small matrix conductivity, the empirical thermal conductivity shall be very small regardless of the values of porosity. Another means of estimating thermal conductivity of sediments is by effective medium theory method. The effective medium theory is a means to describe properties of a composite material from which the fractions of the individual components and their properties are known. An effective thermal conductivity, K for a randomly inhomogeneous medium made of constituents with volume fractions, V_i and thermal conductivity's, k_i is

$$K-1 = 3V_i (2K+k_i)^{-1} \qquad\qquad (2.3)$$

where it is assumed that on a scale much larger than the grain size, the composite is homogeneous and isotropic. This has an advantage over the previous empirical formula since it is applicable for any number of components, any distribution of volume fraction and all values of the individual conductivities (Palciauskas, 1986).

The variation of thermal conductivity of clastic sediments composed of different particles is affected by the ratio of the volume occupied by the fine grained particles (i.e. clays) and the course grained particles (e.g. a mixture of quartz and feldspar) it is composed of
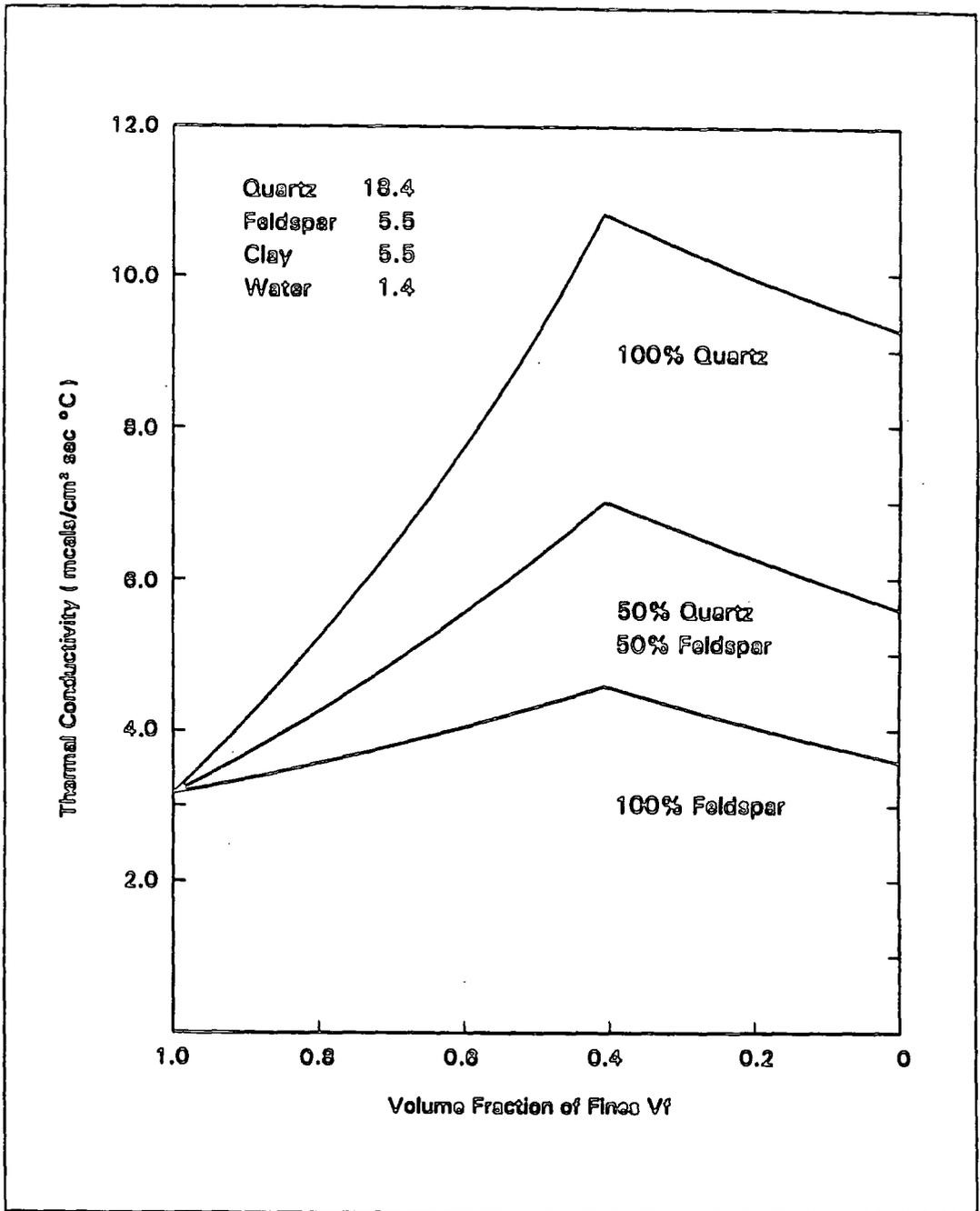
Figure 2.4 : Theoretical relationship of the effective thermal conductivity for clastic rock-water mixtures as a function of Volume of fine (Vf) . (After Palciauskas, 1986)
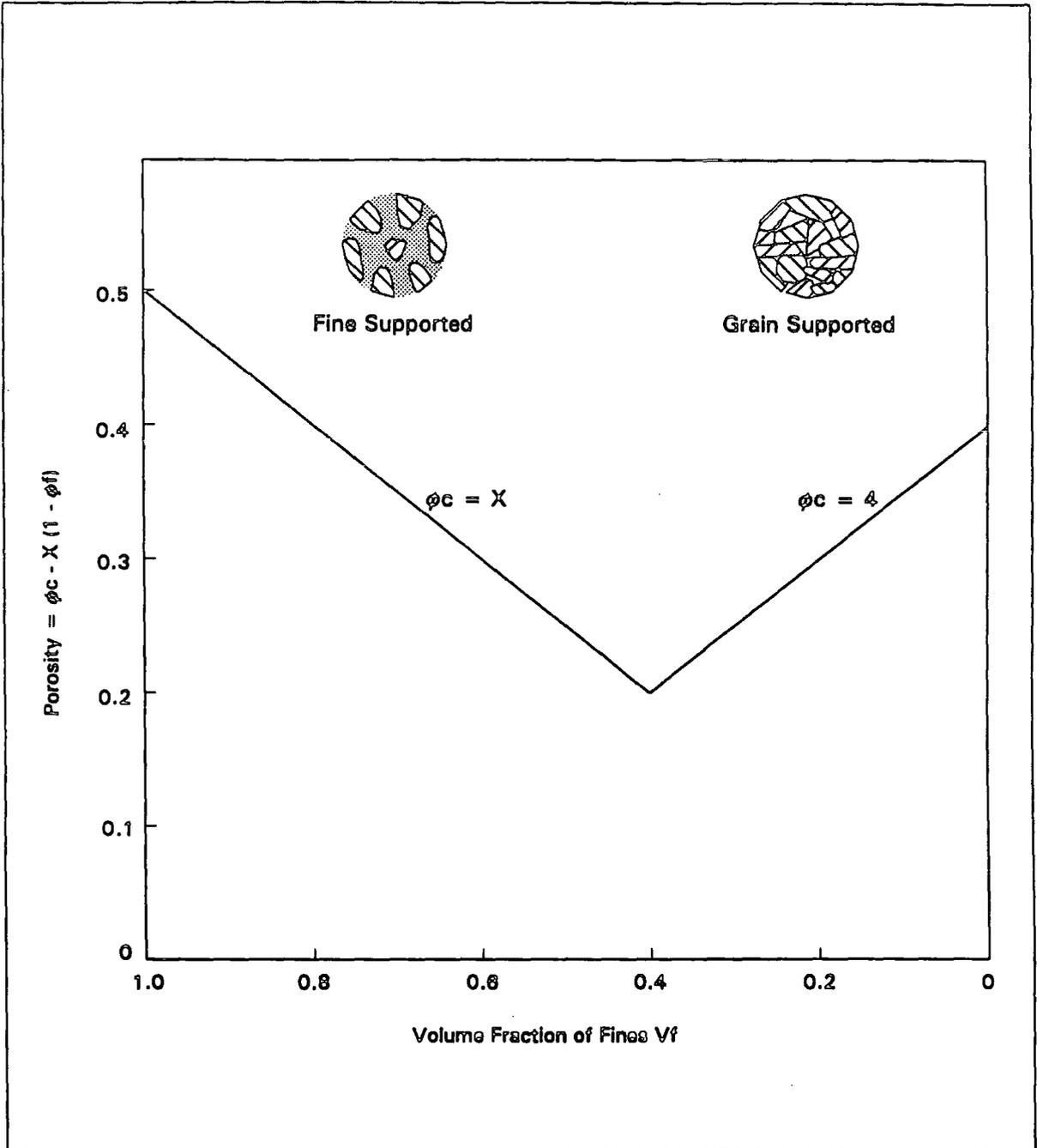
Figure 2.5 : The porosity as a function of Vf, the volume fraction occupied by the fines. (After Palciauskas, 1986)

(Figure 2.4). Hence according to the effective medium theory, in a normally compacting basin, the theoretical effective thermal conductivity is highest for sediment with compositions consisting of 40% volume of fines. This specimen is expected to have the lowest porosity at any specified depth (Figure 2.5). In other words for a siltstone of Vf at the 40% value, it canhave a higher thermal conductivity than a sandstone of Vf less than the value at a specified depth. This phenomenon may explain some of the samples classified as siltstones which show the relatively high thermal conductivity compared to sandstones.

2.2   Calibration of measured thermal conductivity with logs reading

Measured thermal conductivity data are dependent on the amount of cores present in wells. Usually a well is cored for an interval of about 7 to 10 metres of the whole total depth of about 2000 to 3000 metres. Therefore the measured thermal conductivity data are insufficient for constructing a thermal conductivity versus depth profile for the entire well. The samples are only a good representation of wells at coring intervals. Previous studies (Matsubayashi and Uyeda, 1979; Wan Ismail, 1984) in the Malay Basin used the litho-stratigraphic method to estimate the effective thermal conductivity at any well location. The litho-stratigraphic average method only assumes a constant thermal conductivity of individual layers or stratigraphic units in all wells analysed. This will give an estimation of thermal conductivity in some wells biased to the average measured thermal conductivity. However geophysical well logs are available for a better representation of the physical properties of the entire well column. Measured thermal conductivity is one of the physical properties of sedimentary rocks which can be calibrated to well logs (Vacquier et al., 1988; Brigaud et al, 1990; Demongodin, et al., 1991).

Several attempts have been made to calibrate thermal conductivity to logs. Vacquier et al (1988) approached the task by dividing the overall rocks into seven lithological subsets and

used measured thermal conductivity from cores. An empirical relation for each litho subset is expressed by a five-term linear regression equation. The log readings used included density, porosity, transit time and shale volume derived from gamma ray. The correlation coefficient between measured and predicted values ranges from 0.55 (sandstones) to 0.89 (argillaceous rocks). There seems to be a low degree of correlation coefficient for some lithotypes (such as sandstones), which may indicate inadequate treatment of rocks into subsets based only on lithological types. In clastics, for example the variation of porosity seems to affect the thermal conductivity quite substantially. This method needs a lot of log data which normally is not available in all wells. Secondly the lithological subsets need to be ascertained before the equations can be applied. Hence in areas where only well logs are available, the method is not practical. Another means of correlation of thermal conductivity to well logs is based on mineral components of cutting samples and was attempted by Brigaud et al. (1990 & 1992). They used the established geometric means equation 2.2 above, to determine the thermal conductivity at cutting depths along the well. The porosity was estimated from log data while the mineral compositions were analysed from the cutting samples. This method suffers several problems which includes: the examination of numerous cutting samples and tying each set to the log depth. which is always difficult. In addition the mineral composition of ditch cuttings are liable to be altered during the transportation along the wellbore.

In my study an attempt to correlate thermal conductivity measurements to wireline logs empirically is made. The measured thermal conductivity is expressed as a function of porosity and volume of fines determined from the available log data. This method is based on the understanding of the effective medium theory highlighted above and the application of regression analysis demonstrated by Vacquier et al., (1988). Having obtained the empirical equations, the thermal conductivity at any specific depth can be determined exclusively from well logs.

2.2.1 Thermal conductivity data source

The measured thermal conductivity of two hundred and three samples are selected from the data base provided by PETRONAS. The original data has been taken from measurements of thermal conductivity of core sample made by the author in PETRONAS Laboratories Kuala Lumpur, Malaysia in 1983. The selected samples consist of varieties of clastics from wells distributed over the basin with different depths and stratigraphic groups.

A Quick Thermal Conductivity Meter (QTM) was used to carry out measurements on selected cores of the Malay Basin. Conventional cores of about 17 cm (5") in length each were cut in halves along their length and the surface was smoothed to provide a proper surface for taking a thermal reading. Lithological descriptions were made for each sample by physical and chemical examinations on cores. Since all samples are clastics, the classification of lithology are taken according to the grain size. It is possible to classify into sandstone, siltstones, shales and claystones. For fine clastics of finer grains than siltstone, they are classified under shales if there are fissile, otherwise they are called claystones or mudstones. The key properties described include, the lithology, grain size for sandstone, and accessories in the form of cements which is also thought to affect thermal conductivity. The sandstones are described as dolomitic, calcitic, ferruginous, quartzitic or carboniferous, after their prominent accessories.

The samples were immersed in water for 48 hours and kept at a room temperature of about 21 to 24 °C before measurement. Measurements of thermal conductivity were carried out by means of a transient box type thermal conductivity meter (QTM). Details of the QTM and its application procedures were described by Sekiguchi, (1984). The probe was protected from water wet samples by a thin plastic film to avoid damage to the meter. The calibration and drift correction of the meter were made after measuring 10 to 20 samples. Clayey samples

were sealed in plastic to prevent them from disintegration and only cut open at the flat surface during the measurement.The measured thermal conductivity data were compiled according to their respective wells, depths and lithologic descriptions. An average thermal conductivity of each lithologic type in each stratigraphic group is as shown by Table 2.1.

Some problems have arisen in the choice of fluid for soaking the samples. It is recommended that water be used. Although samples can be destroyed whenever there are clays, the samples can be prevented from total destruction by wrapping in plastic. In some practices, mixture of kerosene and water are used for the protection of the sample. But by introducing kerosene as fluid, then we are forcing more unrealistic compositions of the subsurface conditions during the measurements and may reduce the thermal conductivity values as kerosene has a lower thermal conductivity than water. Therefore it is considered that more representative thermal values can be achieved when water is taken as the medium for soaking the cores because water forms the main infills of the pores in the sediments. The effects of air bubbles that may be trapped in the pores are taken into consideration by assuming that the samples have been flushed of air after being soaked for forty eight hours.

2.2.2 Log interpretation and analysis of measured thermal conductivity data

In the present work the sediments are treated as a composite of fines and coarse with the pores filled with water. The principle of the effective medium theory predicts that the thermal conductivity can be written as a function of volume fraction of each components of the sediments and their respective thermal conductivities (Equation 2.3) whereas the empirically derived equation (the geometric mean formula) relate thermal conductivity with porosity and matrix conductivty (Equation 2.2). These approaches are considered in calibration of thermal conductivity with logs readings by taking volume of fines (shales) and porosity to represent the physical properties of the sediments.

Physical properties of the sediment can be deduced from log analysis. This has the advantage over using the raw log data for it eliminates some errors due to the tool sensitivity to borehole size and mud salinity. The volume of shales from log analysis can approximate the volume of fine materials in the sand-shale sequences. In log analysis, the volume of fines, Vf, (which is Schlumberger's (1988) volume of shales) is defined as

$$Vf = (gr\text{-}gmin)/(gmax\text{-}gmin) \qquad (2.4)$$

where gr is the gamma ray reading, gmin and gmax are the minimum and maximum gamma ray values of the particular log run. The interval for assigning each pair of gmin and gmax is taken as the log run depth interval because the interval has similar mud used and also the physical character of formation is quite uniform (for e.g.. hardness). This choice of the depth interval may reduce the effect of physical and chemical influences from the drilling mud and formation on the gamma ray logs reading.

The neutron log (Øn) responds to the total volume of water present in the sediments, including those bound in clays and therefore represents the total porosity in clean sands. The neutron porosity is derived from the hydrogen index (HI) of the compensated neutron log which does not require much corrections to be made on the raw data. HI is directly related to the amount of water in the pore spaces and bound in clays.

Vf and Øn are used here to represent the rock composition, namely the matrix, porosity and fluid contents. The thermal conductivity is expressed as:

$$K = (A^{Vf})(B^{\text{Øn}})(C) \qquad (2.5)$$

where A, B, and C are constants. The above equation is based upon a power function between thermal conductivity with neutron porosity and volume of fines and is solved by regression analysis.

2.2.3 Modelling of thermal conductivity values of clastics rocks

The empirical relationship between log interpreted data and measured thermal conductivity is established using multiple regression analysis. Regression analysis is a mean of choosing the best relation of a dependent variable with independent variables. In this case, the log interpreted data are the independent variables and the thermal conductivities are taken as dependent variables. This gives a means of prediction of the thermal conductivity values based on the given values of the log interpreted data. The multiple regression analysis generates the value of the outcome variables (i.e. thermal conductivity) which depends jointly upon the values of the predictor variables (Aiken and West, 1991), i.e. log interpreted data i.e. $\emptyset n$ and Vf. The solutions can be in the form of either linear or exponential equations. In the case of thermal conductivity it is found that the exponential relationship between the thermal conductivity to the logs' parameters gives better degree of accuracy.

The two hundred and three samples were used in analysis to calibrate the relationship of thermal conductivity to logs using equation 2.5. The well location from which the cores were taken is shown in Figure 2.6. The corresponding logs' data are read from the paper print records. The gamma rays and neutron porosity are from compensated neutron logs which has little environmental effect. Data with severe borehole damage is only considered after borehole correction been made (Schlumberger, 1988).

38
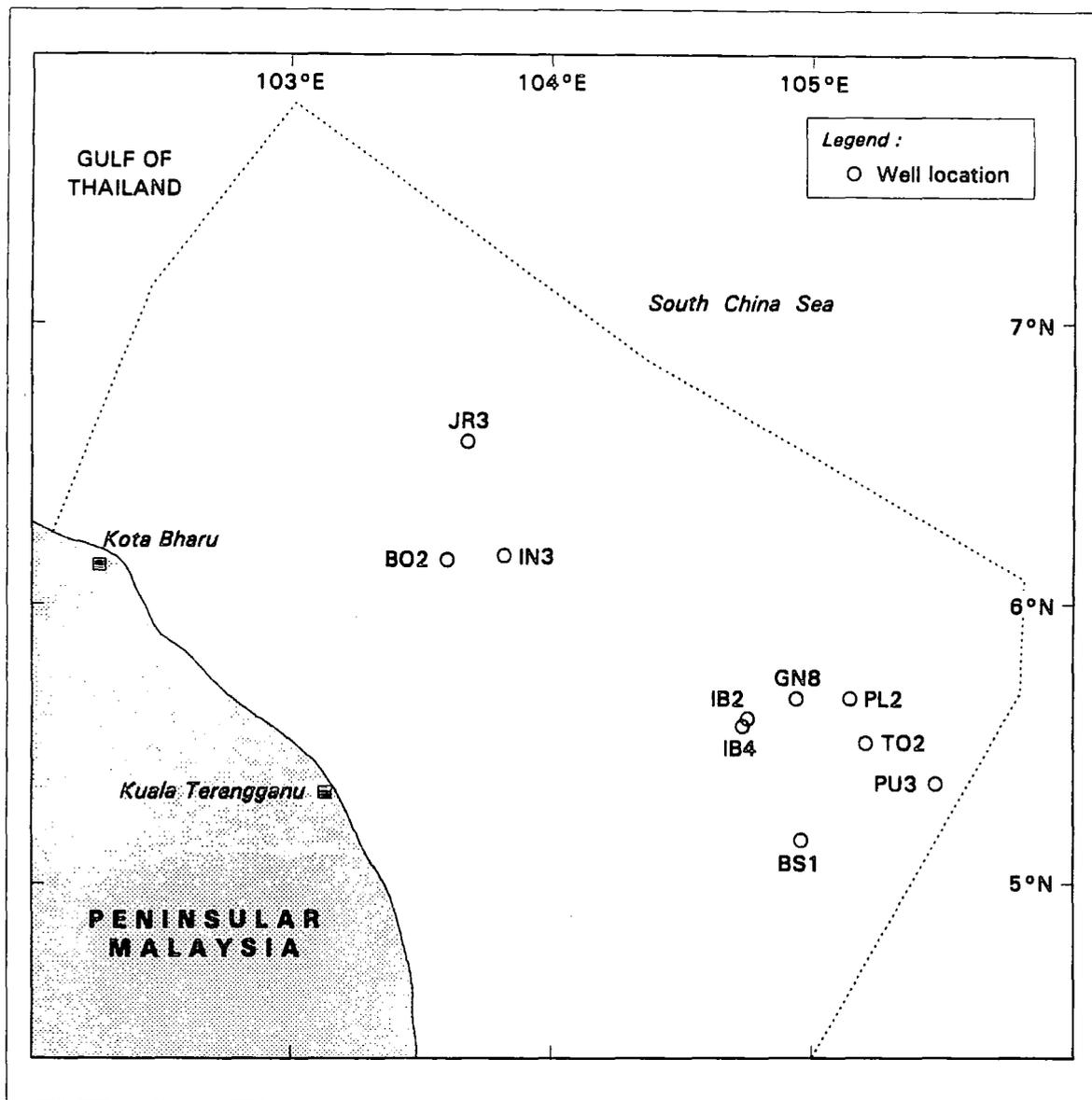
Figure 2.6 : Distribution of wells with measured thermal conductivity data used in current study

The sensitivity of Øn to the sediment's thermal conductivity is compared to the effectiveness of using density and sonic porosities in the empirical equation 2.5. Twenty nine sandstone and thirty mudstone (silty shales, shales and claystones) samples were analysed to compare the thermal conductivity derived by using each of the three different type of log porosities with the Vf (i.e. neutron. sonic and density porosities). The analysis will test the effectiveness of each log porosity, compared to that of Øn. Table 2.2 shows the result of statistical analysis after the predictions of the different rocks' thermal conductivity using the log porosities.

The sonic and neutron porositites are more compatible to each other in the prediction of thermal conductivity while density porosity differs. In general neutron log is the most effective porosity to be used with an average standard error of 5 to 8 %, correlation coefficients of 0.80 to 0.90. The sonic log porosity and density porosity has an average standard error of 8 to 10 % and 10 to 15 % respectively with a correlation coefficient of 0.71 to 0.75 and 0.16 to 0.67 respectively. The good coefficients among the neutron and sonic porosities may be due to the compatibility of lithology and fluid content of rocks with neutron and sonic porosity logs (Figure 2.7). For instance, both neutron and sonic porosity are sensitive to the clay bound water and may give high porosity for these shales whereas the density log is not se-nsitive enough to clay bound water (Etnyre,1989). Both the neutron and sonic porosities respond in a similar way to changes in lithology and thus to thermal conductivity.

Therefore sonic porosity may be used in sections where neutron logs are absent as e.g. in the top sections of a well column. The sonic porosity used in the calibration is determined from Wyllie's time average equation. This model works well in compacted sandstone at depths over 1524 m (Etnyre, 1989). In sediment of shallower depth and in shaly sandstones , the equation has to be divided by a dimensionless correction term known as "lack of compaction" factor, Cp. The Cp can be estimated by dividing 100 with sonic travel time of a nearby shale. The use of sonic porosity is difficult due to unknown sonic transit time of matrix tma, and fluid

Lithology	Sandstone	Øn	Ørb cor	Ørb	Øtt	Øtt cor
Vf(%)						
Maximum	19					
Minimum	2					
Number of Sample	29					
Correlation coefficient		0.80	0.67	0.59	0.71	0.71
Standard error						
Maximum		15.49	29.14	34.18	17.51	18.09
Average		0.18	0.74	0.03	1.09	0.30
Minimum		8.38	10.13	10.96	9.86	9.72
Thermal Conductivity (W/m°k)						
Maximum		6.24	5.86	5.54	5.93	6.15
Minumum		3.03	3.03	2.91	2.88	3.04
Porosity values(%)						
Maximum		28	27	30	35	28
Minimum		4	4	5	7	4

Lithology	Mudstone	Øn	Ørb cor	Ørb	Øtt	Øtt cor
Vf(%)						
Maximum	79					
Minimum	40					
Number of sample	30					
Correlation coefficient		0.90	0.42	0.16	0.76	0.75
Standard error						
Maximum		14.50	32.66	52.07	22.95	23.78
Average		0.44	0.05	0.37	0.47	0.98
Minimum		5.44	12.50	15.28	8.19	8.61
Thermal Conductivity (W/m°k)						
Maximum		3.78	3.46	3.27	3.72	3.81
Minumum		1.89	2.01	2.17	1.94	1.95
Porosity values(%)						
Maximum		45	34	35	64	39
Minimum		27	16	11	21	18

Table 2.2 . The comparison among neutron porosity (Øn), sonic porosity (Øtt)
and density porosity (Ørb) used in predicting thermal conductivity. Øtt c
and Ørb cor are the sonic and density porosity corrected for the clay ef
The sandstone and mudstone samples have been selected
with the specified volume of fines (Vf) ranges shown.
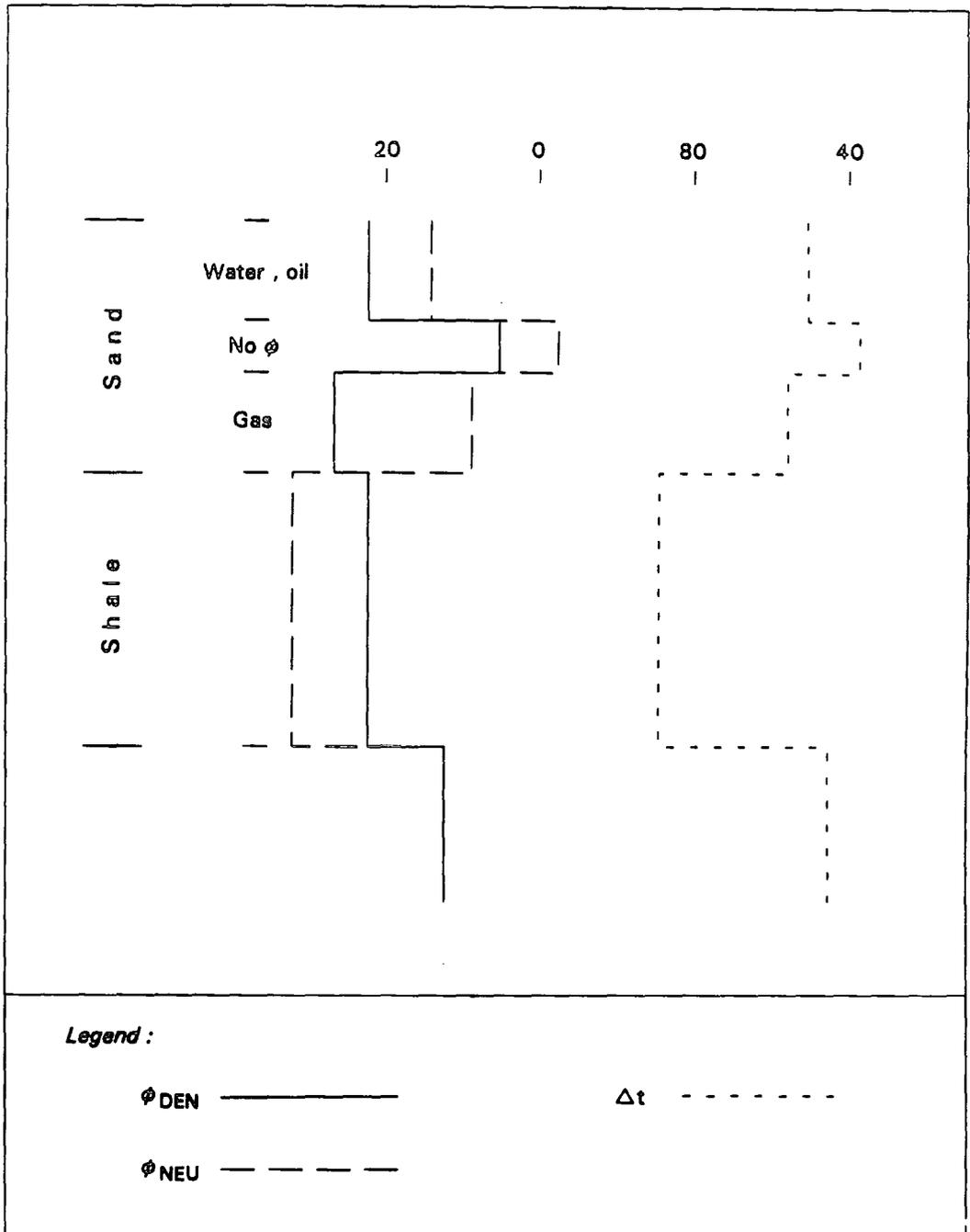
Figure 2.7 : Effect of lithology and fluid contents of clastic rock to neutron, density and sonic logs (Modified after Etyre, 1989).

tsf, and the weakness in estimating Cp. The matrix sonic transit time can range from 5,905 to more than 6,397. m/sec.and for the fluid sonic transit time it is about 1,620 m/sec. Another method used in the determination of sonic porosity is by transforming sonic transit time empirically by the Raymer-Hunt-Gardner method (Raymer et al., 1980). This transformation is used only when there is availability of corresponding bulk density values. This transformationhas an advantage over the Time-average equation method for there is no need to do any estimation of tma and tsf or correction factor, Cp.

The problem in using neutron porosities arises when the sands are filled with gas. In this case both the neutron and sonic porosities give a slightly lower values of porosity compared to those in the fluid-filled sections (Figure 2.7). Since the calibration of the thermal conductivity to log parameters is carried out using the water filled sample , the equation for gas filled sample are not available. Gas sands are mostly associated with either water or oil zones, therefore their porosities can be substantially approximated by those of the adjacent zones.

2.2.4   Thermal facies

In the correlation of measured thermal conductivity to log parameters, there are constraints in selecting the samples with measured thermal conductivity data and the respective parameters in order to get an acceptable degree of confidence in the correlation. By dividing the samples into suitable number of subsets, correlation by regression analysis can become simpler. In the first stage the samples were divided into sandy and shaly subsets. The neutron porosity seems to be the dividing element between the sandy and shaly facies with the former having lower porosities. In the next stage further subdivisions of sand facies were made possible based on their relative grains sizes which are equivalent to ranges in Vf values. Finally it is apparent that the whole samples may be grouped into several facies. The facies can be

defined based on the values of Vf ranges and On ranges. Therefore each facies is then represented by a set of samples having a range of Vsh and On values. An empirical equation is then established defining the thermal conductivity prediction for a pair of known Vf and On. The average standard error is to 5 to 8 % and the correlation coefficient is about 0.80. The facies is termed a thermal facies (kf). The thermal facies can be classified into 7 types each representing a specific lithology. The cleaner sandstone is represented by thermal facies 1 (kf1) and the silty sandstones is kf2. Thermal facies 3 (kf3) and 4 (kf4) is mostly mudstone and silty mudstone while thermal facies 5 (kf5) is the argillaceous sandstones. The clays and silty clays are represented by thermal facies 6 and 7 (kf6 and kf7). The list of samples of each facies with their respective log data and measured thermal conductivity data are listed in Appendix 2.1.

The regression analysis on the measured thermal conductivity values with their equivalent log properties gives the empirical formula for determination of the thermal conductivity of each facies. In initial analysis, a population of samples having specific ranges of Vf with On as the fully independent variable were regressed and the coefficients of each variable were determined and used in the determination of the empirical thermal conductivity. The samples which contribute to maximum error were discarded. Next , the exercise was repeated until an acceptable minimum error is reached with a maximum number of samples being used in the regression analysis. Eventually the regression analysis was carried out over several specific ranges of Vf and On corresponding to the various thermal facies, each of which is overlapping with the other adjacent samples in order to preserve continuity for all thermal facies.

The analysis is in principle somewhat similar to a step-wise regression analysis described by Krumbein & Graybill (1965) whereby a variable is constrained by a constant value and allowing other variables to control the prediction of the independent variables in the regression analysis with step-wise deletion of the weak variables. However in my study, the

variables are grouped into facies and were allowed to define the equation for the determination of the empirical thermal conductivity representing the facies with minimum standard error and with maximum samples being represented. The standard error is presented by absolute percentage calculated from the formula $100(k_{emp} - k_{mes})/k_{mes}$, where k_{emp} is the predicted thermal conductivity and k_{mes} is the measured thermal conductivity. This analysis returned the optimum number of thermal facies (i.e k_{f1}, k_{f2}, k_{f3}, k_{f4}, k_{f5}, k_{f6} and k_{f7}) with ranges of V_f from 0% to over 85% and O_n of 0% to over 45%. Seven empirical formulas have been established representing each of the 7 thermal facies with the standard error between the predicted and measured thermal conductivity equal to about 8%. The thermal conductivities predicted by logs using the empirical equation above are plotted against the measured values. The comparison between the predicted and the measured thermal conductivity are shown in Figure 2.8.

A thermal facies (kf) then has a unique representation by an empirical equation for predicting thermal conductivity as well as representing definitive lithofacies. The thermal conductivity can then be determined exclusively from log where V_f and O_n are available. Figure 2.9 shows the three dimensional relationship among the V_f, O_n and the predicted thermal conductivity from the log interpreted data. For each facies the limit of the ranges of V_f and O_n can be approximated by those in Table 2.3.

2.2.5   Thermal conductivity model of each thermal facies

Model of thermal conductivity determined from logs is as shown by the diagram of Figure 2.9. In the thermal facies 1, k_{f1} the model shows that high thermal conductivity of nearly 7.00 W/m°C corresponds to log values of 0% O_n and V_f. Figure 2.10 (model A) exclusively demonstrate the variation of the k_{f1} thermal conductivity where the increases in both V_f and O_n increase the thermal conductivity. In this clean sandstone facies (k_{f1}), there is
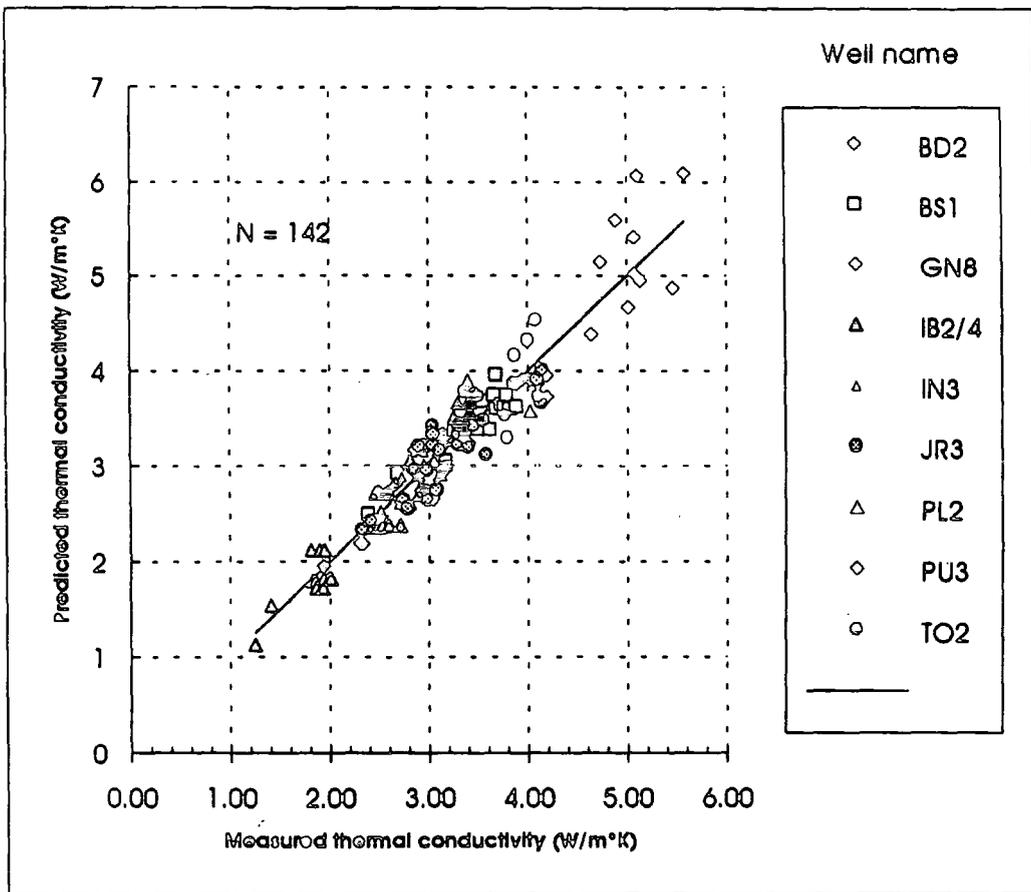
Figure 2. 8 Comparison of measured and predicted thermal conductivity

Table 2.3

The empirical equations relating thermal conductivity and logs parameters. Each thermal facies, kf is defined by the limiting values of logs and having a unique empirical equation relating log parameters to the thermal conductivity.

kf	Limit of Log Parameters	Empirical Equation
kf1	Vf < 20%, Øn < 36%	$k_{emp} = 6.86\ (0.99)^{Vf}(0.98)^{\varnothing n}$
kf2	Vf = or > 20% and < 40%, Øn < 35%	$k_{emp} = 6.43\ (0.99)^{Vf}(0.98)^{\varnothing n}$
kf3	Vf ≥ 40% and < 60%, Øn> 18% < 35%	$k_{emp} = 10.59\ (1.00)^{Vf}(0.96)^{\varnothing n}$
kf4	Vf ≥ 60%< 85%, Øn>18% < 39%	$k_{emp} = 5.83\ (0.99)^{Vf}(1.00)^{\varnothing n}$
kf5	Vf >13%< 30% Øn = or > 33%<60%	$k_{emp} = 13.14\ (1.09)^{Vf}(0.91)^{\varnothing n}$
kf6	Vf ≥ 30% and < 40%, Øn ≥ 35%<49%	$k_{emp} = 12.95(1.03)^{Vf}(0.98)^{\varnothing n}$
kf7	Vf = or ≥ 40%<85%, Øn = or ≥ 35%<61%	$k_{emp} = 15.24\ (1.01)^{Vf}(0.94)^{\varnothing n}$
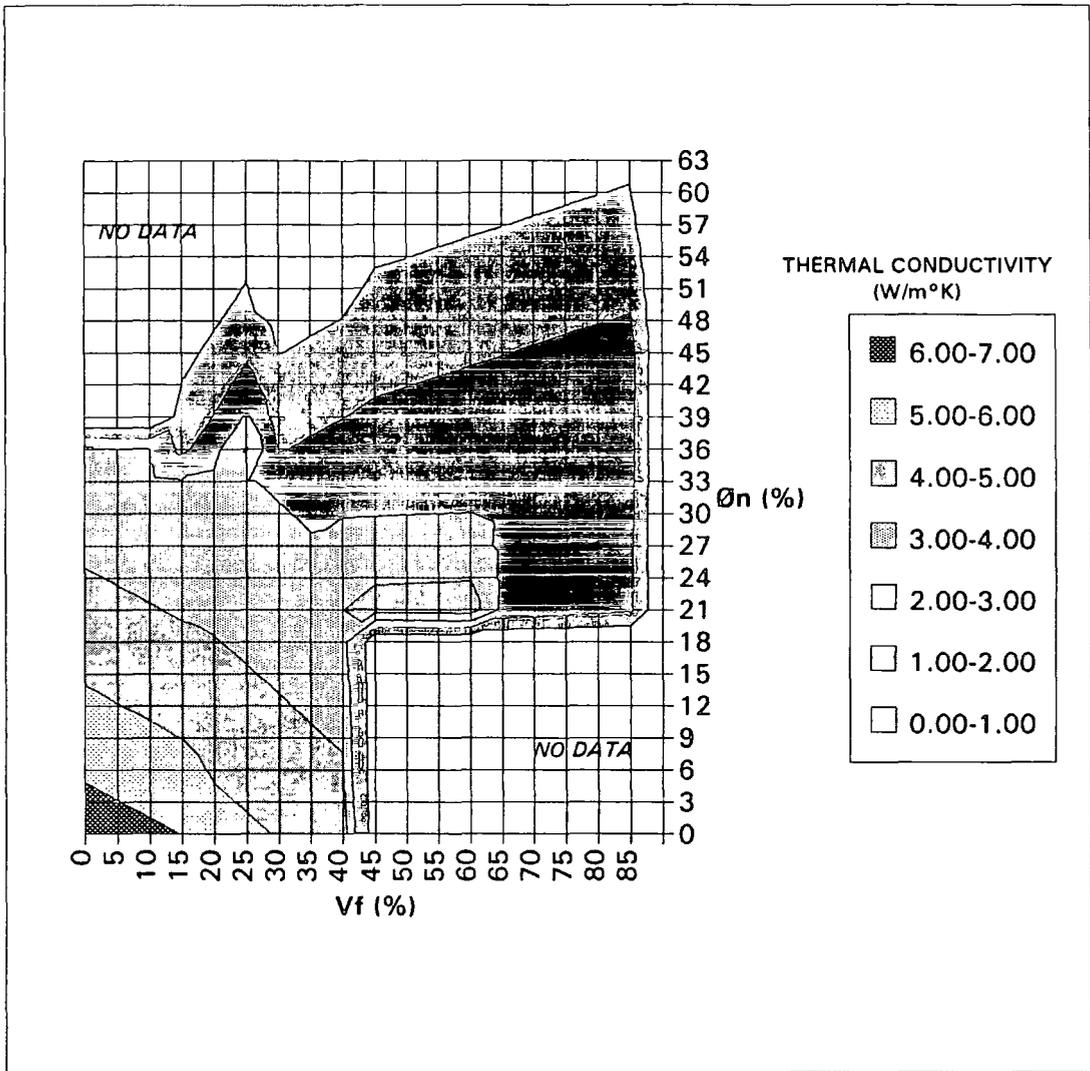
Figure 2.9   The adopted monograph of empirical thermal conductivity
             determined for the whole thermal facies (kf1 -kf7).

an equal weight of influence of porosity and volume of fines to the predicted thermal conductivity. Figure 2.10 (model B) shows the trend between thermal conductivity with Vf and On of kf2 which is slightly curved compared to that of kf1. The kf2 is sandstone facies with more clay content than kf1. However in kf3 (Figure 2.11 (model C)), which comprises mostly siltstone and mudstones with some finer grained sands, the porosity has played a greater influence than that of Vf. This may indicate that this facies is less compacted so that the effect on porosity or water content reduction will increase the thermal conductivity remarkably. But in kf4, which consists of mostly mudstone and silty mudstone, there is a decrease in the influence of porosity to thermal conductivity. The kf4 (Figure 2.11 (model D)) consists of near fully compacted clastics. There is little change in thermal conductivity with further increase in porosity. In other words the thermal conductivity increases with increase in Vf but is insensitive to changes in neutron porosity. In kf5 (Figure 2.12, model E), which consists of porous argillaceous sandstone, the thermal conductivity increases with increases in volume of fine for certain ranges of Vf and is in harmony in part with the theoretical observation of the effective medium theory of Figure 2.4. In kf6 and kf7, where both are mostly consist of claystones, the trend of thermal conductivity to Vf tends to be opposite to those of kf1 and kf2 (Figure 2.13, model F and G). The kf6 has relatively higher thermal conductivity compared to those of kf5, because of the predominance of silty clays in the kf6. The increase in the thermal conductivity with increasing clay content indicates that in the absence of larger grains the only means of heat transfer would be by the finer grain matrices. The above representation shows that there is no single empirical or theoretical formula which can satisfy all clastics in the determination of thermal conductivity.

2.3   Insitu thermal conductivity of rocks

The thermal conductivity of the subsurface can be estimated from the model based on log readings of wells drilled on an area. Detailed study of thermal conductivity-depth profiles
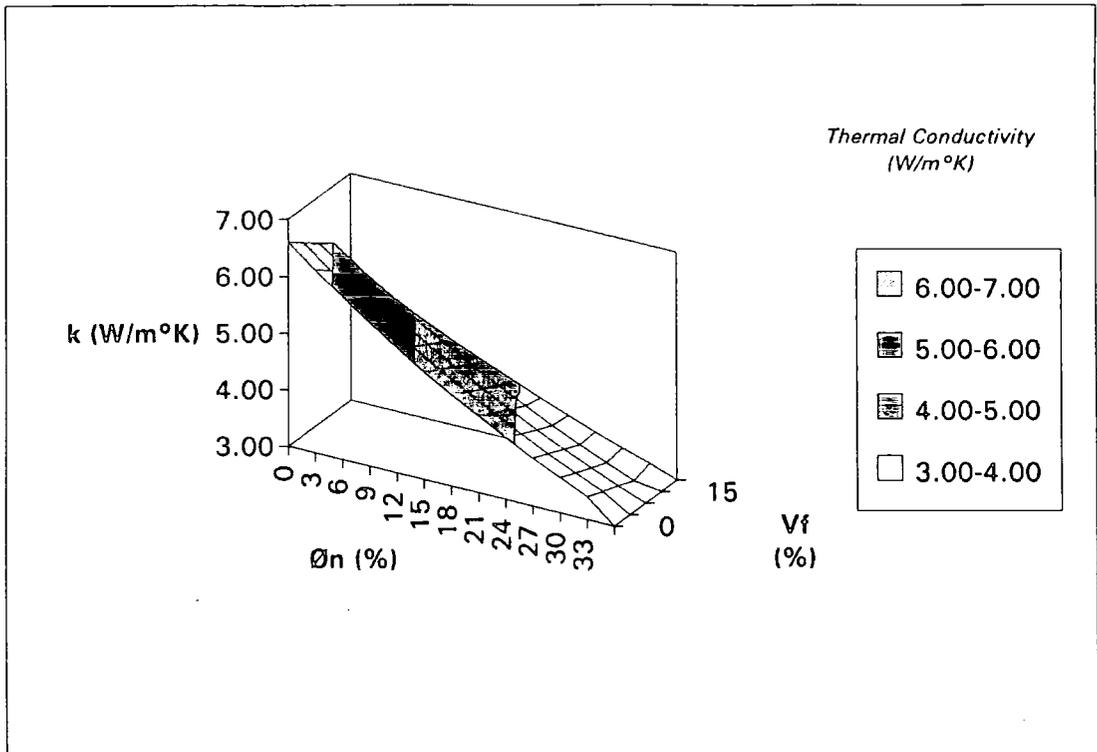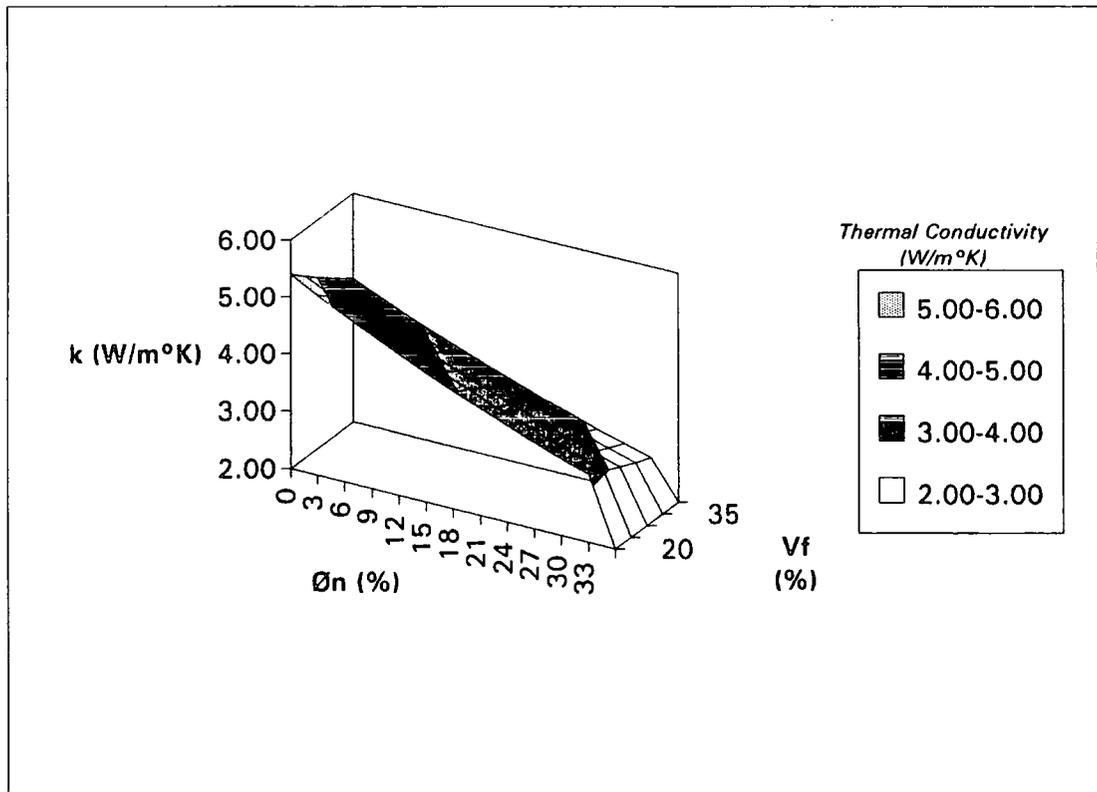
Figure 2.10   The 3D representation of thermal conductivity (k), volume of fines (Vf) and neutron porosity (Øn). Both models are for the sandstone facies. Model (A) is for thermal facies, kf1 and model (B) is for kf2.
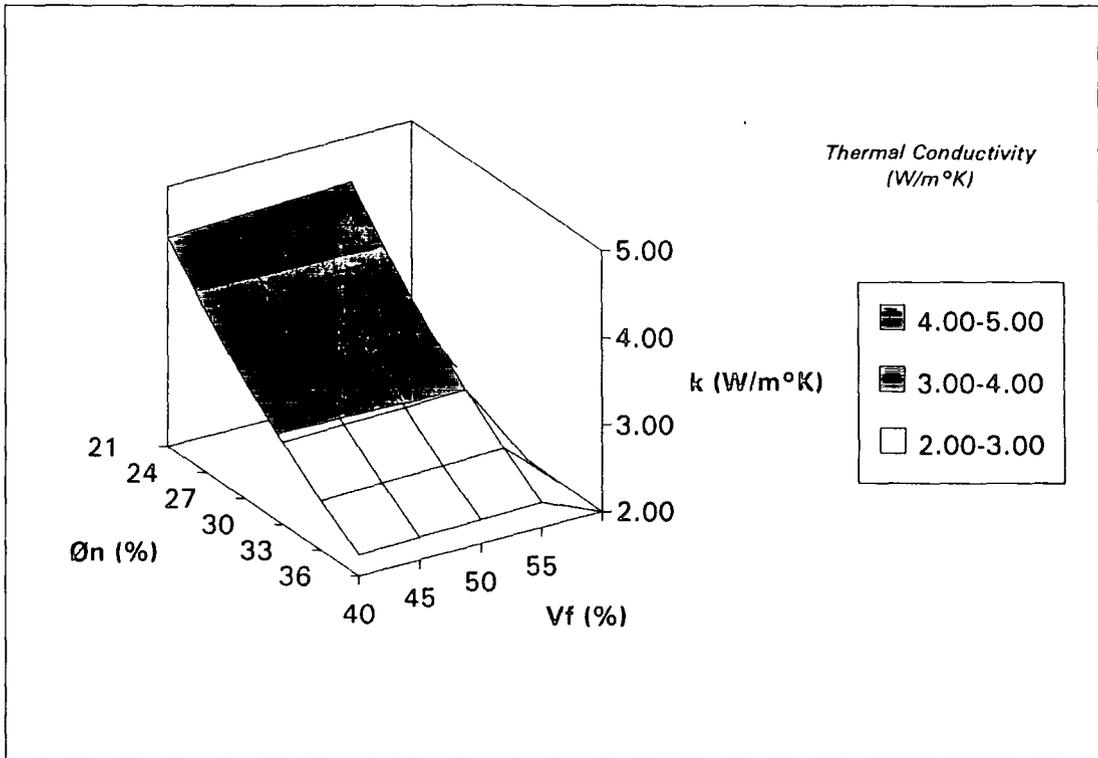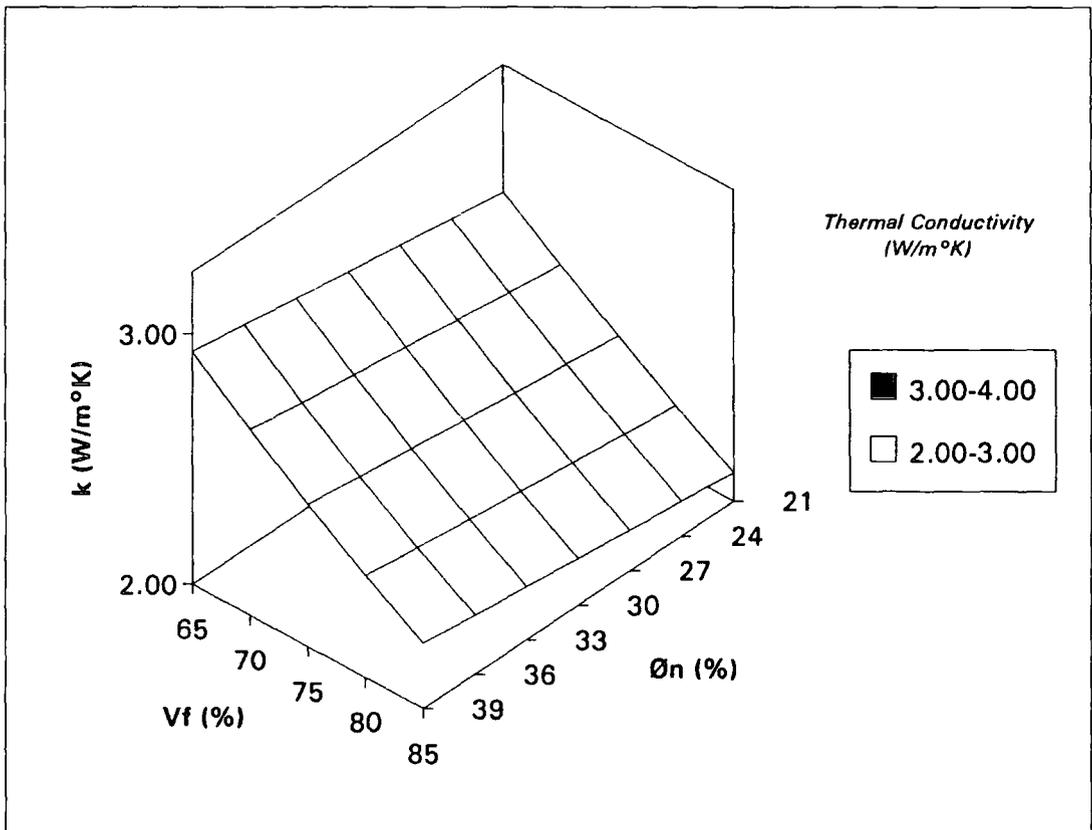
Figure 2.11   3D thermal conductivity model for siltstone/mudstone facies.
Model C is for thermal facies, kf3 and model D is for kf4.
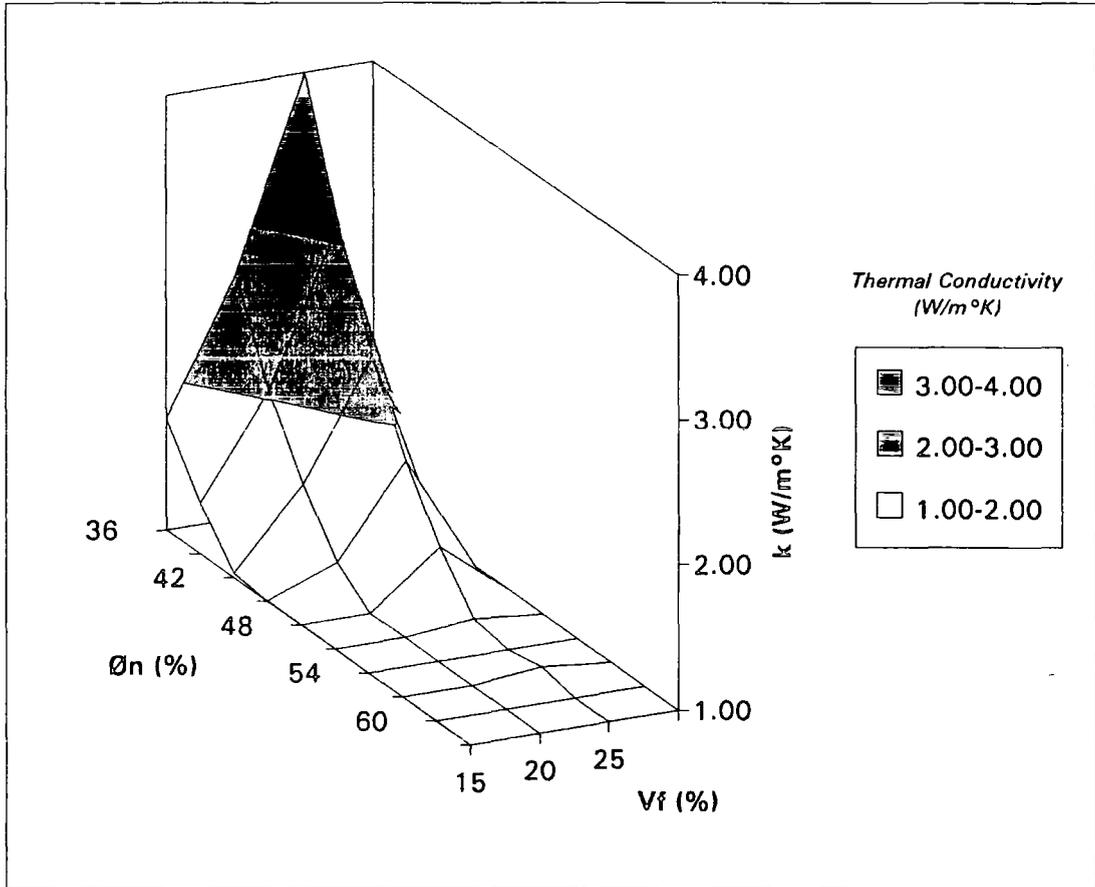
Figure 2.12.   Thermal conductivity 3D model for argillaceous sandstone facies.
              The thermal facies is kf5.
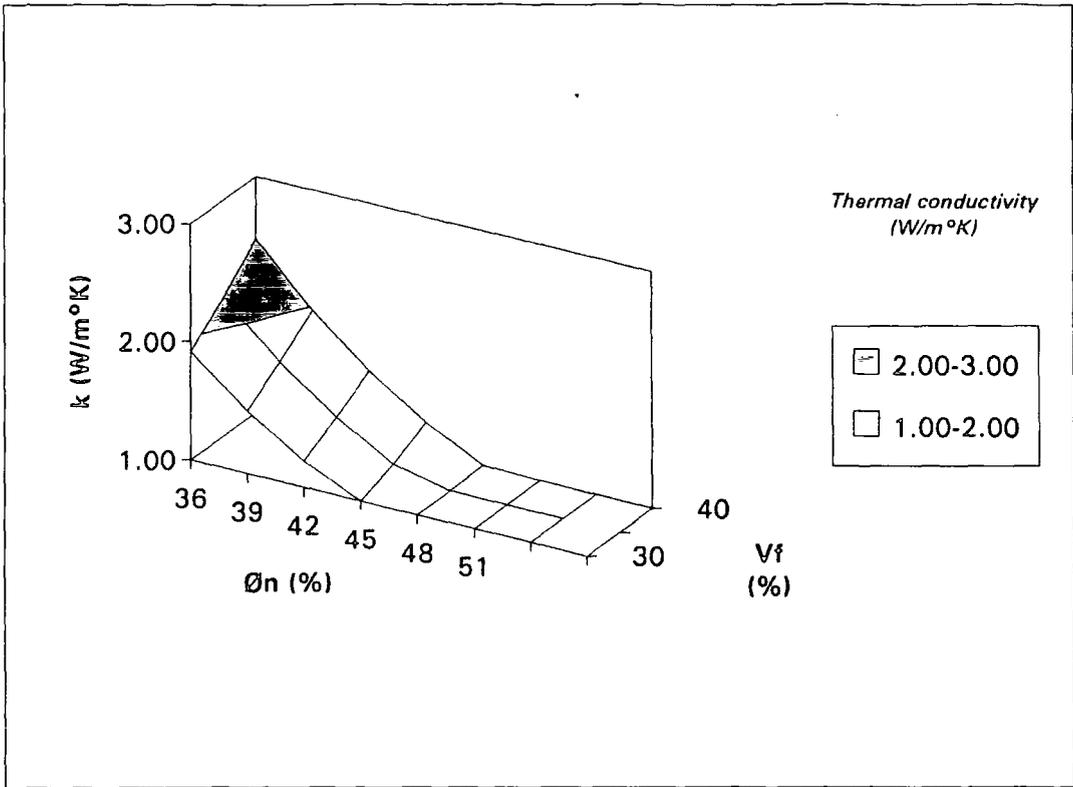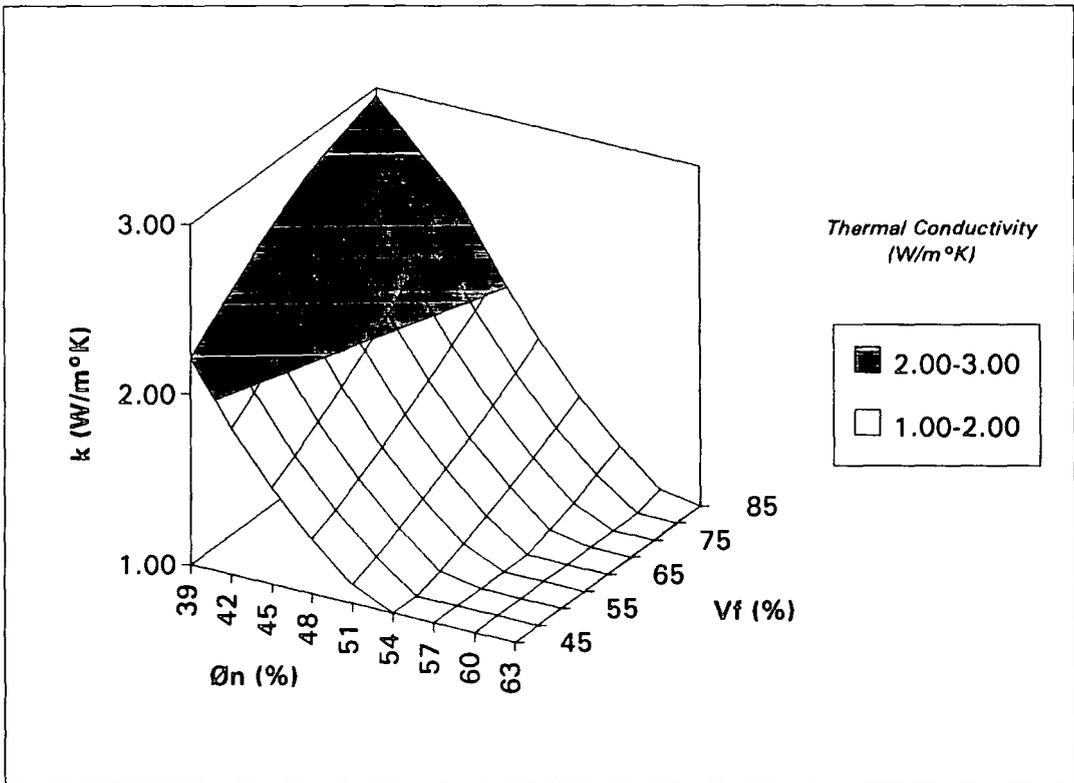
Figure 2.13.   The thermal conductivity 3 D model for claystone facies.
The model F is for thermal facies kf6 and model G is for kf7.

is important for the construction of other thermal parameters. By having the detailed vertical profile the amount of heat flow variation within the basin can be studied. In this section, log data from a well is analysed for predicting the thermal conductivity-depth profile.

The electric logs were firstly interpreted for the Vf and Øn or normalised Øsonic in discrete depth intervals. Readings from the gamma ray and neutron index and/or sonic transit time logs from each log interval were compiled for interpretation of the properties of the sediments. The depth interval is specified based on regular trend of the logs patterns to depth. The data are spaced at about equal intervals along the well. This discrete depth interval would represent as accurately as possible the average response of logs to the rocks in the interval and is kept to within less than 3m. The maximum and minimum of the log curves are taken to represent the values of the log reading for the specified rock. The slope of the curves are taken to represent the intermediate rock unit. The log reading at the middle of the slope would represent the log value for the interval (Figure 2.14). An approach proposed by Griffiths, (1982) bears the similar concept in segmentation and reassignment for petrophysical borehole logs.

The log readings for gamma ray, raw neutron data, sonic transit time are analysed for each depth interval. Then each interval is assigned its thermal facies following the model described in section 2.2.5. Then the empirical thermal conductivity of a discrete depth interval is determined accordingly to its thermal facies. Appendix 2.2 shows an example of a log data compilation and thermal properties of a well.

2.3.1   Temperature correction to thermal conductivity

The measured and predicted thermal conductivity from logs are the values determined at surface temperature and pressure. Thermal conductivity at depth is affected by the
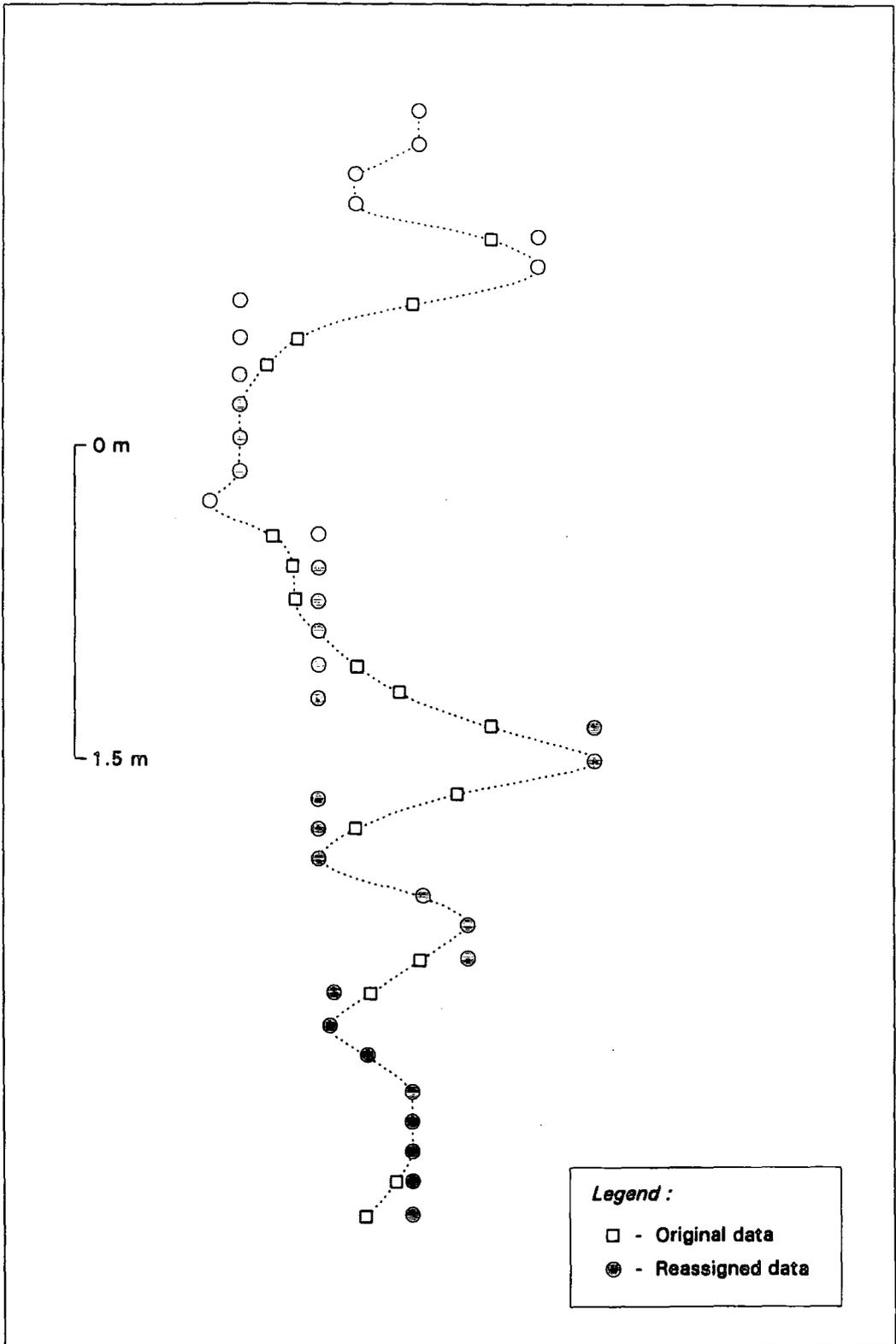
Figure 2.14 :   Example of detailed segmentation of log data
(After Griffiths, 1982)

55

physical conditions of the well. The corrected thermal conductivity is the approximation of the true thermal conductivity of the formation at the depth of the middle of the discrete depth interval and at the estimated formation temperature.

The thermal conductivity of rocks has been known to increase with temperature (Birch and Clark, 1940). The values estimated from the procedures in the sections 2.2 are only fairly good for the rock at the surface because the measurements and calibrations have been done at the surface condition. The insitu thermal conductivity of rocks should be approximated by taking the properties of the subsurface which may affect the thermal conductivity.

Sekiguchi (1984) has made several conclusions on the effect of pressure and temperature on the thermal conductivity. The effect of temperature is taken into consideration while the effect of pressure is not significant as Sekiguchi (1984) observed that the change in thermal conductivity per 100Mpa is about 1% or less for harder rocks or minerals. This variation with pressure does not seem to be so large for the heat flow calculation. The change for softer rocks such as claystone is 10% and more. This presumably resulted from the reduction of the pore space during the measurements. The effect of pressure for the softer rocks seems to have been accounted for into the thermal conductivity predictions whenever measured thermal conductivity has been calibrated to porosity. On the other hand, it has been observed that thermal conductivity of sandstone decreases by 50% with increase in temperature from 20°C to 200°C. For shale and clays and water the thermal conductivity changes very little with the temperature. The changes in some rocks with increase of temperature is shown in Figure 2.15.

By adopting the procedure suggested by Sekiguchi (1984) , the temperature corrected in situ thermal conductivity can be given by :
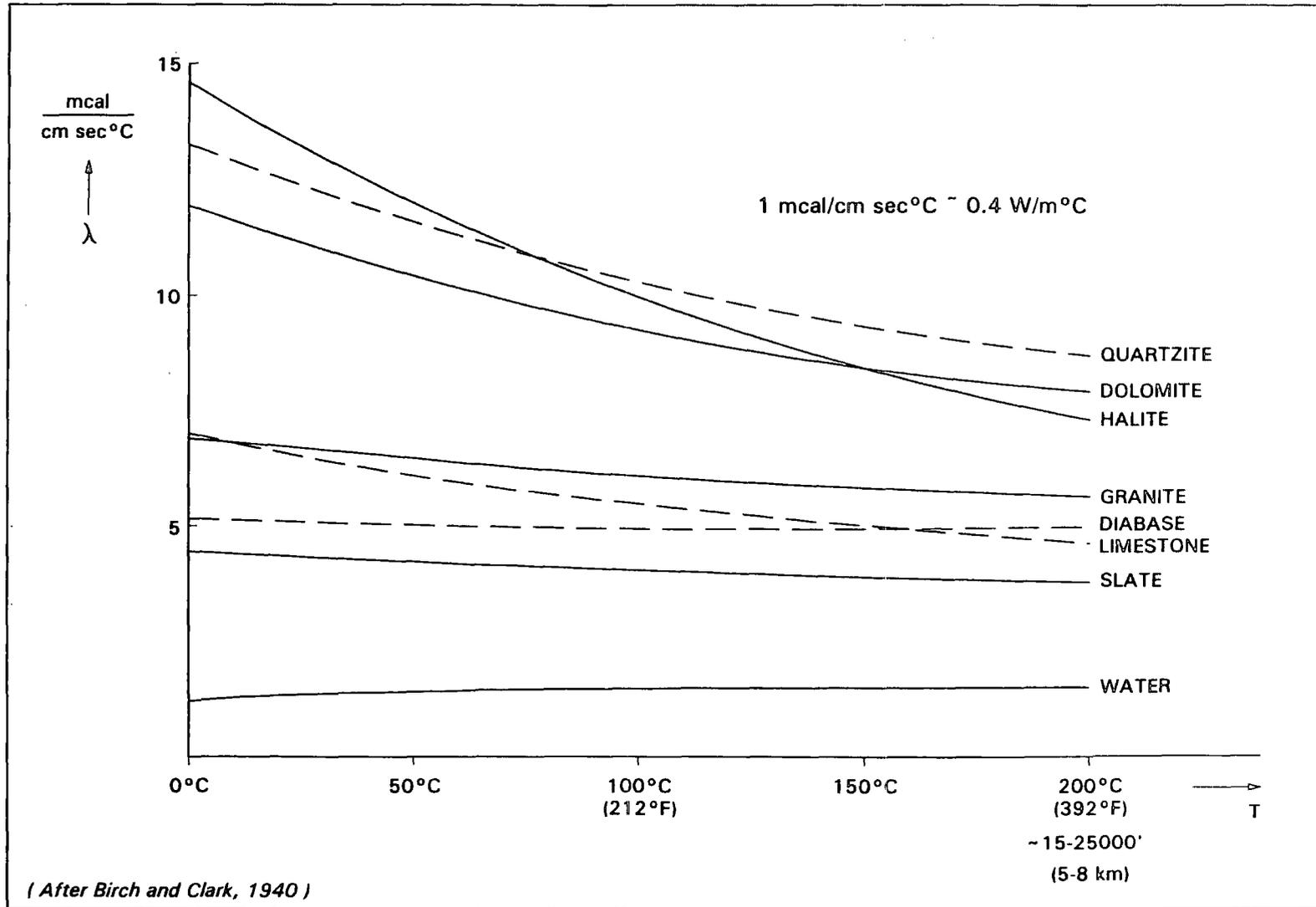
Figure 2.15 : The decrease in thermal conductivity of hard rocks with temperature

57

WIS12-Jan

$$(372 * (k - 1.84)(1/(Tf + 273) - 0.00068)) + 1.84 \qquad (2.6)$$

where k is the thermal conductivity at surface temperature in units of W/m°K and Tf is the

formation temperature in °C. It appears that only sandstone of thermal conductivity higher

than 1.84 W/m°K require correction. For a discrete depth interval, a temperature correction

for the thermal conductivity can be carried out if an estimated formation temperature is

known. The estimated formation temperature can be calculated from the average geothermal

gradient of the location.

2.3.2 The effective thermal conductivity of a rock column

In the determination of a vertical thermal profile of a well site and using the surface

heat flow value, the thermal conductivity of the subsurface rocks is also required. Since the

thermal conductivity varies through out the rock interval, an average thermal conductivity is

useful when an average heat flow over an interval of rocks with different thermal conductivites

is required. The average thermal conductivity of a vertical well has been determined here by

averaging the contributions of the effective thermal conductivity of every rock units that

formed the column of rocks by an harmonic average equation (Vacquier, 1984; Correia, et al.,

1990).

$$K = (d_1 + d_2 + ...d_n) / (d_1 /k_1 + d_2 /k_2 +... \ d_n /k_n) \qquad (2.7)$$

where K is the effective thermal conductivity, $d_1....d_n$ is the thickness of each interval and

$k_1.....k_n$ is the thermal conductivity of rock in each interval. k is computed from thermal facies

equation for each discrete intervals. The thermal conductivity of coal beds, is taken as the

value of an average thermal conductivity of coals (1.45 W/m°K), in the Malay Basin (Wan

Ismail, 1984). The top section of the well is mostly clayey and hence represents the lower

thermal conductivity portion. The details of the thermal conductivity trends with depth are simply a function of lithology and change in porosity of the rocks and are clearly displayed in a well as shown in figure 2.3 earlier.

2.3.3 The average thermal conductivity of the Malay Basin

In the determination of the average thermal conductivity of the Malay Basin wells by the previous method (Wan Ismail, 1984), i. e. the litho-stratigraphic method, LS, wells from 42 fields were analysed. In general, the data distribution over the basin is sufficient to establish contours of thermal conductivity over the area. But in some wells the average conductivity was anomalously high or low. Plot of temperature gradient versus heat flow of the data taken from Wan Ismail (1984) suggested that a possible over or under estimation of some thermal conductivities for certain wells have been incurred in the last study (Figure 2.16). For example, the thermal conductivity for OP-1 was estimated to be 2.25 W/m°K and is considered too high and in SM2 and TJ1 the thermal conductivites are 1.59 and 1.55 W/m°K respectively and is very low. These varied thermal conductivities of wells may be partly due to the bias representation of the sample in the average of the thermal conductivity of each stratigraphic units of the wells which reflects the weakness of the LS method.

In my current study, the thermal conductivities of the wells estimated by the log calibrated thermal conductivity-thermal facies method, LK, shows an improvement. Figure 2.17 is the cross-plot of geothermal gradient and heat flow of the wells in the current study which shows that there is less dispersion in the data compared to those of the previous study in Figure 2.16. The comparison between the old and revised method can be seen as well by looking at the statistics for both methods. The standard deviation has been reduced from 0.16 to 0.10 W/m°k and the differences in the maximum and minimum values are smaller in the new
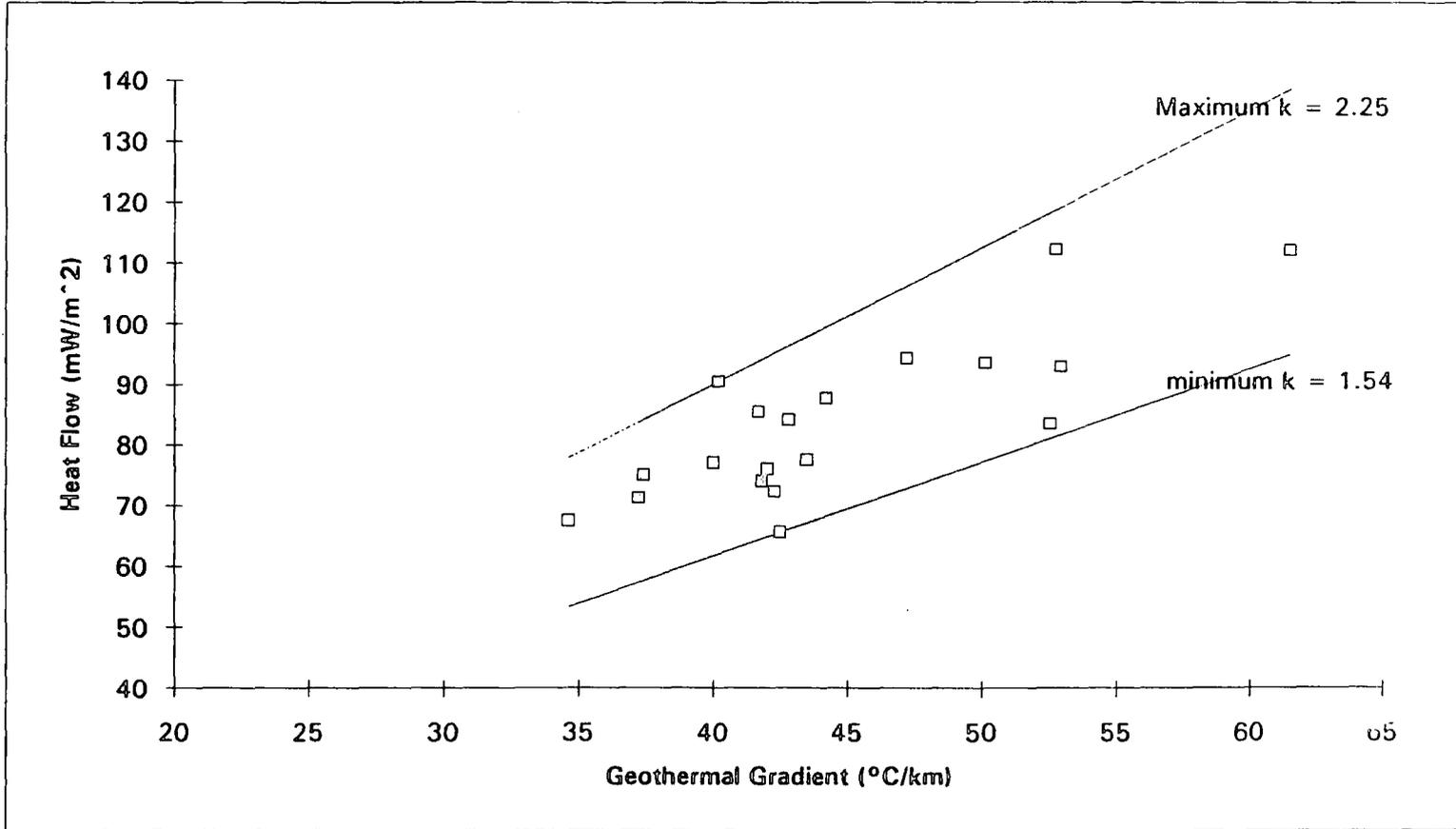
Figure 2.16. Cross-plot of heat flow versus geothermal gradient of previous data (Wan Ismail, 1984). k is thermal conductivity in W/m°K)
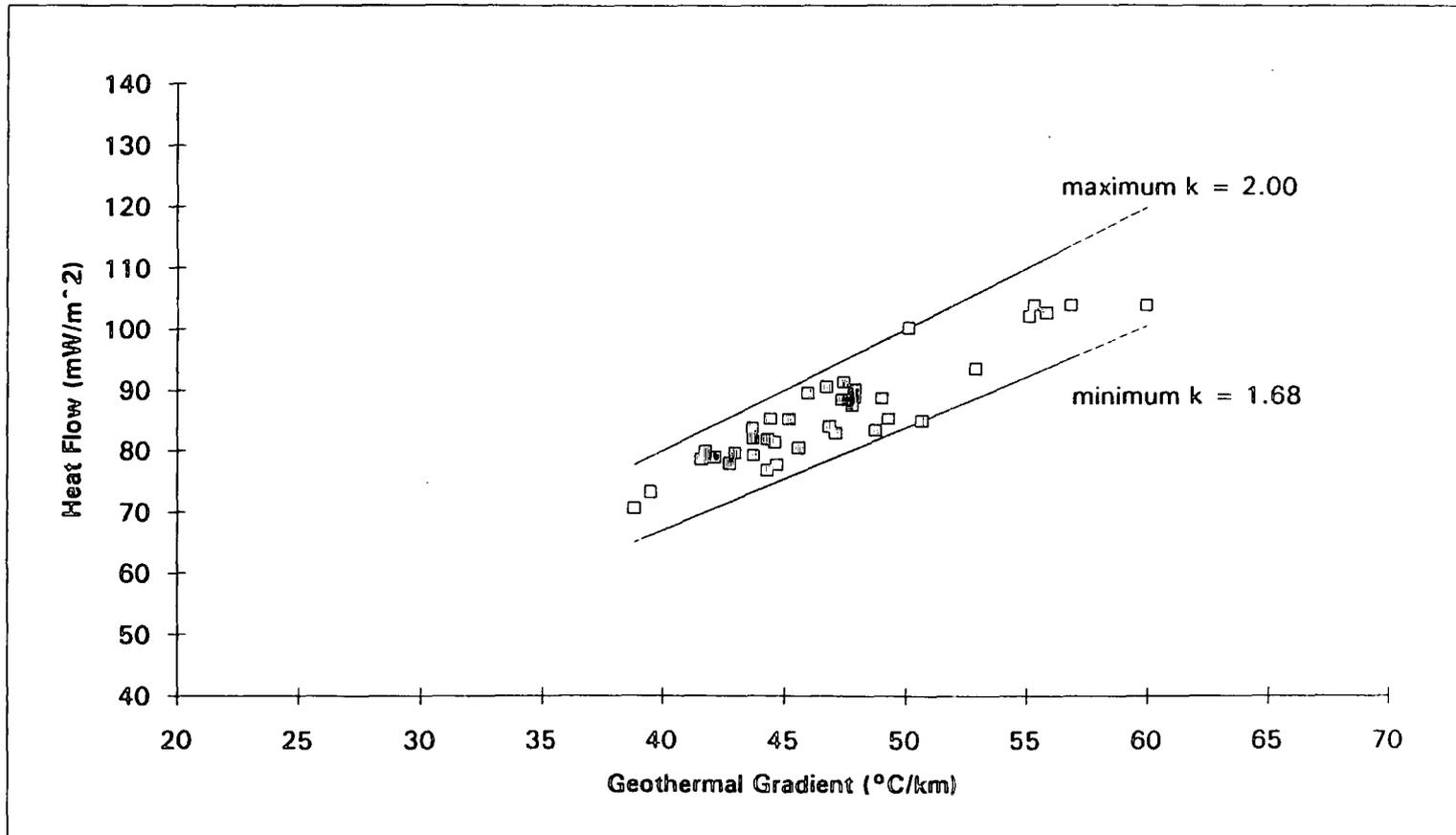
Figure 2.17. Cross-plot of heat flow versus geothermal gradient of present data . k is thermal conductivity in W/m°K

model. Hence some of the extreme high and low thermal conductivities in wells from the previous study can be just bogus values.

Average thermal conductivity of 48 wells are estimated by LK to revise the thermal conductivity contours of the Malay Basin. Thirty of the wells are the old wells which already have the old thermal conductivity data set but have been recalculated by the new method. The rest of the data are of new exploration wells. Comparing the thermal conductivity derived by the two methods for the similar wells, the average calibrated log derived thermal conductivity (LK) value is found to be 9% less than the average of the equivalent wells thermal conductivity from the previous method (LS). The difference of the estimated thermal conductivity between the log calibrated and litho-stratigraphic method values of some wells, with similar stratigraphic sequences is considered small (i. e 9 %).

In constructing the revised thermal conductivity contour of the basin, it is necessary to use some of the well data which were used previously. These are older wells with older logs and are not analysed by the present method. However the LS thermal conductivity can be normalised to that of LK by calibrating the result of the wells that have both data. Some of the wells in the old data set which have the bogus data are neglected in the calibration so as to maintain better accuracy. Hence the average thermal conductivity used previously are then transformed to the equivalent values expected when LK is used. These revised thermal conductivity data and the new estimate data form the data base for production of a revised thermal conductivity map of the Malay Basin. There are 59 selected wells with the average thermal conductivity data over the basin, of which 48 are with the new LK data and 11 are having the normalised LK data. Appendix 2.3 shows the estimated average thermal conductivity of the wells used in contouring of the average thermal conductivity map of the basin.

2.4 Determination of true formation temperature (Tf)

The true formation temperature estimation is one of the important tasks in a study of the heat flow of a sedimentary basin and there is an abundance of literature which describes methods of estimating the formation temperatures. In the oil industry, the temperature recorded during production tests and electric logging are the sources from which the formation temperatures are determined. In electric logs, the temperatures and the logging depth are recorded on log heading. The production test temperature are normally recorded on well completion log of each well. The production test temperature (Tpt) are the most likely records of the true formation temperatures. The true formation temperature at any depth of a well which also has production test temperature can be determined from the temperature gradient. The temperature gradient, G is calculated from the following equation.

$$G = (Tf - Tsb)/(D - Dsb) \qquad (2.8)$$

where Tsb and Dsb is the sea bed temperature in °C and depth in metres respectively. D is the depth of measured Tf. Tsb is taken as constant (27 °C) for the Malay Basin region as the water depths are shallow and consistent (see below).

Temperature recorded in the production test, Tpt, has been considered as the nearest to the formation temperature. These temperatures were only obtained from the reservoir intervals which are mostly deeper than 500m in the Malay Basin. For the top sequence, the seabed temperature is required to complement the other formation temperatures in order to define the gradient for the whole column. In South East Asia, Savin, et.al (1985), indicated that a representative near sea surface temperature is likely to be about 29°C. There has been some observations made in a temperature probe survey conducted on the Louisiana shelf in the tropics that the temperature in the shallow sea was found to be warmer by about 1°C

compared to the sea bed temperature (Cathles and Nunns ,1991). In the Malay Basin , where there is no extensive survey for sea bed temperature, many workers have assigned a temperature of 26.6°C to the sea bed (SEAPEX-IPA, 1977; Matsubayashi and Uyeda, 1979; Wan Ismail, 1984; Thamrin, 1985). In this study the sea bed temperature, Tsb, is assigned as 27°C.

In a well column the formation temperature can be estimated more accurately if the thermal conductivity of each sedimentary beds are known. The temperature gradient provides the linear average increment of the temperature with depth. Since there are differences in thermal conductivity the temperature will be subjected to different gradients along the well profiles. From the equations (2.1) and (2.8), the formation temperature of wells with production test temperature and thermal conductivity can be defined better by:

$$Q = -K(Tf\text{-}Tsb)/(D\text{-}Dsb)$$

or

$$Tf = Tsb + |\ (\ Q\ /\ K\ )(D\ \text{-}\ Dsb)| \qquad\qquad (2.9)$$

The temperature is based on the assumption that all the heat is sourced from the conductive heat flow, which is not always the case for all locations because other sources of heat within the basin such as the radiogenic heat and convective heat transfer can add to and redistribute the conductive heat from basement. However it can form the first approximation of the formation temperatures.

For wells without production test data, bottom hole temperatures (Tbh) recorded during logging are widely used to approximate the true formation temperatures (Oxburgh and Andrews-Speed, 1981; Sekiguchi, 1984; Correia et al., 1990; Brigaud et. al., 1992). Unfortunately, temperatures recorded in most wells during drilling operations are usually

64

lower than the formation temperature because the shut-in time in the wells is too short to enable the mud in the borehole to reach thermal equilibrium. Proper correction of the Tbh are required to estimate the true formation temperatures.

2.4.1 Statistical calibration of bottom-hole temperature with the production test temperature

In correction of Tbh to the true formation temperature (Tf) several models have been developed to obtain the true formation temperatures. Sekiguchi, (1984) provided a method by which the Tbh has been statistically compared with the Tpt in some oil and gas fields in Japan. In this method the Tbh and Tpt were correlated in several oil and gas fields where many development wells had been drilled. It was shown that from the simple linear relation of Tpt, the formation temperature can be estimated with a precision of about 7%. Although this method has been shown to work well in some oil and gas fields in Japan, it does not work satisfactorily in the Malay Basin. This could be due to the different geological styles of the Malay Basin which do not suit the formula used in other basin. In addition every basin may have different hydrodynamic features which can regulate the subsurface temperatures differently. Other calibration of Tpt for the Malay Basin is necessary to understand the temperature distributions within the basin.

The temperature from logs can be calibrated to the production test temperatures for the wells over the Malay Basin by modelling the vertical temperature profiles of production tested wells. Using the procedures described in section 2.3, thermal conductivity profile of wells which have production test data can be produced. Hence the formation temperature at any other depth can be estimated by the equation 2.9. Therefore the respective formation temperature at depths where the logged Tbh has been obtained can also be estimated. Figure 2.18 shows an example of the relationship between the production test temperature, thermal

conductivity profile and the estimated formation test temperature at a specific depth where Tbh has been logged. BHTc is the corrected Bottom-Hole Temperature, Tf is the estimated formation temperature and Tpt is the production test temperature.

The estimation of formation test temperature which incorporate the above procedure is called " Statistical Corrected Bore Hole Temperature ", or SB temperature. This is to differentiate from another method of correction of temperature, which will be discussed later. In SB method, estimated formation temperature at the logging depth is calibrated with the first-run bottom - hole temperature for selected production tested wells. These corrected botom-hole temperatures of production tests well are used as model for the estimation of formation temperatures in other wells which have only log temperature data. The SB temperature model is established by fitting the first run log temperatures with the estimated formation temperatures of selected production test wells over the basin.

The location of wells with production test temperatures selected in the study is shown in Figure 2.19. From the equation (2.9), it is possible to obtain a relationship between estimated Tf and Tbh for all the wells with production tests over the basin. A relationship was obtained by regression analysis given the equation

$$Tf = 1.01(Tbh) + 19.71 \qquad\qquad (2.10)$$

The temperature data for the derivation of the relationship between the estimated Tf and the first-run Tbh at logging depth is in Table 2.4. The Tf estimated by the equation (2.10) above can be determined to a precision of 5%. Therefore Tbh taken from the first-run log reading can be used directly to estimate the formation temperature at the logging depth by using the equation 2.10. The formula is applicable to all locations over the basin as the empirical equations were derived from basin-wide samples.

Figure 2-18. Thermal conductivity and temperature - depth profiles of PL2
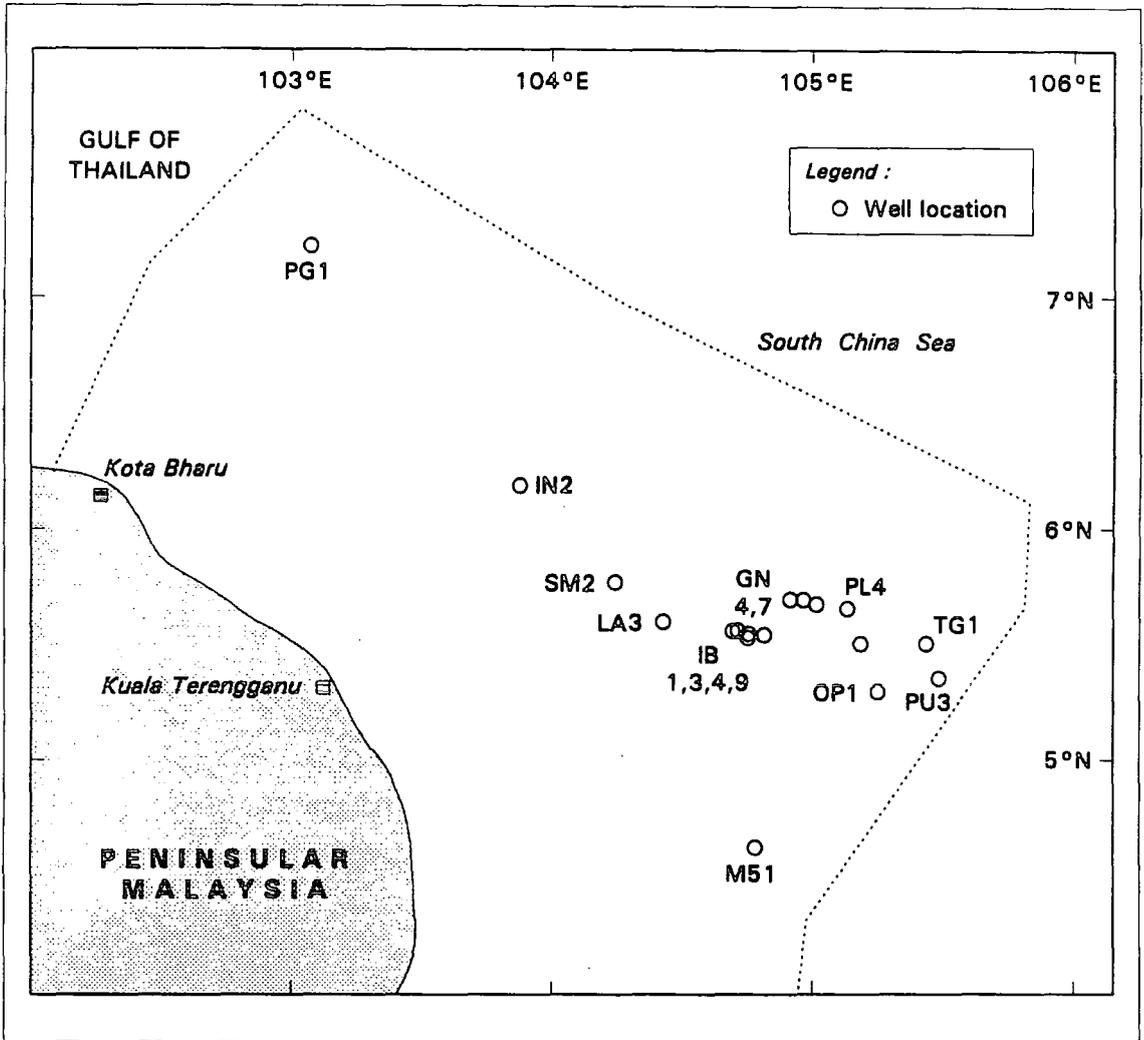
Figure 2.19 :   The location of production test wells used in the estimation
of the formation temperature by calibration with the first
run log temperatures

Table 2.4   Comparison of estimated temperature from direct
calibration of First-run Tbh to equivalent masured temperature (Tpt) .
(page 1/2)

Well	Depth(m)	First-run Tbh (°C)	Equivalent Tpt (°C)	Estimated Tbhcor.(°C)	% standard error
PU3	777	51	65	65	1
PU3	827	53	70	67	4
IB4	788	54	71	69	2
PL1	1014	57	72	73	0
IB9	780	58	71	74	4
TB4	1002	59	74	75	2
IB4	974	60	79	77	3
IN2	1000	62	76	79	3
IB6	809	63	80	80	0
LA3	1123	66	87	84	3
IR1	1006	67	87	85	2
IB1	1013	67	83	85	3
IB3	976	67	81	86	6
PU3	1563	71	96	91	4
IB9	1251	72	90	93	3
SM2	1254	73	97	94	3
IB3	1275	73	97	94	4
IN2	1565	74	97	95	2
OP1	1681	76	85	98	15
IN2	1702	77	102	97	5
SM2	1374	77	102	98	4
TG1	1701	80	106	101	5
PU3	1658	82	98	103	5
IB4	1798	84	111	105	5
PG1	1583	84	99	105	6
IB4	1966	85	117	106	10
IN2	1862	85	108	106	2
IB9	1820	86	100	106	6
PL4	2061	87	122	107	12
TB3	2014	87	121	107	11
IB6	1750	88	115	109	6
GN7	1774	88	108	109	1
TG1	2050	88	117	109	7
IB4	1701	91	107	111	4
PU3	1994	92	110	113	2
TB4	1992	92	107	113	5
TP3	1855	92	113	113	0
TO1	2163	92	119	113	5
IB1	1736	92	106	113	7
PG1	1930	93	123	114	8
TO2	2046	94	112	115	3
LA3	1686	96	115	117	1
TO1	1975	98	114	119	4

Table 2. 4   Comparison of estimated temperature from direct
calibration of First-run Tbh to equivalent masured temperature (Tpt) .
(page 2/2)

IB1	2218	100	127	121	5
PU3	2214	101	117	122	5
GN7	2575	101	132	122	8
TB3	2645	102	141	123	13
IR1	1985	102	120	123	3
PL1	2326	103	120	124	3
OP1	2517	107	135	128	6
PL2	2424	107	126	128	1
TB4	2632	108	126	129	2
IB3	2118	108	136	129	5
PG1	2292	112	143	133	7
PL4	2357	113	130	133	2
LA3	2181	114	141	134	5
LA3	2276	117	141	137	3
PL1	3085	122	145	141	3
OP1	2572	123	137	142	4
IR1	2678	138	166	155	7
PG1	2622	147	152	163	7
PG1	2774	152	160	167	5
PG1	2804	154	167	169	1

In the SB method for correction of Tbh, the estimation of Tf is done empirically by direct calibration of Tbh from first-run log with the estimated formation temperature in production test wells. The true formation temperature (Tf) may be estimated better if several factors are taken into considerations in the correlation. Glaser and Hurtig (1984) observed that the rate of thermal equilibrisation at the borehole is dependent on the logging depth. In addition, the thermal equilibrium in the borehole may be affected by the fluid movement in and out of the hole (Hearth and Nelson, 1985). It is obvious that the lithology surrounding the borehole could impact on the thermal recovery with time since the warming up rate of rocks depends on their respective thermal conductivities. Hence, it is necessary to consider converting each Tbh data by considering other factors that may affect the thermal recovery at the boreholes. Generally methods to correct Tbh comprise forward and inverse procedures (Cao et al., 1988). The forward procedures attempt to posit parameters and perform calculation of temperatures, and then adjust parameters until some acceptable degree of fit to the observed data is achieved. Here the forward procedure is used whereby the temperature data set on logs are analysed to predict the true formation temperatures by estimating the parameters that affect the prediction, such as the duration of cooling effect on mud during drilling.

Hermandrud and Shen (1989), has made a comparison of the various methods that are available at present, and concluded that the estimated temperatures determined have to be compared to measured temperatures in order to evaluate their accuracy. In the current study, the production test temperatures are assumed to be the true formation temperatures.

2.4.2 Horner-plot analysis of bottom-hole temperatures

The most popular method to estimate the true formation temperature from the logs is the time- sequential Tbh whenever multiple log runs are made and is known as Horner- plot (Dowdle and Cobb, 1975; Brigaud, et al., 1992). Newer methods of correction based on fairly

advanced physical description of the borehole are believed to give a more unbiased formation temperature. These various methods have yet to be judged in the light of the accuracy of the resulting formation temperature.

In the Horner-plot method the increase in temperature of the formation is monitored through several bottom hole temperature readings. The true temperature of the formation is than taken as the temperature at infinite time after the cessation of mud circulation. This time depends on the type and character of formation, depth, mud and the most prominent is the cooling time of the formation due to drilling or circulated mud in drilling. The Horner-plot equation is given as

$$Tf = BHT + A \ln ((1+tc/te)$$ \hspace{2cm} (2.11)

where Tf is the formation temperature, A is the slope, te is the elapse time after circulation stopped and logging started and tc is mud circulation or drilling time before logging. te is related to the warming up time for mud and tc is the cooling time (Dowdle and Cobb, 1975.; Jessop, 1990)

One of the problems in implementing the Horner plot method is to estimate the cooling time, tc, of the formation prior to the first measurement of the temperature at the bottom-hole. The circulation time of mud is normally not measured during logging, hence many workers have estimated the time to be between 1 to 6 hours (Thamrin, 1985; Majorowicz et al., 1990; Brigaud et al. 1992). While Jessop, (1990) suggested that the cooling time interval is the time of drilling operation before recording the first temperature reading. This means that the time of cooling the formation can be longer than has been estimated by some workers. In a statistical study of real circulation time, in the Mckenzie Delta Basin, northern Canada, Majorowicz et al. (1990) showed that a circulation time of 8 hours is common but that some reached as long

as 30 hours. The actual time of cooling of the formation due to circulated mud or drilling needs to be considered as there is otherwise serious errors in the estimated formation temperature (Majorowicz et al., 1990). The duration of the sediments experiencing cooling effects may be more than any recorded drilling or mud circulation time prior logging. The time taken for the borehole to return to equilibrium after logging would be very long because the activities before logging are all condusive to the cooling of the formation. Further cooling may be affected by fluid flow from the borehole into the formations. The cooling time of the formation at certain logging depth is, therefore need to be ascertained for the estimation of the temperature by the Horner-plot method. In this study the formation effective cooling time has been evaluated first, before the Horner-plot equation is used in the estimation of the true formation temperatures. The effective cooling time is postulated empirically from its relationship with known formation temperatures (from production test or Bottom-hole temperature, Tbh, from known heat flow and thermal conductivity of the formations) the warming up rate and the depth of the formation.

The effective time for mud circulation for a recorded bottom hole temperature can be deduced from a known true formation temperature (estimated from the production tests temperature gradients by equation 2.9), and the time elapsed, te, after circulation of mud and drilling stopped, prior the temperature being recorded, by applying equation 2.11 (the Horner plot equation). The analysis here assumes that the Horner plot method is applicable for most data sets, although there are studies which indicate that the method is not ideal for small te (Majorovicz et al., 1990). The Horner plot will be used in estimating the cooling time from known formation temperature, regardless of te. Hence all ranges of te shall be accommodated by the resultant tc. The cooling time, tc may be different from the real circulation times since the postulated values depend on the recorded te, estimated Tf, and the logging depth. In other words, the value of tc will vary according to the condition of the borehole portrayed by the

estimated Tf, the length of warming up period recorded, i.e. te, and the specified depth along the well where logging is done.

A list of ideal cooling times, tc, is determined for each logging depth of the production test wells, where the estimated Tf has been established. Table 2.5 shows the list of cooling time estimated for Tf and other corresponding temperature parameters, such as Tbh, and te and depth. Other parameters are the derivatives of the three main measurements at the specific depth. All these parameters will be used later for establishing the equation to predict cooling time for other boreholes where the true formation temperature is unknown.

From Table 2.5, the relationships between cooling time and the logs parameters can be observed. If the initial temperature recorded at a logging depth is Tbh_{min} and the final temperature recorded after an elapsed time after circulation of te_{max} is Tbh_{max}, then the increase in temperatures (Tbh_{max}- Tbh_{min}) is the instantaneous heating temperatures during a time interval of (te_{max}- te_{min}). The instantaneous warming up rate, WUR is given by (Tbh_{max}-Tbh_{min})/(te_{max}- te_{min}).

Analysis of the contribution of the various parameters obtained from the log data as described above has been done to assess the relationship among them in the prediction of formation temperature. Thus an empirical equation is obtained from the set of data deduced from the temperature and cooling time of Table 2.5. There are five sets of such data from a total thirty three sampling logging depths which are coded as thermal recovery types, denoted by Rt1 to Rt5. Each data set give a unique equation for the prediction of effective cooling time. These data are arranged in increasing instantaneous warming up gradient, WUG. Warming up gradient is the gradient of WUR with depth, i.e WUG = WUR/depth (column 13 in Table 2.5). The warming up gradient increases with increasing component of shales samples (kf 4 to kf7) in each Rt. In Rt1, there seven sandstone samples (kf 2 and kf3) out of ten in the

Table 2-5 List of estimated circulation time, tc, and log parameters which are used to predict effective circulation time, tceff (column10). Included in the list is kf (column 1), and the Tr types.

Column	1	2	3	4	5	6	7	8	9	10	11	12	13
Well	tc hr.	kf type	Depth m.	teMin hr.	teMax hr.	Tbhmin °C	Tbhmax °C	tec (5-4) hr.	Tc (7-6) °C	tcemp hr.	std. error (%)	Rt type	Inst. Warming rate °C/hr/m
PL2	410	kf3	2424	9	16	107	110	7	3	392	4	Rt 1	0.000164
PL4	98	kf3	2357	11	7	110	113	3.5	3	111	14	Rt 1	0.000337
OP1	545	kf2	2517	6	9	107	110	3.5	3	551	1	Rt 1	0.000341
PU3	370	kf3	1994	8	5	89	92	3	2	319	14	Rt 1	0.000372
GN4	12	kf7	1309	16	18	78	79	2	1	12	1	Rt 1	0.000382
LA3	5	kf2	2276	9.5	22	117	129	12.5	13	5	5	Rt 1	0.000449
M51	13	kf4	1645	8.5	34.75	79	99	26.25	19	13	2	Rt 1	0.00045
IN2	481	kf3	1862	3.8	7	85	88	3.2	3	527	10	Rt 1	0.000466
IB4	275	kf3	1701	3	6.5	91	93	3.5	3	269	2	Rt 1	0.000467
TO1	0	kf7	1975	21	18	98	95	3	3	0	0	Rt 1	0.000469
M51	13	kf4	1645	8.5	34.75	79	99	26.25	19	13	1	Rt 2	0.00045
IN2	481	kf3	1862	3.8	7	85	88	3.2	3	506	5	Rt 2	0.000466
TO1	0	kf7	1975	21	18	98	95	3	3	0	0	Rt 2	0.000469
PG1	75	kf2	1930	5	12	93	101	7.5	8	66	11	Rt 2	0.000522
LA3	25	kf3	1686	10	13	96	99	3.25	3	25	1	Rt 2	0.000547
PG1	0	kf2	2804	5	10	154	162	5	8	0	1	Rt 2	0.000555
GN7	1	kf4	2575	4	20	101	125	16	24	1	1	Rt 2	0.000583
TG1	225	kf4	2050	4	8	88	94	4.5	6	237	5	Rt 2	0.000602
GN4	42	kf4	2445	5.5	10	100	107	4.5	7	41	3	Rt 2	0.000636
GN7	1	kf4	2575	4	20	101	125	16	24	1	1	Rt 3	0.000583
GN4	42	kf4	2445	5.5	10	100	107	4.5	7	42	2	Rt 3	0.000636
IN2	505	kf7	1000	2.5	5.75	62	64	3.25	2	507	0	Rt 3	0.000684
IB3	80	kf4	2118	3	7	108	114	4	6	79	1	Rt 3	0.000708
IB3	50	kf7	976	4	8	67	70	4	3	53	5	Rt 3	0.000768

Table 2-5 (continued)

Column	1	2	3	4	5	6	7	8	9	10	11	12	13
well	tc hr.	kf type	Depth m.	teMin hr.	teMax hr.	Tbhmin °C	Tbhmax °C	tec (5-4) hr.	Tc (7-6) °C	tcemp hr.	std. error (0)	Rt type	Inst. Warming rate °C/hr/m
TB3	50	kf4	2645	4	10	102	114	6	12	52	3	Rt 3	0.00077
IR1	0	kf3	2678	6	13	138	153	7	15	0	1	Rt 3	0.0008
PU3	397	kf7	777	3	6	51	53	3	2	379	4	Rt 3	0.000858
PU3	397	kf7	777	3	6	51	53	3	2	342	14	Rt 4	0.000858
LA3	285	kf7	1123	3	7	66	69	4	4	316	11	Rt 4	0.000866
PG1	13	kf2	2292	4	10	112	124	6	12	12	7	Rt 4	0.000905
IB1	34	kf7	1013	6	9	67	69	3	3	35	3	Rt 4	0.000914
TG1	18	kf1	1701	4	7.75	80	88	3.75	8	20	12	Rt 4	0.001219
IM2	6	kf4	1702	4.45	5.75	77	79	1.3	3	6	3	Rt 4	0.001255
IB9	22	kf7	1251	3.5	6	72	76	2.5	4	23	2	Rt 4	0.001279
TB3	2	kf3	2014	8	12	87	97	4	11	2	2	Rt 4	0.00131
IB9	80	kf6	780	3.16	6.5	58	61	3.34	3	83	4	Rt 5	0.001066
IM2	6	kf4	1702	4.45	5.75	77	79	1.3	3	6	2	Rt 5	0.001255
IB9	22	kf7	1251	3.5	6	72	76	2.5	4	21	5	Rt 5	0.001279
TB3	2	kf3	2014	8	12	87	97	4	11	2	1	Rt 5	0.00131
PG1	20	kf4	2144	4.5	9.5	94	109	5	15	20	0	Rt 5	0.001389
SM2	15	kf4	1374	4	5.21	77	82	1.63	4	15	3	Rt 5	0.001984
LA3	0	kf4	2181	4.75	6	114	119	1.25	6	0	1	Rt 5	0.002038
IB4	33	kf7	1750	4.5	4.75	88	99	0.25	11	33	1	Rt 5	0.02539

set while in Rt5 there is only one silty sand (kf3) sample among the eight samples.The observed trend of increasing shaliness with increasing instantaneous warming up rate gradient suggests that lithology effects the efficiency of the temperature recovery to true equilibrium formation temperature at the logging depth. Other parameters which effect the temperature recovery (such as the effect of fluid flow) have been indicated by the variation of the instantaneous warming up rate of each log depth.

The empirical equations for a thermal recovery (Rt) set are determined by regression analysis on the data for the samples in each set (column 3 to 9, in Table 2.5). The circulation time deduced here is termed as the effective circulation time (tc_{eff}). When a formation temperature is to be determined than the te_{eff} is firstly obtained and followed by the execution of the Horner -plot (equation 2.11) to obtain the expected true formation temperature at the logging depth. The five sets of empirical equations for the determination of tceff is as shown in Table 2.6. Each Rt is classified according to the instantaneous warming up rate gradient intervals observed in Table 2.5 and summarised in Table 2.7. The formation temperature for each well can be calculated by the Horner-plot by using the log parameters (Tbh, te) and the tc_{eff}. This method of calculating formation temperature by the Horner-plot that incorporate tceff is called HP-TR method which is the acronym for Honer-plot - thermal recovery method. A list of the estimated formation temperatures of selected wells are as shown in Appendix 2.3.

2.4.3   Comparison among the various methods of estimation formation temperature

The formation temperature determined by the two procedures above is compared to estimated formation temperature from the gradient of production test temperature in several wells in order to compare and check accuracy. Figure 2.20 is the histogram of estimated temperature by the Horner plot method and by the former statistical method (SB) and the

Table 2.6 The general equation for the determination of effective cooling time from the thermal recovery parameters at a logging depth of a well and the respective standard error and r.m.s. error for the estimated cooling time derived using the equation.

$$tc_{emp} = (b)^D (m_1)^{te_{min}} (m_2)^{te_{max}} (m_3)^{T_{min}} (m_4)^{T_{max}} (m_5)^{tec} (m_6)^{T_c}.$$

where
D	depth at logging
te_{min}	minimum elapsed time after mud circulation prior stopped
te_{max}	maximum elapsed time after mud circulation prior stopped
T_{min}	minimum temperature measured
T_{max}	maximum temperature measured.
te_c	time interval between the measurement of T_{min} and T_{max}
T_c	increase in the measured temperature after time te_c.
m_1 to m_6	the coeficient of the independent variables.

The values of m_1 to m_6 are determined for each recovery type, Rt.

Rt	Rt 1	Rt 2	Rt3	Rt4	Rt5
Coefficient					
b	2.88E+03	4.39E+06	6.27E+04	6.07E+02	9.03E+05
m1	0.81	0.06	0.21	0.44	0.22
m2	0.96	13.39	1.82	1.58	2.57
m3	0.09	1.61	1.06	0.89	0.88
m4	10.69	0.55	0.85	1.05	1.00
m5	1.29	0.08	0.61	2.54	0.31
m6	0.06	1.37	0.80	0.62	1.43

Table 2.7 Summary of the limit of instantaneous warming -up rate of each type of thermal recovery for Bottom-Hole Temperature

Thermal recovery type	Instantaneous warming rate ($^{\circ}$C/hr/m)	
	>	< or =
Rt1		0.0004595
Rt2	0.00046	0.0006095
Rt3	0.00061	0.00085
Rt4	0.00085	0.001188
Rt5	0.001188	

production test temperature extrapolated to the same logging interval. It is shown that the estimated temperature of the formation from the Horner-plot method which has thermal recovery type estimated tceff, HP-TR, is better than SB as shown by the respective standard errors between the predicted and true temperatures deduced from the adjacent production tests data. In addition an assumed fixed value of tc is not as thorough as the thermal recovery estimated tc (tc_{eff}).

2.4.4 Geothermal gradient map of the Malay Basin

The geothermal gradient of 59 exploration wells in the Malay Basin have been interpreted from the new formation temperatures obtained and as shown in Appendix 2.3. The geothermal gradient map will be constructed and discussed in Chapter 3. There are fifteen new geothermal gradient data obtained from temperature data set determined for the new exploration wells while the rest are the geothermal gradient reinterpreted using the raw log data in wells from the previous study which have been recorrected using the new established HP-TR method. The revised geothermal gradients are about 4.65% higher than those obtained from the previous work (Wan Ismail, 1984)). The previous work was based on the Horner plot calculation where the circulation time were assumed to be between 1 and 3 hours.

In summary the formation temperature has to be determined by a more rigorous method, HP-TR in order to predict a better estimated formation temperature. The HP-TR method is more reliable than the other methods as discussed above. One of the main reasons is probably because the circulation time, tc_{eff}, has been obtained from the analysis of recorded log data rather than from pure assumptions. The Tf estimated has been derived based on analysis involving the Tpt values which have been established as the true formation temperature.
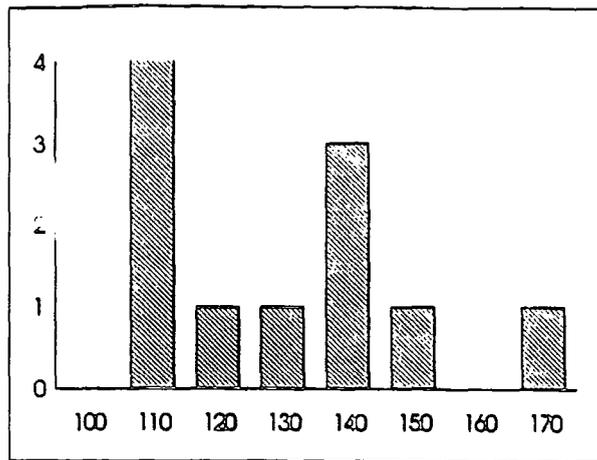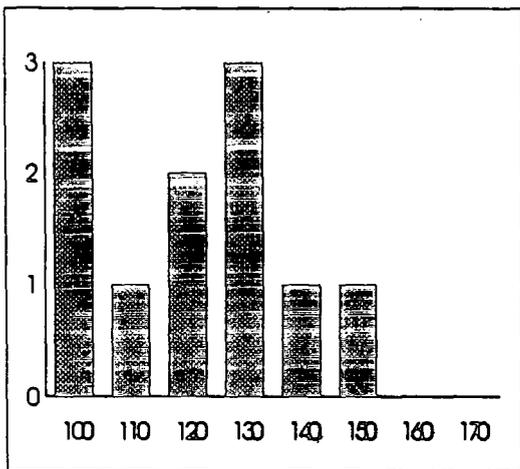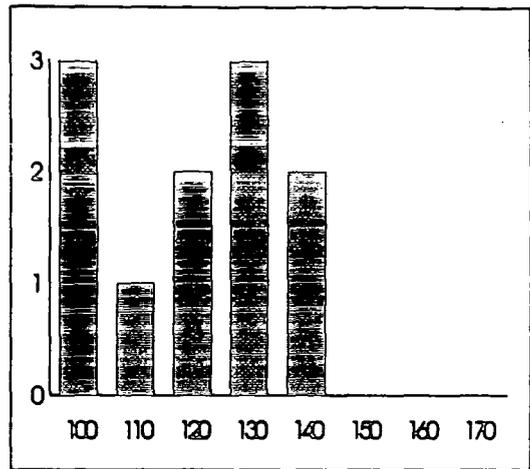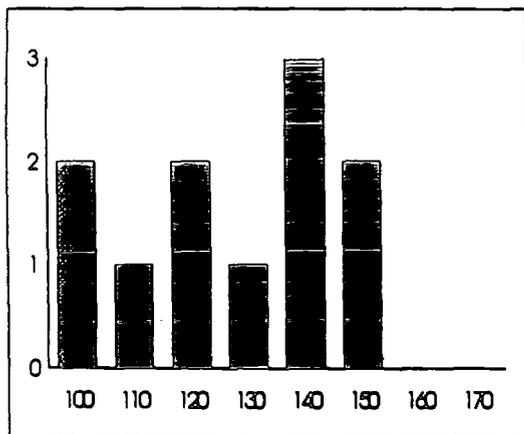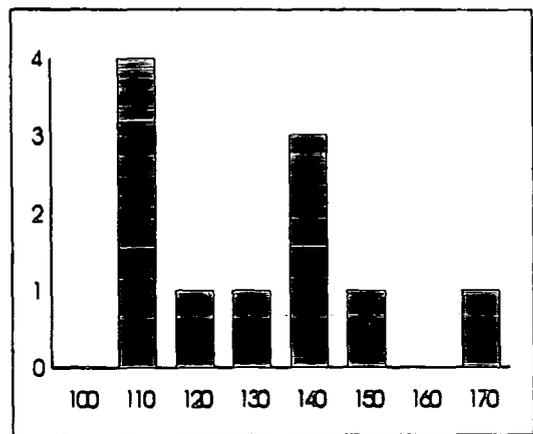
Figure 2.2 0 Comparison of estimated formation teperatures with temperatures derived
by statistical and Horner plot method. The histograms are the temperature (in °C) for the
expected true formation temperature (A), statistical Tbh-Tpt relationship (8), the Horner plot
with tc = 15 hr. (C) the Horner plot with tc= 80 hr. (D)and the HP-TR plot
(E) methods. The histogram of the measured production test temperatures
appeared to be concordance with that of thermal recovery-effective circulation
time temperature distributions (E).

2.5   Conclusions

1.   Thermal conductivity of boreholes in which conventional wireline logs have been run can be estimated to a reasonable level of accuracy for offshore Malay Basin wells. The method relies on the measured thermal conductivity data from cores but yields better results than the previous method. The method can be applied in any area where there core and borehole data are available.

2.   Thermal conductivity is estimated from gamma-ray and a porosity tool, preferably the neutron porosity, in combination with lithological information incorporated into "thermal facies".

3.   Thermal facies can be determined exclusively from the log data when calibration has been established with Lithological information. Each thermal facies is related empirically to the thermal conductivity by an empirical equation defined by the values of the log readings.

4.   The neutron porosity, one of the log readings used in identifying thermal facies and consequently the prediction of thermal conductivity is more useful than other porosity logs, probably due to the effectiveness of the neutron log in detecting water content of the rocks than any other tools.

5.   The thermal conductivity profile of a vertical well can be useful in determining the continuous heat-flow as well as the temperature profiles. The interval heat flow profile can be derived if there are temperature readings along the wellbore. In addition the continuous temperature log in the interval can be estimated using the heat flow-thermal conductivity relationship.

6.   The Horner-plot method for estimating true formation temperature from wireline log data is improved by incorporating an effective circulation time. Comparison with the true formation temperature from the production tests shows the method to be significantly more precise and reliable than previous methods where assumption for circulation time is used.

7.   The improved estimation of thermal conductivity and temperature will allow a better estimate of heat distribution in the subsurface of the Malay Basin and improved input to the geochemical basin modelling. In addition identification of temperature anomalies due to subsurface fluid movement will also be facilitated.

CHAPTER 3

Thermal regime of the Malay Basin

3.1   Introduction

The thermal state of a basin is a critically important parameter in the study of the

tectonics and petroleum geology of a basin. The Malay basin has been known to have high

heat flow. The nature of the high heat flow over the basin has been suggested to be caused by

magmatic extrusions (Matsubayashi, and Uyeda, 1979), or rifting events (Wan Ismail, 1984)

during the history of basin development. In my present study, the average heat flow of the

Malay Basin is estimated to be 85 mWm^{-2} with a standard deviation of 9 mWm-2. .The heat

flow is found to be higher than the estimated average heat flow of thermally subsiding rift or

passive margins basin. With reference to Allen and Allen's (1990) compilation of heat flows of

the world's main genetic classes of sedimentary basins, the average heat flow for the Malay

Basin is in the range of active (synrift) rift or passive margin basins. If the Malay Basin is

considered as an ancient continental rift basin then heat flow of about 50 mWm^{-2} would be

expected (Figure 3.1). Interpretations of the available seismic data suggests that there is a late

extensional event in the Malay Basin which may relate to a possible contribution to the

presence of high heat flow. Hellinger and Sclater, (1983) suggested that the Pattani Basin,

which lies to the north of the Malay Basin, and believed to be genetically similar has the same

heat flow. They believed that the Pattani Basin has experienced late thermal subsidence at 12

m. a. which has caused the high heat flow. In my present study the observed areal and vertical

heat flow patterns suggest that other thermal factors besides the basement may have affected

the distribution of the heat in the Malay Basin.
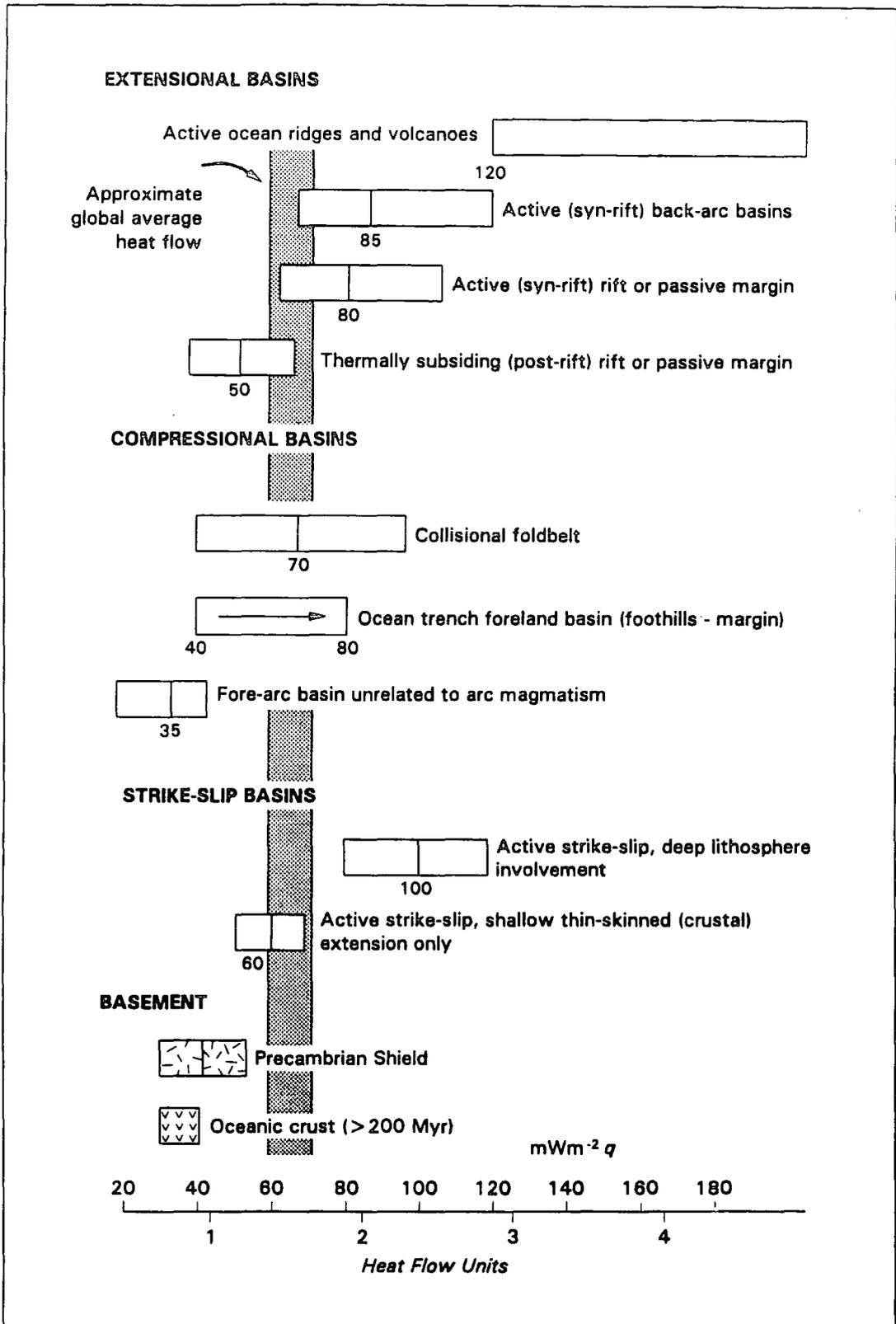
Figure 3.1 : The heat flow of the main genetic classes of sedimentary basin (after Allen and Allen, 1990). The Malay Basin's average of 85mWm^{-2} heat flow is higher than the global average.

The areal heat flow patterns observed (as in the next Figure 3.5) indicate the amount of heat flowing out of the surface per unit area. In the current study, areas of anomalously high heat flow has been observed in several parts of the basin. These are areas with more than 90 mWm^{-2}. In other localities there are areas of relatively low heat flow, with estimated values of about 65 mWm^{-2}. Investigations on heat flow patterns in other basins suggest that heat flow anomalies in sedimentary basins can be associated with fluid flow in the sediments (Majorowicz and Jessop, 1981, Willet, and Chapman 1987, Brigaud, et al. 1992). In addition, the ground water flow in the sediments may be related to hydrocarbon migration within the basin (Zeilinski and Bruchhasen, 1983, Meyer and Mcgee, 1985) also observed that there are geothermal anomalies in certain fields in Rocky Mountain Region of USA associated with oil and gas accumulations.

The possible causes of heat flow anomalies in sedimentary basins are being continuously discussed and investigated. The cause of variable heat flow distributions may differ from one basin to another and may depend on the nature of the basin and the underlying basement. A study by Speece at al., (1985) indicated that the influence of changes in basement heat flow is the main cause of the observed geothermal gradient pattern in Michigan Basin. Similarly a study on vertical changes in thermal properties by Forster and Meriam, (1993) shows that variations in the geothermal gradient are mainly caused by the effect of thermal conductivity variations in Tertiary and Mesozoic rocks which overlie Precambrian basement in Kansas, the mid continent in USA.

In the Western North Sea, although geothermal gradient changes can be mostly attributed to changes in the thermal conductivity of the rocks, the positive (high) temperature gradient anomalies within the basin has probably been controlled by heat advection. Other causes of heat pulses in the history of the basin development, such as tectonics, cannot explain the shallow anomalies observed (Andrew-Speed et al., 1984).

In order to investigate the nature of heat flow distribution within the basin, areal patterns and vertical profiles of thermal properties are important criteria to study the nature of the thermal state of the sedimentary basin. In this chapter, the observed heat flow anomalies, changes in the thermal conductivity and temperature gradients over and within the basin shall be investigated to understand the thermal state of the Malay Basin.

3.2   Construction of areal thermal maps of the Malay Basin

The data presented in Chapter 2 are mapped using a software, UNIMAP. The software package is a powerful mapping tool whereby the irregular data sets can be transformed into regular set by several methods, which includes, the binomial, polynomial, statistical krigking and fault. The thermal data are chosen from randomly spaced wells which construed to the irregular data set. The data set is firstly interpolated to facilitate contouring using the `fault' method option. The `fault' interpolation is chosen because it maintains the original data points effects while reproducing the regular data set during mapping. The contour line is placed at an average distance from the data points. The interpolation process is done through a grid system, whereby the smoothness of the curves can be regulated by the number of grid specified during the interpolation process. Another feature is that the contours generated from the programme `fault' is that the range of the area of interpolation can be controlled by a technique called search angle. The larger the search angle the more detailed contour lines and more extensive coverage can be attained.

The data used include the co-ordinates of each well. The original geographical co-ordinates of the wells are first transformed into a new grid system for making data access into the UNIMAP software package. The relationship between the geographical co-ordinates and the grid system used in this report is as follows:

For the Easting grid, the longitudinal co-ordinate, Y is expressed as

$$Y = 30(d° - 102) + (m'/2) + (s'')/120. \qquad (3.1)$$

and the latitudinal grid, X is given by:

$$X = 30(d° - 3) + (m'/2) + (s'')/120 \qquad (3.2)$$

where the degree (d°), minutes (m') and seconds (s") is the expression of latitudes and longitudes used in the geographical presentation. The location 3° 0' 0" N and 102° 0' 0" E is given by a new grid (0,0). A subsequent increase of 1° is equivalent to 30 unit in the new grid system. 1 new grid unit is equal to approximately 3.67 km in distance.

The Malay Basin has been divided into 6 geographical sectors in order to analyse the thermal properties (Figure 3.2). The subdivision of the Malay Basin into sectors is felt useful for describing the thermal state of the basin fully. Since the basin has varied tectonics and stratigraphic styles (Chapter 2), there is a need to define sectors. Each sector is chosen so as to conform closely with the geology.

The NW sector comprises sediments drilled to H group (Middle Miocene). The deepest well drilled in this sector is coded PG1 in the Pilong field which reaches a depth of 2782 m and a well, TK1, has reached a basement at total depth of 2653 m , SW portion of this sector (Figure 3.2). The TK1 was drilled in a depression on the basin edge which may be independent of the basin proper. The structural styles of the area to the west of Bergading and Bintang Line (approximated by line joining wells BG1 and BT2) is of extensional tectonics. The main faults and features are aligned north - south which is similar to the alignments in the Thai basins to the north. This part of the basin is known as the NW province or sector 1.
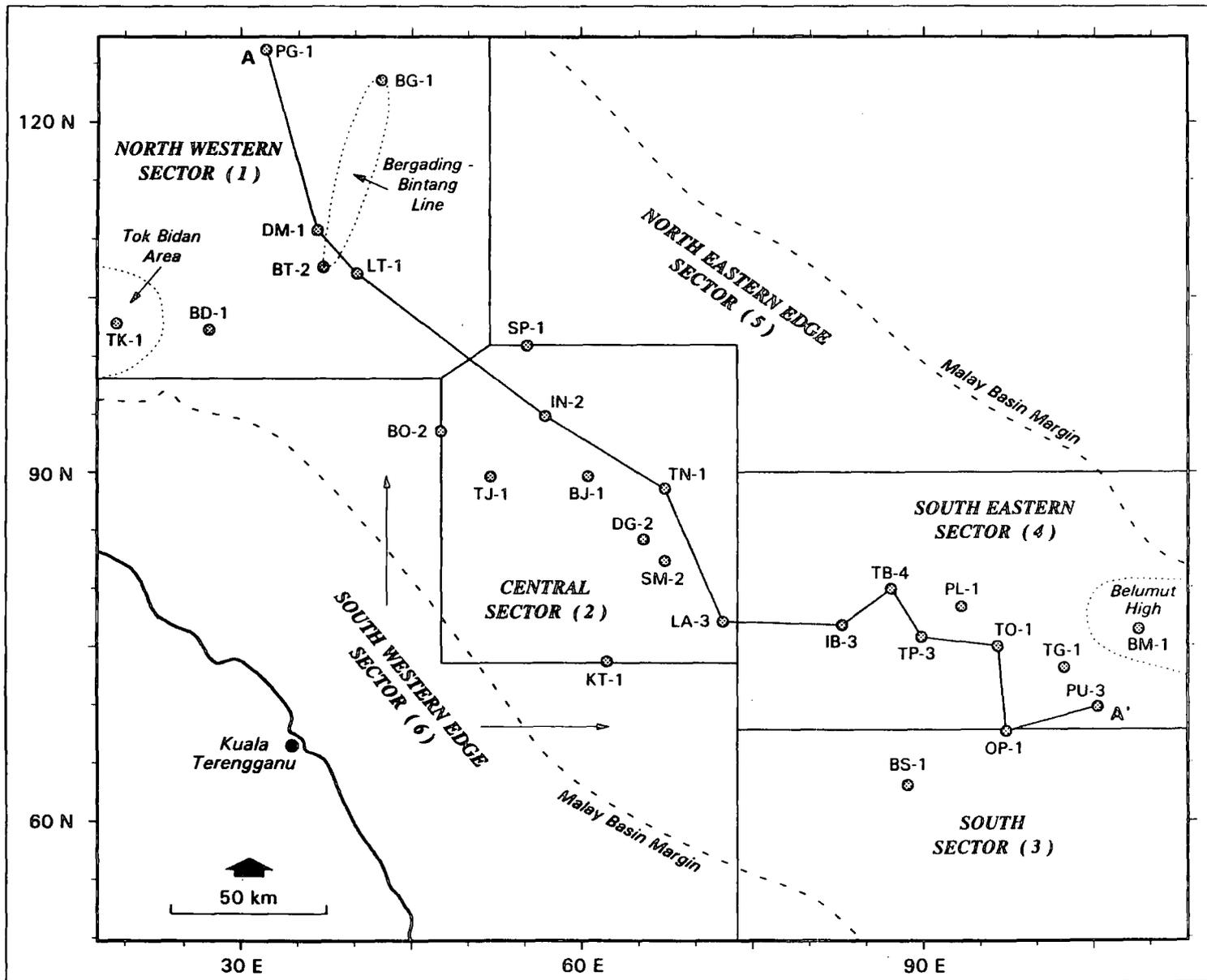
Figure 3.2 : The geographical sectors of the Malay Basin. The location grids are those adopted for used in mapping.

A - A' refer to location of isotemperature-depth profile cross-section shown in Figure 3.8

To the east of the Bergading - Bintang Line, the structural styles differ from those of the sector 1. Compressive domes and anticlines with north-south faulting covers the area from the southern portion of the basin to the Jerneh feature in the west, adjacent to the Bergading structure. This region are divided into three sectors, namely the Central Sector (coded sector 2), the Southern sector (coded sector 3) and the South-eastern sector (coded sector 4) . The south eastern sector has been uplifted and eroded during Plio-Miocene times. The deepest well PL1 reached a total depth of 3074 m in group L in Late Oligocene. A thick lacustrine shales of about 150 m to 300 m is present in the south Malay Basin and extends into the South-eastern region, sector 3. The shale is commonly known as the Terengganu or K shale.

The north eastern sector is the region with gentle basement gradient. The structural features are marked by NW- SE extensional faults parallel to the edge of the basin. The faults dissect the gentle onlapping sediments over the NE edge. This portion is known here as North-eastern (NE) sector, or sector 5. The south western edge of the basin is called sector 6.

Exploration wells drilled in each of the sectors are not evenly distributed among the sectors. The most explored South eastern sector is where most data has been selected. The least amount of data is from the newly explored North east sector (sector 5) and sector 6. On average, about 50 km separates each of the 59 locations which represent data points used for the evaluation of the thermal properties in the Malay Basin.

3.3   The thermal maps

The thermal conductivity of the basin has been mapped to determine the pattern of thermal conductivity data averaged for the locations over the basin (Figure 3.3). The thermal conductivity patterns can give some clues to the nature of the heat flow in the sedimentary

Legend :

- - - - Malay Basin Margin
——— Sector Boundary

C.I. = 0.04 W/m°K

7°N

6°N

5°N

Kuala Terengganu

0   50
KM

103°E   104°E   105°E

Figure 3.3   : Average Thermal Conductivity of Malay Basin

basins. A geothermal gradient map is shown in Figure 3.4. The geothermal map is produced from the corrected BHT and production test temperatures of Chapter 2. In this chapter, the analysis of the geothermal and thermal conductivity patterns is carried out to investigate possible causes of heat flow distribution areally as well as vertically.

The heat flow map (Figure 3.5) is constructed from the product of the thermal conductivity and geothermal gradient of each sites. The heat flow patterns will be influenced by the magnitude of the thermal conductivity and the temperature gradients. Therefore anomalies of heat flow over the surface is, either the manifestation of the thermal conductivity or geothermal gradient or both.

The construction of the heat flow map is made with the assumption that the heat flow behaves according to the conductive heat transfer given by Fourier's Law, $Q = - K(dT/dY)$. Therefore under normal circumstances, the heat flow shall varies according to the principle given by the conductive heat transfer, i. e. the any changes in thermal conductivity will induce an inverse change to the geothermal gradient. This relationship between the thermal conductivity and geothermal gradient is known as negative correlation. Hence areas of strong negative correlation between the two elements of the heat flow values will indicate a conduction heat transfer (Figure 2.1). On the other hand, positive correlation between the thermal conductivity and geothermal gradient will indicate a weak influence of the conduction heat transfer and an increase in other types such as an advective heat transfer. Hence the relationship between the geothermal gradient with the thermal conductivity is used to infer the factors that influence the relative near surface or seabed heat flow values. In areas where thermal conductivity is remarkably has strong influence on the temperature field then, one can observed a negative correlation of geothermal gradient with thermal conductivity (thermal correlation) patterns. Anomalous heat flow associated with positive correlation between geothermal gradient and thermal conductivity may suggest a high degree disturbances in the
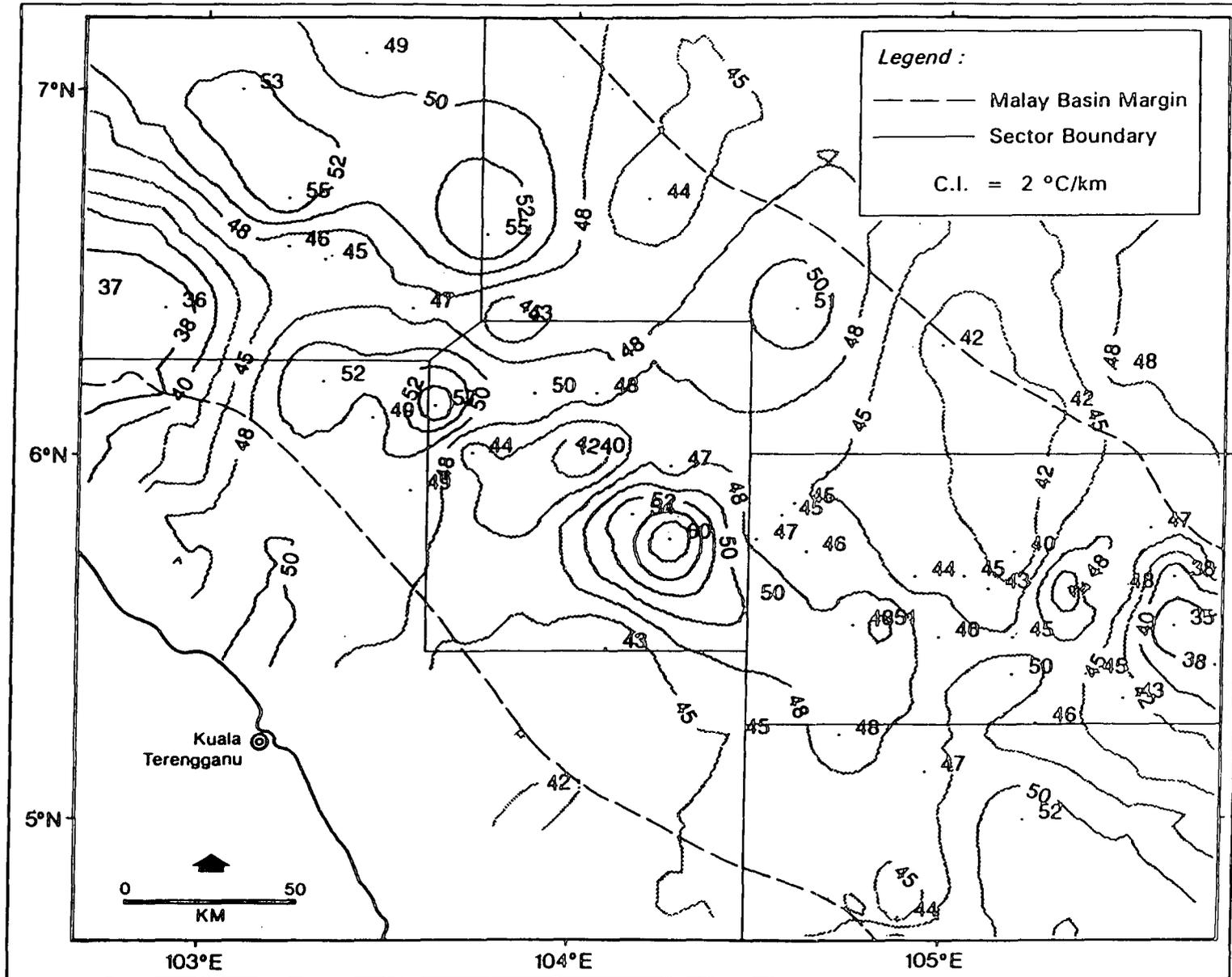
Figure 3.4 : Average Geothermal gradient of the Malay Basin
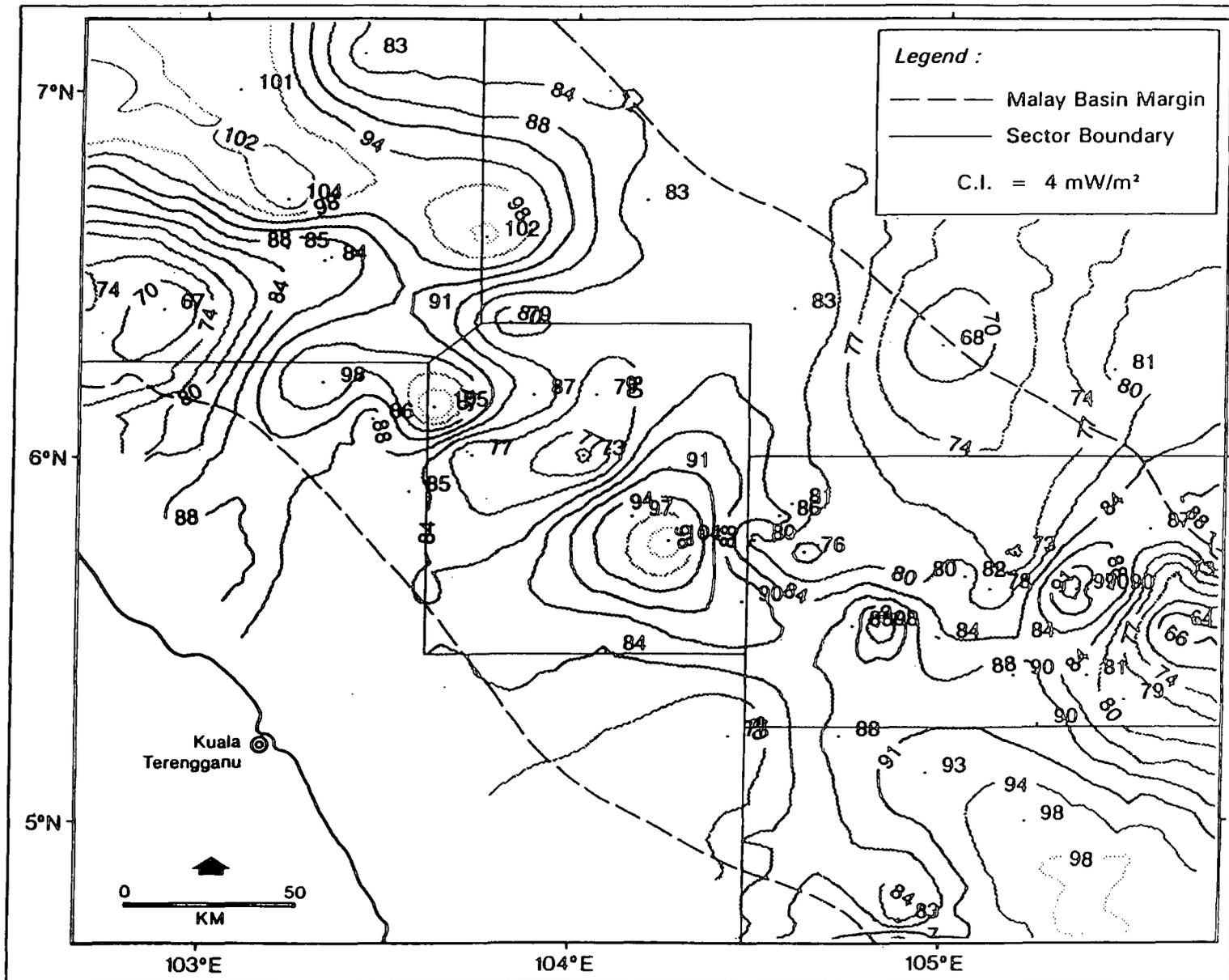
Figure 3.5 : Heat Flow Over Malay Basin

temperature fields that the conductive heat flux is redistributed vertically and horizontally (Brigaud, F. et al., 1992).

3.3.1 The surface thermal patterns

Statistical compilation of the estimated thermal values of each well, and in each sectorand basin wide average is shown in Appendix 2.3 and Table 2.1 respectively. The patterns displayed by the thermal parameters at the surface can be summarised by the maps shown in Figure 3.5 for heat flow, Figures 3.3for thermal conductivity and Figure 3.4 for geothermal gradient.

Each of the sectors are dispalying different surface thermal patterns which may be related with the geology and thermal field within the sedimentary basin. The following descriptions will show the regional and basin wide variation of surface heat flow density and other thermal parameters.

The average thermal conductivity of wells in sector 1 (1.88 + 0.08 W/m°K), is slightly higher than the values for the whole basin (1.84 W/m°K). A gradual increase in average thermal conductivity from the north eastern edge towards the south western edge of the basin is observed. The lowest estimated thermal conductivity is for well BG1 (1.71 W/m°K) situated near the north eastern edge, whereas the highest is for TK1 (2.02 W/m°K) in the south western edge and is concordant with the nature of the structural styles of this part of the basin. The basin is asymmetrical with a gentler, passive north east edge and a steeper and structurally active south-western edge. The steeper gradient of the south west edge must have been prone to more sand deposited due to erosion of the basin edge escarpment which gives the higher thermal conductivity. The average geothermal gradient varies according to the changes in thermal conductivity in a highly negative correlation manner in Tok Bidan and KT1 area,

Table 3.1 Statistics of the thermal data for the Malay basin

Sector	Number of wells	Thermal conductivity		Geothermal Gradient		Heat Flow	
		W/m°K	Standard Deviation	°C/km	Standard Deviation	mW/m^2	Standard Deviation
1	11	1.88	0.08	48	6	90	12
2	11	1.80	0.13	49	6	88	11
3	6	1.86	0.09	48	3	89	8
4	25	1.86	0.09	45	4	84	8
5	6	1.71	0.09	46	4	79	6
The Malay Basin	59	1.84	0.11	47	5	86	10

over the basin edge. In the centre there is an extremely high (over 50.0 °C/km) geothermal gradient. The geothermal gradient contours decreasing rapidly towards the south western edge. The heat flow is high and extensive over this part of the basin. which may be related to some regional consequences. At the central axis of the basin, the heat flow is of over 90mWm^{-2}. The highest heat flow, in particular is shown by well DM1 with a value of 104 mWm^{-2}.

In the central portion of the basin, sector 2, the average thermal conductivity of the wells (1.80 + .13 W/m°K) which is slightly lower than the basin wide average. As in the sector 1, low thermal conductivity (of below 1.75 W/m°K) is observed over the areas in the Northeastern edge. Thermal conductivity increases towards the southern edge and reaches a maximum of over 2.00 W/m°K at well KT1 (Figure 3.3). The higher conductive southern section may be due to increase in the sandstone percentages deposited from the eroded escarpment of the basin edge faults. The geothermal gradient is higher in the central axis, but is disrupted by a low in the middle. It appears that there is negative correlation in general between the geothermal gradient and thermal conductivity over the southern edge. In the area of low thermal conductivity in the centre and over the north-eastern edge, a positive correlation of low geothermal gradient with low thermal conductivity patterns is observed. The two thermal anomalies at the basin centre are separated by the low heat flow area around wells TJ1 , SP1 and BJ1. This low heat flow portion seems to be unique for the central axis of the whole Malay Basin which is predominantly a high heat flow regime.

In Sector 3, the south Malay Basin, high thermal conductivity and geothermal gradient contours cover most of the area investigated with only a small portion on the western side, where heat flow is low. The average heat flow is generally as high as the North- western part (sector 1), which is about 90 mWm-2 (Figure 3.5). This area portrays mainly positive thermal correlations with a low conductive portion in the middle of the sector.

In sector 4, which is commonly referred as the South-east Malay Basin, geothermal gradient and thermal conductivity show mostly a fair positive correlation except over the Belumut High. High thermal conductivity is recorded in wells around the Belumut High (Figure 3.4). The well BM1 has penetrated basement rock at about 1289 M. The geothermal gradient is low, less than 45 °C/Km and represents a thermally high negative correlation spot. The low geothermal gradient is present in the northern portion of the sector as well, with a moderate thermal conductivity which indicate a partial negative or positive correlation. However, in the central portion of the sector, the geothermal gradient and thermal conductivity values are moderate which suggest a fair positive correlation. The heat flow is high in places surrounding the Belumut High and over the central portions. These areas also shows a positive thermal correlation.

The most distinguishable areas of low thermal values is over most of the eastern part of sector 5, areas near the north-eastern edge. Over this area, the thermal conductivity is low while the geothermal gradient is also low. Anomalous low heat flow are observed. This part of the basin has a uniformly strong positive correlation of low thermal parameters. In the west part of sector 5, the heat flow is higher with a moderate geothermal gradient values (45 to 50 °C/km). The thermal conductivity moderate to low. It is a region of negative thermal correlation. The negative thermal correlation zone present here continues into central sector.

The heat flow map (Figure 3.5) shows a general Northwest - Southeast trend with major areas of high heat flow (thermal highs) along the axis. Two major highs are found at the Northwest and Southeast ends of the basin. The flanks are normally the low heat flow areas. There are exceptions to these general patterns, firstly there is a pronounced thermal low located along the axis, which disrupts the general trend of high heat flow along the axis of the basin. Another feature is the north east - south west trends of several high heat flow which in the vicinity of the structural highs (The Belumut High and Bintang - Bergading Line). The

presence of a low heat flow area in the centre of the basin suggest that the basement heat has

been redistributed, since the basin is deeper along the axis (which would contribute to low

thermal conductivity and make high geothermal gradient), the heat flow should remain high.

The presence of some minor thermal highs alongside with the topographic highs is another

indication of a possible effect of heat flux redistribution.

3.3.2 Causes of surface heat flow anomalies

Figure 3.6 shows the relative domains of mechanism of heat flow over the basin which

is deduced from the correlations of the thermal conductivity and geothermal gradient. The

strong negative correlation is inferred as prominently conductive and the strong positive

correlation part is areas of prominent advective heat transfer. Other intermediate domains

belong to some mixtures of conductive and advective components of heat flow which are

deduced from the relative influence of conductive and convective types of heat flow.

Although parts of the Malay Basin has negative thermal correlation which indicate the

conductive mechanism of heat flow (Figure 3.6), but a sizeable portion of the basin have a

positive thermal correlation which indicate, mainly the effect of possible fluid flow. Thermal

pattern in the Malay Basin appears to be influenced by the basin structural configuration and

some possible internal processes which redistribute the heat flow and produced the anomalies.

The size of high heat flow anomalies as well as strong positive thermal correlation localities

are of tens of kilometres may suggest that the fluid flow is of crustal origin (Willet and

Chapman, 1989). The mechanism of the redistribution of heat flows within the basin may be

related to either the effects of high temperature fluid moving up from the deeper sections of

the basin or the movement of water which has been forced by conditions in part controlled by

topography, precipitation or evaporation (Lachenbruch and Sass, 1977). Both mechanisms

that cause the anomalies could take place in this basin. The two ends major high heat flow area

may have been partly affected by topographically forced water movement due to the
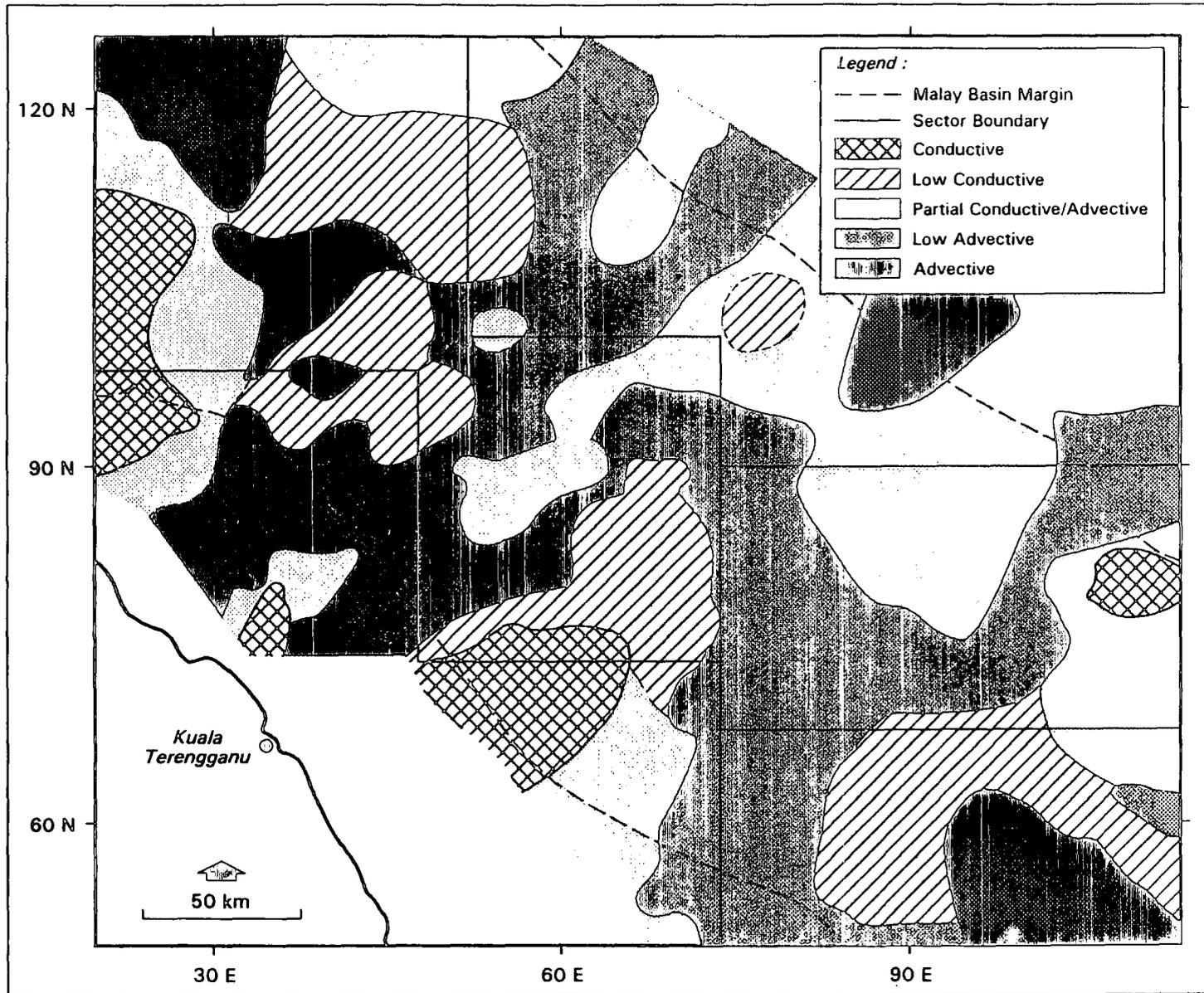
Figure 3.6 : Distribution of relative mechanism of heat flow inferred from
relative thermal correlation patterns

WIS17-Feb

adjacent highs i. e. the Belumut High in the SE and the Bergading - Bintang Line and Tok

Bidan High in NW. The chain of heat flow anomalies along the centre of the basin (Figure

3.5) may have been mainly due to the effect of upward movement of water from deeper

sections which has been produced within the sediments probably by compaction or gas

conversion processes. However, the differences and varieties in stratigraphical, structural and

sedimentological patterns over the basin may suggest that basin wide hydrologic control is not

important in the dispersion of the heat flow in the Malay Basin.

3.4   Components of heat flux affected the surface thermal pattern

We have seen a mixture of negative and positive correlation of the geothermal gradient

and the thermal conductivity distribution patterns over the Malay Basin. A larger portion of

the basin is under a positive thermal correlation including the basin axis, which include the

prominent high heat Flow in the NW, sector 1 and SE, sector 3 and a lower heat flow locality

in SE sector 4 of the basin. The areas in the fringe of the Northeastern edges, are where

positive correlation covers a very large areas. These are areas of possible heat flow

distribution influenced by fluid flow. The heat flow values are a mixture of highs and lows .

The areas of negative thermal correlation occur along the edges of the basin. The

strongest negative correlation between the geothermal gradient and thermal conductivity

occurs in the south-eastern and some lighter ones in the south western edges of the basin and

in the north eastern sector as well (Figure 3.6). The negative thermal correlations suggest that

the conductive heat flow is a major contributor to the surface heat flow distribution. The heat

flow values around 65 to 70 mWm^{-2} occurs over these areas which is comparatively low for

the basin as a whole.

In the South-eastern sector, the region where the evidence of strong negative correlation of geothermal gradient to thermal conductivity has been observed is over the Belumut High. The Belumut High is an area of granitic rocks of Cretaceous age. The area which has been a long-lived topographic high and has been an early source of sediments for the Malay Basin. The basement granite is possibly similar to the one which forms the crust of the land mass in Peninsular Malaysia.

Another area of strong negative correlation of geothermal gradient but to a lesser intensity is observed around the wells TK-1 and BD1 in the Southwestern edge of sector 1. The area has been drilled to basement which is at a depth of about 2600m. It is relatively high topographically compared to the basin proper. The area around TK1 was possibly a platform as in the Belumut High, but it has been separately sagged during the earlier stage of basin development (Esso, 1976).

The Belumut High heat flow of 65 mWm^{-2} is slightly higher than the average continental heat flow of 62.3 and 56.6 mWm^{-2} reported by Jessop et al. (1976) and Sclater et al, (1981) respectively. The Belumut High probably has been unaffected much by thermal perturbations during basin inception due to its all time higher than the basin proper The heat flow is considered as basement heat flow which comprised of crustal radiogenic and aesthenospheric convected heat.

3.4.1   Basement radiogenic heat production

The crustal heat flow in the Malay Basin may be similar to the nearby continental value. A survey on radioelement (U, Th and K) data onshore Peninsular Malaysia suggests that the mean heat production values of the different plutons here ranges from 5.32 to 7.72 Wm^{-3} which are comparatively higher than the values of many known granites (Chakraborty,

1992). The depth - distribution of the radioelements is uncertain, but no downward depletion is apparent for a vertical depth range of about 1 km. Hence the total contributions of the crustal radio elements to the total surface heat flow is quite uncertain. If the radiogenic heat production is confined to the continental crust, the basal heat flux from the aesthenosphere is approximately one half of the total basement heat flux (Sclater et al. 1981). Hence, for the heat flow of 65 mWm^{-2} the basal heat flux is about 33 mWm^{-2} over the Belumut High. Then the radioelements apparent depth-distribution in this area is estimated to be the region of 5 km (33 mWm^{-2} divided by 6.42Wm^{-3}). In a study by Birch et al. (1968) and Roy et al. (1968), the depth of radiogenic heat production for rocks in New England, USA is found to be about 6 km which approximately matched the one deduced from the above estimation. Therefore it is likely that the basement heat flow is probably about 65 mWm^{-2}

3.4.2   Radiogenic heat production of sedimentary rocks

In the basin proper where heat flow is mostly high (about 85 mWm^{-2}) and there is positive correlation of geothermal gradient to thermal conductivity, the excess heat (above the basement conducted heat) sources have been suggested to come from the advective heat transfer due to fluid flow, internal heat production and the thermal perturbation associated with basin development. The two former causes are to be considered in the present study but the later source is considered minimal (Blackwell and Steele, 1989). By taking crustal back ground heat flow of 65 mWm^{-2} (observed over the Belumut High), than for most parts of the basin, the excess heat flow is about 20 mWm^{-2}

The contribution to heat flow by the internal radioactive elements can be significant in producing the excess heat flow in a basin. The heat production of the sediments caused by radioelements in a sedimentary basin is important for basin deeper than 5 km and older than 10 million years (Rybach, 1986). It can be estimated empirically using log data.

Table 3.2. List of wells with radiogenic heat production (A) data.
The radiogenic heat production is estimated from logs.

Well	A $(\mu W(m)^\wedge 3)$	Well	A $(\mu W(m)^\wedge 3)$
PU3	0.82	BN1	1.26
SM2	0.92	PL2	1.26
CM1	0.99	IN2	1.27
PG1	1.00	TG1	1.29
IB9	1.00	BU1	1.29
TP3	1.00	GN 4	1.30
BE2	1.04	IR1	1.32
DG1	1.07	BG1	1.34
AG1	1.07	TB4	1.34
OP1	1.07	PL1	1.35
LT1	1.08	GN7	1.36
BS1	1.08	LA3	1.38
BT2	1.12	KP1	1.38
IB6	1.18	TN1	1.40
IB3	1.19	IB1	1.41
TB3	1.21	DM1	1.47
GN2	1.22		

104

Values in miligram equivalents

Figure 3.7 : Mineral contents-depth trend of a well (Zyke field, Baku) showing
evidence for upward movement of water

(Adopted after Roberts, 1980)

In the Malay Basin, the high heat flow anomalies are found in association with almost all oil fields structures. There are data for some formation water recovered by repeat formation tests from wells in sector 2 (DG2, SM2 and BO2 in Table 3.3). There is a significant increase in chlorine and nitrate within some intervals in the upward direction. The observed trend in water salinity concentration may be related to the upward movement of formation water as well.

Independent studies on the present day distributions of temperature fields and their relation with heat flows in sedimentary basins has been carried out (Majorowicz and Jessop, 1981, Chapman et al., 1984, majorowicz et al., 1985 Speece et al., 1985, Bethke, 1986, Willet and Chapman, 1987, Blackwell and Steel, 1988, Brigaud et al. ,1992). The analysis has resulted in a common conclusion that underground water circulation may have disturbed significantly the temperature fields in the basin. They have suggested that underground water movement can be the result of hydraulic variations over the region as well as fluid expulsion processes during the burial of sedimentary rocks. In the Malay Basin, there is the possibility of both mechanisms playing a role in the distribution of heat flux.

In another study, mathematical modelling has been developed to understand and establish the relationship of fluid flow to thermal properties in sedimentary basins. The models try to explain the nature of the fluid flow in the above two conditions, i.e fluid flow by hydraulic variations and expulsion processes during burial. Most of the models are complicated which make their practical application difficult. Further more the models are mostly limited to simple cases such as horizontal aquifers. However, mathematical modelling is required to assist in estimation of the nature of vertical flow of fluid which is important in the understanding of the thermal anomalies observed in the areal heat flow distribution over the Malay Basin.

106

Table 3.3. The upward increase in concentrations (in parts per millions, ppm) of salts
in some wells in the Malay Basin, indicating a possible upwards fluid movement is taking place.
(tr denotes trace amount of the ion is present; and un is for result not stated or no test.)

Well	Depth K. B. (m)	Cloride (ppm)	Nitrate (ppm)
DG2	666	2600	160
	805	1900	140
	964	2900	180
	1120	1760	100
	1176	2300	120
	1195	1120	50
	1230	920	tr
	1230	480	80
	1230	920	tr
	1311	2540	110
	1311	2440	95
	1322	2400	192
	1353	200	175
	1353	700	tr
	1415	1200	22
	1415	2280	32
	1420	1260	14
	1420	860	4

Well	Depth K. B. (m)	Cloride (ppm)	Nitrate (ppm)
BO2	879	2800	20
	1292	1950	tr
	1292	un	20
	1686	1500	tr
	1686	1300	tr
	1817	1900	tr
	1817	1800	tr
SM2	1008	2400	70
	1024	2400	30
	1180	2300	90
	1198	2200	120
	1212	2000	100
	1212	2000	12
	1247	2400	70
	1253	2300	80
	1253	2300	80

In trying to evaluate the vertical flow of fluid associated with heat flow anomalies, a model is selected to estimate the probable vertical displacement of fluid movement. The model was introduced by Lachenbruch and Sass (1977). The relationship between heat flows and the vertical fluid flow is given by

$$Q/q = e^{z/s} \qquad (3.4)$$

where Q is the heat flow over the anomaly where fluid flow is active and q is the average heat flow in the surrounding region (Vacquire, 1984). z (in km) is the thickness of the vertical flow and $s = K/upc$, where p and c are the density and the heat capacity of water respectively (unity in cgs unit). $\pm u$ in mm/sec is the velocity of fluid flow, and K is the thermal conductivity (in cgs unit. 1 mWm°K = 2.388(10^{-3}) cal/cm sec °C)

It has been established that for the heat flow to be increased, then it is sufficient to have fluid to moves upward a few mm per year (Lachenbruch and Sass, 1977, Andrew-Speed et al., 1984, Zielinski and Bruchhausen, 1983, Vacquier, 1984.). The thickness of the vertical flow can be estimated by equation 3.4 ,which can be expressed as

$$z = K \left(\ln[Q/q] \right) / cpu \qquad (3.5)$$

The model describes whether the surface heat flow (Q) is significantly different from the regional heat flow (q) depending upon whether the depth of vertical water flow is small or large in relation to s, which is dependent on thermal conductivity of rocks, density and heat capacity and velocity of water. The equation is applied to the heat flow anomalies and the thickness of vertical flow is estimated when the water velocity is assumed to be 3 mm per year. The thickness of the vertical flow has been estimated at 9 localities where the heat flow anomalies are very pronounced. The estimated vertical flow thickness of fluid flow at each

anomaly is given in Table 3.4. The thickness of the vertical flow ranges from 1.80 to 0.92 km . The thicker vertical flow is found to be in sectors 1 and 3 with the estimated thickness of 1.80 and 1.75 km respectively. These are the regions of high heat flow and where most of the basins gas reserves are trapped.

The base of the vertical fluid flow interval is assumed to be the regional surface of constant regional heat flow (Lachenbruch and Sass ,1977). This model can be described by the base plane where water flows with constant temperature. The extent of the upward flow of fluid which causes the anomalous heat flow can be seen from vertical thermal profiles of individual well. Whether the vertical flow heat flow can cause the high heat flow or lower the heat flow depends on the direction of flow.

3.5   Vertical thermal profiles.

It has been shown that among the internal heating source in the Malay basin about 50% are likely to be from the radiogenic production The amount of heat flow in excess of this can be related mostly easily to the vertical fluid flow component. Further observations can be deduced from analysis of the character of the vertical profiles. One of the element to look upon here is temperature. The temperature is an important asset in the study of chemical reaction in sedimentary basin, such as in the conversion of kerogen to hydrocarbon, and smectite illite transformation as well in relation to occurrences of geopressures.

3.5.1   Temperature-depth profiles

A profile of iso temperature lines is constructed along the basin in Figure 3.8 (Location of wells in Figure 3.2). It is intended to demonstrate the changes in the depth of iso-temperature surfaces and reflects the changes in geothermal gradient with depth and

Table 3.4 The thickness of the section of vetical fluid movements
in anoamlies over the Malay Basin. The anomalies quoted can
be refered from the heat flow map of Figure 3.5.

Sector	Anomaly (coded)	K (W/mK)	q (mWm²)	Q (mWm²)	Z (km)
1	1W 1	1.92	70	102	1.80
	1W 2	1.88	70	94	1.38
2	2C 1	1.84	77	94	0.92
	2C 2	1.80	77	96	0.98
3	3S 1	1.92	68	98	1.75
	3S 2	1.88	77	94	0.93
4	4E 1	1.84	70	91	1.22
	4E 2	1.88	68	91	1.36
5	5N 1	1.80	80	98	0.92
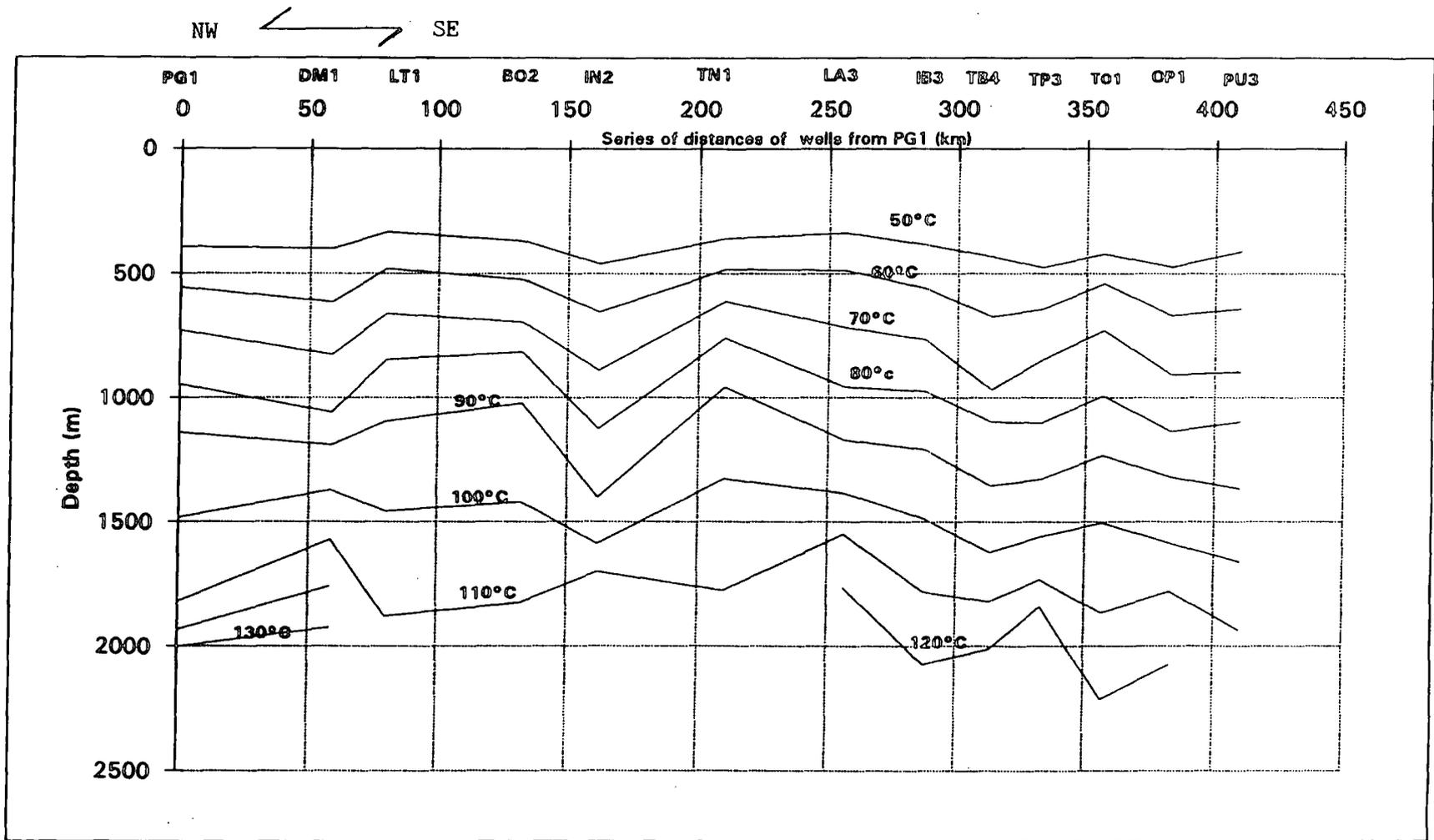
Figure 3.8. NW-SE cross section of iso-temperature lines through the selected wells
Well location is as shown in Figure 3.2.

horizontal distances. A cross section of temperature - depth profiles is made to see the overall changes in temperature with depth. The section (A - A' in Figure 3.2) trend NW-SE from well PG1 to PU3. and passed through other 11 well locations.

One of the important observations is that the temperature profiles at top of the section is quite regular but at the base of the section they are an alternate highs and lows. The iso-temperature lines are not regular with depth which suggest that the thermal conductivity do not play major role in defining the temperature profile. The surface of iso-temperatures of 130 °C is shows a high degree of depth variability and becoming deeper towards the south west sector (sector 4). Hence there are much variations in geothermal gradient in the horizontal planes as well. The changes in the temperature along a horizontal plane indicates an effective horizontal fluid motion's contribution to the heat flow patterns (McCord et al., 1992). The trends reflect the increasing geothermal gradient towards the north west, in particular within the upper intervals (above the 90°C iso-temperature line).

Another observation is that there are regional variations in interval geothermal gradients. In the north west the gradient is higher in upper sequence than the lower sequences where as in the Southeast, it is quite uniform with depth. The increasing geothermal gradient, within the sections above 90°C as compared to the sections below the lines may suggest a possible upward fluid movement (Reiter et al. 1989, Wang and Xiong, 1989, McCord, et al. 1992). The high geothermal gradient intervals within the upper layers is prominent in wells LT1 and BO2 within sector 2, while in PG1 the iso temperature lines tends to close up at depth lower than 1800m. In DM1, the trend is uniform in the upper interval but tends to close up at about 1200m. Closer examination on the isotherms, reveals that those wells from LA3 towards PU3 in the south-eastern parts (sector 4) are about uniform with depth while the wells towards the Northwest tends to decrease in geothermal gradient with depth. The regional variation of iso- temperature lines reflects the variation in heat flow patterns with

depth. Most location in the Northwest will have a higher interval heat flow at shallower depth than the deeper parts.

Figure 3.9.1, 3.9.2 and 3.93 show variations of temperature over groups D, F and Klw which cover mainly the North-western(sector 1) and central sector (2). The temperature over group D is high (75°C to 93°C) in sectors 1 and 2. The highest temperature being over the central portion of the basin (over 90°). In the deeper layer of the top of group F, the maximum temperature has shifted to areas over the NW portion (over 120°C). Therefore, generally the temperature is higher in sector 1 and 2 than in sector 4 because of the deeper depth equivalent of each group in the former sectors. The shift in the maximum temperature contours for each group indicate the influence of redistribution of heat flow within the sediments. In sector 3 and 4, the deeper temperature distribution which is represented by that of top of group Klw Figure 3.9.3 shows a higher temperature over the SW corner (over 115 °C) and lower in the E part. The differences is partly due to differences in depths as well as heat flow over the region.

The variation of heat flow with depth can be shown by Figures 3.10.1 and 3.10.2 for groups D and F. The heat flow contours are produced by assuming conductive heat transfer. Over group D the heat flow varies from about $55mWm^{-2}$ in sector 2 to over120 in sector 1. The lowest heat flow is over the centre of the basin, i. e. in the area over the NE corner of sector 2. The highest heat flow areas is over the NW corner of sector 1. There is a drastic change in heat flow distribution over the top of F group with a high heat flow in the centre of the basin. Where as in the South-eastern sector, sector 3 and 4, heat flow is comparatively uniform with depths (compare heat flow contours of sector 3 in Figures 3.10.1, 3.10.2, and 3.10.3). the higher heat flow over the top of Klw (Base of the Terengganu shale) of over 100 mWm^{2} in the southern part of the sector is probably due to the shielding effect of the overlying shales.
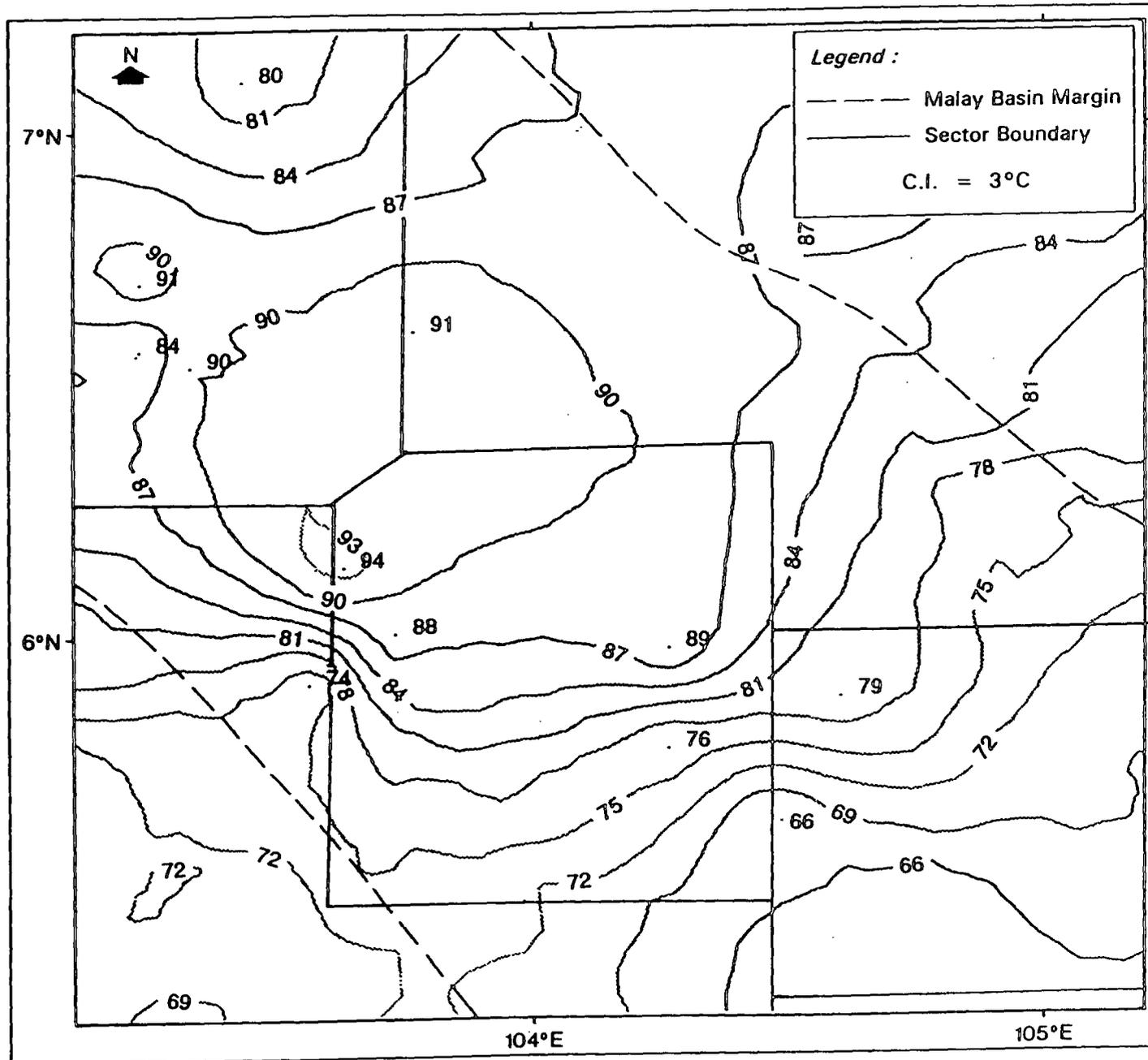
Figure 3.9.1 : Temperature at Top of Group D
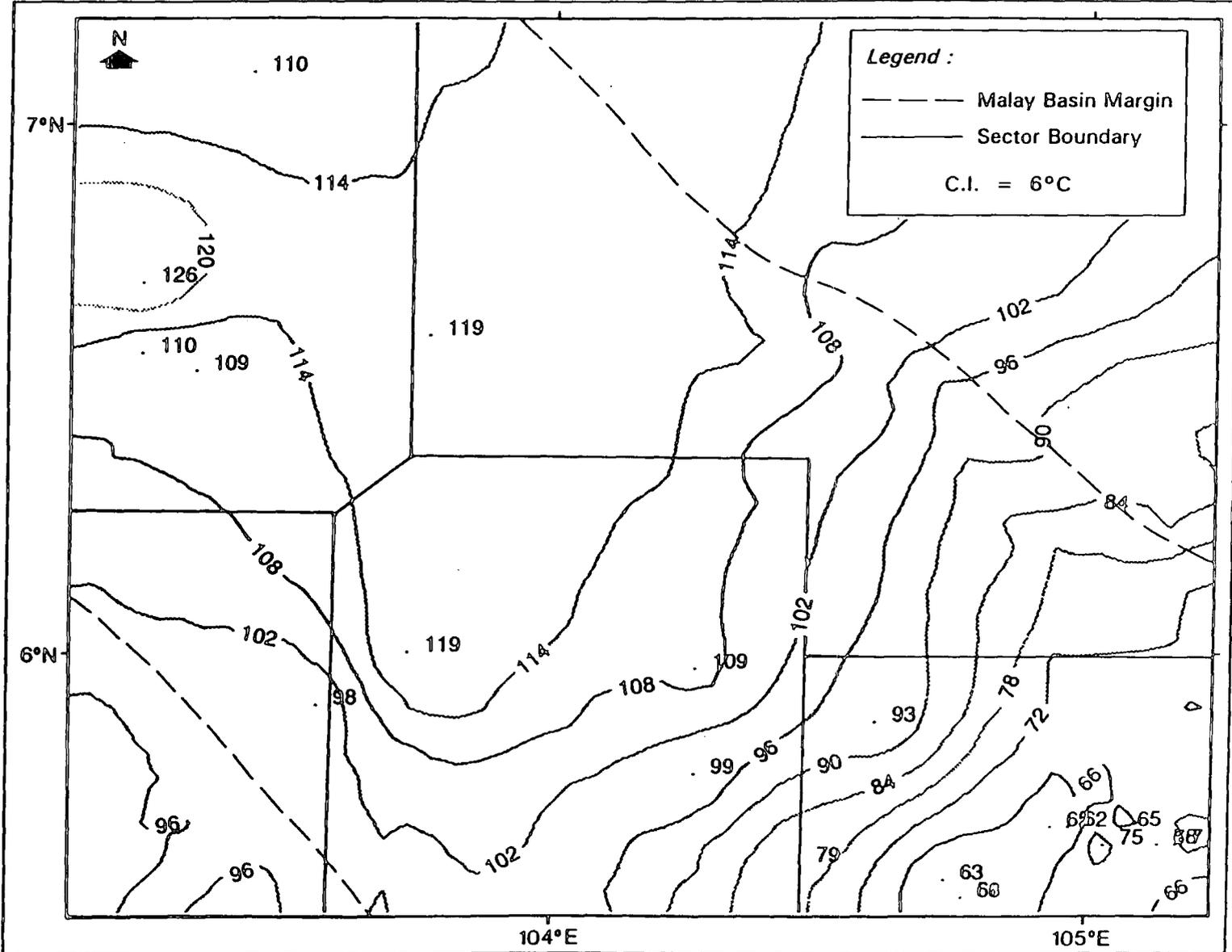
Figure 3.9.2 : Temperature at Top of Group F
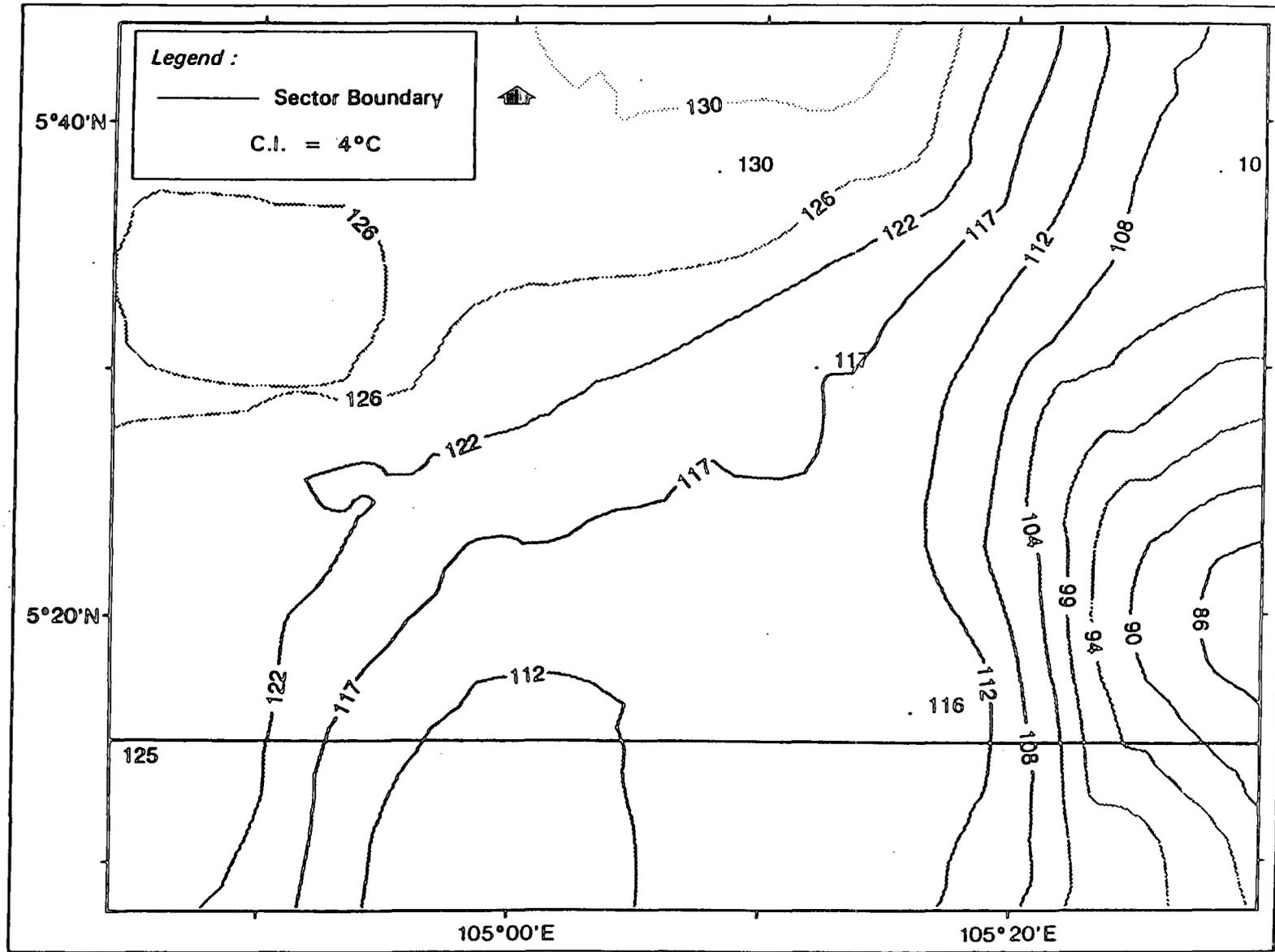
Figure 3.9.3 : Temperature at Top of Group Klw
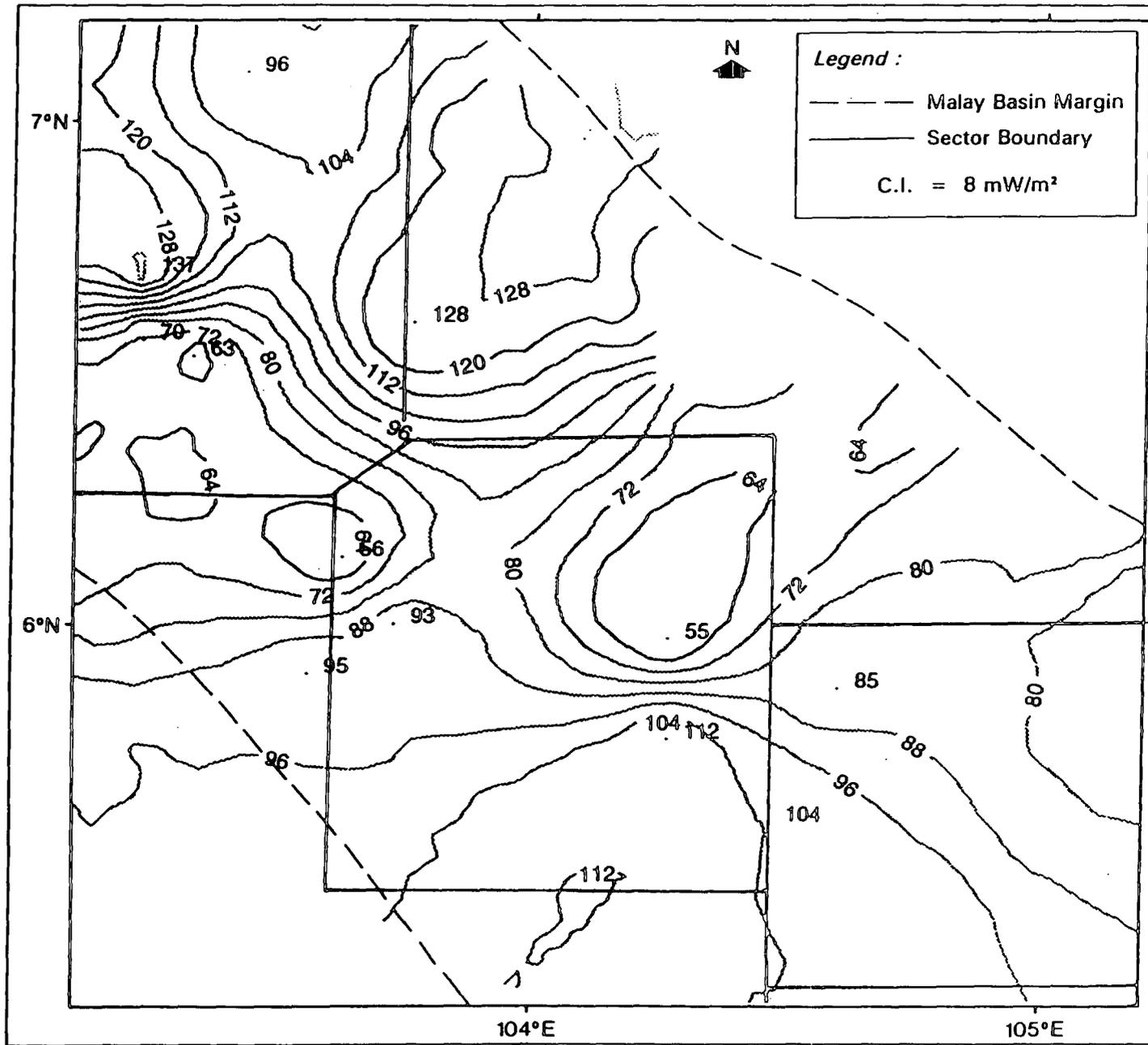
Figure 3.10.1 : Heat Flow Over Group D, Malay Basin
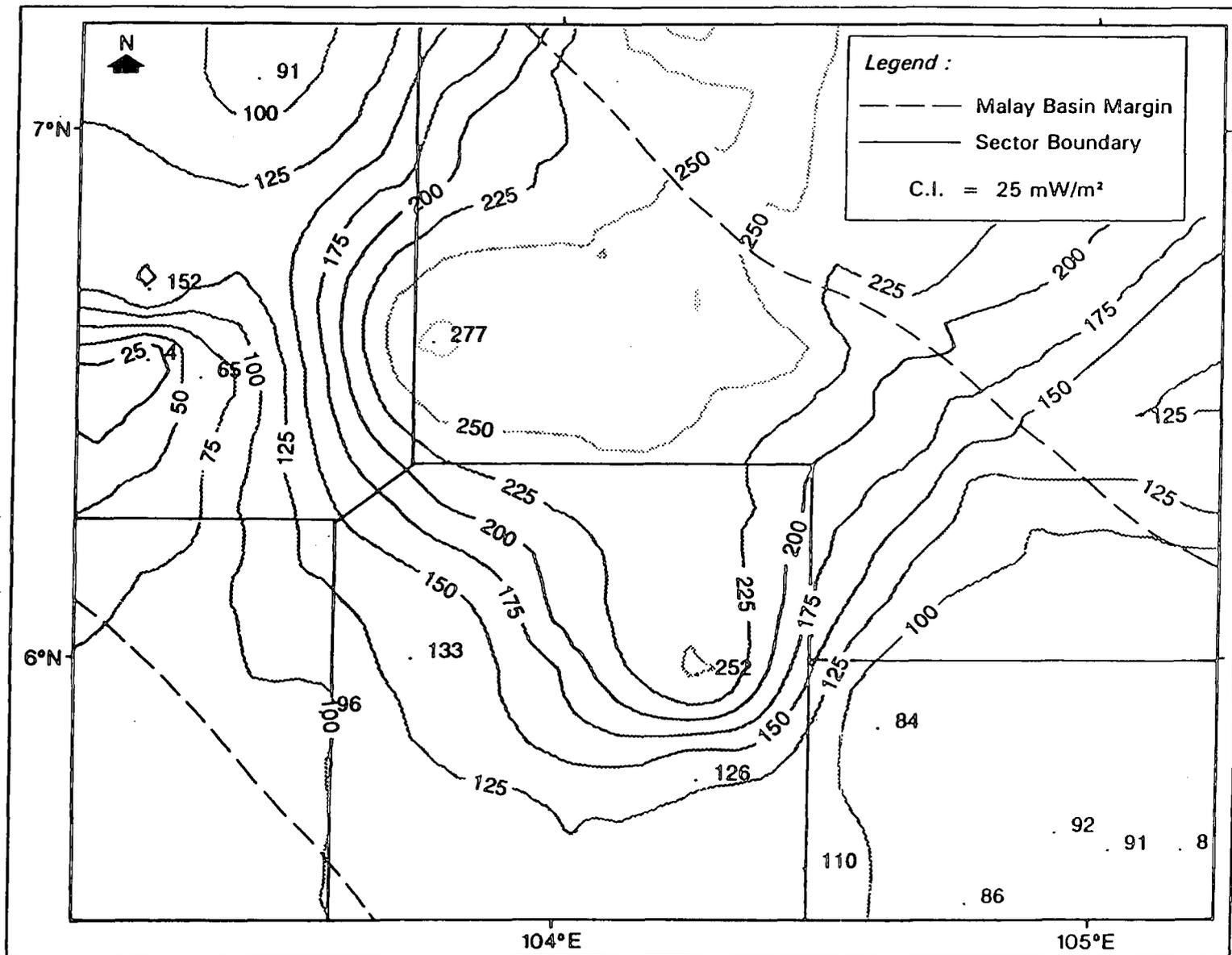
Figure 3.10.2: Heat Flow Over Group F, Malay Basin
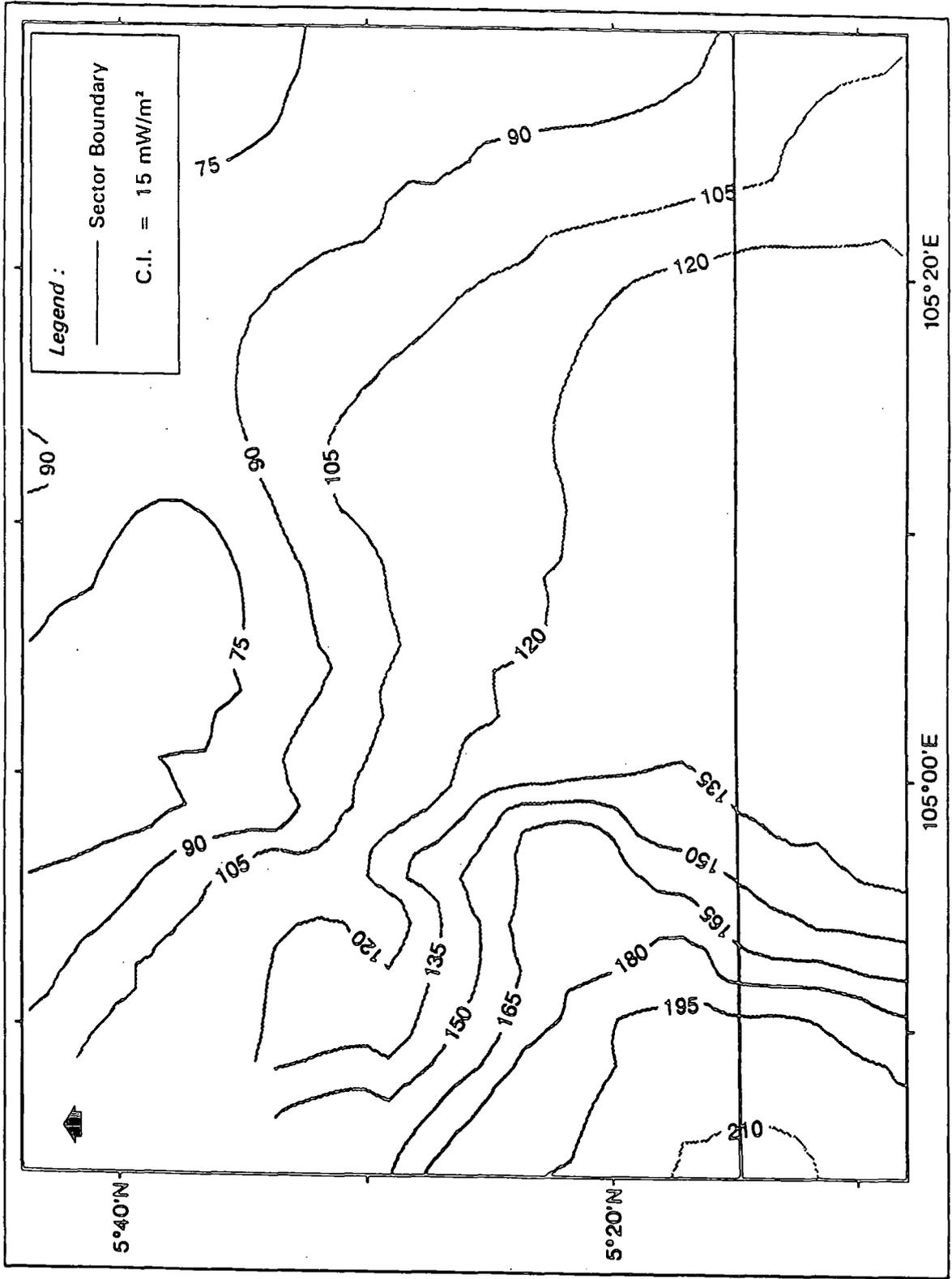
Figure3.10.3: Heat Flow Over K Sands (Group Klw)

119

The North-western and Central Malay Basin is the area of active fluid movement compared to the South and South-eastern part of the basin. The vertical fluid base interval is deeper in the NW part than the rest. The heat flow changes with depth and as well as temperature is apparently greater in the central and the Western region. All these factors indicate active fluid movement associated with heat flow anomaly. The high heat flow in and below group Klw in the Southern portion of the basin may be related to the fluid movement with good thermal insulator and fluid insulator layers above. The Kup group, the Terengganu shale with thickness of up to 300m at some location may form thermal insulator which conserve heat flow.

For well PG1, the 1800m depth seems to be critical, since it is the depth at which overpressured section started, and it coincides with the depth at which the base for fluid to flow vertically is estimated. If the model for fluid flow is taken, then it has predicted that the base of no vertical fluid motion nearly match with the top of overpressured zone. If this is true than overpressures in sector 2 shall be shallower at depth less than 1000m (Table 3.4) This is in harmony with the temperature isolines which indicate that the high geothermal gradient base is at depth about 1000m.

3.5.2   Hydrologic discharge

The interval heat flow can be determined when the interval geothermal gradient is available over a vertical column with known average thermal conductivity. Then the temperature-depth profile can be determined from the known interval heat flow and thermal conductivity-depth profile. The vertical variation of temperature with heat flow is interpreted as an indication of the effect of fluid flow in the vertical plane. Mean while the horizontal variation in heat flow may account for the horizontal fluid flow component. (Reiter et al., 1989, Jessop, 1990, McCord et al, 1992).

In a study to determine the vertical discharge of water, Reiter et al. (1989) showed that constant vertical discharge along an interval can be determined for incompressible fluid with advective heat flow. The specific discharge, V_z across an interval of interest in the vertical direction can be determined by

$$m_z = dQ/dT = pcV_z \qquad (3.6)$$

where mz is the slope of the plot of heat flow, Q versus temperature, T. p is the fluid density and c is the heat capacity per unit mass of fluid.

The vertical specific discharge gives the amount of fluid discharge in vertical component. In cases where there is only flow in the horizontal, (x) direction then the change in vertical conducted heat flow is nearly equal to the net amount of energy advected in or removed from a given volume (McCord et al., 1992). The change in the heat flow, dQ, is given by the equation

$$dQ = pcV_x(dT/dx)dz \qquad (3.7)$$

where Vx is a constant specific discharge in x direction. A plot of dQ versus dz will give a slope mx which is expressed

$$mx = pcV_x(dT/dx) \qquad (3.8.)$$

where dT/dx is a comprehensive horizontal geothermal gradient, and can be evaluated with the availability of the temperature data in the x (horizontal).

A study of the horizontal and vertical discharge of fluid is important in the part of the basin where there is evidence of fluid movements. Estimates of horizontal discharge are much greater than the vertical discharge in the Fruit land Basin (McCord et al., (1992) because more volume of horizontal movement has to take place to bring the change in the temperature data observed. In the Malay Basin, a similar effort is made in this study to do some quantitative estimation of vertical versus horizontal component of fluid flow within the basin.

The study on the fluid discharge will be made in localities where the possible upward movement of fluid is taking place more vigorously. In the previous application of vertical heat flow (section 3.4.3), it was found that anomalies with higher heat flow is most favourable condition to have vertical fluid flow (advective heat transfer mechanism). Therefore the thermal data from these anomalies is considered to be applied in the estimation of the specific fluid discharge. the knowledge will enhance the understanding of the fluid movement within the basin.

In this report, no attempt is made to analyse in detail the role of hydrology in causing the heat flow anomalies. But a simple numerical evaluation of upward specific discharge of fluid will be demonstrated to augment other observations. Two wells are used to analyse the hydrologic discharge in areas of anomalous heat flow: Well PG1 in the NW (sector 1) and another well is TG1 in the SE (sector 4). Both wells are situated near the edge of the basin and in case of TG1 is near to the Belumut High. The calculation of specific discharge is made using the equation 3.6 based on Heat Flow-Depth and Heat Flow-Temperature profiles of Figures 3.11 and 3.12..

The result of the preliminary simple analysis (using equation (3.6)) for these wells indicate an upward movement of fluid flow by -0.32 and -0.20 (10-9m s-1) recorded in PG1 and TG1 respectively. In PG1 the fluid flow is active from the depth above the overpressured
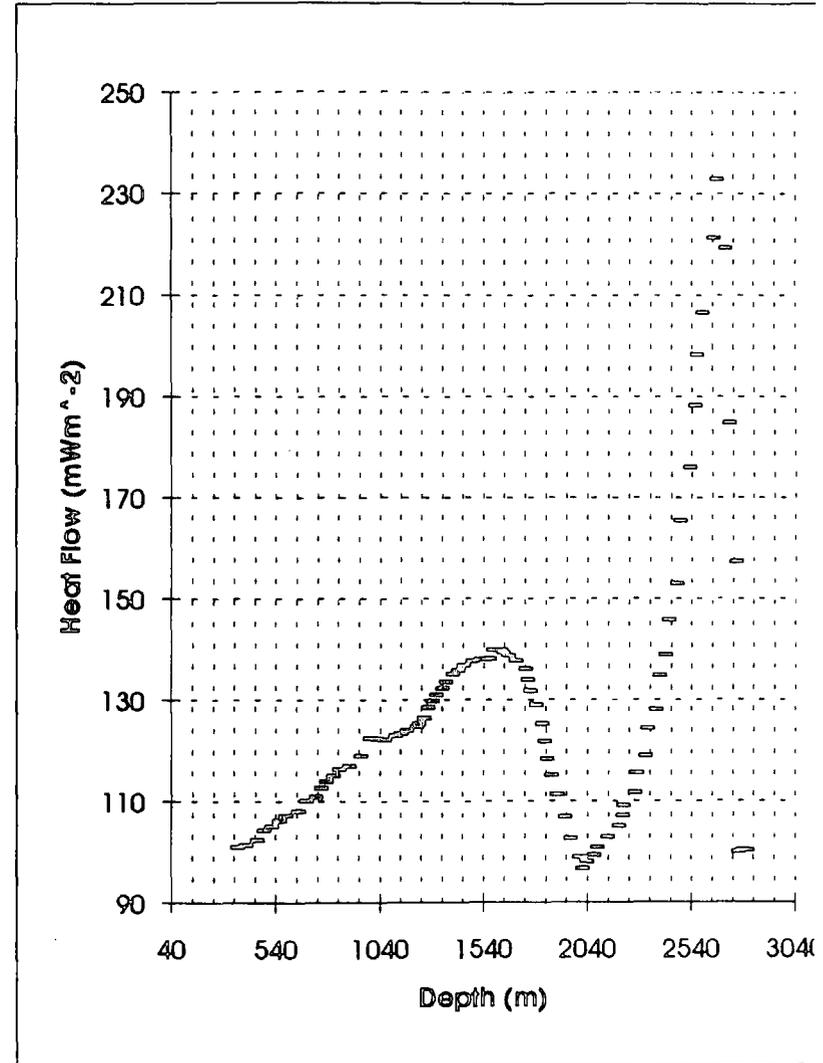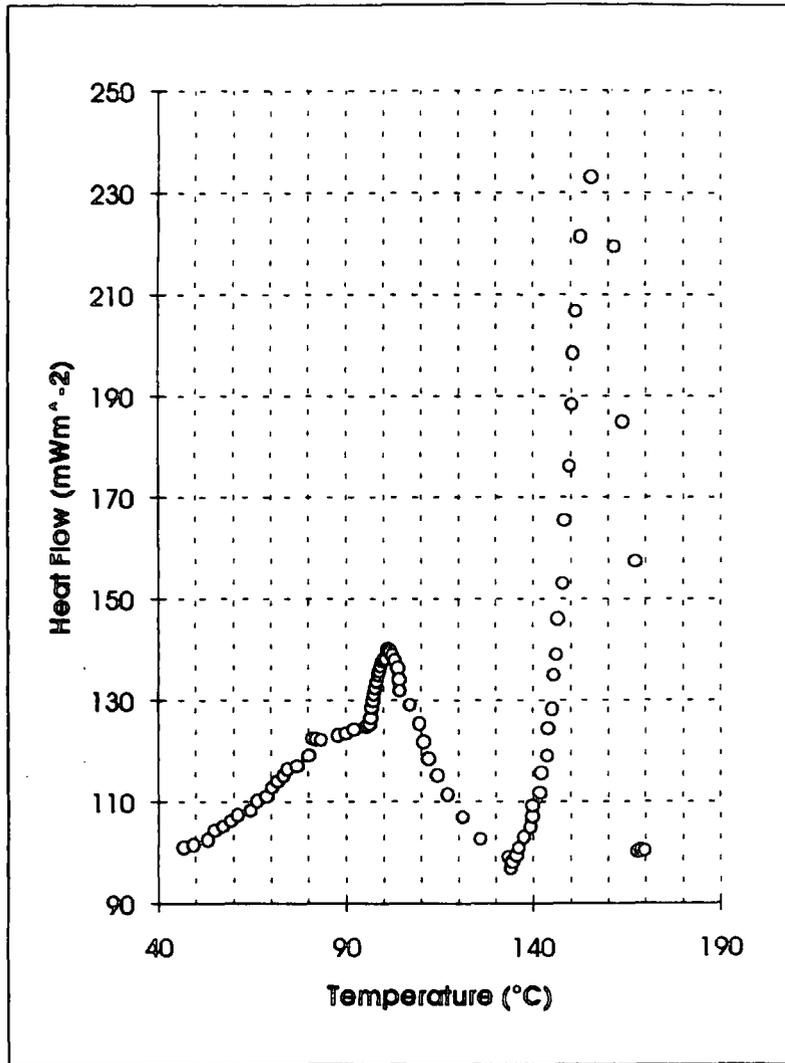
Figure 3.11 Plot of Heat flow versus Temperature and Depth for well PG1.
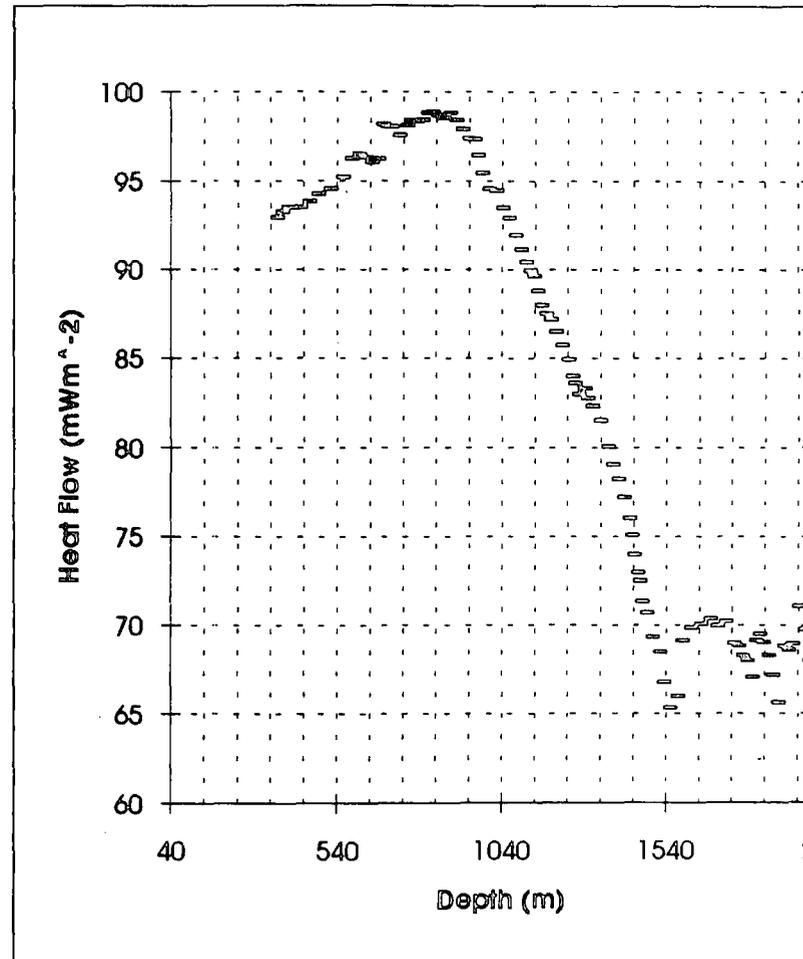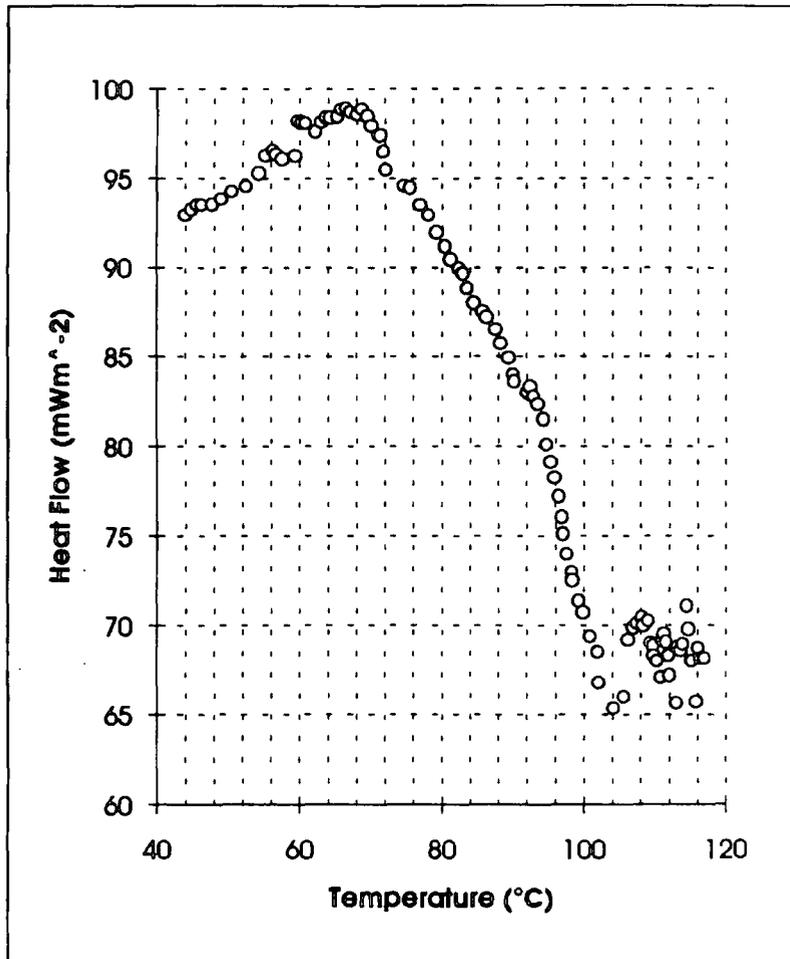
Figure 3. 12 Plot of Heat flow versus Temperature and Depth for well TG1

Table 3.5. An example of a quantittative estimation of upward
fluid flow by heat flow-temperature depth profiling.
(^ sign means to the power of)

Well	Depth interval		Temperature interval		Q-T Slope	Specific Discharge
	Top	Base	Maximum	Minimum		
	m	m	°C	°C		(10^-9)ms^-1
PG1	2018	1625	134	102	-1.35	-0.32
TG1	1555	831	104	67	-0.85	-0.20

Note: Q-T slope is calculated by regression of plots in figure 3.11 and 3.12 .
Specific discharge is estimated by eqation 3.6 and using
c = 4.184kJkg^-1°K^-1 and p = 10^3kgm^-3.
The negative of specific discharge denotes an upward fluid flow.

zone at about 2000m. In the last estimation of the base of the vertical flow at PG1 is 1,800m .

The depth is estimated from the anomalous heat flow pattern by Equation 3.5. In TG1 the

depth of base of vertical fluid flow estimated from the anomalous heat flow data for the region

is 1,360 m while the estimated depth in specific discharge of upward fluid flow is is 1,555m.

(Table 3.5).

The base of upward fluid flow estimated from equations 3.5 and 3.6. may be

coincidentally similar and appropriate for the 2 wells and the models, but if both mathematical

models are reliable, then the upward fluid movement is proven as one of the causes of the

anomalous heat flow. A general distribution of upward component of fluid flow may be

estimated from a regional heat flow pattern over a surface and the equivalent temperature of

the surface by applying the concept shown by equation (3.6).

Another out come of the specific discharge evaluations for PG1 and TG1 is that the

advective heat component is of about $10mWm^{-2}$ The value matches to the one predicted in

earlier sections (3.4). The thermal figures obtained in this exercises are compatible to the

estimated average heat flow values over the Malay Basin of about $85mWm^{-2}$. The internal

sources due to processes within the basin is expected to be about on average $20mWm^{-2}$.of

heat flow. The areas with heat flow higher than average of $85mWm^{-2}$, may be due to excess

heat flux of probably due to tectonics which are recently or currently active. The shallower

sections in the Northwest may have received extra heat flux from the younger faults and

fractures produced by the extensional event currently active. In other words, part of the heat

flux may come from thermal events associated with the young structuring . However in the SE

area, excess heat flux can be associated with deeper fractures and shale diapirisms (Figure

3.13) which release fluids, hotter than the regionally present shales. Figure 3.13 shows a

seismic section across TP3 area where there is an anomal;ous high heat flow at depth (please

see the diagram in the next chapter).
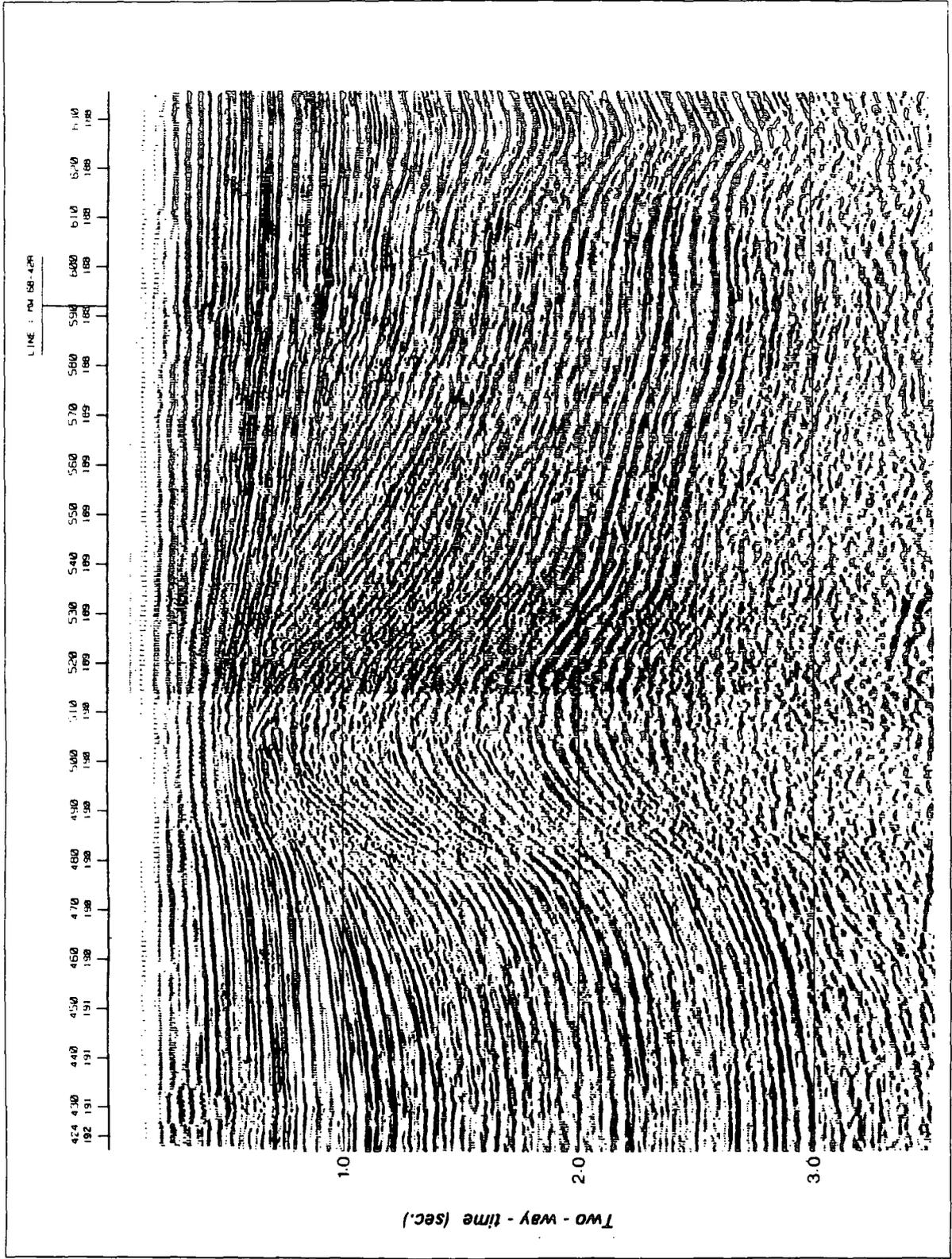
Figure 3.13 : Seismic section at TP3 locality illustrating possible shale diapir which may contribute to excessive heat flow

127

2.5.3 Causes of upward fluid flow

The cause of the upward fluid flow is numerous. In the ancient basins of the continental interiors, topographic relief provides drives for ground water migration. (Bethke, 1993). In the Malay Basin, there are small topographically highs, the Belumut High in the Southeast, the Naratiwat Highs and the Tenggol Arc in the Southwestern edge and the Khorat High to the Northeast. (Location in Figure 1.1). These structures may be able to help ancient hydrostatic drive but now the pressure within the basin and the topographic highs are likely to be in equilibrium. The transient drives for the fluid flow in the basin can be derived from processes within the basin itself

The agent of fluid drives in a sub sea basin includes processes such as the compaction of sediment during burial, the expansion of petroleum fluids during organic maturation, and the rebound of the sediment porosity after erosion (Bethke, 1993). All these possibilities are satisfied within the Malay Basin. The basin must have rapid sedimentation rate with alternate shale and sand sequence in a lacustrine to inner neritic environment. There are wide spread of overpressured zones which suggest that, the compacted waters of sedimentation are trapped due to rapid burial.

3.6   Summary and conclusion

1.   A new distribution map of surface heat flow (sea floor as datum) has been produced from new temperature and thermal conductivity data set derived from the method described in chapter 2. The average heat flow is about 86 mWm^{-2}, which is about the same as estimated previously reported (Wan Ismail, 1984). However the average geothermal gradient is higher and the thermal conductivities are slightly lower than the previously reported. The higher geothermal gradient (47 $°Ckm^{-1}$) and lower thermal conductivity (1.84 W/m°K) is obtained by

the improved temperature and thermal conductivity estimation methods explained in the last chapter. Overall there is a better coverage especially in the NE sector where new data from the latest exploration wells are incorporated.

2.   The heat flow, thermal conductivity and geothermal gradient maps portray the patterns which suggest, apart from conductive heat source, advective heat is as important factor for contributing about 10 mWm^{-2} of heat flow values. The advective heat causes anomalies over the basin, where the surface heat flow are estimated at over 100 mWm^{-2}. in some locations.

3.   An estimated 10 mWm^{-2} of heat flow are produced from the radiogenic heat generation within the sediments in the basin. The basement heat flow is probably about 65 of which 50% or about 33 mWm-2 is estimated sourced from the crustal radioelements based on the radioelemnts heat generation of onland batholiths. The rest of about another 33 mWm-2 is the sub lithosphere component as estimated by Reiter et al, 1989 and McKenzie, 1978.

4.   The thermal anomalies heat flow excess of 10 mWm^{-2} is estimated for most part of the basin. A calculation using a mathematical model of Lachenbruch and Sass (1977) estimates the base of vertical fluid flow associated with the thermal anomalies varies from 1,800m to about 1000m. Below this the model predicted that the heat source are constantly supplied by basement heat.

5.   Specific discharge of fluid of about 0.30 x10-9 ms-1 is estimated from two tests well which are located in the thermally anomalous areas. The advective heat associated with the fluid discharge is about 10mWm-2 which is similar to the value estimated from the heat flow budget for advective heat component after deducting the basement and radioactive originated heat flow average values.

6.   The heat flow - depth profile of the wells in the NW showed higher heat flow in the shallower sections while in the SE, the thermal anomalies are mostly seen at deeper in stratigraphic column. The NE wells probably has attained the higher heat flux due to recent extensional events, which may have perturbed heat flux . The SE part, thermal anomaly at greater depths are thought due to the processes which involved shale diapirism and fracturings which brings up basement heat faster than it is dessipated out of the surface.

CHAPTER 4

Thermal modelling and pressure distribution

4.1. Introduction

In the last chapter, the regional investigation of the thermal state of the Malay Basin was reviewed. The main observation of the thermal state is that the basin has a high heat flow which is not typical of a passive intracratonic extensional basin. The heat flow anomalies are distributed in localised high spots mainly along the basin axis and areas around the paleo topographic highs. The cause of the anomalies is believed to be mainly due to advective heat as a result of fluid flow. Water chemistry of some wells show the upward fluid movement associated with heat flow anomalies as well.

When the fluid is trapped or filtered in a sealed or partially sealed compartment, which retards the flow, then the heat energy carried by the moving fluid will be held as well. Areas where fluid flow is sufficiently checked conform to areas where pressure is above the normal hydrostatic pressure and are termed be "overpressured". In an overpressured compartment, heat flux may be confined and only released through some fractures or faults.

Abnormal formation pressure is defined as any formation pressure deviating from hydrostatic pressure. Fertl (1976) suggested two types of abnormal pressures exist which are categorised as "subpressure" and "surpressure". Subpressure is the formation pressure which is less than hydrostatic pressure while surpressure is the formation pressure which is more than the hydrostatic pressure. Since in the Malay Basin, all known abnormal pressures belong to

surpressure, therefore the abnormal pressures, surpressure and overpressures are used synonymously. Abnormal pressures are sometimes referred as geopressures (Gretener, 1979).

Most of the wells drilled by the operating companies in the Malay Basin have been terminated due to overpressures at depth of about 2000 m to 2500m. Other occurrences of overpressures take place at shallower depths. Table 4.1 shows the estimated depth of inception of overpressures in some wells studied in this report. The pressure values are taken from repeat formation tests during well logging and also from production tests, while the temperature data are taken from the studies described in the previous chapter. The depth of the beginning of overpressures was estimated when the measured pressure values are deflected from the hydrostatic pressure trend. The depth referred to logging depth, since the datum for the measurement of depth is about the same for every well. The depths are measured from the Kelly Bushy which is at an elevation of 12 to 15 metres above sea - level.

Detecting overpressured zones before drilling is necessary in order to prevent lost time and accident in drilling. In industry, many techniques have been developed to detect overpressures prior to drilling. Normally overpressured zones are reported to be associated with increasing temperature. In the Malay Basin the overpressured areas are where most commercial hydrocarbon resources are often discovered. According to Jones (1980) large amount of commercial accumulations of petroleum and natural gas in many of the world's deep sedimentary basins can be explained in terms of a fluid pressure cycle which occurs early in their structural evolution. The fluid pressure cycle is transient lasting 10 to 20 million years or more, during which rapid deposition and/or crustal tectonics compartmentalise sand-bed sequences and cause progressive rise of pore fluid pressure. Associated with the rise of fluid pressure are changes in mineral and hydrocarbon solubility and chemical reactions which is partly helped by temperature.

Table 4.1. Temperature and seismic group at top of estimated
overpressures in selected wells in the Malay Basin

Sector	Well	Seismic Group	Depth of Overpressures' top (m)	Temperature at Ovepressures' top (°C)
2	SM2	F	1143	92
4	IB1	I	1494	93
4	LA3	H	1250	93
2	IN2	E	1615	102
4	LB1	H	1615	105
3	BS1	J	1372	110
4	TP3	K	1951	111
2	BO2	E	1905	112
2	TJ1	E	1981	112
1	PG1	F	1859	115
1	KP1	H	1935	119
5	JR2	F	1859	120
4	TB3	I	2164	124
3	AG1	K	2286	126
1	DM1	F	1951	131
4	OP1	L	2438	133
4	SR1	I	1981	133

Several processes can lead to overpressures in Malay Basin. In this chapter, stratigraphic data and thermal data are employed to understand the nature and causes of overpressures based on the observed relationship of the occurrences of overpressures, thermal and sediment - depth profiles. Investigation of typical thermal-depth profiles in areas of overpressures are made for selected wells in several sectors of the basin. The investigation includes the thermal characteristic of overpressured sections and the possible influence of temperature on their occurrences.

Most of the wells in the Malay Basin are overpressured, at several depths and in various stratigraphic groups. Although there are several factors that may cause the overpressures, the effect of temperature and heat may be quite substantial as a consequence of the wide spread thermal anomalies in the basin. The thermal parameters may be related with other physical and chemical factors that control overpressure development.

Four wells are chosen from different sectors of the basin to investigate the role of heat in the overpressured zones (Figure 4.1). These wells are PG-1 from the NW sector, BO-2 from the central, LA-3 in the central sector nearer to SE sector and BS1 from the south sector. BS-1 and PG-1 is chosen among these wells as type wells for the thermal-pressure study. PG-1 penetrated most of the stratigraphy covered by the other wells in the basin, and has good quality temperature and pressure data while BS-1 has similar data and reaches older stratigraphic groups.

4.1.2 Geological data

The well PG-1 has penetrated the sequence of mostly younger group of sediments. The total depth reached is group H of Middle Miocene. Apart from BS-1, all the other wells
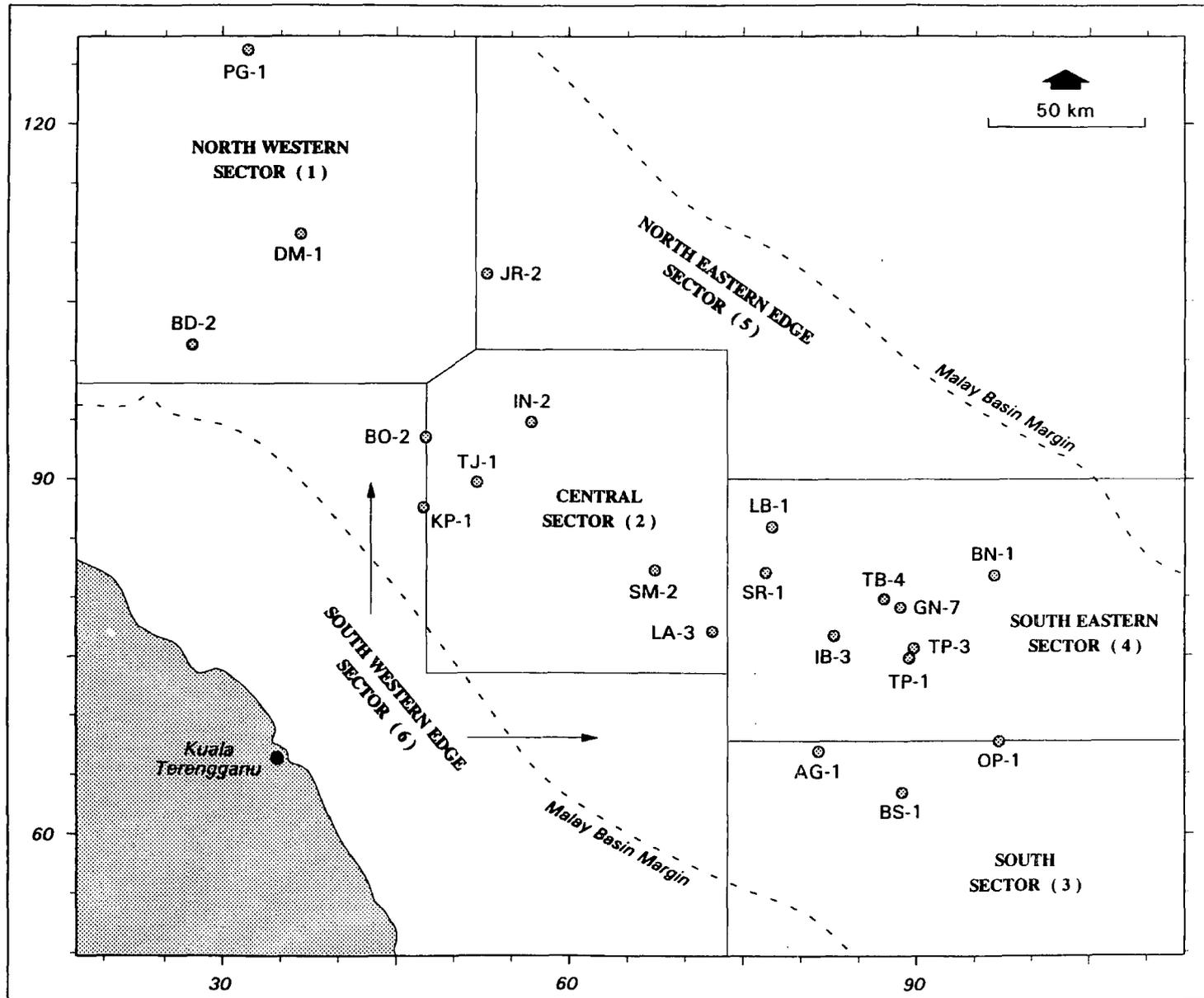
Figure 4.1 : Location of key wells in overpressures study

penetrated the groups represented in PG1. The BS-1, a more southerly well has been uplifted and hence penetrated stratigraphically deeper rocks than the rest. Lithology of various stratigraphic group are influenced by their environment of deposition (Figure 4.2). In group D through I, the deposition has been interpreted to be in a low to medium energy shallow water environment. The low energy and shallow water conditions are favourable for coal beds to be formed as found in these groups.

The sediments in PG-1 was deposited mostly as mixture of shales or clays, siltstone and sandstone. In the interval of the upper 1200m, the lithology is mostly an inter lamination of clay and siltstone. Figure 4.3 illustrates the relative lithologic composition from the Vf curve, where higher Vf indicate more shales and clays than sandstones. The sandstones occur intermittently in beds below. In depth between 1200m to about 2300m the rocks are increasingly shaly. Below the depth 2300m, mostly shales are observed. However quite thick sandy beds are interpreted down to the 2400m depth. The most shaly zone is the interval just below the sand at 2400 to about 2500m. From here the rocks are increasingly sandy to total depth. There is comparatively little calcareous sediment present in the upper part above the overpressured zone. Slight dolomitization is noted near the base of the well..

Most coals are found in wells BO-2 (Figure 4.4) and LA-3 (Figure 4.5) among the wells above. In groups J to L, which has been reached by well BS-1 (Figure 4.6), the environment of deposition is high energy and fluvial dominated. Most of the sediments are recognised as sandstones and brackish shales. Note that in wells BO-2 and LA-3, generally the sediments are increasingly shaly with depth. In BS-1 (Figure 4.6), there is an interval of high sand to shale ratio (low Vf) in the J group (at depth interval between 1400 to 1700m) and a thick Kup shales underlying it (at depth interval of about 1700m to 1800m). The thick shales bed is commonly known as the Terengganu shales.

NW   SE

MY	GP	AGE
0	A	RECENT TO
	B	PLIOCENE
5.2	D	LATE MIOCENE
	E	
9.8	F	MIDDLE MIOCENE
	H	
16.5	I	EARLY MIOCENE
	J	
22.5	K	
	L	
	M	LATE OLIGOCENE
	O	
	N	
32.0	P	

00

GP A

GP H

GP B

GP I

GP D

GP J

5,000

GP E

GP K

GP F

GP K

GP L

GP M

10,000

GP H

GP N

GP O

GP I

GP J

GP P

GP K

LATE CRETACEOUS

15,000

GP = GROUP   Modified after ESSO

EXPLORATION PLAYS
o Gas   ● Oil

DEPOSIT ENVT. & FACIES
Fluvial Deltaic
Marsh
Shore Face
Restricted Marine
Bay / Lacustrine
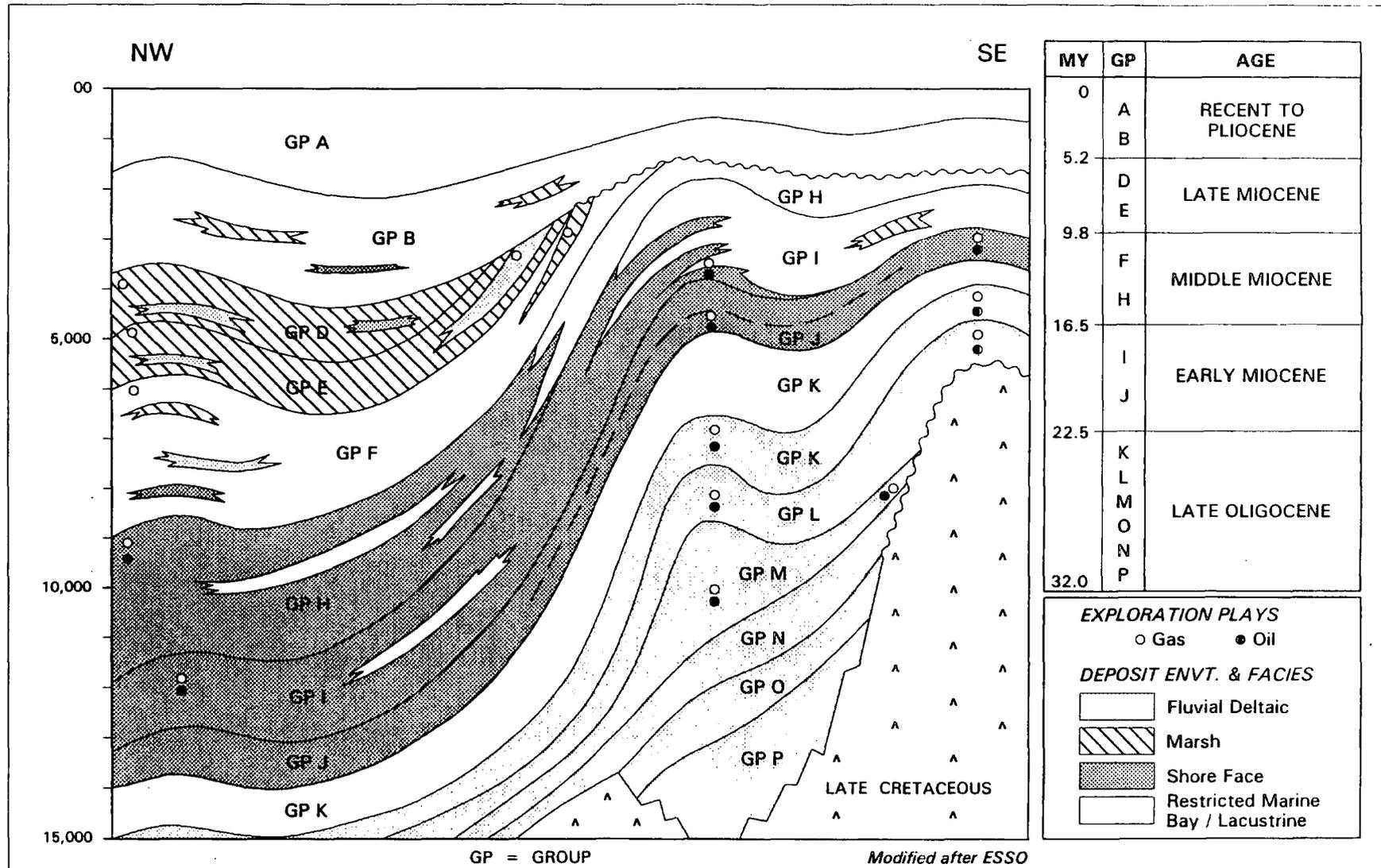
Figure 4.2 :   Diagramatic geological cross-section with depositional environment and facies
of the Malay Basin
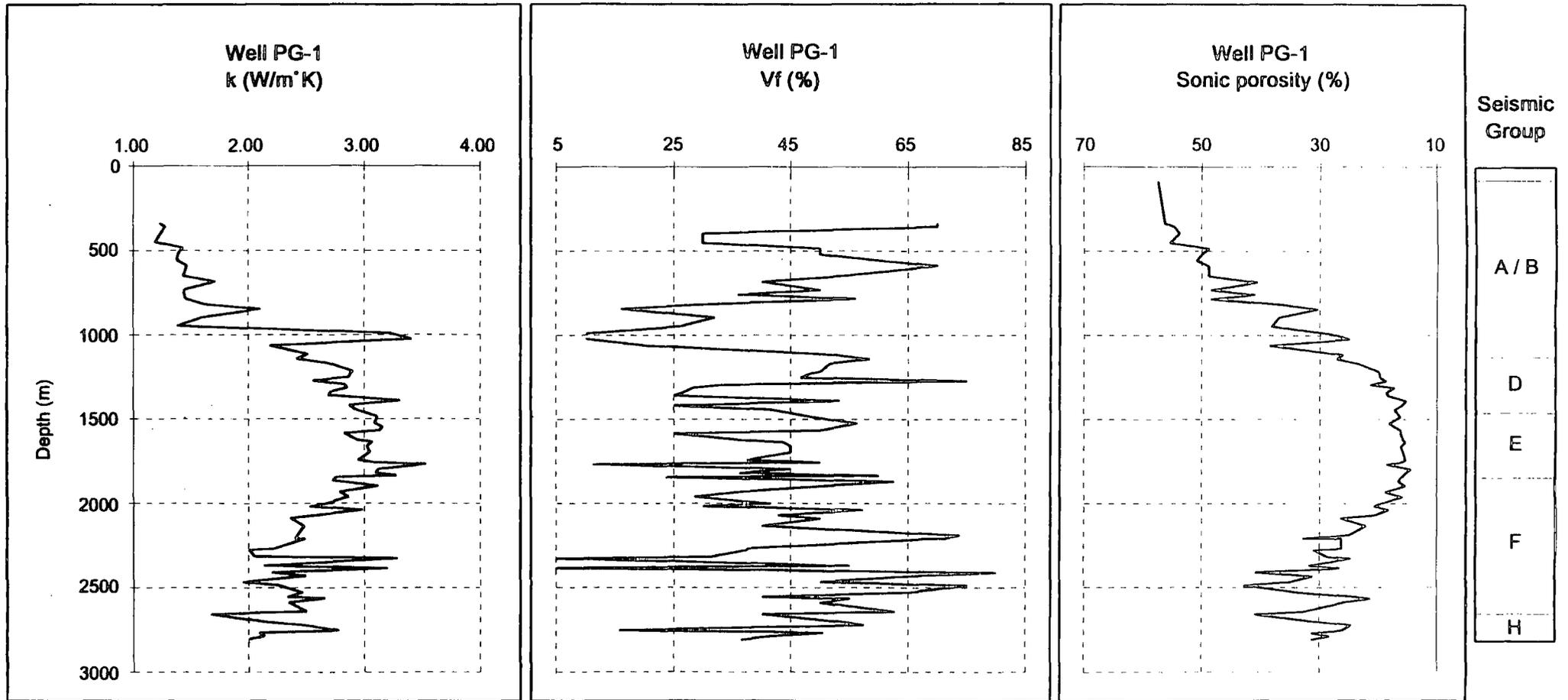
Figure 4.3 : Thermal conductivity (k), Volume of fines (Vf) and porosity of well PG-1, Northwest Malay Basin
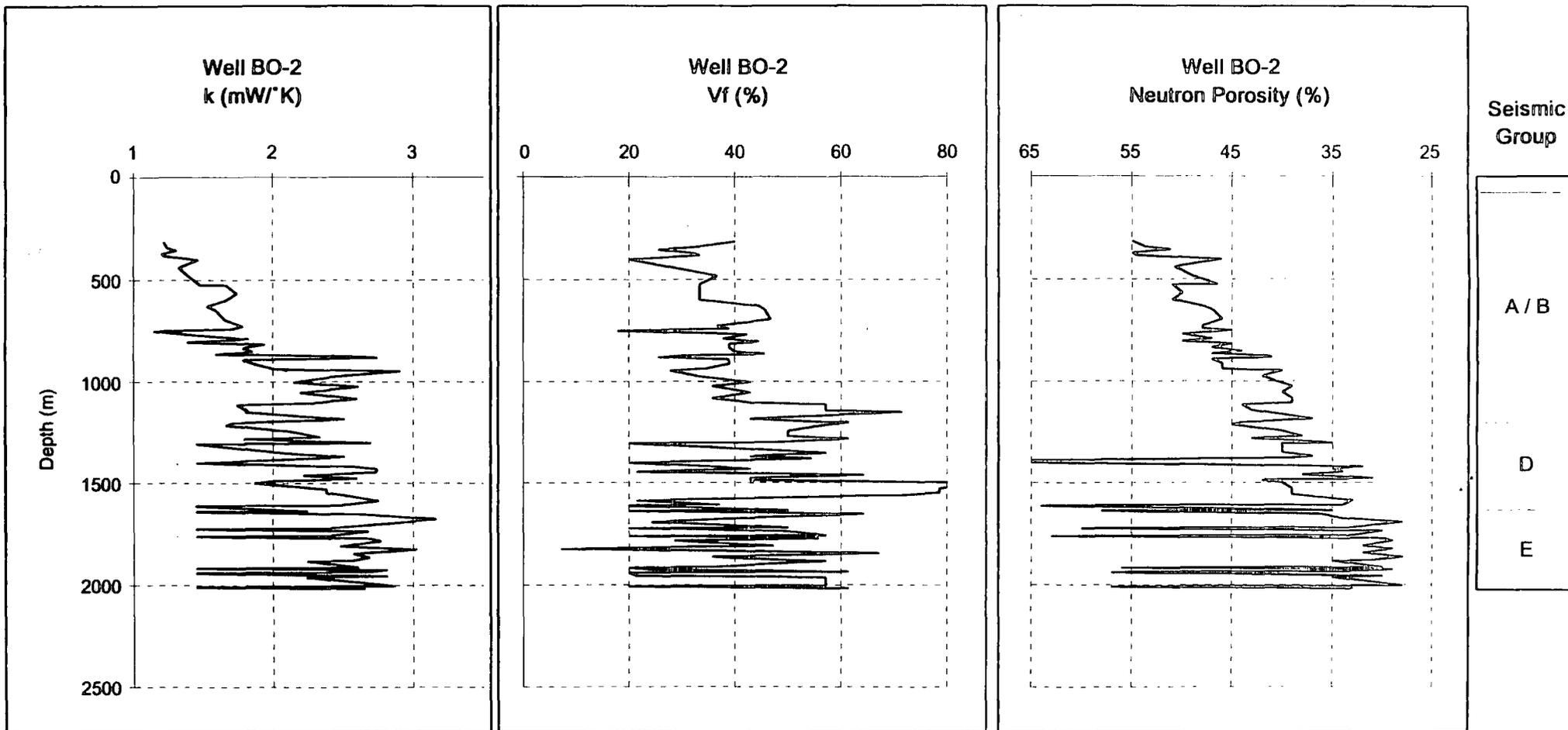
Figure 4.4 : Thermal conductivity (k), Volume of fines (Vf) and neutron porosity of well BO-2
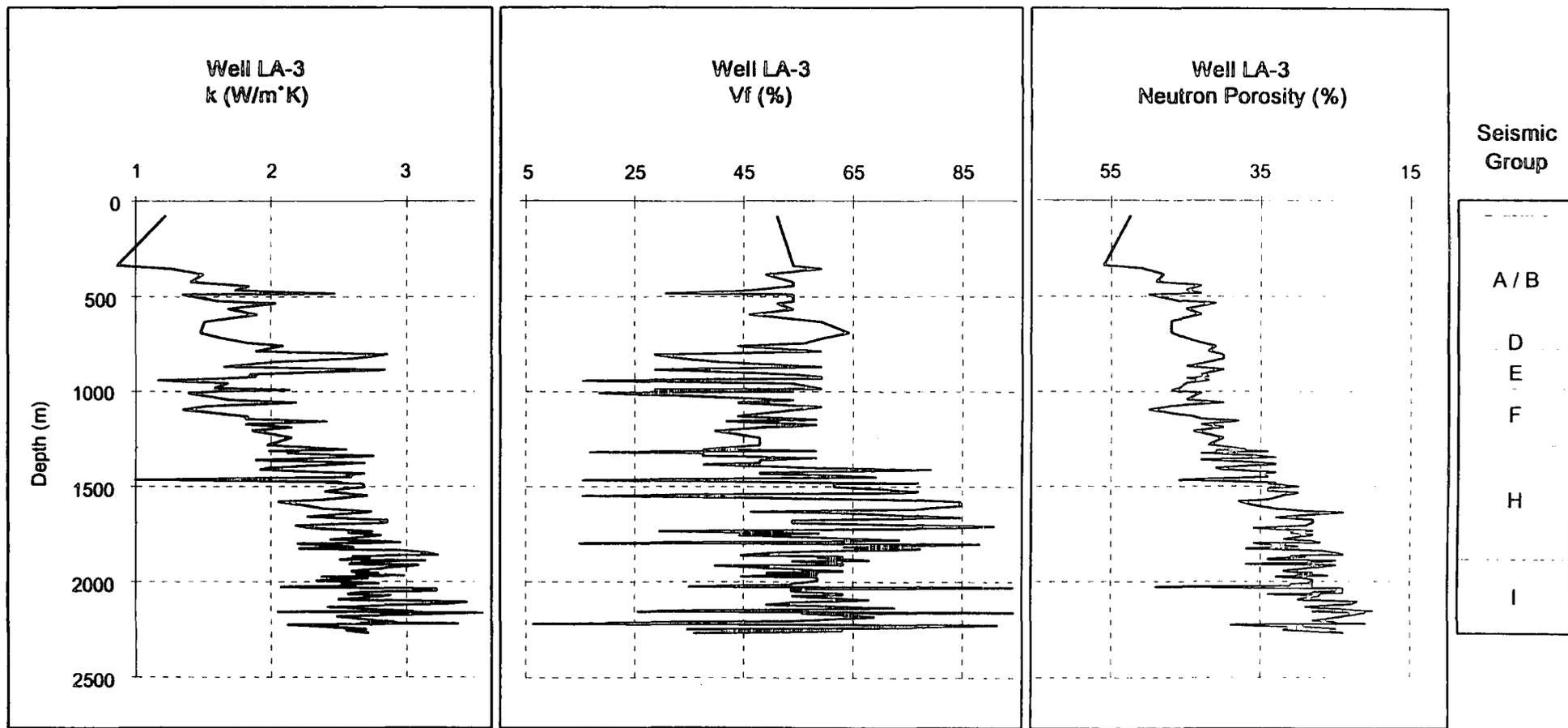
Figure 4.5 : Thermal conductivity (k), Volume of fines (Vf) and porosity of well LA-3, Central Malay Basin
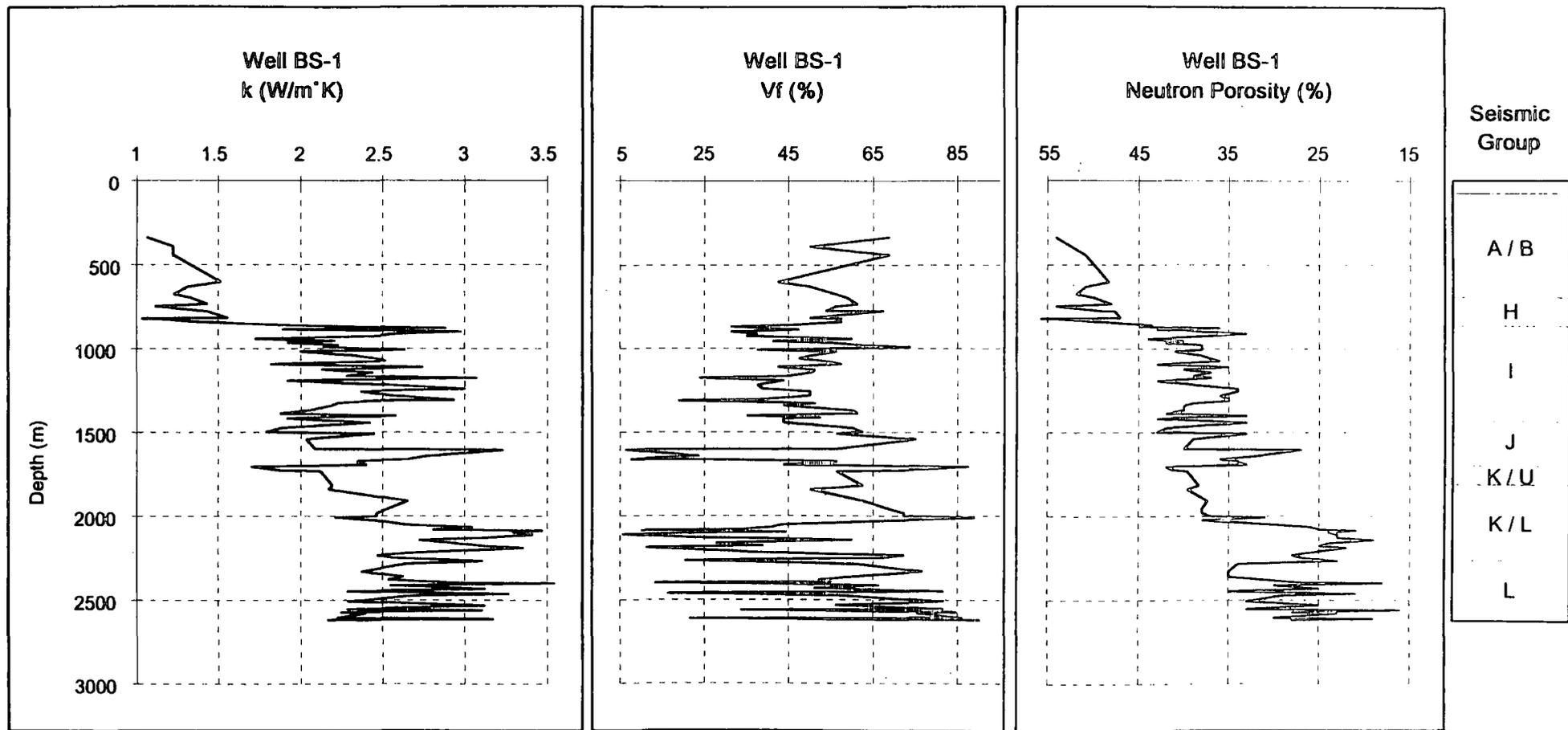
Figure 4.6 : Thermal conductivity (k), Volume of fines (Vf) and porosity profiles of BS-1, South Malay Basin

In PG-1, the porosity has been estimated by sonic log. Sonic transit time are used to compute the sonic log by using Wyllie's equation with correction for lack of compaction .(Etnyre, 1989). The sonic porosity-depth profile is as shown in Figure 4.2. Most of the sections have porosities of more than 30%. The interval between 1500 to 2000m (in group E and F) however have lower porosity of 15 to 20%.

In other wells the porosity is derived from the neutron logs. The porosity trends in BO-2 and LA-3 show a decreasing trend with depth. In BS-1 the trend of decreasing porosity with depth is interrupted by massive sands which has lower porosity than the dominant silty sands. A high porosity interval is also shown by the Terengganu shales. In BO-2 and LA-3, the trend is obscured by some low porosity beds at the deeper sections due to coal and possibly the undercompacted clays associated with coal beds. In PG-1 and BS-1, there is porosity inversion at deeper interval probably due mainly to overpressures. Tight zones are observed in BS-1 as well, where porosity of nearly 15 % is found in Klw sands at depth interval of about 2100 to 2,300m (Figure 4.6).

The neutron porosity and sonic indicate the total porosity of the rocks. The density porosity is equal or less than the sonic or neutron porosity. The difference in sonic and neutron porosity to that of density porosity indicate the presence of secondary porosities which may be due to fractures or diagenesis.

Hydrocarbon occurrences are wide spread over the Malay Basin as shown in Figure 1.2. Two wells selected for profiling are gas wells i.e. BO-2 and BS-1 and the other two are oil and gas wells. The gas sands mostly belong to younger groups D and E in the PG-1 and BO-2 as well as in groups I, J and K in BS-1. The oils are found in group H in PG-1 and LA-3. The gas sands are mostly in PG-1. and in BS-1. In general the Malay Basin has three times more gas than oil reserves.

4.2   Thermal-pressure vertical profiles

Figures 4.7, 4.8 and 4.9 show the temperature, heat flow and pressure - depth profiles of PG1, LA3 and BS1 wells respectively. The thermal profiles are constructed by linking each data point in order to show clearly the trend as well as the magnitude with depth. The thermal conductivity (please see the Figures 4.3, 4.5 and 4.6) varies considerably with small depth intervals. The temperatures are connected to show the gradient with depth. The more abundant temperature data will give more gradients with depth. The heat flow profiles are represented by the interconnected points of average vertical heat flow at the particular points. These representations enable interpretations of the changes of the thermal parameters with depth to be more easily recognised. The pressure profiles are presented with the data points from the values taken from measurement records. The units are in S. I. where the pressure is expressed in mega pascal (Mpa, 1 Mpa = 106 Nm^{-2} = 145 psi)

4.2.1   Construction of pressure and thermal-depth profiles

The pressure data are taken from the Repeat Formation Test (RFT) and Drill Stem Test (DST). The Initial Shut In Pressure (ISIP) is preferred to the Final Shut In Pressure(FSIP) because it registers greater value which is probably nearer to the equilibrium pressure. However due to data shortage, some pressure data in BS-1 and some of PG-1 are those of FSIP. For RFT data, there is small differences between the FSIP and ISIP readings which is negligible.

The temperature and thermal conductivity profiles are derived from the estimated formation temperatures by the method outlined in Chapter 2. Vertical heat flow profiles are determined by calculating an interval temperature gradient with the corresponding average

Well PG-1
Pressure (Mpa)

Well PG-1
Heat flow (mW/m²)

Well PG-1
Temperature (˚C)

H

H'

Depth (m)

Top of overpressure
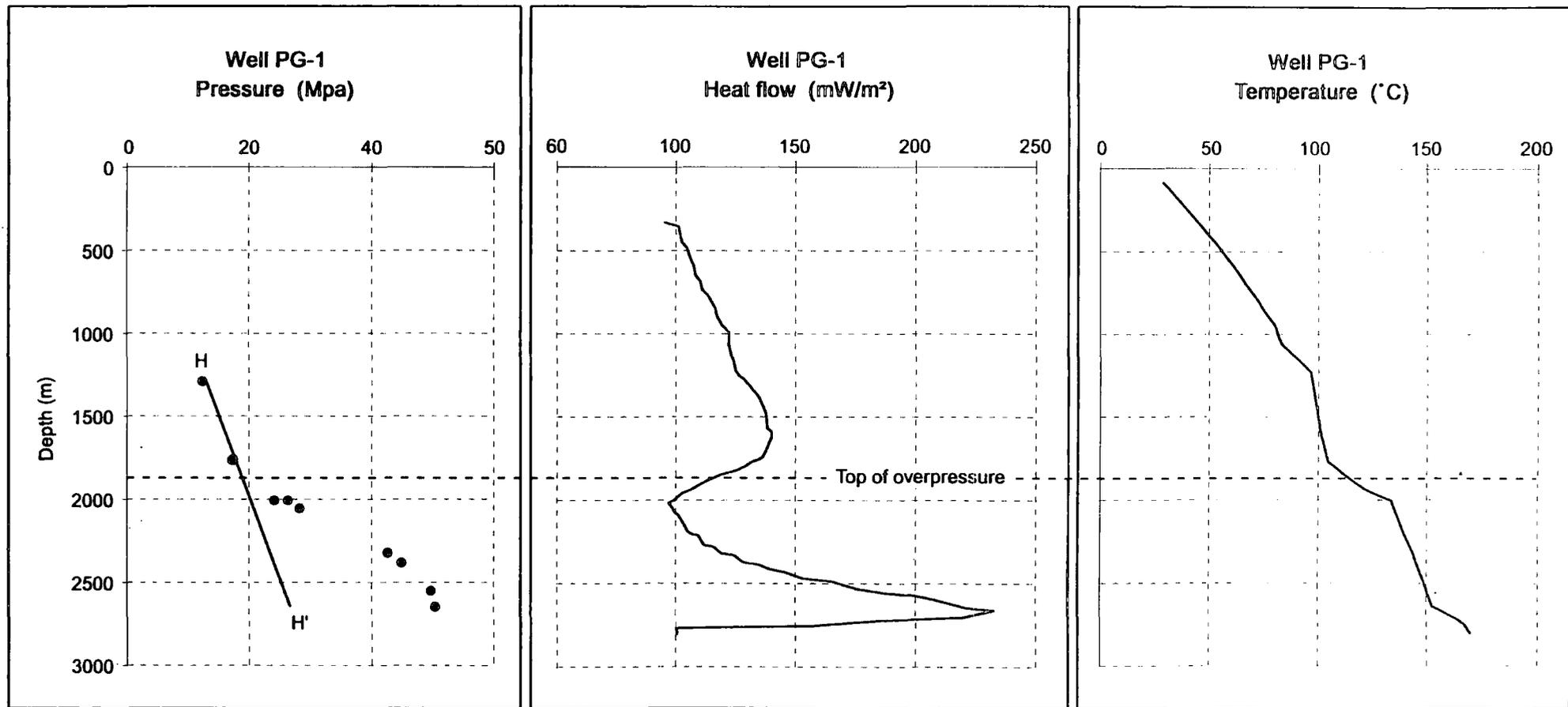
H - H' is the hydrostatic pressure gradient

Figure 4.7 : Pressure and thermal profiles of well PG-1, Northwest Malay Basin

H - H' is the hydrostatic pressure gradientVI

Figure 4.8 : Pressure and thermal profiles of well LA-3, Southeast Malay Basin

Figure 4.9 : Pressure and thermal profiles of well BS-1, South Malay Basin

H - H' is the hydrostatic pressure gradient

thermal conductivity of a rock column in the well. Each rock interval has its own thermal conductivity and temperature (as has been determined in chapter 2). By multiplying the average thermal conductivity and the temperature gradient, the heat flow of the rock interval is known. The procedure can be carried out for the whole well, or for any arbitrary sections of the well. The arbitrary section is defined for interval which start at an original depth point within the well. Since most of the heat flow is vertical and originates from the crust, the original depth reference is taken as the deepest measured depth of the well. Then the heat flow - depth profiles of a well can be determined by plotting the heat for values of all arbitrary sections, starting from the bottom most sections and moving up the well column. This process of heat flow profiling enable us to detect the composite effect of changes in temperatures and thermal conductivity within the well column. The method used here is in principle similar to a method normally known as 'Bullard method' (Bullard, 1939 and Jessop,1990).

4.2.2   Interpretation of the thermal-pressure profile

The top of the overpressured section of wells in the Malay Basin is assigned when the pore pressure exceeds the hydrostatic pressure of about 10 Mpa/km (8.5 ppg MWE). Wallace (1980) indicated that any measured formation pressure of slightly in excess of 8.5 ppg should be considered as the onset of abnormal pressure based on the operational experience in the Malay Basin. Other figures have been quoted in several other studies, for the top depth indicators of the overpressures. Mudford and Best's (1989) and Mudford's (1988) work in offshore Canadian Basins have referred the top at about similar measured pore pressure (10.1 Mpa/km) as indicator of the top of overpressure. According to Freed and Peacor (1989) although pore pressures exceeding 10Mpa/km indicate the presence of overpressures, the gradient of 15.8 Mpa/km is commonly used simply because the resistivity changes dramatically and electric logs can be used to identify the depth at which the pressure can be encountered.

The pore pressure in excess of 10 Mpa/km is taken as overpressures in this study since it is more commonly used in this area.

Of the 4 wells chosen, three wells have entered into some thick overpressured zones. The well BO-2 had just penetrated the zones at near total depth (about 2000m), typical of most wells here, where drillings have been terminated on reaching the overpressured zone. The three thermal-pressure profiles are shown in figures 4.7, 4.8 and 4.9 portraying differences in trends and curves with depth. Note that H - H' represent hydrostatic pressure profile of 10.1 Mpa per km. The figures show that, the pressure - depth trends of wells PG-1 and BS-1 are remarkably different. In PG-1 the trend changes quite abruptly from hydropressures to overpressures compared to that of BS-1. The gradient of the geopressure in PG-1 tends to change faster than that of the BS-1. The difference in the relative change of pressure gradient may be related to factors which control the overpressure. The trend of the overpressure gradient of the LA-3 is in between the two extremes.

The depth of onset of overpressures in PG-1 is at about 1850m in group F (Figure 4.7) while the BS-1 top is at about 1370m (Figure 4.9) in group J. The corresponding temperature at the top of overpressured zones in PG-1 and BS-1 is about 114°C. The BO-2 well which is in the central sector has top of overpressures at 1910 in group E at a temperature of about 112°C. while LA-3 (Figure 4.8) has the top of overpressure at about 1250m in group H with temperature of 95 °C.

The differences in top depth and group of the overpressures for most of the wells suggest that the overpressured zones can be encountered in various intervals and stratigraphic groups. The temperatures at top of the overpressure are about 100°C. The profiles of PG-1 and BS-1, show that the overpressures zones are associated with anomalously high heat flow. The heat flow high in the overpressure section may have been developed due to the shielding

of heat flux by the overpressured compartment. The middle intervals in the overpressured zones have developed very high heat flow. Heat flow profiles, indicate that the background (deeper) heat flux may have been trapped within the overpressured zone. This is made possible by the low conductivity of the rocks (Figures 4.3, 4.5, and 4.6) associated with the overpressured zone. The heat preserved in the overpressured zone must have been more than the heat relieved to the overlain zones.

The geothermal gradient is observed to increase on reaching the top of overpressured zone (Pressure Transition Zone, PTZ) in the temperature profiles of PG-1 and BS-1 (Figure 4.7 and 4.9). The characteristically higher geothermal gradient on sections with temperatures below the 90 °C can be seen occurring across the basin in particular over the NW and central portions as has been shown in Figure 3.8. In the overpressured zone intervals the geothermal gradient varies. Deeper within the overpressures interval the temperatures pick up and geothermal gradient increases which is likely due to the increase in heat flow. In BS-1 (Figure 4.9) the heat flow tends to decrease again which indicates another change in geothermal gradient. In LA-3, (Figure 4.8) however there is a uniform increase in heat flow with depth of up to total depth. The base of the overpressured zones has not been reached by any of the observed wells.

The above profile of heat flow and temperature with depth indicate that within the overpressured zone there is no constant temperature gradient as well as heat flow. The changing thermal profiles here may suggest, existence of fluid circulations within the overpressured zones. Accordingly, the zones can have variation in permeability which may affect the degree of overpressures within the zones (Mann and Mackenzie, 1990). The differences in the permeability can affect the hydrocarbon entrapment.

In BS-1, Kup (Figure 4.6) group which is the main shale bed in the SE Malay Basin (Terengganu shale) has constant temperature with depth and slight reversal of temperature is noticed at the base of the shale bed. This effect could be caused by loss of fluid from the shales into the sandstones underlying and overlying the shale (i.e. the J sandstone and the Klw sandstone) meaning that the low permeability shales are dissipating fluid and subsequently increasing pressure in the higher permeable sandstones.

The high neutron porosity of the shale indicates that probably the shale has been undercompacted or fractured. In PG-1, a similar trend of sonic is seen in the H shales which is overpressured. The density of the shale is estimated from logs to about 2.6 gm/cc which is probably normal for the depth of over 2000m. If the high sonic porosity is coupled by normal density than it may indicate that within the overpressured shale in PG-1, secondary porosities has been developed. The porosities may be in the form of cracks and fissures.

4.2.3 Possible cause of overpressure in Malay Basin

The cause of overpressure has always been the subject of much debate. Among the mechanisms for overpressuring to develop are: (a) Rapid sedimentation and burial or commonly known as disequilibrium compaction, (b) Aquathermal pressuring ,(c) Conversion of smectite to illite and (d) Conversion of kerogen to hydrocarbon. Most authors now agree that the first process, the disequilibrium compaction is the predominant cause of most overpressures observed in sediment (Bethke, 1985; Shi and Wang, 1986; Mann and Mackenzie, 1990).

In the Malay Basin, the causes of overpressure are not fully understood. Apart from the thermal regime, other parameters of importance in the study of pressure which is not fully studied are the clay mineralogy and the tectonic development. In this chapter some

speculations about the mechanism of overpressuring shall be discussed. The purpose of this exercise is only to get a conceptual understanding of the different mechanism of overpressuring and the basin setup.

Data in Table 4.1 indicated that occurrences of overpressures are not related directly to depths and stratigraphy as well as temperature. However apparently temperature can be shown to have some relationship with the regional overpressuring in the Malay Basin. Figure 4.10 shows distribution of temperatures of tops of overpressure zones for some selected wells in the Malay Basin. The overpressures depth started at about a uniform temperature in a sector. For example, wells in sector 2 (the Malay Basin Centre) start to overpressuring at temperatures of less than 110°C. Most of the wells in the Southeastern Malay Basin (sector 4) are with top of overpressures at temperatures of over 120 °C. The relationship between temperatures and top overpressures vis-a-vis geologic sectors may suggest that temperature can play a role for the mechanisms of overpressuring in the basin.

Illitization

Occurrences of overpressures in the central Malay Basin (sector 2 and part of sector 4) are at temperatures of about 100 °C or less. In this sector, most of the sediments are in groups D and E which are composed of mostly interlaminations of clays, silt, sand and coals. If by assuming that the clays are composed of smectite in sufficient amount and in a condition fravourable for the conversion of smectite to illite, then considerable fluid from the bounded water of clay particles can be generated. The water, inturn is released into the surrounding permeable rocks and produces overpressuring (Hower et al., 1976; Dutta, 1987; Freed and Peacor, 1989). The transition of smectite to illite is independent of geologic age and formation boundaries (Perry and Hower, 1970) and mainly temperature dependent. The start of optimum rate of the transition is at temperature of about 100 °C (Figure 4.11). Freed and Peacor (1989)
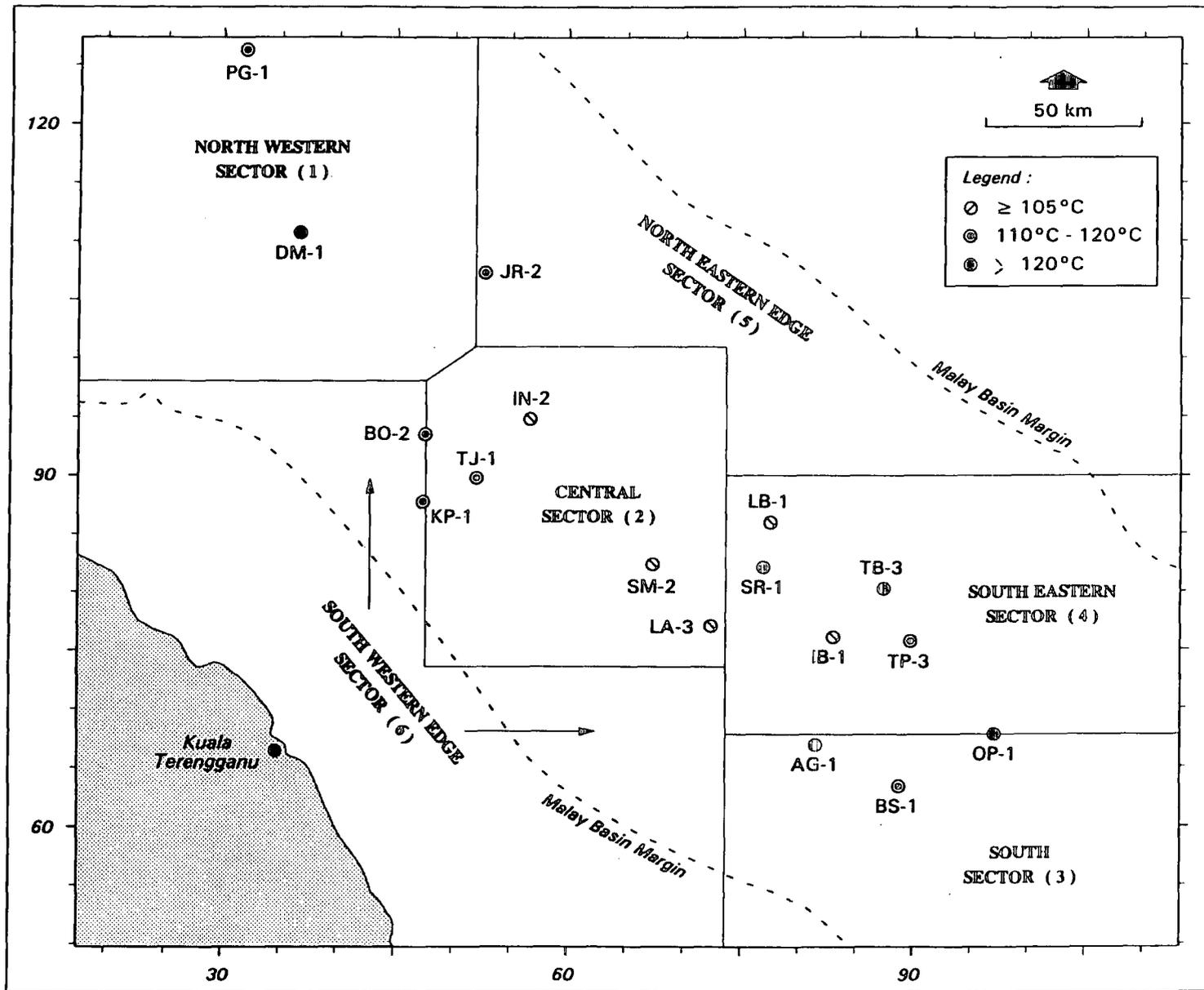
Figure 4.10 : Temperature at top of overpressure of selected wells in the Malay Basin
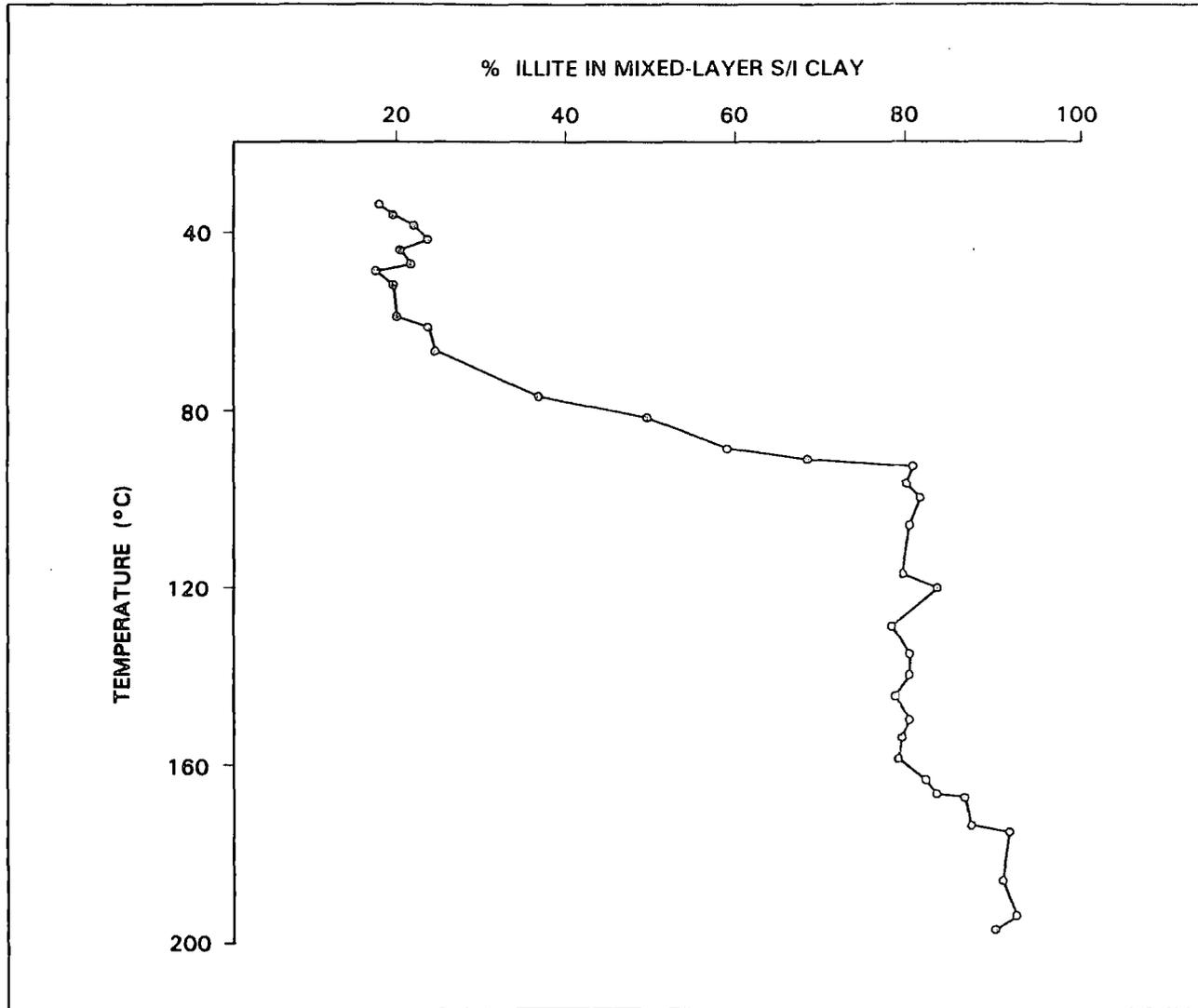
Figure 4.11 : Percent illite in mixed-layer smectite/illite (S/I) clay vs. temperature
for a deep, geopressured well in onshore, Louisiana area
(Modified from Dutta, 1987)

observed that the base of normal hydropressure coincided with the depth of onset of the smectite-illite transformation in geopressured shales in Texas. The start of geopressured zones by illitization can be at temperature lower than 100 °C (Jones, 1980).This process of illitization may have caused the overpressuring in particular at the central parts of the Malay Basin. This hypothesis is yet to be thoroughly studied before any concrete solution can be made.

Aquathermal

In several wells, the temperatures at the onset of overpressures is slightly higher than those in the central part of the basin. Most of the overpressures are found in groups older than E, meaning that the overpressuring may have taken place earlier than those in locations in the central sectors. Furthermore, other groups have different facies deposited under different environments(Figure 4.2). Nevertheless, the same process in the generation of the overpressuring as speculated in the central region may have taken place in this part of the basin as well. However, investigations on well PG-1 has suggested that aquathermal pressuring may have taken place in the Malay basin as well.

The well PG-1 has been shown to be overpressured in stages with depths (Figure 4.7).The pressure gradient changes slowly with depth in the lower section of the zone and increased in the upper section . Figure 4.12 shows sketch of Vf, sonic transit time (Dt) and porosity (Ø) of the well. The sketch shows the area of overpressured zone, corresponding to sections of lower porosity in the upper portion than the lower interval. The lower interval of the zone, where the pressure gradient is lower (below 2500m), the Dt is apparently lower than the above interval with Ø increasing with depth.
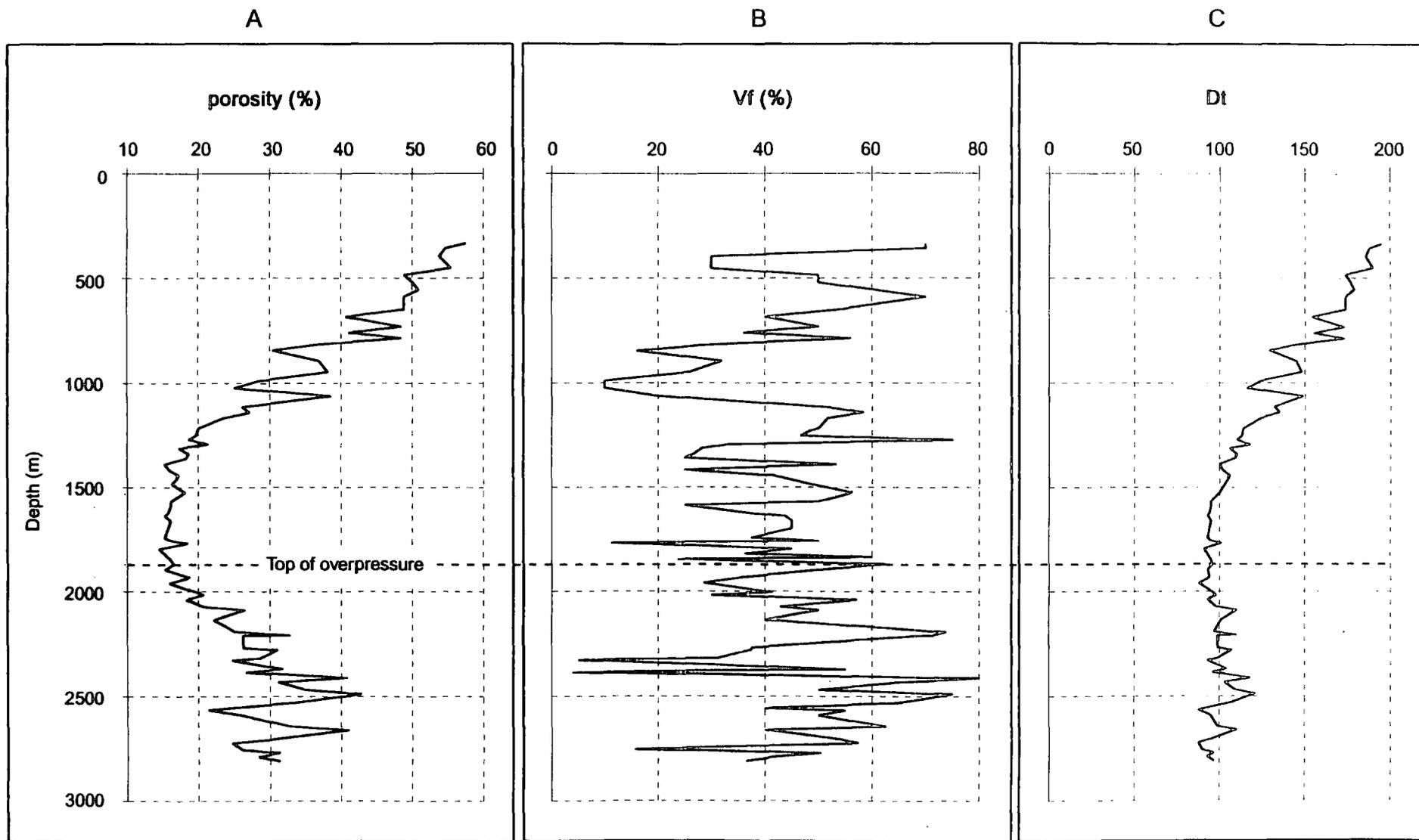
Figure 4.12 : Log data of PG1 showing (A) porosity , (B) Volume of fines and (C) Sonic transit time, Dt (μ sec/ft.)

The above log trend suggests that the top part of the upper interval is comparatively a tighter zone than the interval below. This tight zone is in an intermediate pressure zone. The tight zone has resulted in the low temperature gradient and lower heat flow. Below the tight intermediate zone is the loose, high ϕ zone of high pressure with higher geothermal gradient. This is the main overpressured section. The higher porosity, is however corresponded by lower Dt.(and so possibly higher density) than the intermediate zone. Therefore most likely, in the main overpressured zone, the secondary porosity may have been developed due to tectonics or thermal effect.

A pressure - temperature plot of the main overpressured zone in PG1 has been made to demonstrate the relationship between pressure and temperature. Figure 4.13 part (B) shows that a high pressure-temperature gradient has developed within the overpressured zone. The observed gradient exceeded 1.6 Mpa/°C, which is equivalent to the pressure increased in sealed compartment as suggested by Barker (1972). The high pressure-temperature gradient has been implied to be a very effective pressure generating mechanism (Gretener, 1979) under condition of near total confinement (sealing). Therefore the mechanisms of overpressures in PG1 can be suspected of an aquathermal nature.

Meanwhile, aquathermal pressuring mechanism has not been regarded as the main cause of the overpressure due to the fact that there is little chance that there exist an isolated environment as such (Chapman, 1980; Shi and Wang, 1986.). Furthermore the viscosity of water decreases fast with increase in temperature and allows the total seal unlikely to be preserved with depth (Mudford and Best, 1989). The mechanisms of overpressures can be an indirect result of temperature, whereby other processes contribute to the direct mechanism of overpressure with the presence of appropriate temperature condition.

156
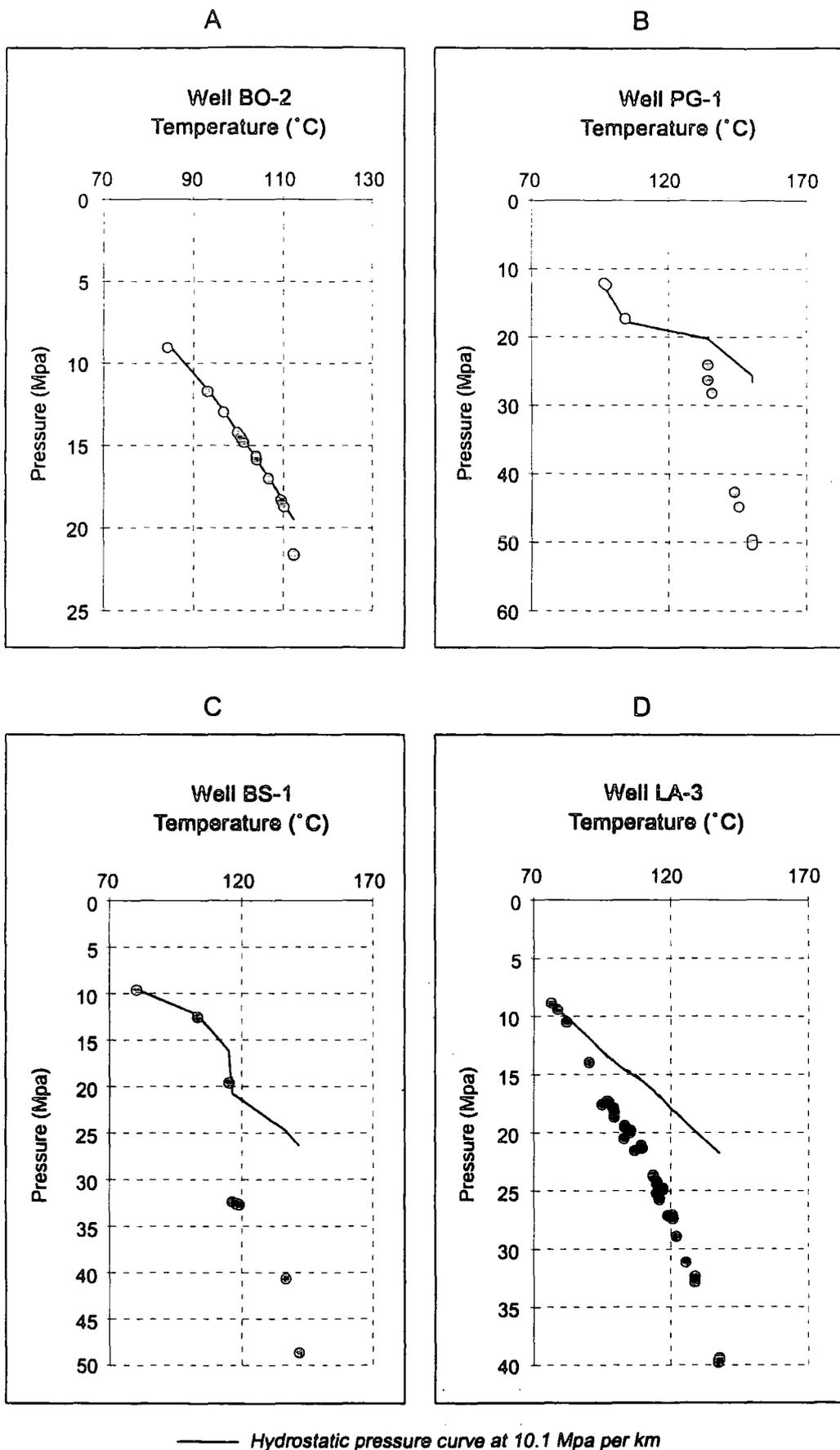
Figure 4.13 :   Pressure vs. temperature curves for wells BO-2 (A), PG-1 (B),
                 BS-1 (C) and LA-3 (D)

Hydrocarbon generation

The observed occurrences of hydrocarbon within the overpressured zones and the adjacent sand beds may have affected the overpressures in the basin. Table 4.2 shows top of seismic groups with the hydrocarbon type present in the selected wells. The hydrocarbons are distributed over and within the overpressured zones. The conversion of kerogen to hydrocarbon may have caused the overpressuring and affected the generation and migration of hydrocarbons. Althogh more evidences are required to analyse the conversion of the kerogen to hydrocarbon in the overpressured zones, however some observations described below may suggest that the above mechanism may contribute to overpressuring here.

The onset of hydrocarbon generation is likely to take place in the range of 80° to 93°C (Waples, 1980; Jones, 1980; Bonham, 1980). It has been have observed that the temperatures at the top of most geopressured zones are near the range of those of the onset temperatures (i.e 80°C to 93°C) for hydrocarbon conversions. While the peak hydrocarbon generation temperature is at about 120°C (Tissot et al., 1980; Bonham, 1980) is within the overpressured zones observed in the basin. The temperature of the overpressured zones seems to be correlated with the spectrum of temperatures of kerogen conversions.

In well BS1, the Terengganu shale (seismic group Ku), which is overpressured, lies in between the gas sands (Table 4.2). This shale may be releasing fluid (may be gas saturated) to the adjacent reservours. There are areas in the Malay Basin where shale diapirs has been observed to be associated with high pressure, one of which is seen in TP3 (Figure 4.14 and Figure 3.13). In both locations of BS1 and TP3, the methane gas generated from kerogen conversion may generate the overpressures. Later, micro fractures may have developed in the shales relieving the overpressures and followed by hydrocarbon migration in the nearby

Table 4.2   The hydrocarbon type present in each stratigraphic group
of the selected overpressured wells. Depth is below K. B.

Well	PG-1		BO-2		LA-3		BS-1	
Seismic Group	Top of Group (m)	Type of Hydrocarbon	Top of Group (m)	Type of Hydrocarbon	Top of Group (m)	Type of Hydrocarbon	Top of Group (m)	Type of Hydrocarbon
A/B	82		71		78		79	
D	1063	GAS	1197	GAS	632			
E	1484	GAS	1637	GAS	744			
F	1821	OIL			941			
H	2566				1242	OIL	694	
I					1880		860	GAS
J							1418	GAS
Ku							1695	
KI							1842	GAS
L							2252	
Total depth	2804		2020		2281		2626	
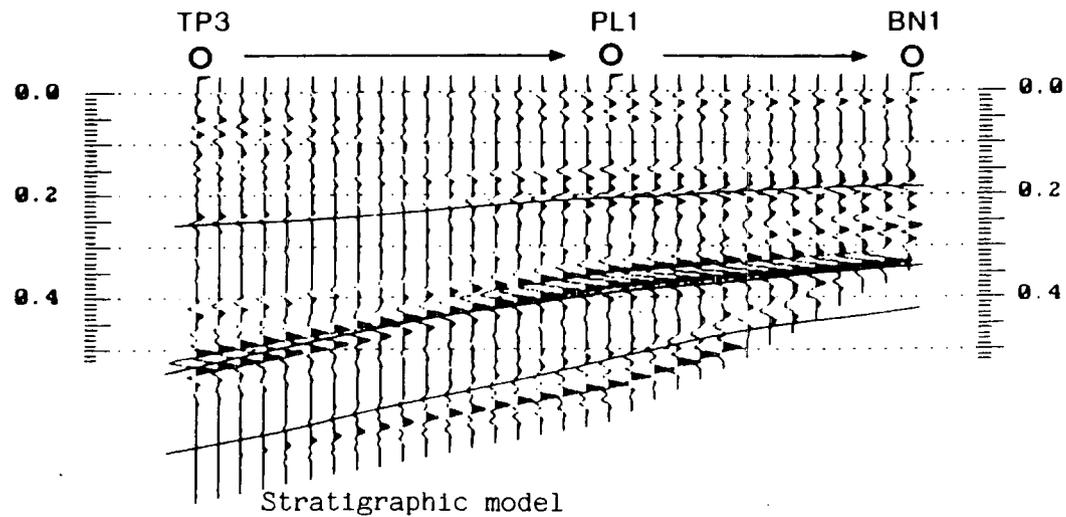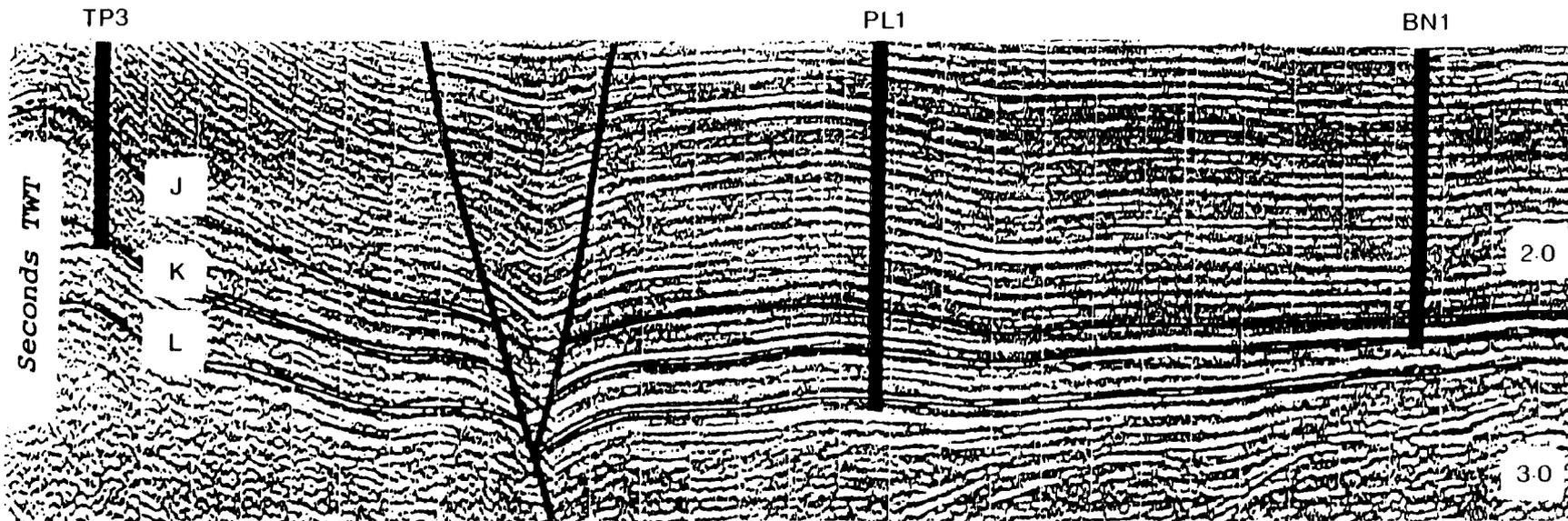
Figure 4.14 : NE-SW seismic cross-section along TP3, PL1 and BN1. J, K, L are tops of groups.
The arrow show possible transient Fluid Flow before structuring.

reservoirs (Hedberg, 1980). Figure 4.14 suggest fluid flow may follow the direction shown by the arrow, i.e. from TP3 toward BN1. The fluid movement would contribute to the horizontal migration of hydrocarbon following the model in equation 3.7 and coupled by prevailing pressure conditions which could occur during instantaneous shales diaperism before the effective uplift of the structures. The vertical component of hydrocarbon migration by bouyancy will accordingly overtake the horizontal flow when structuring has taken place and hydrodynamics is in equilibrium. Eventualy a condition is met where degree of sealing of the reservoir is sufficient for the trapping of the hydrocarbon to be effective.

The relationship between the temperature and pressure regimes in the geopressured zones with the conversion of kerogen to hydrocarbon and the expulsion of these fluid has been suggested by several authors. Among others, Spencer (1987) concluded that the overpressuring in the Rocky Mountains , USA is caused by hydrocarbon generation mechanism. He found that nearly all the overpressured zones and source rocks are at temperature of about 93°C. The observed association of shales and reservoirs containing overpressured gas in BS-1 can be considered to indicate importance of hydrocarbon conversion mechanism taking place in the Malay Basin. However, there is lack of data on the source rocks in order to evaluate whether this mechanism of overpressuring could adequately explain the observed overpressure.

Disequilibrium compaction

The main factor that permits the development of overpressures is believed to be by disequillibrium compaction. The main process that lead to the disequillibrium compaction is the rate of sedimentations (Magara, 1978; Bethke, 1985). Disequillibrium compaction can take place when the sediments have been deposited at a fast rate so that the water in the underlying sediment is trapped. It has been suggested that the rate of sedimentation of about 100m/million

years and above favours the disequilibrium compaction occuring (Waples, 1991). In order to have some clues for the possibility of this mechanism to take place in the basin, isopachs of the formations are estimated from wells' data. The rate of sedimentation has been approximated for each stratigraphic group of key wells as shown in Table 4.3. Since the thicknesses of sediments in the Table 4.3 is the un decompacted thicknesses, the rate of sedimentation is lesser than if it has been approximated from decompacted beds. The result will not differ much in the final interpretation of the mechanism of disequilibrium compaction. The rate is approximated by dividing the thickness of each group by the age duration (with estimates of maximum and minimum age of each groups) in million years each section has been deposited.

The figures in Table 4.3, shows that , the rate of sedimentation in most groups can exceed 100m/m.y. which is considered high enough for disequilibrium decompaction to take place. Therefore by taking rapid sedimentation rate as the ultimate cause for the development of over pressure then most of the overpressure can be caused by disequilibrium compaction mechanism. Higher sedimentation rate is observed in groups older than H because of the high energy of deposition environment. The group D and E sediments in well LA-3 has been seen to be devoid of overpressures which is in agreement with the expectation following the concept of disequilibrium compaction.

Most of the groups older than the H group has high sedimentation rate in well BS-1 except in the Terengganu shale. The thick shale has a very low sedimentation rate and most likey is unaffected by disequillibrium compaction. The Terengganu shale is observed to have normal compaction based on the neutron porosity decreasing trend with depth. Hence with low sedimentation rate of about 40m/m.yr. it is likely that disequilibrium compaction may not be the major mechanism of overpressuring here. However the bulk density log showed a higher porosity at depth which may be due to the effect of overpressuring as it lies within the

162

Table 4.3. Estimated rate of sedimentation at key wells.
(in metre per million years)

Well		PG-1			LA-3			BS-1		
Depth Top (m)	Age Begin (m.a.)	Depth Top (m)	Sedimentation Rate (m/m.y.) Max	Min	Depth Top (m)	Sedimentation Rate (m/m.y.) Max	Min	Depth Top (m)	Sedimentation Rate (m/m.y.) Max	Min
A/B	5.2	82	189	100	78	107	57	79	118	63
D	6.6	1063	301		632	79				
E	9.8	1484	105		744	62				
F	13	1821	233		941	94				
H	16.2	2566	119	74	1242	199		694	52	
I	20				1880	143	105	860	147	
J	22.5							1418	111	
Ku	26.2							1695	40	
KI	28.1							1842	216	
L	29							2252	468	416
TD	32	2804			2281			2626		

163

overpressured zones. The sediments below the Terengganu shale is seen to have very high sonic transit time and probably undercompacted due to high sedimentation rate. It is likely that several mechanisms may have shared the process of overpressuring in this well and needed further analysis.

In summary, the overpressures in the Malay basin can be caused by several mechanisms. The central portion of the Malay Basin may have been caused by illitization process more than the other mechanisms. In BS1, hydrocarbon generation may have played major role in overpressuring. Meanwhile in PG1, temperature may be speculated to be one of possible factors for aquathermal mechanism as caused of the overpressures. The most common mechanism of overpressuring is probably the disequilibriuim compaction of sediments since almost all (group D and Klu are the prominant exceptions) columns of sedimentary rocks experienced high sedimentation rates.

4.2.4 Prediction of thermal and pressure distribution

The above discussions and the general description of the thermal profiles described in chapter 3 suggested that there are several factors that affect the temperature distributions within the basin. The thermal conductivity of the basin may only control the mega terrestrial heat transport from the crust but other mechanisms has disrupted the heat flow very enormously in the upper layers of the basin. The major processes which have been descrbed (i.e overpressures, fluid flow and sediment radioactivity) may have redistributed the heat flow.

In areas where there is no active fluid flow and overpressuring than the temperature-depth profle varies nearly linear with depth. Well BN-1 is an example of such profile (Figure 4.15). Heat flow anomalies is absent within the depth of the section. The well is located in an area which is believed to be tectonically quiet and no ovepressuring is seen. In

Figure 4.15 : Estimated formation temperature and heat flow profiles with depth of well BN1

BN1CPT

Figure 4.16 : Estimated formation temperature and heat flow profiles with depth of well GN7

Figure 4.17 : Estimated formation temperature and heat flow profiles with depth of well PL1

GN- 7 and PL-1(Figures 4.16 and 4.17) thermal profiles, no observed overpressure is observed in the well sections.Therefore the observed heat flow anomalies of group I is likely due to the fluid flow. The heat flow returns normal at the shallow intervals and indicate possible filtration of water into the sediments. In TP-3 (Figure 4.18) there is a commulative effect of both overpressure and fluid flow in the area. The anomalous heat flow occur in two intervals. At near the total depth the interval is overpressured. The cause of the anomalous heat fow near the total depth is regarded mainly due to the observed overpressures. While overlying the overpressured zone is the heat flow anomalous zone which is due probably mainly to lateral fluid flow.

In the central portion of the basin, most of the wells reached the overpressured zones near total depth. There are two type of thermal profiles common in this area. One is demonsrated by the TJ-1(Figure 4.19) well where the overpressured zone at near total depth has caused the anomalous heat flow. But the heat flow has returned to normal due to probably less effective shallow fluid movement. A combination of effective thermal disturbances by overpressure and nearsurface fluid flow are shown by well LA-3 (Figure 4.21). Apart from the deeper heat flow anomaly due to overpressures, the well showed another anomaly near the surface. The near surface anomaly is mainly due to fluid movement.

4.2.5   Heat flow Provinces of the Malay Basin and implication to fluid flow

From the observations of the regional profile in chapter 3 and the discussions of the type wells above, the basin can be categorised into heat flow provinces. The south east sector is comprised of a mixed thermal pattern which is controlled by overpressure and deeper fluid flows. The effect of shallower fluid has not yet been seen. The trend of active fluid flow anomaly is increasing from the north eastern edge towards the centre of the basin as shown by the thermal profile in Figure 4.20. In the South Malay basin the thermal regime is probably
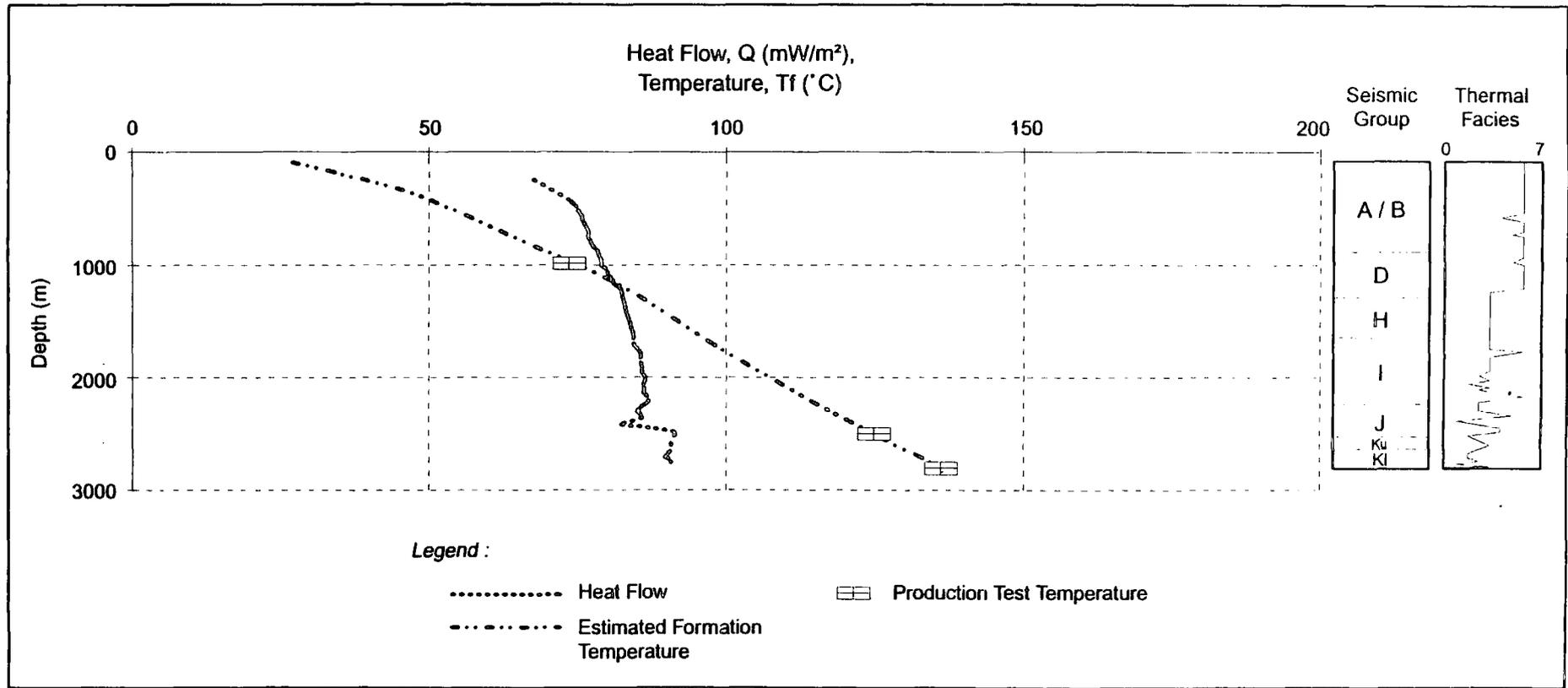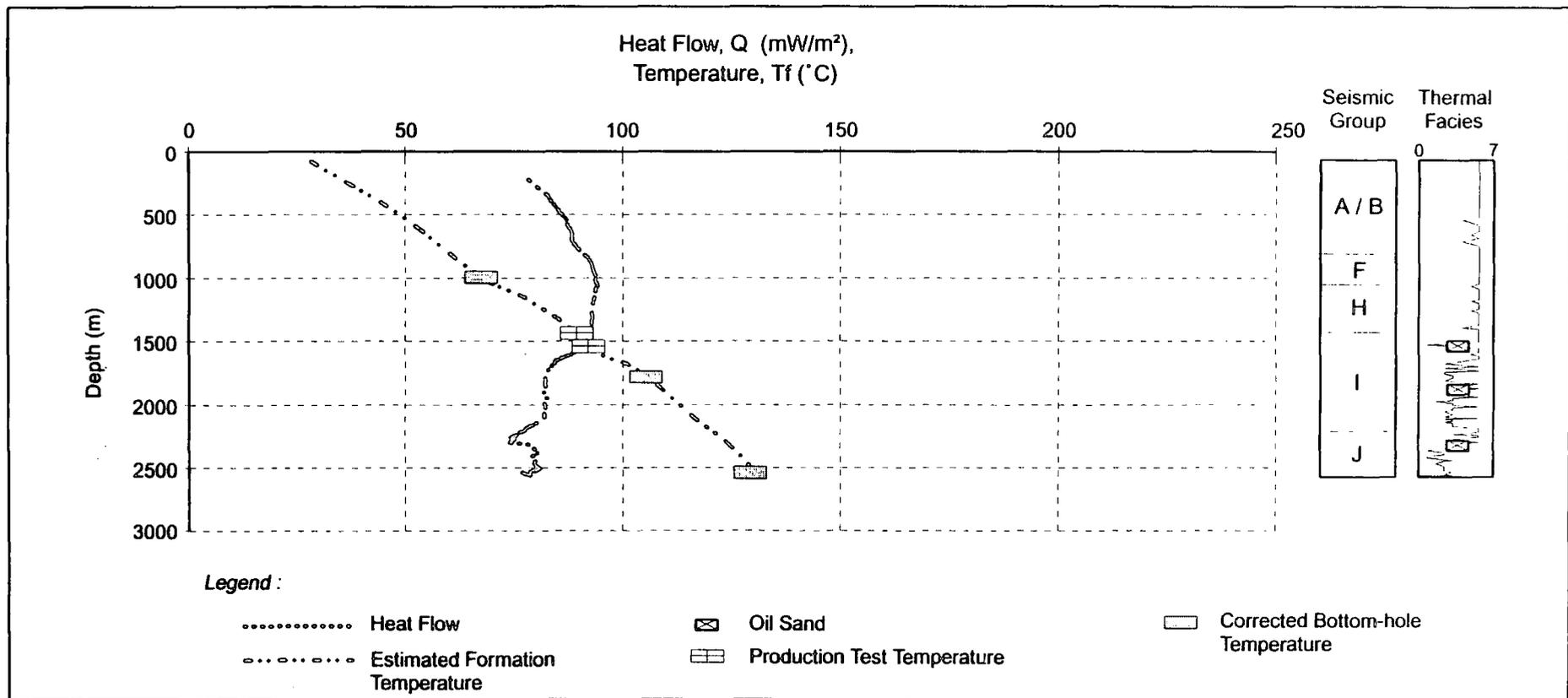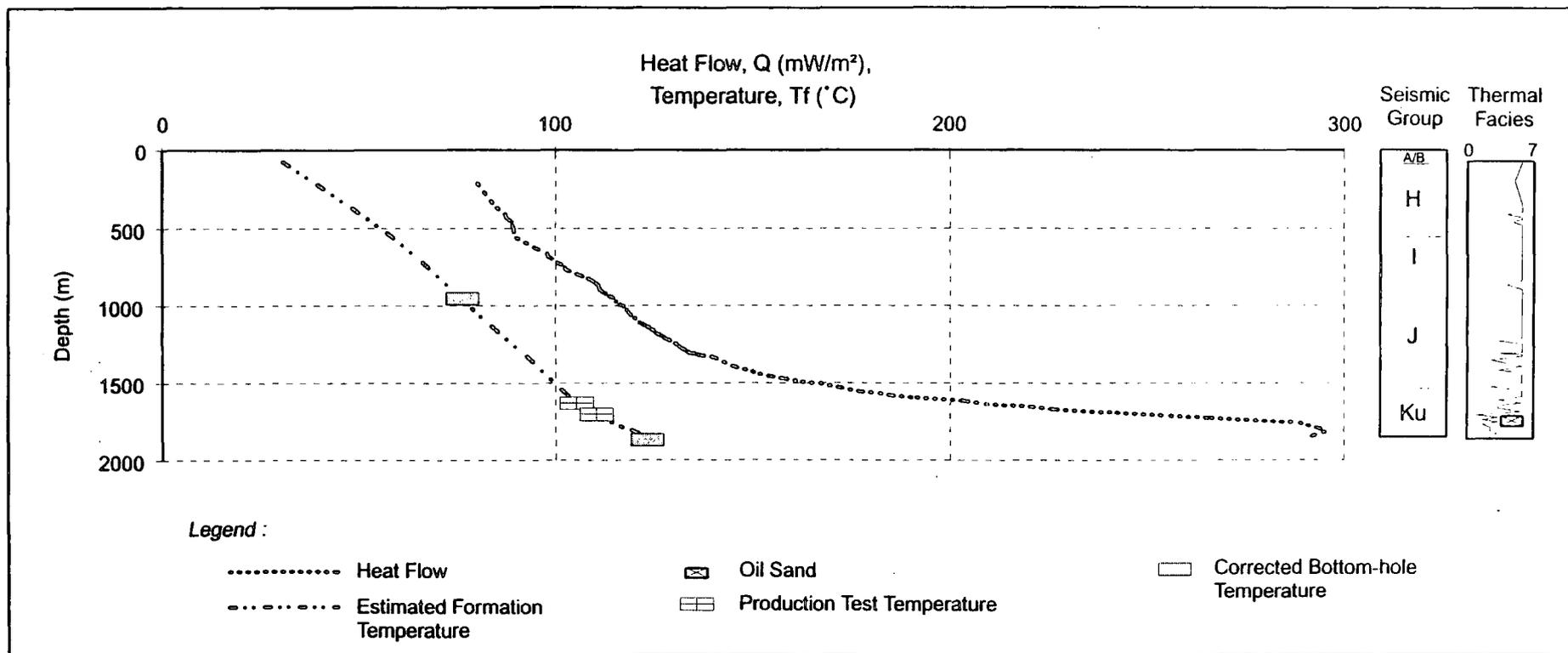
Figure 4.18 : Estimated formation temperature and heat flow profiles with depth of well TP3

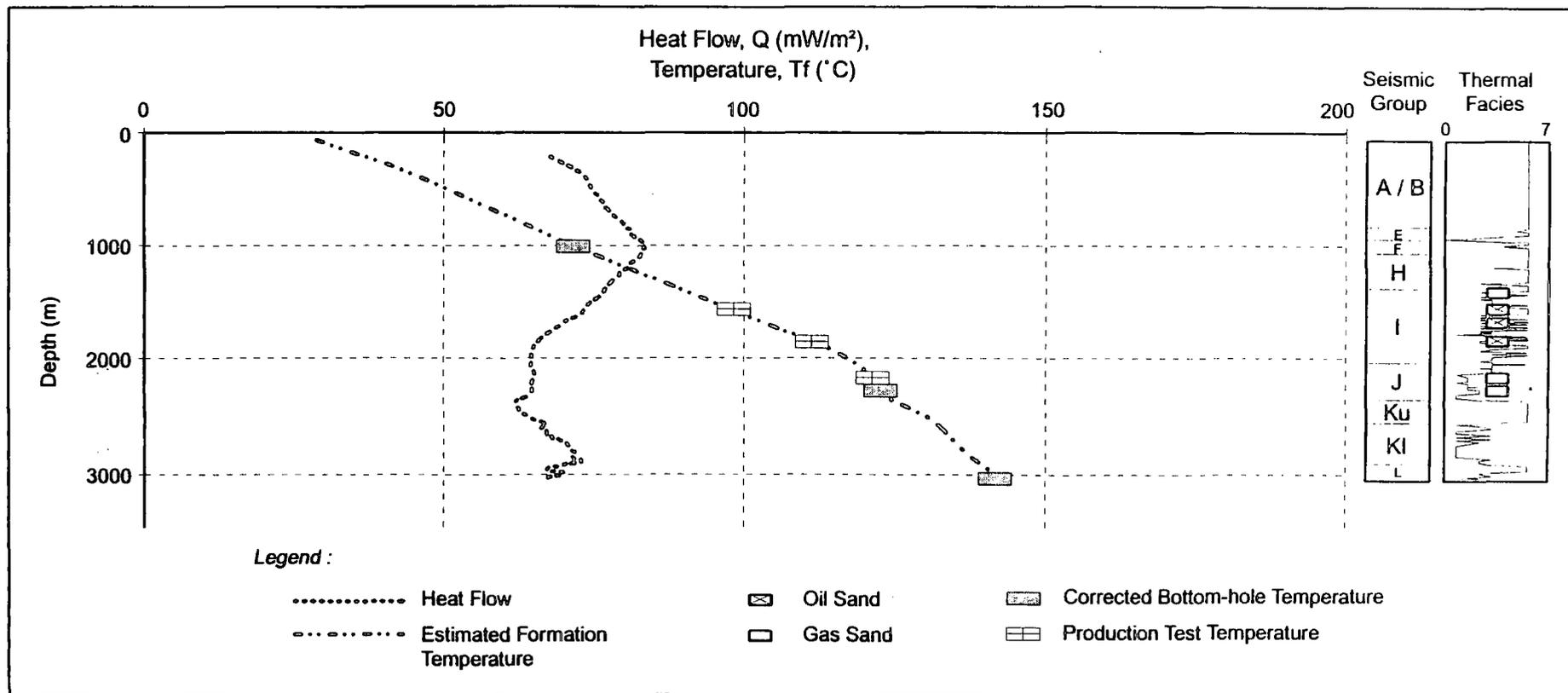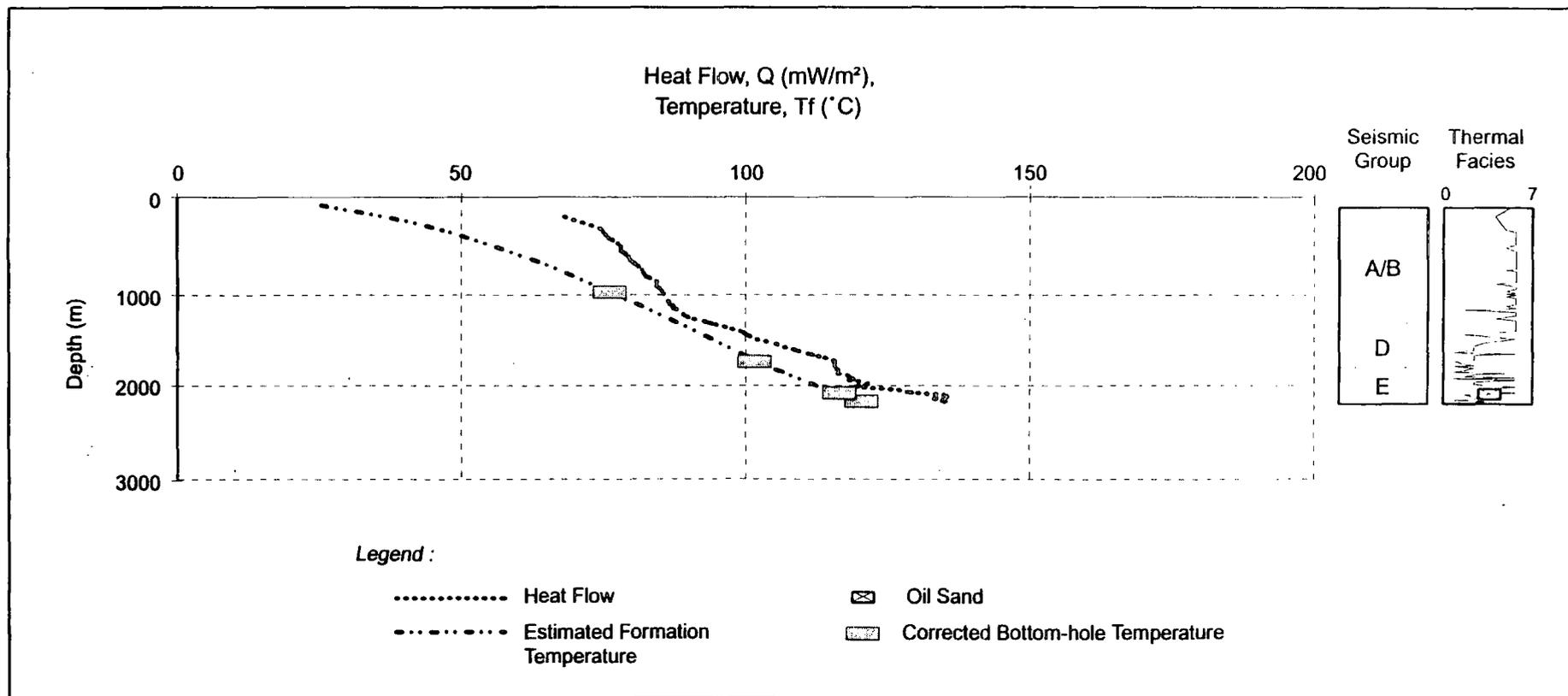Figure 4.19 : Estimated formation temperature and heat flow profiles with depth of well TJ1

170
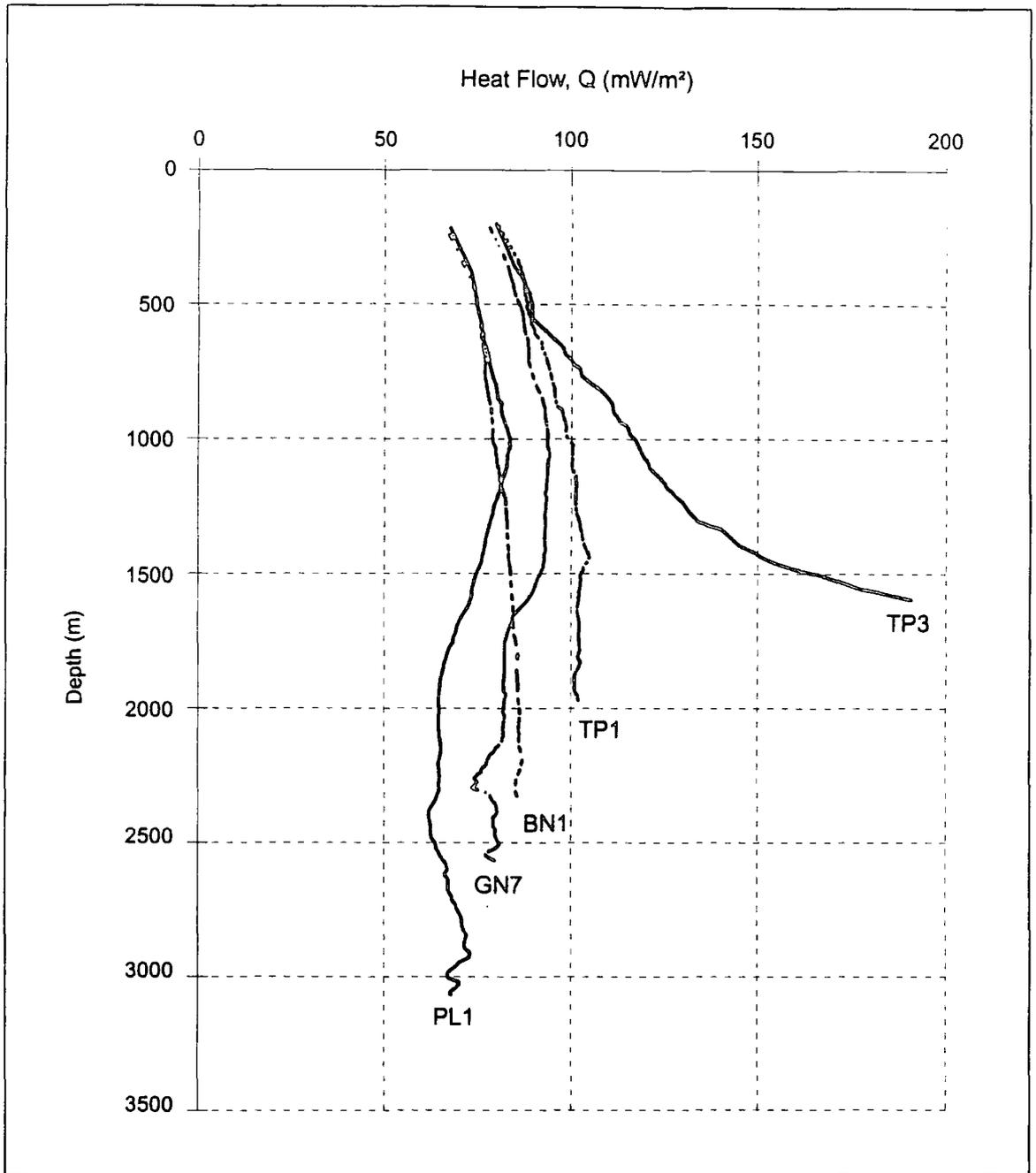
Figure 4.20 : General heat flow profiles in Southeastern Malay Basin
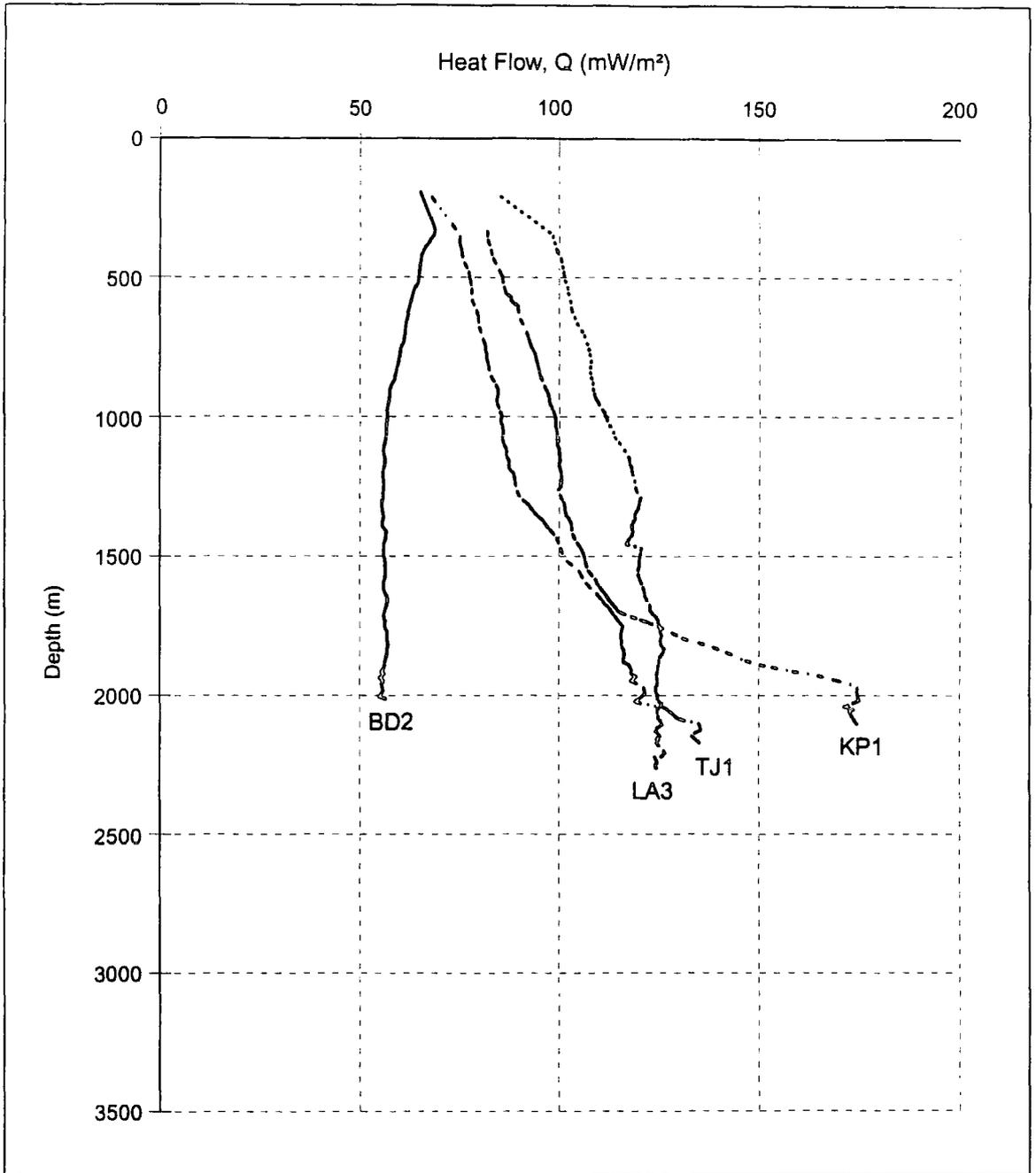
Figure 4.21 : General heat flow profiles in Central Malay Basin

similar to those of the central southeastern portion. The profile of BS-1 probably potrays the typical South Malay Basin thermal state.

While in the central portion the anomalous heat flow is composed of some overpressures related to the shallow water circulation type. When there is no shallow fluid movement effect the heat flow near the surface is about normal. Therefore the normal heat flow of about 75mWm-2 observed in Chapter 3 for the central region (Sector 2) of the basin is probably due to the lesser contribution of the near surface water flow (as in TJ-1 of Figure 4.19).

In the north west sector the wells are possibly overpressured at depth as shown by the PG-1 well. The upper intervals, above the overpressures are probably affected mostly by the upward fluid movement. Although no anomalous heat flow is present above the overpressures, the heat flow is higher and the temperature gradient has become higher than elsewhere.

The general model of the fluid movement that affects the heat flow is not feasible to construct at this point. The difficulty lies mainly in the lack of structural, stratigraphical and geochemical control. However, not all factors are equally important in the production of the thermal anomalies. The illitization which causes overpressures and heat flow anomalies may only be relevant at certain temperatures. The recent tectonics which effect sediment following the regional plio-Miocene unconformity may have introduced probable additional heat in the north west sector. In the SE, because of the compressions and uplifts events, cracks may have formed which acts as the fluid movements conduit. Shale diaperism, shown by the TP-3 well area, may have caused the anomalous heat flow in association with overpressures. The overpressured shales can be saturated with gaseous fluid from the decomposition of carbonaceous matter within the shale. These fluid pressure compartments will form the thermal shields which inhibit the flow of heat.

In summary the thermal state of the Malay Basin is patterned mainly by hydro dynamics, recent structuring as well as the basement tectonics. The hydrological movement may have affected mostly the hydrocarbon migration within the basin. Accordingly, Magara (1987) has suggested that, the fluid flow due to compaction which took place in the geological past is probably important in the primary migration of hydrocarbon. While, the present fluid movement, as in the case of meteoric water is important in trapping hydrocarbon in a pool and unimportant in the primary migration.

In this study, the anomalous heat flow within the centre of the basin is highly contributed by the shallow fluid movement component which is probably not important in the generation of hydrocarbon. The anomalous heat flow at depth is probably important in the maturation of the source rock and generation of hydrocarbon.

With the detailed heat flow profiles of wells, the pressure profile can be estimated provided the causes and nature of the heat flow and pressure are known. Approximation to heat flow profiles can be done if the existing wells in the basin are mapped in vertical and horizontal profiles . The overpressures profiles can be approximated from known temperature profile if the fluid flow pattern is known. To now the temperature profile require input of thermal conductivity which can be approximated from seismic data in undrilled areas. Overpressured zone can now be estimated and hence hydrocarbon migration direction can be deduced (Magara, 1987). However, in this study no attempt shall be made to use the said method in overpressure prediction, the suggestion is only intended for future venture in the field.

174

4.3   Thermal modelling

The aim of thermal modelling in this section is to test and utilise the thermal data resulted from the analysis in the previous sections. The data is used for input into a basin modelling programme, BasinMod to simulate present and paleo temperature from thermal, Stratigraphic, lithologic and petrophysics data.

Thermal history of a basin is an important tools in the basin analysis for predicting the timing of source rock maturity and hydrocarbon generation and expulsion from the source rock. The process and timing of the kerogen - hydrocarbon conversion is also an important criteria in analysing the migration of hydrocarbon, leading to the reservoirs. The timing of the hydrocarbon generation can be compared to the tectonics events and other mechanisms which create the traps for the hydrocarbon. If a structure was formed before the migration than the hydrocarbon may be able to be detained in the trap. Other kind of traps are not as many as the structural traps but their importance is increasing due to exhaustion of the structures.

In this report, a brief model for prediction of the present and paleotemperature is made. The application of the observed present day thermal properties and other supporting data shall be used to determine the oil window as it is today and in the past. Thermal history of a sedimentary basin is constructed from the knowledge of the sediments burial history and their associated temperatures. An essential part of the study is to have a model for the prediction of the thermal history. The modelled temperature profile is then compared to the measured values in order to get a good fit. In case there is a good fit then the same parameters can be used to predict temperatures at unknown location. Therefore a suitable geologic model has to be obtained to get the best predicted thermal properties.

4.3.1 Present-day temperature model

Among the analysis to predict the temperature in subsurface includes the burial history analysis and organic matter maturity analysis. The output of the burial history can be in the form of compacted or uncompacted subsidence curve. The tectonic subsidence can be generated. The data which are relevant to the analysis can either be extracted from the built in (default) values or input from measured or predetermined value.

In this report the models are made using thermal and stratigraphic data taken from the well records while petrophysical data is from the default values. Four wells are selected from the respective sector for the temperature modelling, i.e. DM1, SM2, TP1 and AG1 (the location is shown in Figure 4.1, TP1 is at TP3 locality.). The wells are chosen in order to represent different sector of the basin. The aim is to have a conceptual model of thermal properties of the basin.

All the stratigraphic interval and ages are assigned according to the stratigraphic scheme described in chapter 1. Although there are several unconformities reported but they are minor and localised and hence not considered in this analysis. The major unconformity, considered in this study is the Plio-Mio unconformity which is believed to have taken place in between 9.8 to 5.2 m.a.

Since only the S and SE portion of the basin has been subjected to uplift (Figure 1.8), then an important event which is associated with the unconformity is the erosion thickness. To simplify the analysis the section that is interpreted to be eroded is assigned the missing section as has been estimated by earlier workers mentioned in Chapter 1.

The lithology of each group is assumed by the average contribution of thermal facies of the group. In other word, a group is assigned one lithologic type which has been determined from the average thermal facies from the well data as described in chapter 2. The use of thermal facies is considered adequate in the programme for the thermal facies has been determined from lithologic log and calibrated to cored samples. The petrophysical data are supplied by the default values of the programme and is assigned accordingly to each group. The porosity-depth profile is given by the default selected Baldwin and Butler, 1985 method.

For the thermal conductivity data, the well data set is preferred and used as input for determining the thermal conductivity. The programme. has specified that the minimum thermal conductivity of each group has to be given. Theoretically the minimum thermal conductivity should be the thermal conductivity of the sediment for the top of the group. Since the top most thermal conductivity of each group need not be the minimum in the real situation therefore the minimum thermal conductivity has to be estimated . The estimated minimum thermal conductivity is determined by an effective heat conductivity equation, (Atroshchenko, et al. 1982)

$$k_e = (k_1^m)(k_2^{1-m})$$

where ke is the effective thermal conductivity, k_1 and k_2 is the minimum thermal conductivity of sand and shale respectively and m = volume fraction of the sand and (1-m) is the volume fraction of shale.The thermal conductivity-depth trend will be estimated by the programme for each group during the analysis.

The temperature data set is provided from the corrected formation temperature and production test temperature. The temperature will be used to compare with the modelled temperature.

There are options in modelling the present day temperature. The options available are either to use the temperature or heat flow data. First the present day temperature data was tried as the thermal parameter. The model returns temperature- depth profile from the backstripping technique. But, this option does not give consistent fitting of the modelled and measured temperature for all the wells.

The modelling by tectonophysical method is the next options where heat flow is taken as the thermal parameter. The heat flow which contribute most to the development of the present-day thermal profiles may be the background heat flow. The total surface heat flow has been raised probably recently and advective in nature and probably not an important control of maturation. Hence the background heat flow values, which is often less then the surface heat flow values are used. The background heat flow used is about $65mW/m^2$, which has been estimated for the basin, as described in chapter 3. The temperature model returned by the programme is consistent with the measured temperatures.

4.3.2 Paleotemperature modelling

When the present-day temperature has been satisfactorily modelled, the next stage is to evaluate the paleotemperature. The database used to predict the present day temperature has been fixed for the wells used in the paleothermal modelling. The paleotemperature can be estimated by the BASIN-MOD programme. Paleothermal indicator has been used to check the predicted thermal history constructed from the model. The vitrinite reflectance data has been considered as the measured paleothermal indicator.

The heat flow option allows several variations of time variant heat flow in the programme. One of the variations tried out is based on the regional understanding of thermal history. It is believed that the Malay Basin has been subjected to several heat flow

perturbations as a result of the opening of the South China Sea (Ru and Piggot, 1986). Several estimated heat flow - time data has been tried in the analysis. The resultant temperature did not match with the observed paleothermal indicator.

However, with the heat flow option based on extensional tectonics and background heat flow satisfy the prediction of the thermal maturity history. The heat flow model is based on extensional tectonics introduced by Mckenzie (1978) and modified by Jarvis and Mackenzie (1980). One requirement for the modelling to be made is the extension factors (β) of the basin. Since the deeper sediments are not known, then the ß can be best estimated from the tectonic subsidence curve. Several wells are backstripped and the tectonic subsidence curve is produced. The tectonic subsidence curves for the selected wells in the Malay Basin, shown in Figure 4.22 are similar in shape to those of the Pattani and Saigon Basins (Figure 4.23). The subsidence curves shown in the Figures have been modified after Azim, (1993, personal communication). ß factor has been estimated for the Pattani basin by Hellinger and Sclater (1983) and is used in the basin as well. A single ß factor of 2 can be applied to all wells' studied here, although a better approximation is by assigning each well a ß value. However for regional approximation a single ß value is sufficient , considering the wells chosen in the analysis are all near the basin central axis. The background of 65mWm-2 is used. The comparison between the model and measured vitrinite reflectances and Oil and gas window can be determined after the thermal history has been established and maturity modelling being done.

4.3.3 Maturity profiles

The maturity modelling used in this study is based on kinetic model developed at Lawrence Livermore National Laboratory (LLNL). The model uses a distribution of Arrhenius rate constant to calculate global vitrinite maturation, then correlate maturation with
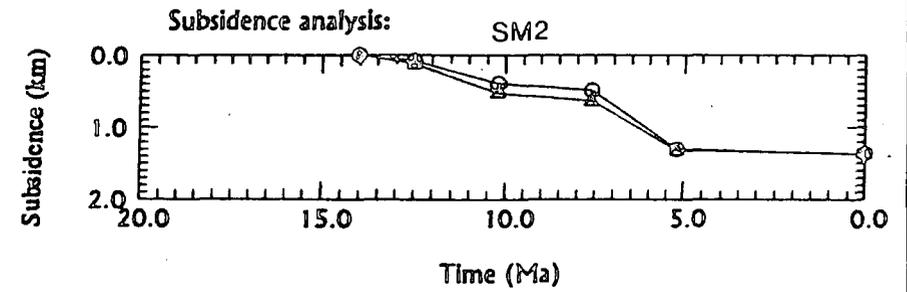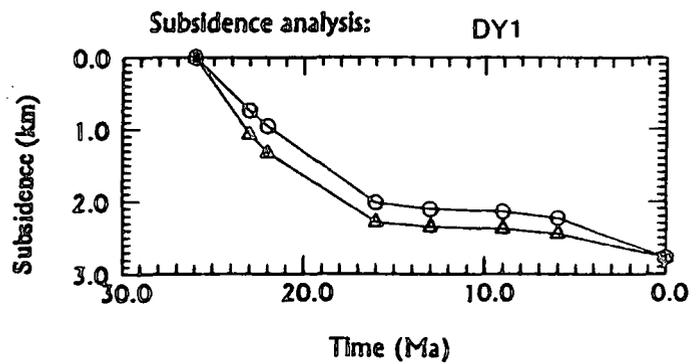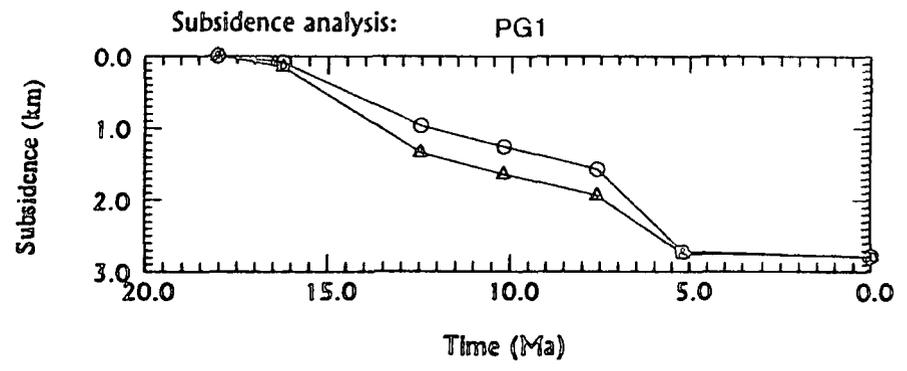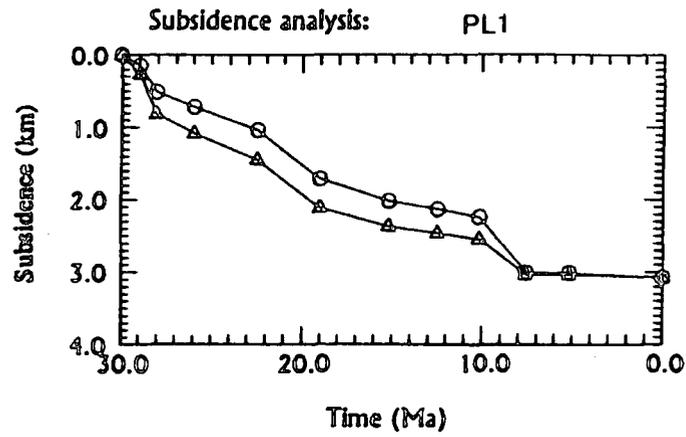
Figure 4.22 : Subsidence curves of selected wells in Malay Basin
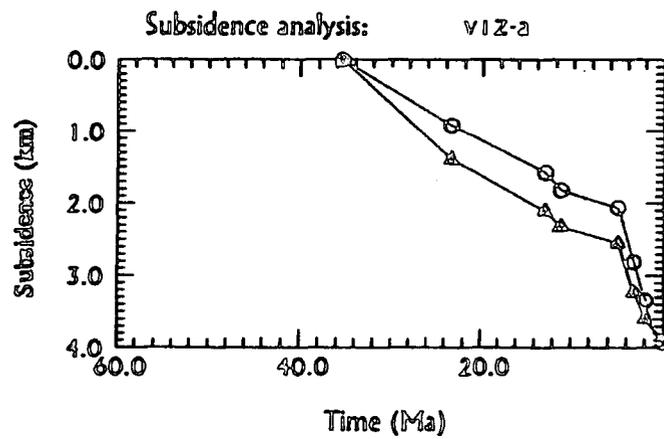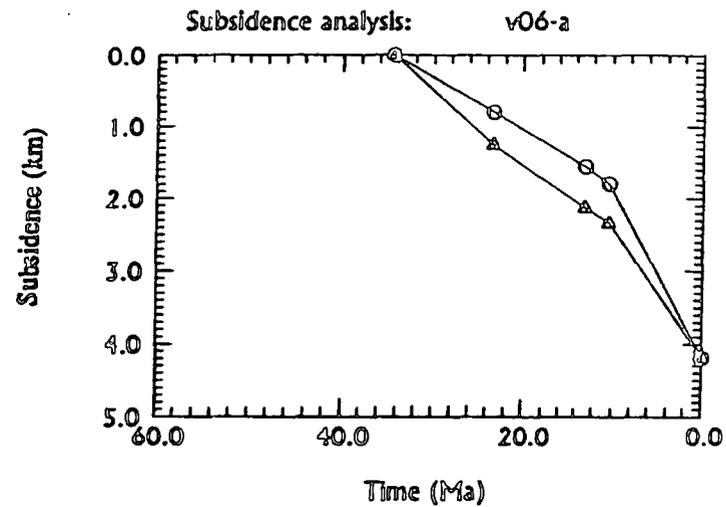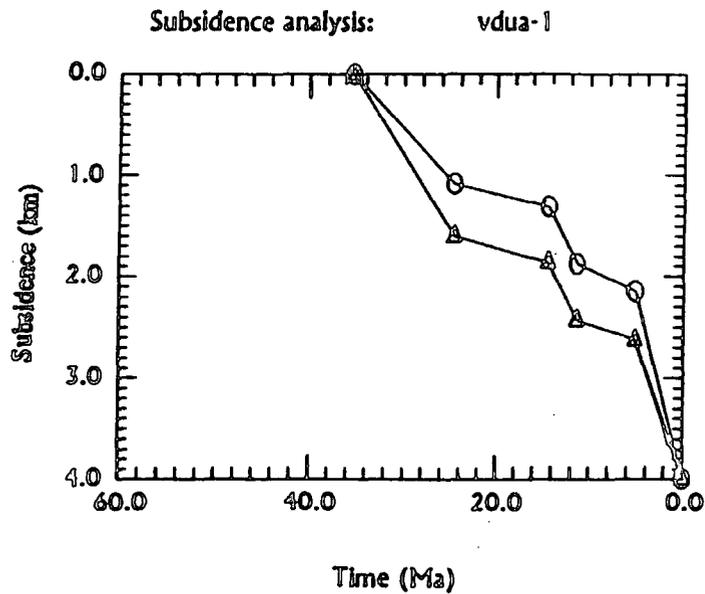
Figure 4.23 : Subsidence curves of selected wells in Saigon Basin

reflectance. This is a more acceptable method of maturity modelling than the other option, the Time Temperature Index method of Lopatin provided by the BASINMOD. Furthermore LLNL model gives the same answer as a more detailed model, VITRIMAT, which calculates vitrinite elemental composition, then correlates composition with reflectances(Sweeney and Burnham, 1990).

The maturity profiles for wells DM1, SM2, TP1 and AG1 are selected to represent the basin and are shown in Figures 4.24, 4.25, 4.26 and 4.27. The fit between the measured and modelled vitrinite reflectances indicated that the rifted model is applicable for the wells paleothermal modelling.

The modelled maturity curves are slightly and consistently higher than the vitrinite data in the upper column of every wells studied. A good match between the vitrinite and thermal model can be seen at the deeper intervals only. The suppression of the vitrinite along the upper column of the wells may be due to consistant low in reflectance readings or a possible lack of constrains in thermal modeling parameters such as the episodic changes in heat flow (Ru and Piggot, 1986) and the amount of erosions. In this study, for simplification, a single heat flow pulse due to rifting is assumed, during Late Oligocene. An example of the basement heat flow history can be seen from Figure 4.28. However the thermal models are considered to be in a general agreement with the measured vitrinite reflectances.

Wells TP1 and AG1 were drilled to depth of matured rocks within the oil windows. Oil window has been defined for 0.5 to 0.7% Vitrinite reflectance (Vr or Ro) to be Early Mature for oil, Vr of 0.7 to 1% is Mid mature for oil, and Vr of 1.3 % as Late Mature. Main Gas generation window is within Vr of 1.3 to 2.6%.
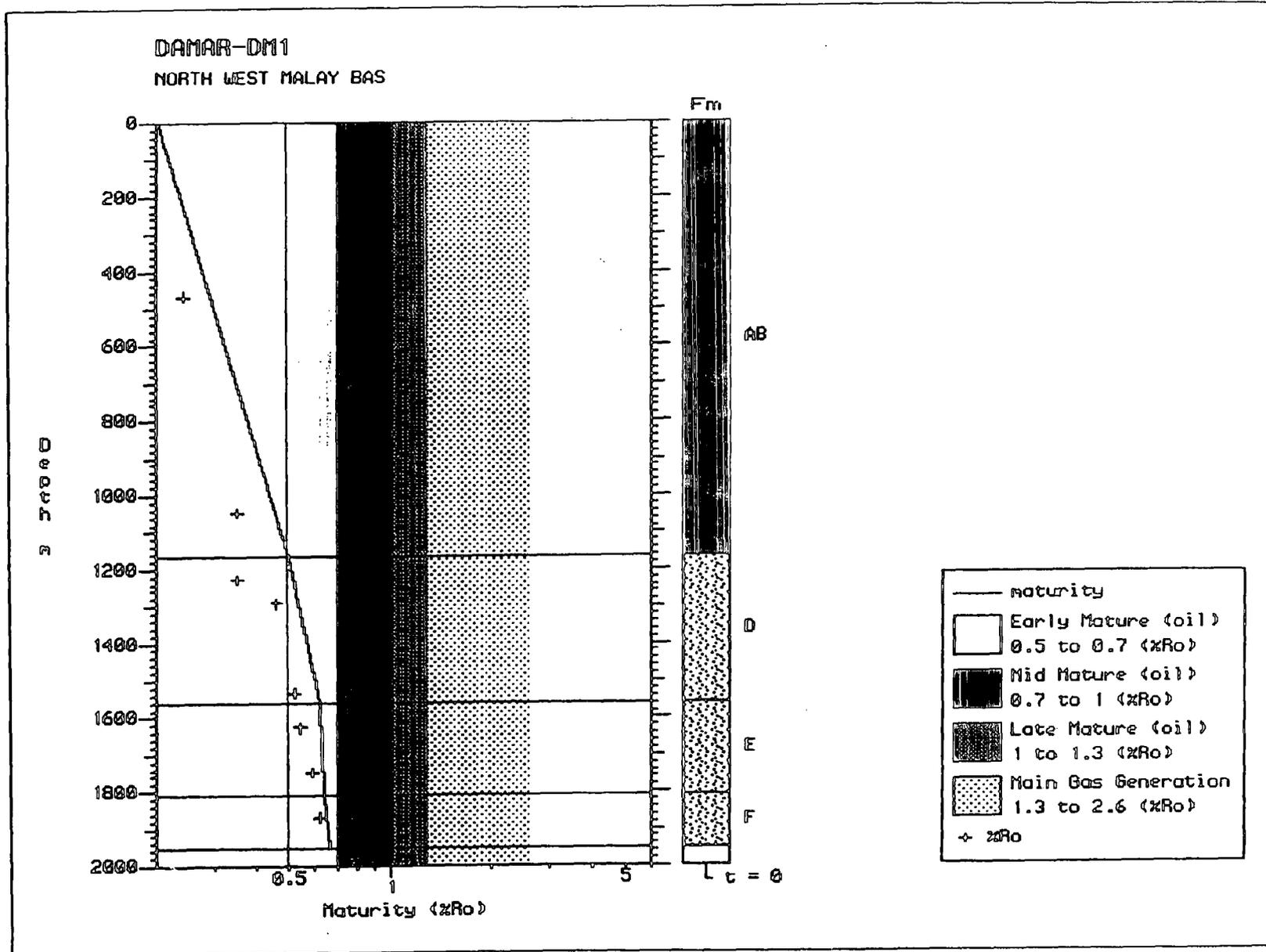
Figure 4.24 : Comparison between measured vitrinite reflectance and maturity model of well DM1
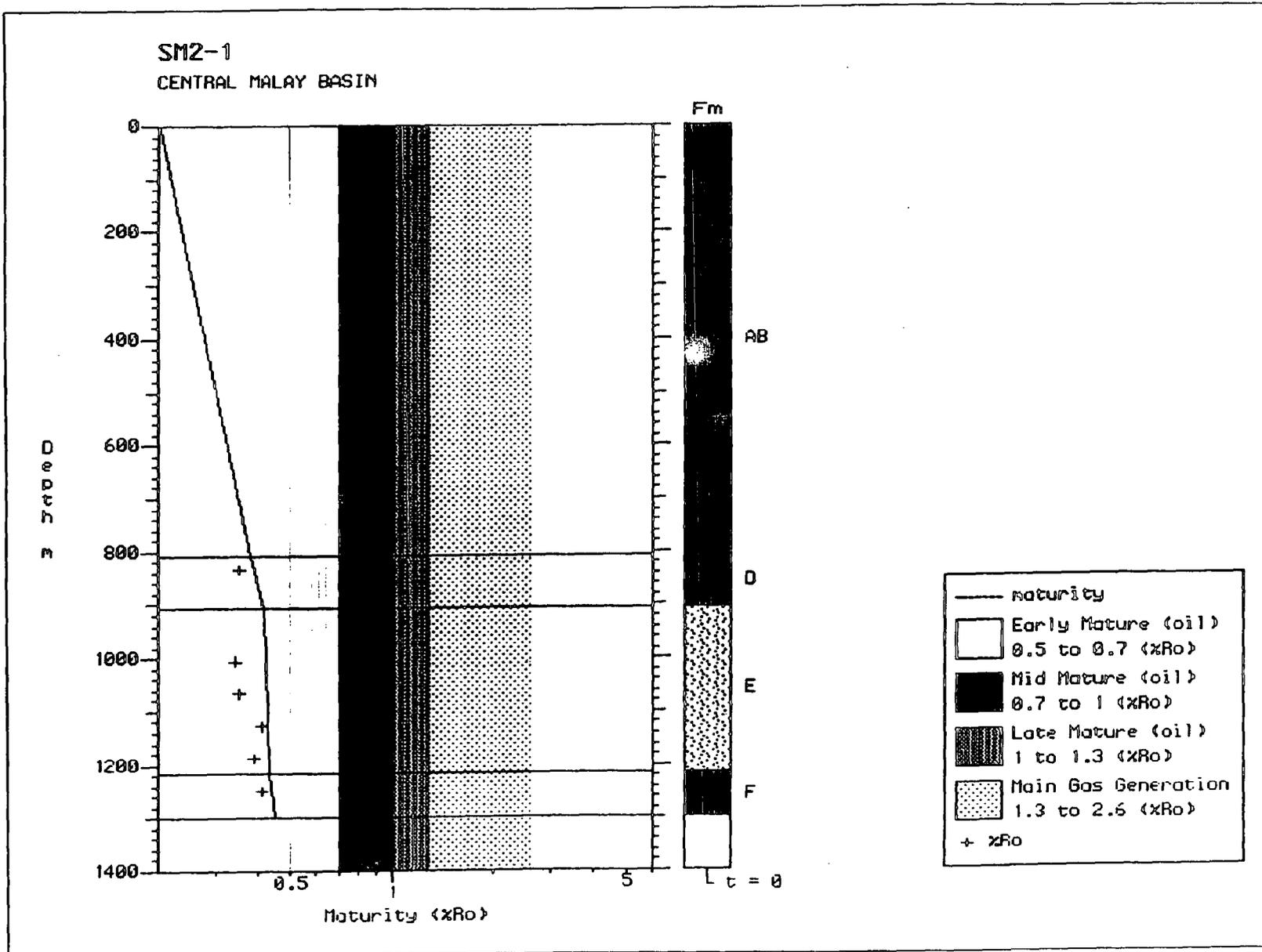
Figure 4.25 : Comparison between measured vitrinite reflectance and maturity model of well SM2
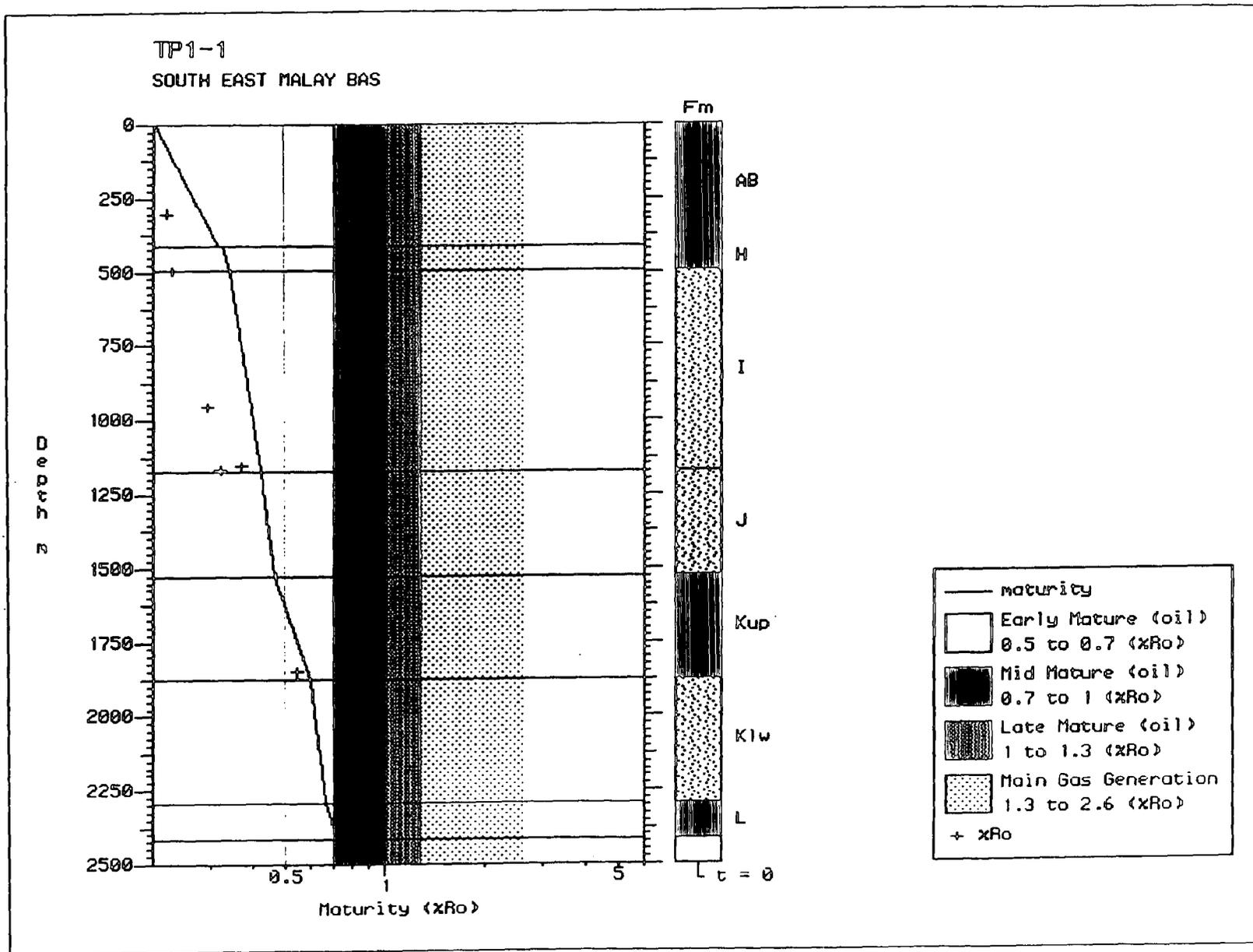
Figure 4.26 : Comparison between measured vitrinite reflectance and maturity model of well TP1
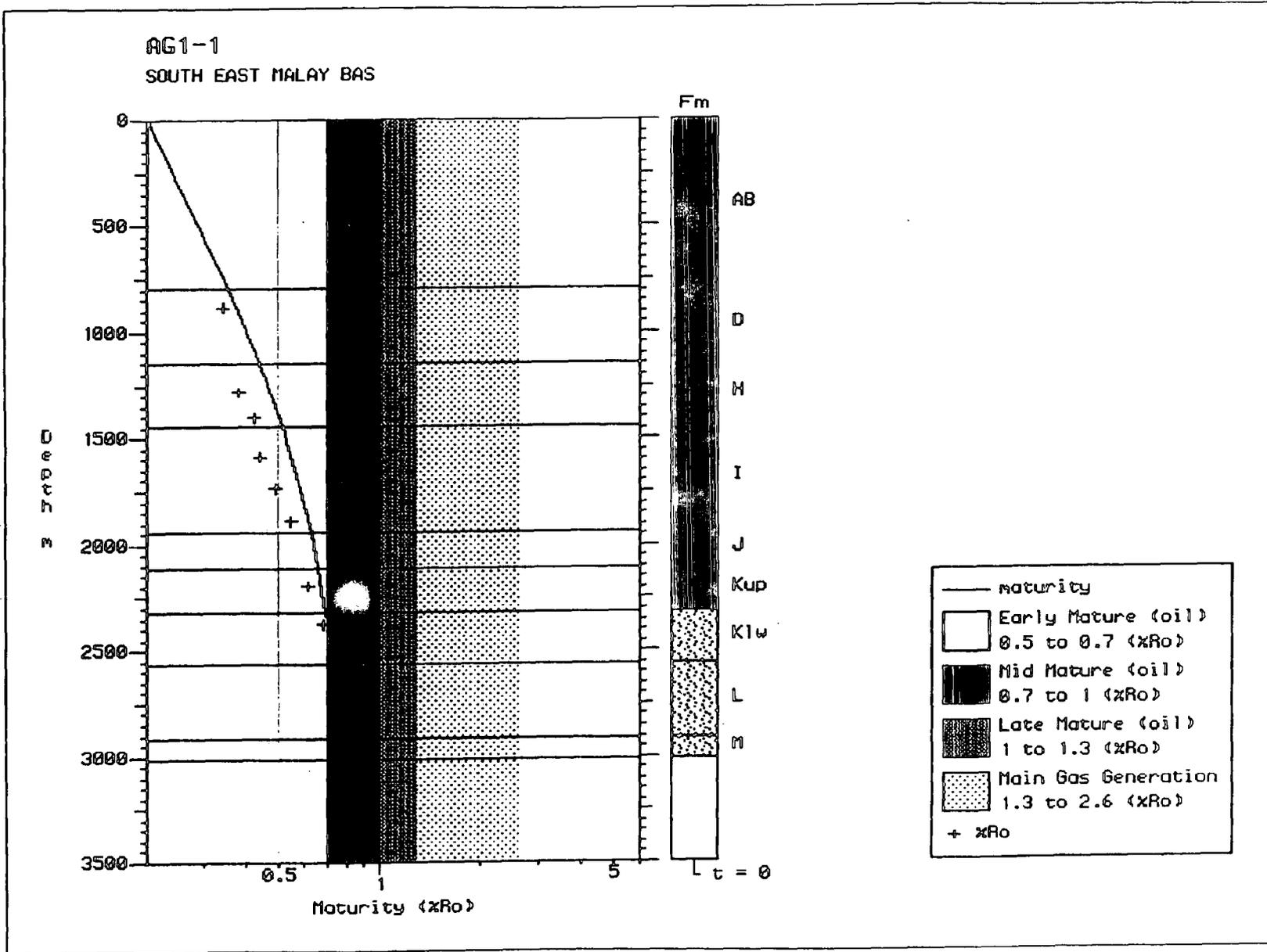
Figure 4 .27 : Comparison between measured vitrinite reflectance and maturity model of well AG1
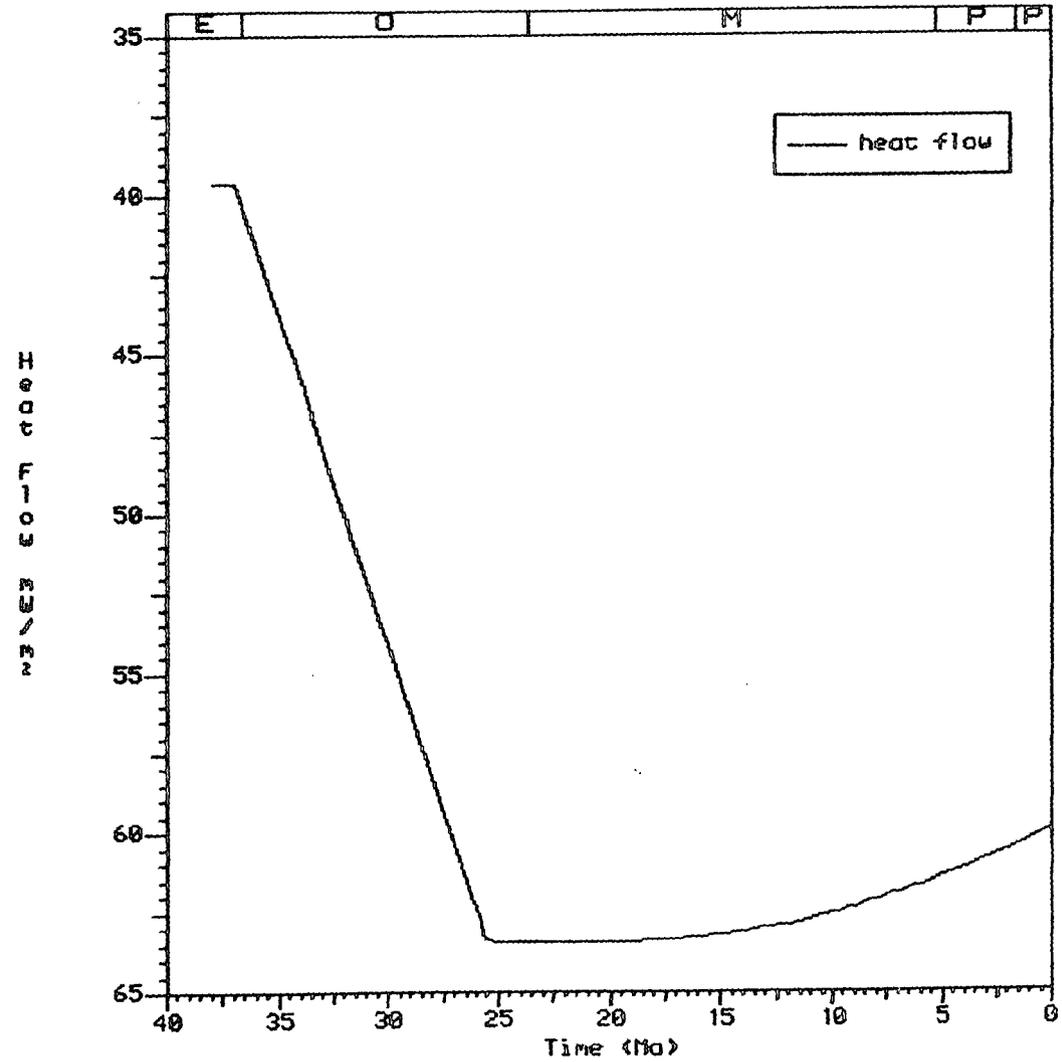
Figure 4 .28 : Paleo heat flow profile of well AG1

The Mid mature oil window of AG1 has been reached in Klw group at depth of 2325m and in TP1 at 2275m in the L shales. The probable source of oil in the Southern portion of the Malay Basin is the Klw and L shales. In the Northern portion, the wells studied do not reach the mid mature oil window. However from maturity profile of DM1 (Figure 4.24), the mid mature oil window is probably reached in H shales at depth below 1950m. The H shales can be the possible source for the Northern portion of Malay Basin. Therefore, the models suggest that the mid mature portion of the wells are the possible source beds.

4.3.4 Oil migration and deep prospects

The regional occurrences of oil windows are likely to be mostly below the overpressures. The reservoirs are mostly above the overpressured zones. There is possibility that oil has been migrated into the reservoirs from the depth below the overpressures. The migration of oil can take place laterally and vertically. The vertical migration took place from the source rocks below the overpressures only during episode of normal pressuring or near hydrostatics condition (Swarbrick and Edwards, 1993). The normal pressuring can be seen to have taken place during 16 to 12 ma and 9 to 2 m.a. period in Lower L sand of TP 1 (Figure 4.29). Maturation of hydrocarbon in the Southern portion of the Malay Basin occurred during Klw and L shales time (28 ma) and thus predated the episodes of hydrostatic pressure conditions. In the Northern portion the Maturation of source rocks in H group (before 13 ma) appears to predate the second episodes of normal pressuring. Therefore much of the oil have been migrated and trapped as most of the structures have been fully developed at about 13 and 5.2 m.a. in the Southern and Northern portion of the Malay Basin respectively (Figure1.8 and 1.6). In addition, possible hydrocarbon being trapped in the stratigraphic plays at the edges of the basin in the groups younger than Klw and H within the Southern and Northern portions of the basin respectively.The latest (later than 2 ma) episode of overpressuring in
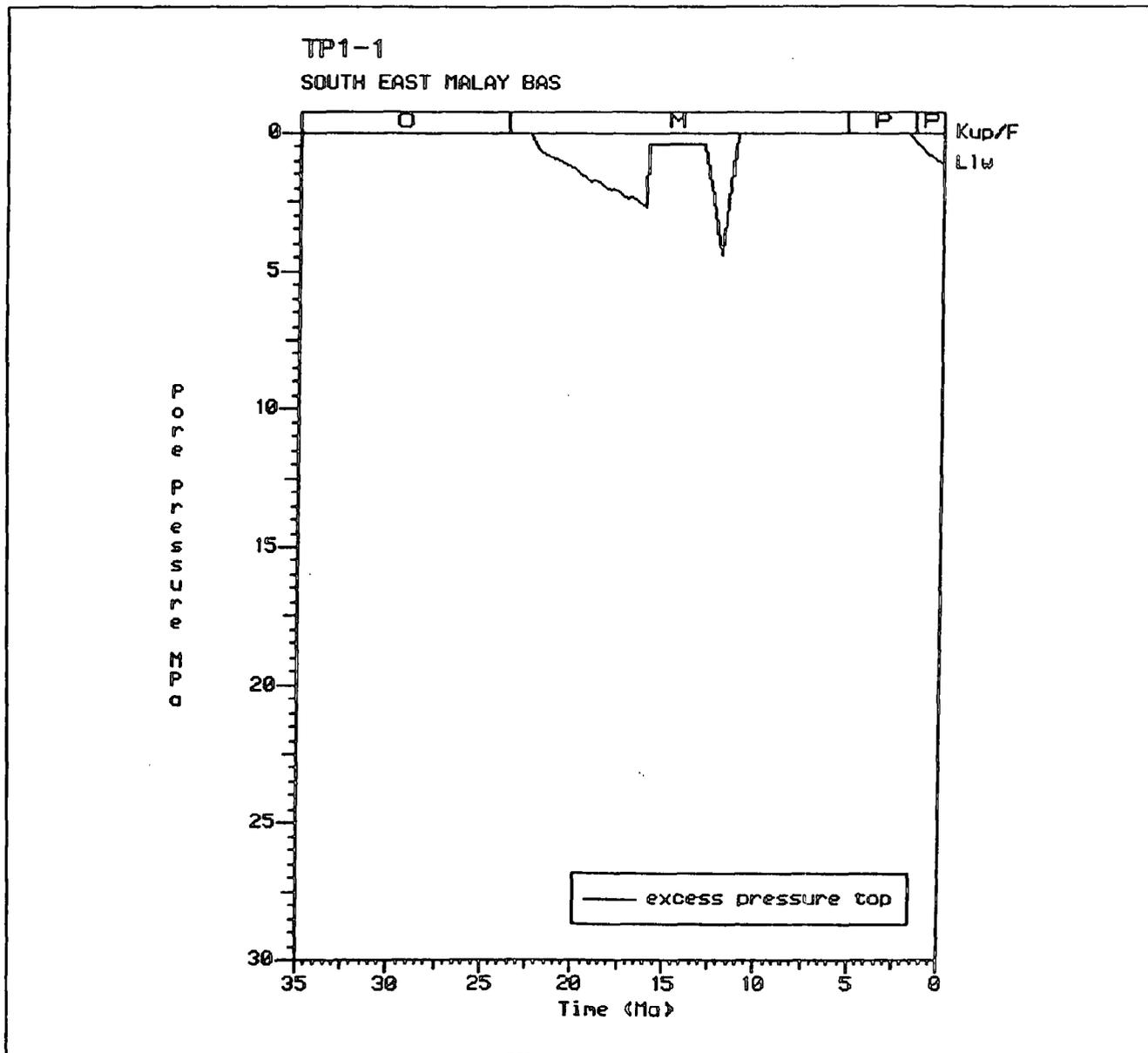
Figure 4.29 : Paleo pressure development of well TP1

the deep L sands can act as fluid flow barrier from the deeper reservoirs and hence increasing their sealing capacity. Therefore future drillings of deep reservoirs below the overpressures appear to be a good prospecting for hydrocarbon in the Malay Basin.

4.4   Conclusion

1.   High heat flow anomaly has been observed in the overpressured intervals of a well column. The temperature gradients can vary within the overpressured zone. In the transition zone just over the proper overpressured zone, the geothermal is high and is interpreted to be due to the thermal insulating effect of the zone.

2.   The surface heat flow anomalies are likely to be an indicator to the presence of overpressures at depths. Prediction of overpressured zones can be made if details on heat flow depth profile over an anomaly is known.

3.   There are evidences for multiple mechanisms of overpressuring in the Malay Basin. The prominent evidence being the disequilibrium compaction.

4.   The temperature history of the Malay Basin can be satisfactorily modelled by using extensional basin model with present-day background heat flow of about 65 MW/m2 .

5.   The oil windows in the Malay Basin are found below the overpressured zones and reservoirs. Migration of oil from source rocks to the reservoirs may have taken place during episodes of normal pressurings which predate the structuring of the basin.

6.   There are possibilities of deeper reservoirs below the overpressured zones which have enhanced trapping capacity by the overpressuring.

CHAPTER 5

Conclusions and recommendation for future studies

5.1   Findings and Conclusions

1.   A new method for calibration of measured thermal conductivity to borehole log records has been established for the wells in the Malay Basin. The procedure involves the use of two log parameters i.e. gamma ray and neutron porosity for calibration to the measured thermal conductivity of conventional cores.

2.   Seven thermal facies have been recognised, each of which is empirically related to the thermal conductivity by an empirical equation. From the reading of gamma ray and neutron porosity, thermal facies at any depth of a well column can be established and hence the thermal conductivity can then be determined. The thermal facies is related to the lithology, since they are calibrated to known lithologies.

3.   A new method for correction of bottom-hole temperature in estimation of true formation temperature at the wellbore has been established. The Horner plot equation is used for correction of the bottom hole temperature by allowing the cooling time to be predetermined. The cooling time is estimated from the known formation temperature taken from wells which have production test temperatures. The estimated cooling time obtained is known as the effective cooling time. From 58 readings of known effective cooling time, 5 equations relating them to the log readings have been established.

4.   The vertical profile of thermal parameters for 55 exploration wells have been determined which show the trend of heat flow, thermal conductivity and temperature with depth.

5.   Revised heat flow, thermal conductivity and geothermal gradient maps have been made for the Malay Basin which incorporate the new exploration well data. Several thermal anomalies have been identified. Estimation based on data from 59 wells, the average heat flow, geothermal gradient and thermal conductivity is estimated to be $86 + 10$ mWm^{-2}, $47 + 5$ °C(km)$^{-1}$ and $1.84 + 0.11$ W(m°K)$^{-1}$.

6.   The anomalous heat flow in vertical profile of the wells has been found to be related to advective heat associated either with (i) overpressured zones or (ii) the effect of fluid. Normally, the heat flow anomalies due to overpressure is larger than an anomaly resulting from fluid flow. Other factor of excessive heat transfer is inferred to be due to young structurings and shales diapirisms.

7.   The temperature of the onset of the overpressured zone has been observed to vary from about 90°C to 120°C. The distribution of the onset temperatures are concordance with the geological setup suggest that temperature can be an indicator to the mechanisms for overpressures, such as illitization and hydrocarbon generation. However, due to the fast rate of sedimentations in most of the stratigraphic units where a mix sandstone/shale lithology present, disequillibrium compaction is speculated to be the main cause of the overpressures.

8.   Of the Malay basin's total heat flow, about 65 mWm-2 is estimated to comprised of the background heat flow. The excess heat flow is due to fluid flow and internal radioactive has been estimated to be about 20 mWm-2. The overpressures and late tectonics account for the rest.

9.   Models for fluid flow based on the thermal properties of the Malay Basin has been adopted, using the newly interpreted thermal parameters of the basin. A fluid flow above the overpressured zones of selected wells are illustrated. Regional fluid flow pattern can be deduced from the models.

10.   Thermal maturity of the sediments of the Malay Basin can be estimated from the heat flow, thermal conductivity and temperature data , since the measured thermal maturity indicators has been used to calibrate the thermal data. Data from selected wells studied indicate that the maturity windows of the well columns has not been reached at all locations. However the model suggest that the H, Klw and L shales are matured for oil generation.

11.   Episodic overpressuring history of TP1 indicated that the normal pressuring episodes post dated the maturation of the source rocks. The timing of hydrocarbon generation and migration were appropriate for the hydrocarbon being trapped in the reservoirs.

5.2   Recommendation for future studies

1.   The present study has established a better method to determine the thermal properties of the basin. Coupled with pressure data and observations which relate to fluid movement (e.g. diagenetic cements, hydrocarbon migration) a fluid flow model could be attempted.

2.   A pilot study has been carried out by the author to investigate fluid flow history by analysis of reservoir petrography and fluid inclusion in diagenetic cements. Preliminary results (not reported in this thesis) lead me to recommend that a larger study can be conducted.

3.   Thermal maturity of the deeper part of the basin and in frontier areas can be analysed using the paleothermal model established here. In these areas thermal conductivity

approximation can be established from seismic data available. This could be achieved by linking seismic facies to sand-shale ratios (and pseudo gamma response) and velocity to pseudo porosity. The thermal conductivity can be estimated from the sonic velocity and seismic facies after being calibrated to thermal facies.

4.   The heat flow anomalies may be strongly influenced by the distribution of overpressure and the access for deep basin fluids to reach high stratigraphic levels. Consequently a full review of pressure distribution throughout the basin would yield insights into the interpretation the observed heat flow data and their implications for fluid flow.

REFERENCES

AIKEN, L. S. AND WEST, S. G. , 1991. Interaction between continuous predictors in multiple regression. *In Testing and Interpreting Interaction in Multiple Regression, Sage Publication, UK.*

ALLAN, P. A. AND ALLEN J. R., 1990. Thermal History, *Basin Analysis, Blackwell Scientific Publication, pp 301.*

ANDREW-SPEED, ET AL.,. 1984. Temperature and Depth-Dependent Heat Flow in Western North Sea. *The American Assoc. Petroleum Geol. Bull. V. 68, No. 11, pp 1764 - 1781.*

ARMITAGE, J. H. AND VIOTTI, C. 1977. Stratigraphic nomenclature-southernend Malay basin. *Proceeding Indonesian Petroleum Assos. Vol. 6, pp. 69-94.*

ATROSHCHENKO, P. P. , BOGOMOLOV, Y. G. AND PARKHOMOV, M. D. , 1982. Multifator dependences of thermophysical properties of rocks. *In Cermak, V. and Haenal, R. (Editors), Geothermics and Geothermal Energy, E. Schweizerbart'sche Verlagsbuchhandlung (Nagele u. Obermiller) Stturgart. pp. 129 - 132.*

BALDWIN, B. AND BUTLER, C. O., 1985. Compaction Curves. *The American Association of Petroleum Geologists Bulletin, V. 69, No. 6, pp 622 - 626.*

BARKER, C., 1972. Aquathermal pressuring: role of temperature in development of abnormal pressure zone. *The American Assos. Petrol. Geol., V. 56 pp. 2068-2071.*

BETHKE, C. M., 1993. Causes and Effects of Regional Fluid Migration within Sedimentary Basins (extended abstract). *In Parnell, J., Ruffel, A. H. , and Moles, N. R. . (Eds.) Geofluids '93, International Conference on fluid evolution, migration and interaction in rocks, Torquay, England. pp.241 - 243.*

BETHKE C. M., 1986. Inverse hydrologic analysis of the distribution and origin of Gulf Coast-type geopressured zones. *Journal of Geophysical Research, v. 91, pp. 6535-6545.*

BETHKE, C. M.,1985. A numerical model of compaction-driven ground water flow and heat transfer and its application to the paleohydrology of intracratonic sedimentary basin. *Jour. Geophys. Res. V. 80, p.6817-6828*

BLACKWELL, D. D. AND STEEL, J. L., 1989. Thermal conductivity of sedimentary rocks: Measurement and Significance. *In N. D. Naeser and T. H. McCulloh (Eds.), Thermal History of Sedimentary Basins, Methods and Case Histories., Springer-Verlag, New York pp. 13 - 36.*

BIRCH, F. , ROY, R. F. AND DECKER, E. R., 1968. Heat flow and thermal history in New York and New England. *In E. Zen, W. S. White, J. B. Hadley and J. B. Thomson (Eds.), Studies of Appalachian Geology: Northern and Maritime Interscience, New York, pp. 437 - 451.*

BIRCH, F AND CLARK, H. , 1940. The thermal conductiviy of rocks and its dependence upon temperature and composition, *American Journal. of Science., V. 246, pp 729-760.*

BONHAM, L. C., 1980, Migration of hydrocarbons in compacting basins, *In Roberts III, W. H. and Cordell, R. J. (eds.), Problem of petroleum Migration, The American Assos. Petrol. Geol., AAPG studies in Geology No. 10., pp. 69 - 88.*

BRIGAUD, F. , CHAPMAN, D. S. & DOUARAN, S. L. , 1990. Estimating Thermal Conductivity in Sedimentary Basin Using Lithologic Data and Geophysical Well Logs. *American Assos. Petrol. Geol. Bull. V. 7 , N. 9, p. 1459 - 1477.*

BRIGAUD, F. VASSEUR, G. AND GAILLET, G. , 1992. Thermal state in the north Viking Graben (North Sea) determined from oil exploration well data. *Geophysics, Vol. 57. No. 1 pp 69 - 88.*

BULLARD, E. C., 1939, Heat flow in South Africa. *Proceedings of the Royal Society of London Series A, V.173, p. 474-502.*

CAO, S., LERCH, I., AND HERMANRUD, C., 1988.Formation temperature estimation by inversion of borehole measurements. *Geophysics, V. 53, No. 7, p. 979-988.*

CATHLES, L. M. and NUNNS, A. G, 1991. A temperature Survey un Louisiana Shelf: Effects of Bottom-Water Temperature Variations. *The American Assos.of Petrol. Geologist, V 75, No. 1 p 180 - 186*

CHADWICK, R. HOLLIDAY, D. W, & ROWLEY, W. J. , 1991. Thermal History of Petroliferous Basins of the CCOP Region.2. The Malay Basin. *British Geol. Survey technical Report WC/91/02C.*

CHAKRABORTY, K. R., 1992. Geothermal energy and uranium mineralisation potential of the Main Range granite province, Peninsular Malaysia. *Abstract of Symposium on Tectonic Framework and Energy Resources of the Western Margin of the Pacific Basin, Kuala Lumpur. pp 59.*

CHAPMAN, R. E. ,1980. Mechanical versus thermal cause of abnormal high pore pressure in shales.*The American Assos. Petrol. Geol., V. 64 pp. 2179-2183.*

CHAPMAN, D. S. , KEHO. T. H. , BAUER, M. S. , AND PICARD, M. D. 1984, Heat flow in the Uinta Basin Determined from Bottom Hole Temperature (BHT) Data. *Geophysics, V. 49. No. 4, pp. 455 -466.*

CORREIA, A., JONES, F. W. AND FRICKER, A. 1990. Terrestrial heat flow density estimaties for the Jeanne D' Arc Basin, Offshore eastern Canada. *Geophysics, V. 55. No. 12, p. 1625-1633.*

DALY, M. C.,COOPER, M. A., WILSON, I., SMITH D. G., & HOOPER, B. G. D.1991. Cenozoic plate tectonics and basin evolution in Indonesia. *marine and Petroleum Geology, 1991, Vol. 8, pp. 2-21.*

DEMONGODIN, L., PINOTEAU, B., VASSEUR, G. AND GABLE, R.; 1991. Thermal conductivity and well logs: acase study in the Paris basin. *Geophy. J.Int. V.105, pp 675-691.*

DOWDLE, W. L. AND COBB, M. W., 1975. Static formation temperature from well logs, an empirical method. *J. Petr. Tech. V. 27, p. 1326-1330*

DUTTA, N. C., 1987. Fluid flow in low permeable porous media. *In DOLIGEZ, B. (Ed.), Migration of hydrocarbon in sedimentary basins, Editions Technip, pp.567-595.*

ESSO, 1976. Review of the geology of the Malay basin concession area, *Unpublished PETRONAS internal report.*

ETNYRE, L. M. , 1989. Neutron-Density Log Combination , *Finding Oil and Gas from Well Logs,* Van *Nostrand Reinhold , New York p 258 -269.*

FERTL, W. H., 1976. Abnormal formation pressure, *Elsevier Scientific Publishing Co., New York..*

FÖRSTER, A. ,MERRIAM D. F., 1993. Heat Flow changes and relation to fluid flow -an example from the Midcontinent, USA.(Extendned Abstract). *In Parnell, J., Ruffel, A. H. , and Moles, N. R. . (Edits.) Geofluids '93, International Conference on fluid evolution, migration and interaction in rocks, Torquay, England. pp. 103-106.*

FREED, R. L. AND PEACOR, D. R. , 1989. Geopressured Shale and Sealing Effect of Smectite to Illite Transition. *The American Assoc. of Petroleum Geol.,V 73, No. 10, pp 1223-1232.*

GLASER, S. AND HURTIG, E., 1984. The establishment of thermal equilibrium in deep borehole in the northern part of German Democratic Rep.. *Tectonophysics, V. 103, p. 47 - 54.*

GRIFFITHS, C. M., 1982. A proposed Geologically Consistent Segmentation and Reassignment Algorith For Petrophysical Borehole Logs. *In CUBITT, J. M.and REYMENT R. A. (Edit.), Quantitative Stratigraphic Correlation, John Wiley & Sons, p 287-298.*

GRETENER, P. E. , 1979. Pore pressure: Fundamentals, General Ramifications and Implications for Structural Geology. *AAPG Continuing Education Course Note Series 4 (Revised Edition).*

HEARTH , J. R., & NELSON, P. H., 1985. Well logging for Physical Properties. *MacGraw Hill, New York.*

HEDBERG, H. D. , 1980. Methane generatiopn and Petroleum Migration.. In Roberts III, W. H. and Cordell, R. J. (edit.), Problem of petroleum Migration, *The American Assos. Petrol. Geol., AAPG studies in Geology No. 10., pp. 179 - 206.*

HELLINGER, S. J. AND SCLATER, J. G. , 1983. Some comments on two-layer extensional models for the evolution of sedimentary basins. *Jour. of Geophysical Res. Vol. 88, No. B10, p. 8251-8269.*

HERMANRUD, C. AND SHEN, P. Y., 1989. Virgin rock temperatures from well logs accuracy analysis for some advanced inversion models.*Marine and Petroleum Geology, Vol.6, pp 360-363.*

HITCHON, B. 1984. Geothermal gradients, hydrodynamics and hydrocarbon ccurrences, Alberta, Canada. *Bull. Am. Assoc. petrol. Geol.V. 68, pp.713-43.*

HOWER, J.; ESLINGER, E. V.; HOWER, M. E.; PERRY, E. A. , 1976. Mechanism of burial metamorphism of argillaceous sediment: 1; mineralogical and chemical evidence. *Geol. Soc. of America Bull. V. 87, pp. 725-737.*

HUTCHISON, C. S. 1986. Tertiary basins of S. E. Asia - their disparate tectonic origins and eustatic stratigraphical similarites. *GEOSEA V proceedings Vol.1,Geol. Soc. Malaysia Bulletin 19, pp. 109-122*

HUTCHISON, C. S., 1989. The Paleo-Tethyan Realm and Indonesian Orogenic System of Souteast Asia.*In A. M. C. SENGOR (Ed.), Tectonic Evolution of the Tethyan Region, pp. 585 - 643. Kluwer Academic Publishers.*

JARVIS, G. T. AND McKENZIE, D. P. , 1980. Sedimentary basins formation with finite extension rates. *Earth Planet. Sci. Letters, V 40, p. 42-52.*

JESSOP, A. M. , HOBART, M. A. , SCLATER, J. G. , 1976. The World Heat Flow data collection - 1975. In *Energy, Mines and Resources, Ottawa, Canada, Geothermal Series No. 5, p. 125.*

JESSOP, A. M., 1990. Measurement of heat flow on land. *In: Thermal Geophysics. Elsevier, New York.*

JONES, F. W. & MAJOROWICZ, J. A.,1987.. Some aspects of the thermal regime and hydrodynamics of the western Canadian sedimentary basin. In: GOFF, J. C. & WILLIAMS, B. P. J. (eds.) *Fluid Flow in sedimentary Basins and Aquifers, Geologic. Soc. Special Pub. 34, pp. 79-85.*

JONES, P. H. 1980. Role of Geopressurein the Hydrocarbon and water System. *In Roberts III, W. H. and Cordell, R. J. (edit.), Problem of petroleum Migration, The American Assos. Petrol. Geol., AAPG studies in Geology No. 10., pp. 207 - 216.*

KRUMBEIN, W. C. AND GRAYBILL, W. C.; 1965. An Introduction to statistical model. *McGraw Hill Book, London.*

LACHENBRUCH, A. H. AND SASS J. H. 1977.Heat flow in the United States and the thermal regime of the earth. In HEACOCK, J. G. (Ed.) *The Nature and Physical Properties of the Earth Crust. Geophysics Monograph, Am. Geophysical Union, V. 20, pp 626 675.*

MAGARA, K. , 1987. Fluid flow due to sediment loading - an application to the Arabian Gulf region.. In GEOFF, J. C. AND WILLIAMS, B.P. J. (Eds), *Fluid Flow in Sedimentary Basins and Aquifers, Geological Society Special Publication No. 34, pp. 19-28.*

MAGARA, K. , 1978. Compaction and Fluid Migration.*In Practical Petroleum Geology, p. 11-25. Am. Elsevier, New York.*

MAJOROWICZ, J. A. , JONES, F. W., & JUDGE A.S., 1990. Deep subpermafrost thermal regime in the Mackenzie Delta basin, northern Canada - Analysis from petroleum bottom-hole temperature data. *Geophysics, V. 5, N. 3, p 362-371.*

MAJOROWICZ , J.A. , JONES, F. W., LAM, H. L. ,1985. Regional variations of heat flow differences with depth in Alberta, Canada. *Geophy. J. R.. Astr. Soc. V. 81, pp. 479 - 487.*

MAJOROWICZ, J.A., JESSOP, A.M., 1981 Regional heat flow patterns in the Western Canadian sedimentary basin, *Tectonophysics, vol. 74 pp 209 - 238.*

MANN, D. M. AND MAcKENZIE, A. S. , 1990. Prediction of pore fluid pressures in sedimentary basins. *Marine and Petroleum geology, V. 7, pp. 55-65*

MATSUBAYASHI, O. and UYEDA, S., 1979. Estimation of heat flow in exploration well in offshore areas of Malaysia. *Bull. of Earthquake Res. Inst. Tokyo, pp. 54.*

MAYER, H. J., MCGEE, H. W. 1985. Oil and Gas Accompanied by Geothermal Anomalied in Rocky Mountain Region. *The American Association of Petroleum Geologists Bulletin, V. 69, No. 6, pp 933 - 945.*

McCORD, J.; REITER, M. AND PHILIP, F.; 1992.Heat flow data suggest large ground water fluxesthrough Fruitland coals of the northern San Juan basin,Colarado-New Mexico. *Geology, v. 20, p. 419-422.*

McKENZIE, D. 1978. Some remarks on the development of sedimentary basins, *Earth and planetary Science Letters, Vol. 40, pp. 25-32.*

MUDFORD, B. S. AND BEST, M. E. , 1989. Venture Gas Field, Offshore Nova Scotia: Case Study of Overpressuring in region of Low Sedimentation.*The American Assos. Petrol. Geol., V. 73, No. 11 p. 1384-1396.*

MUDRORD, B. S., 1988. Modeling of the occurence of over pressures on the Scotian Shelf, Offshore Eastern Canada. *Jour. Geophys. Res. V. 93,No B7, p. 7845 -7855*

NG T. S. , 1987. Trap styles of the Tenggol Arch and the Southern part of the Malay Basin. *Bull. Geol. Soc. of Malaysia, No. 21 pp 177 - 193.*

NGAH, KHALID B. , 1990. Deposition and diagenesis of Oligocene-Lower Miocene Sandstones in the Southern Malay Basin. *Phd. thesis, ImperialCollege, London.*

NIK RAMLI, 1988. Humid tropical fan-delta sedimentation: An ancient model from the K sandstones (Late Oligocene-Early Miocene), Southeastern part of Malay Basin, Offshore West Malaysia. *In W. NEMEC AND R. J. STEEL (Eds.), Blackie Publication Co. , p. 341-353.*

OXBURGH, E, R. AND ANDREW-SPEED, C. P. ; 1981. Temperature, Thermal Gradients, and heat flow in the Soutwestern North Sea. .*in L. V. Illing and G. D. Hobson, (Eds.), Petroleum Geology of the continental shelf of North West Europe: London, Institute of Petroleum, p. 141 - 151.*

PALCIAUSKAS, V. V. , 1986. Models for thermal conductivity and permeability in normally compacting basin.*In: BURRUS, J. (Ed.), Thermal Modeling in sedimentary basin, Edition Technip p. 323 -335.*

PERRY, E.,AND HOWER, J. 1970. Burial diagenesis in Gulf Coast pelitic sediments. *Clays and Clay Minerals, v. 18, p. 165-177.*

RAYMER, L. L. ,HUNT, E. R. AND GARDNER, J. S., 1980. An improved sonic transit time to porosity transformation. *Soc. of Professional Well Log Analysis, Twenty first Anual logging symposium, p. 1 - 13.*

REITER, M.; COSTAIN, J. K. ; MINIER, J. , 1989.Heat flow data and vertical groundwater movement , examples from Soutwestern Virginia. *Jour. Geophys. Res. V. 94,No B9, p. 12423-12431.*

ROBERT, P., 1988. Method and means of paleothermal analysis. *In: Organic Metamorphism and Geothermal History, Elf-Aquitaine and D. Reidel, Ch. 2, p. 33.*

ROBERTS, W. H. , 1980. Design and Function of Oil and Gas Traps. *In* ROBERTS, W. H. III AND CORDELL, R. J. *(Eds.). Problems of Petroleum Migration, AAPG Studies in Geology No. 10, p. 217-240.*

ROY , R. F. , BLACKWELL, D. D. , AND BIRCH, F. ,1968. Heat Generation of plutonic rocks and continental heat flow provinces. *Earth Planetary Science Letter V. 5. pp. 1 - 12.*

RU, K. AND PIGOTT, J. D., 1986. Episodic rifting and subsidence in the South China Sea. *The American Assos. Petrol. Geol., V. 70, pp. 1136-1155.*

RYBACH, L. 1986. Amount and Significance of Radioactive Heat Sources in Sediments. *In BURRUS, J. (Ed.) Thermal Modelling in Sedimentary Basins,Editions Technip p. 311 - 322.*

SOUTH EAST ASIA PETROLEUM EXPLORATION SOCIETY (S. E. A. P.E X.) ,1977. Geothermal gradient map of Southeast Asia, *Indonesian Petroleum Assoc., Jakarta*

SAVIN, S. M. ET AL., 1985. The evolution of Miocene surface and near-surface marine temperatures: Oxygen isotopic evidence. *Geol.Soc. of America memoir V.63, p. 49 - 72*

SCLATER, J. G. AND CHRISTIE, P. A. F., 1980.Continental stretching: An explaination of the Post-Mid-Cretaceous subsidence of the Central North Sea basin. *J. of Geop. Reaserch, V. 85, No. B7, p. 3711-3739.*

SCLATER, J. G. , PARSON, B. AND JAUPART, C. 1981. Oceans and continents: similarities and differences in the mechanism of heat loss. *J. Geophysical Res., V. 86, pp 11 535 - 11 552.*

SEKIGUCHI, K. , 1984. A method for determining terrestrial heatflow in oil basinal area. *Techtonophysics, V 103, p 67-79.*

SCHLUMBERGER, 1988.Shaly sands interpretation. *In Basic Log Interpretation Seminar, UK1 Division, Chapter 13. p. 4.*

SHI, Y. AND WANG, C - Y. , 1986. Pore pressure Generationin Sedimentary Basins: Overloading Versus Aquathermal. *J. Geaophy. Res.V.91, No. B2, p. 2153- 2162.*

SMITH, L. AND CHAPMAN, D. S. 1983. On the thermal effects of ground water flow in Regional scale systems. *J. Geaophy. Res. V. 88, p. 593-608.*

SPEECE, M. A.; BOWEN, T.D.; FOLCIK, J. L. AND POLLACK, H. N.; 1985. Analysis of temperatures in sedimentary basins: the Michigan Basin. *Geophysics, V. 50, No. 8, pp 1318 - 1334.*

SPENCER, C. W.; 1987. Hydrocarbon generation as a mechanism in overpressuring in the Rocky Mountain region, *The American Assos. Petrol. Geol.Bull., V. 71, p. 368-388.*

SWARBRICK, R. E. AND EDWARDS, S. C. , 1993. Overpressure and Paleopressure (Extendned Abstract). *In Parnell, J., Ruffel, A. H. , and Moles, N. R. . (Edits.) Geofluids '93, International Conference on fluid evolution, migration and interaction in rocks, Torquay, England. pp. 333-337.*

SWEENEY, J. J. AND BURNHAM, A. K. , 1990. Evaluation of a simple model of Vitrinite Reflectance Based on Chemical Kinetics.*American Assos. of Petr. Geologist, Vol. 74 No.10 p. 1559-1570.*

TAPPONNIER, P., PELTZER, G., Le DAIN, A. Y. , ARMIJO, R. AND COBBOLD, P., 1982. Propagating extrusion tectonics in Asia: New insights from simple experiments with plasticine. *Geology V. 10 No. 12 p. 611-616.*

THAMRIN, M, 1985. An investigation of the relationship between the geology of Indonesian sedimentary basins and Heat flow density. *Tectonophysics, V. 121.p. 45-62.*

TISSOT, B. P. , FORD, J. F. AND ESP*I* TALI$\tilde{E}$, J. , 1980. Principle factors controlling the timing of petroleum generation. In Fact and Principles of World Petroleum Ocurrences. *Canadian Society of Petroleum Geologist Memoir 6, p. 143-152.*

TISSOT, B. P. , PELET, R. AND UNGERER, P. , 1987. Thermal History of sedimentary basins, maturation indices, and kinetic of oils and gas generation. *The American Assos. Petrol. Geol., V. 71, p. 1445-1466*

TURCOTTE, D. L.AND AHERN, J. L., 1977. On the thermal and subsidence history of sedimentary basins, *Jour. Geophys. Res. V. 82, p. 3762-3766.*

VACQUIER, V., 1984. Oil field - A source of Heat Flow data. *Tectonophysics, V104, p. 81-97.*

VACQUIER, V., MATHIEW, Y., LGENDRA, E. & BLONDIN, E., 1988. Experiment on estimating thermal conductivity of sedimentary rocks from oil well logging, *American Assos. of Petr. Geologist, Vol. 72 No. 6 p. 758-764.*

VAIL, P. R., & MITCHUM, R. M. , 1979. Global cycles of relative changesof sea level from seismic stratigraphy, *Geological and geophysical investigations of continental margins, American Assos. Petrol. Geol. Memoir No. 29, p.469-472.*

WALLACE, J., 1980. EPMI Peninsular Malaysia Contract Area abnormal pressure study. *Unpublished PETRONAS internal report.*

WAN ISMAIL W. Y., 1984. Heat flow study in Malay basin, *Combined proceedings of the Joint Ascope/CCOP Workshop 1 and 11, Ascope/Tp 5, CCOP/TP 15. p. 77-87.*

WANG, J. -Y. AND XIONG , L. -P., 1989. Ground water flow and Geotemperature pattern. *Geophysical.Monograph of International Union of Geodesy and Geophysics and American geophysical Union.p. 87 - 105.*

WAPLES, D. W. , 1991. Generation and Migration of Petroleum from Abnormally pressuredFluid Compartments: Discussion. *The American Assoc. of Petroleum Geol.,V 75, No. 2, p. 326 - 327*

WAPLES, D.W. , 1980. Time and temperature in petroleum formation, application of Lopatin's method to petroleum exploration.*The American Assoc. of Petroleum Geol., V. 64, pp 916-926*

WILLET, S. D. AND CHAPMAN D. S., 1987. Temperatures, Fluid Flow and the Thermal History of the Uinta Basin. *In Doligez, B. (Ed.), Migration Of Hydrocarbons In Sedimentary Basins, p 533 - 551.*

WILLET, S. D. AND CHAPMAN, D. S., 1989. Temperatures, Fluid Flow and Heat Transfer Mechanisms in The Uinta Basin. *Geophysical.Monograph of International Union of Geodesy and Geophysics and American geophysical Union.p. 29 - 33.*

WODSBURY, A. D.AND SMITH, L. 1985. On the thermal effects of three dimensional groundwater flow. *J. Geaophy. Res.* 90, 759-67.

ZIELINSKI, G. W., AND BRUCHHAUSEN, P. M. , 1983. Shallow Temperatures and Thermal Regime in the Hydrocarbon Province of Tierra del Fuego. *The American Assoc. of Petroleum Geol. Bull. v. 67, No. 1 p. 166 - 177.*

APPENDIX

Appendix 2.1:

List of measured thermal conductivity, log parameters, description of lithology and thermal facies of the sample used in the analysis

Appendix 2.2

An example of thermal - log analysis data sheet

Appendix 2.3

List of estimated thermal data of selected wells in the Malay Basin

Appendix 2.1 List of measured thermal conductivity, k, and log data used in the calibration. Thermal facies are shown to relate with the lithological facies (see Section 2.2.4).
Note that the lithological description is brief. sst = sandstone slt = silstone, shl = shale, cly = clay and ms = mudstone. Other abreviations are mostly for grainsizes, e.g. f = fine, m = medium, arg = argillaceous.

Well	Depth (m)	k (W/m°K)	lithology	Vf (%)	Øn (%)	Thermal Facies
JR3	1937	3.66	sst,f	0	24	kf1
JR3	1940	3.90	sst,f	0	25	
PU3	1931	6.10	sst	2	9	
PU3	1931	4.88	sst	2	10	
PU3	2165	4.95	sst	2	13	
PU3	2168	5.41	sst	2	14	
PU3	2169	5.02	sst	2	14	
PU3	1921	5.15	sst	4	16	
TO2	1838	4.53	sst,mu	4	23	
TO2	1844	3.73	sst,ml	6	22	
PU3	2173	5.60	sst	7	14	
PU3	1932	4.67	sst	7	12	
BS1	1625	3.39	sst	8	29	
TO2	1847	4.32	sst,ml	8	23	
TO2	1841	3.53	sst,f	9	25	
TO2	1845	3.29	sst,ml	10	24	
JR3	1734	3.87	slt	11	23	
GN8	2407	3.95	sst,sl,arg	11	19	
BS1	2130	3.64	sst,vfu,aa	12	24	
TO2	1831	4.16	sst.fl	13	22	
BS1	2110	3.96	sst,fu,crg,fe	14	24	
GN8	2397	3.73	sst,sl,arg	15	18	
BS1	2113	3.38	sst,vfu,aa	16	24	
JR3	1397	3.42	sst,f,r	18	32	
GN8	2410	3.91	sst,sl,arg	19	19	
BS1	2120	3.61	sst,vfu,aa	19	22	
BS1	2126	3.63	sst,vfu,aa	19	21	
JR3	1403	3.22	sst,f,r	19	31	
JR3	1410	3.33	sst,f,r	19	31	
JR3	1412	2.95	sst,f,r	19	34	
BS1	2121	3.75	sst,vfu,aa	20	22	
TO2	1803	3.29	sst,mud	22	22	
TO2	1821	3.49	sst,f	22	25	
BS1	1620	2.74	sst,vfl,arg,	23	31	
GN8	1790	3.29	sst,fl	24	28	
JR3	1263	3.76	sts,fl,qcd	24	26	
JR3	1401	3.16	sst,f,r	24	32	

Well	Depth (m)	k (W/m°K)	lithology	Vf (%)	Øn (%)	Thermal Facies
			Appendix 2.1 (continued)			
BS1	2114	3.69	sst,vfu,aa	24	24	kf1
BS1	2125	3.17	sst,vfu,aa	24	22	
TO2	1865	3.74	sst,fu	25	24	
PU3	1929	3.86	slt	28	16	kf2
GN8	2410	3.91	sst,sl,arg	19	19	
GN8	2414	3.24	sst,sl,arg	36	20	
BS1	2126	3.63	sst,vfu,aa	19	21	
BS1	2120	3.61	sst,vfu,aa	19	22	
BS1	2121	3.75	sst,vfu,aa	20	22	
BS1	2114	3.69	sst,vfu,aa	24	24	
TO2	1865	3.74	sst,fu	25	24	
BS1	2118	3.37	sst,vfu,aa	33	24	
TO2	1821	3.49	s,f	22	25	
JR3	1263	3.76	sst,fl,qcd	24	26	
TO2	1791	3.44	sst,f,arg	26	26	
TO2	1819	3.30	s,f	26	26	
TO2	1882	3.78	sst,ms,v f	26	26	
PL2	1933	2.80	sst,fl	41	27	
TO2	1879	3.45	sst,msv, f	26	27	
JR3	1748	3.20	slt,sal	40	28	
GN8	1790	3.29	sst,fl	24	28	
TO2	1873	2.98	sst,f,lenses	29	28	
IN3	1452	2.69	sst,arg,sl	40	28	
BD2	1986	3.16	slt	39	29	
IN3	1700	2.99	slt,arg	35	30	
JR3	1720	2.55	sst,vf	40	30	
JR3	1403	3.22	sst,f,r	19	31	
JR3	1410	3.33	sst,f,r	19	31	
IN3	1699	3.03	slt,arg	32	31	
IN3	1705	2.96	slt,arg	33	31	
JR3	1716	2.64	sst,vf,fls	40	31	
JR3	1397	3.42	sst,f,r	18	32	
JR3	1401	3.16	sst,f,r	24	32	
IN3	1705	2.60	slt,arg	35	33	
JR3	1412	2.95	sst,f,r	19	34	
PL2	1931	3.90	sst,vf	35	28	kf3
IN3	1700	2.99	slt,arg	35	30	
IN3	1705	2.60	slt,arg	35	33	
BD2	1986	3.16	slt	39	29	
JR3	1716	2.64	sst,vf,fls	40	31	
JR3	1748	3.20	slt,sal	40	28	
IB4	963	2.72	cly	40	36	
IB4	966	2.38	cly	40	35	
BD2	1985	3.42	slt	41	28	
GN8	2413	4.38	sst,sl,arg	41	19	
IB4	966	2.36	cly	42	37	

Appendix 2.1 (continued)						
Well	Depth (m)	k (W/m°K)	lithology	Vf (%)	Øn (%)	Thermal Facies
PL2	1933	3.72	sst,vfu	44	27	kf3
PL2	1935	3.67	sst,vfl	44	27	
PL2	1936	3.67	sst,vfl	44	28	
IB4	704	1.83	cly	46	41	
IN3	1698	2.97	slt,arg	48	31	
PL2	1937	3.52	sst,vfl	49	28	
GN8	1579	3.03	sst,vf,arg	50	30	
IB4	710	1.72	cly	51	43	
IB4	712	1.80	cly	51	43	
GN8	1483	2.66	sst,fu,arg,cbr	52	30	
IB4	713	2.12	cly	53	43	
JR3	1726	2.74	ms	53	29	
BS1	1609	2.50	ms	54	36	
BD2	1987	3.22	slt	57	30	
BD2	1987	3.33	slt	57	29	
BD2	1988	2.95	slt	57	31	
BD2	1989	3.31	slt	57	28	
BS1	2057	3.05	sl,crb	57	28	
IN3	1701	2.56	sl,arg	60	34	
GN8	1581	2.75	sl,crb,fe	61	30	
PL2	1928	2.91	l,arg	63	28	
GN8	1512	2.48	slt,crb,fe,arg	65	34	
BD2	1987	3.22	slt	57	30	kf4
BD2	1987	3.33	slt	57	29	
BD2	1988	2.95	slt	57	31	
BD2	1989	3.31	slt	57	28	
BS1	2057	3.05	slt,crb	57	28	
GN8	1581	2.75	slt,crb,fe	61	30	
PL2	1928	2.91	slt,arg	63	28	
IB2	1103	3.05	sst,arg	63	42	
JR3	1945	2.63	shl/l	67	26	
GN8	1516	2.81	sst,arg,	69	29	
PU3	1234	2.73	slt	79	43	
JR3	1933	2.33	sst,vf	80	30	
PU3	1232	2.19	slt	85	46	
JR3	1397	3.42	sst,f,r	18	32	kf5
JR3	1393	4.00	sst,vfu,fls	22	33	
JR3	1412	2.95	sst,f,r	19	34	
IB2	1109	1.54	sst,arg	13	37	
IB2	1106	1.13	sst,arg	17	42	
IN3	1697	2.89	slt,arg	27	42	
IN3	1705	2.60	slt,arg	35	33	kf6
BD2	1696	1.96	sst	25	34	
JR3	1284	2.43	sst,fl,rtec	33	34	
IN3	1697	3.16	slt,arg	40	34	
PL2	1929	3.59	slt,arg	53	34	

Well	Depth (m)	k (W/m°K)	lithology	Vf (%)	Øn (%)	Thermal Facies
IB4	966	2.38	cly	40	35	kf6
IB4	963	2.72	cly	40	36	
BS1	1610	2.92	ms	46	37	
IB4	966	2.36	cly	42	37	
IB4	704	1.83	cly	46	41	
IB2	1103	3.05	sst,arg	63	42	
IB4	710	1.72	cly	51	43	
IB4	712	1.80	cly	51	43	
IB4	713	2.12	cly	53	43	
IN3	1697	3.16	slt,arg	40	34	kf7
IB4	963	2.72	cly	40	36	
IB4	966	2.38	cly	40	35	
IB4	966	2.36	cly	42	37	
BS1	1610	2.92	ms	46	37	
IB4	704	1.83	cly	46	41	
IB4	710	1.72	cly	51	43	
IB4	712	1.80	cly	51	43	
IB4	713	2.12	cly	53	43	
IB4	713	2.12	cly	53	43	
PL2	1929	3.59	slt,arg	53	34	
GN8	1487	3.86	sst,fu,arg,cbr	64	33	
PU3	1234	2.73	slt	79	43	
PU3	1232	2.19	slt	85	46	

Appendix 2.1 (continued)

Appendix   2.2   An example of thermal analysis data sheet. This sheet is extracted from IR1 data base used for the prediction thermal conductivity, formation temperature and other thermal parameters.

Well	IR1	Average k	1.92	(W/m°K)	G		51 °C/Km	Q		98 mW/sq. m.		
K.B. Elev.		47 ft		14 m	Water Depth		209 ft		64 m	T. Depth	2691 m	
										Thermal Conductivity		
Base depth	gr	npi/stt	Base depth	Tfavg	Mid depth	kf	Vsh	Ø	raw	Tcorr.	Gg insitu	Tf
feet	API	%/mic.s./ft.	metre	(°C)	metre		%	%	(W/m°K)	(W/m°K)	(°C/Km)	(°C)
256			78	27	78	7						28
1220	100	180	372	35	225	7	40	52	1.27	1.27	67	48
1290	100	175	393	43	383	7	40	52	1.33	1.33	65	49
1375	105	167	419	44	408	7	50	50	1.36	1.36	63	51
1440	90	200	439	45	429	5	20	56	0.61	0.61	139	54
1580	105	165	482	47	460	7	50	50	1.39	1.39	62	56
1610	115	140	491	48	486	7	70	45	1.58	1.58	54	57
1810	95	145	552	50	521	6	30	46	2.24	2.20	39	59
1900	103	170	579	52	565	7	46	51	1.35	1.35	63	61
2080	111	165	634	53	593	7	62	50	1.33	1.33	65	64
2250	105	150	686	57	660	7	50	47	1.57	1.57	55	67
2277	110	166	694	58	690	7	60	50	1.33	1.33	65	68
2350	86	132	716	59	705	5	12	44	0.78	0.78	110	70
2457	107	148	749	61	733	7	54	47	1.57	1.57	55	72
2590	108	140	789	62	769	7	56	45	1.66	1.66	52	74
2740	110	135	835	65	812	7	60	44	1.70	1.70	50	76
2850	111	146	869	67	852	7	62	46	1.55	1.55	55	78
2930	104	134	893	68	881	7	48	44	1.80	1.80	48	79
3000	101	134	914	69	904	7	42	44	1.84	1.84	47	80
3090	104	133	942	71	928	7	48	44	1.81	1.81	47	82
3230	100	130	985	72	963	7	40	43	1.91	1.91	45	84
3300	95	130	1006	74	995	6	30	43	2.54	2.41	36	84
3350	80	35	1021	75	1013	6	38	41	2.47	2.36	44	85
3388	75	34	1032	76	1027	6	38	41	2.47	2.36	44	86
3417	85	36.5	1042	76	1037	7	45	41	2.13	2.13	49	86
3436	75	36	1047	77	1044	6	38	40	2.53	2.40	43	86

Apendix 2.3. List of estimated thermal parameters of of Malay Basin
Wells in italics are those with normalised LK thermal conductivity

No.	Well Code	Location Grid N	Location Grid E	Thermal Conductivity (W/m°K)	Geothermal Gradient (°C/km)	Heat Flow (mW/m^2)
1	AB1	99	94	1.76	42	74
2	AG1	82	67	1.83	48	88
3	BD2	27	102	1.85	36	67
4	BG1	43	123	1.71	49	84
5	*BJ1*	61	90	1.82	40	73
6	*BK5*	96	72	1.82	50	91
7	*BM1*	109	76	1.84	35	64
8	BN1	96	82	1.85	40	74
9	BO2	49	94	1.84	57	105
10	BS1	89	64	1.98	47	93
11	BT2	37	107	1.83	46	84
12	BU1	66	111	1.88	44	83
13	CM1	113	82	1.9	47	89
14	DG1	65	85	1.8	54	97
15	DM1	37	111	1.88	55	103
16	*DY2*	97	60	1.89	52	98
17	*FR1*	87	50	1.86	52	97
18	GJ1	33	120	1.91	52	99
19	GN2	92	80	1.8	45	81
20	IB1	83	76	1.82	48	87
21	IN2	57	95	1.75	50	88
22	IR1	85	76	1.92	51	98
23	JR2	53	108	1.85	54	100
24	*KB1*	44	93	1.76	49	86
25	KD1	40	96	1.9	52	99
26	KP1	47	87	1.72	49	84
27	KT1	63	74	2.01	43	86
28	*LA1*	74	78	1.79	50	90
29	LB1	78	86	1.82	45	82
30	LC1	77	85	1.86	45	84
31	LE1	78	102	1.63	51	83
32	LT1	40	106	1.86	45	84
33	LU1	90	99	1.64	42	69
34	LW1	107	84	1.86	47	87
35	ML1	62	95	1.67	48	80
36	NR1	47	102	1.92	47	90
37	OB1	55	126	1.69	49	83
38	OP1	98	68	1.95	46	90
39	PG1	33	126	2	50	100
40	PL1	94	79	1.81	43	78
41	*PT1*	109	80	1.92	38	73
42	PU3	105	70	1.84	43	79
43	RD1	75	83	1.69	47	79
44	RE1	102	79	2.06	44	91
45	RO1	101	79	1.83	53	97

No.	Well Code	Location Grid		Thermal Conductivity (W/m°K)	Geothermal Gradient (°C/km)	Heat Flow (mW/m^2)
		N	E	.		
46	SI1	104	97	1.69	48	81
47	SL3	102	72	1.83	45	82
48	SM2	68	83	1.73	60	104
49	SP1	55	101	1.83	43	79
50	SR1	79	82	1.68	46	77
51	ST1	87	52	1.88	44	83
52	TB3	88	80	1.81	44	80
53	TG1	104	79	1.88	48	90
54	TJ1	52	90	1.73	44	76
55	TK1	20	103	2.02	37	75
56	TM1	73	67	1.69	45	76
57	TN1	68	89	1.93	47	91
58	TO1	96	75	1.88	45	85
59	TP1	90	75	1.82	46	84